CHEMICAL REVIEWS

pubs.acs.org/CR

Review

# Fe(II) Redox Chemistry in the Environment

Jianzhi Huang, Adele Jones, T. David Waite, Yiling Chen, Xiaopeng Huang, Kevin M. Rosso, Andreas Kappler, Muammar Mansor, Paul G. Tratnyek, and Huichun Zhang*

Cite This: *Chem. Rev.* 2021, 121, 8161–8233

Read Online

ACCESS | Metrics & More | Article Recommendations

**ABSTRACT:** Iron (Fe) is the fourth most abundant element in the earth's crust and plays important roles in both biological and chemical processes. The redox reactivity of various Fe(II) forms has gained increasing attention over recent decades in the areas of (bio) geochemistry, environmental chemistry and engineering, and material sciences. The goal of this paper is to review these recent advances and the current state of knowledge of Fe(II) redox chemistry in the environment. Specifically, this comprehensive review focuses on the redox reactivity of four types of Fe(II) species including aqueous Fe(II), Fe(II) complexed with ligands, minerals bearing structural Fe(II), and sorbed Fe(II) on mineral oxide surfaces. The formation pathways, factors governing the reactivity, insights into potential mechanisms, reactivity comparison, and characterization techniques are discussed with reference to the most recent breakthroughs in this field where possible. We also cover the roles of these Fe(II) species in environmental applications of zerovalent iron, microbial processes, biogeochemical cycling of carbon and nutrients, and their abiotic oxidation related processes in natural and engineered systems.

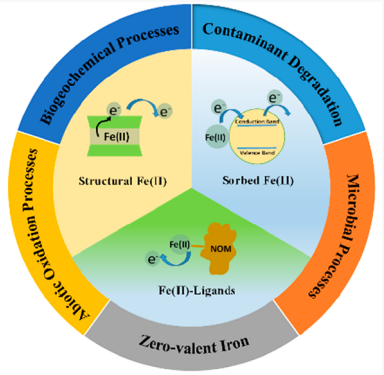


## CONTENTS



**Received:** December 6, 2020
**Published:** June 18, 2021









https://doi.org/10.1021/acs.chemrev.0c01286
*Chem. Rev.* 2021, 121, 8161–8233

## 1. INTRODUCTION

Iron (Fe) is the fourth most abundant element in the Earth's crust and is present in virtually all aquatic environments.[1,2] Average quantities of Fe in sedimentary rocks are approximately 5−6% by weight, with approximately $3.5 \times 10^{12}$ mol/year of Fe involved in redox reactions in the environment.[3] Iron plays an important role in the global biogeochemical cycles of many other major and minor elements (e.g., C, O, N, and S)[4−6] and also has direct and indirect impacts on corrosion,[7] degradation of organic and inorganic compounds,[8,9] mobility of metals,[10,11] evolution and sequestration of natural organic matter (NOM),[12−15] mineral dissolution,[16] nutrient availability,[17] and the weathering of rock and diagenesis,[2,18] in addition to microbial activity.[19] Iron is also central to many chemical aspects of the built or human-impacted environments including catalysis,[20−22] corrosion,[23] environmental remediation,[9] medical diagnosis and therapy,[24] pigments manufacture,[25,26] sensors,[27] solar cell operations,[28,29] water treatment,[30,31] and development of cost-effective iron-based materials for environmental and energy applications.[32−34] Iron redox chemistry is involved in all of the above processes.

Iron has a variable range of oxidation states from −2 to + 6[35] but, in natural environments, exists in two main redox states: ferrous iron (Fe(II)) and ferric iron (Fe(III)). Fe(II) is much more soluble than Fe(III) resulting in its high abundance in bioavailable forms.[36−38] In the environment, Fe(II) can originate from many sources including chemical and physical weathering,[39] reduction of iron(III)-bearing minerals including ferrihydrite, goethite, lepidocrocite, hematite, and magnetite[40−42] as well as different Fe(III)−ligand complexes[43−45] by photolysis,[46,47] chemical reductants such as sulfide[48] and dithionite,[49−53] and dissimilatory iron(III)-reducing bacteria,[54−58] and oxidation of zerovalent iron (ZVI) systems.[59]

Probably the most influential overarching development in the conceptual understanding of iron-based redox chemistry in the environment is the recent recognition that combining aqueous Fe(II) with iron-based solid phases results in materials with much greater and more diverse reactivity than the more familiar and widely studied iron minerals. This development has led to a paradigm shift regarding the reactivity of iron in the environment, with many new (and old) studies being reframed around the idea that the association of Fe(II) with many iron minerals (or ligands) results in an "activated" phase that can serve as a reactive intermediate in biogeochemical and environmental engineering processes.

In the past three decades, there has been a large number of papers reporting important reduction processes involving various Fe(II) species, which belong to four categories: aqueous Fe(II), Fe(II) complexed with ligands (Table 1),[60−63] structural Fe(II) (Table 2),[64−70] and surface-sorbed Fe(II) (Table 3).[8,71−74] Fe(II)−ligand complexes refer to aqueous Fe(II) cations complexed with different, typically organic ligands, resulting in a decrease in the Fe(II)/Fe(III) redox potential and consequently an often higher reduction reactivity than uncomplexed $Fe(II)_{aq}$. Structural Fe(II) reductants refer to those originating from iron minerals that contain Fe(II), such as magnetite, green rust, FeS, and Fe(II) within Fe-containing clays. Surface sorbed Fe(II) reductants refer to the sorption of Fe(II) onto the surface of (oxyhydr)oxide minerals but also include the prospect of electron exchange with metal ions in the mineral substrate.

While there have been many reviews on iron in mineralogy, (green)catalysis, biogeochemistry, and environmental remediation technologies,[3,75−78] none to date have reflected the paradigm shift described above, despite major breakthroughs in the understanding of the reactivity of these Fe(II)-associated reductants in the last 15 years. So far, only narrow aspects of Fe(II)-associated reductants toward select groups of contaminants have been reviewed. Usman et al. (2018) reviewed the occurrence, properties, and synthesis methods of mixed-valent Fe minerals and briefly discussed their environmental applications.[79] Strathmann (2011) summarized the reductive reactivity of soluble Fe(II)−ligand complexes.[80] Neumann et al. (2011) discussed the effects of structural Fe redox reactions on the clay mineral structures and properties.[81] He et al. (2009) evaluated the abiotic degradation of chlorinated organic compounds by the major classes of reactive minerals.[82] Rickard and Luther (2007) reviewed the chemistry of iron sulfide minerals.[83] In addition to these more recent reviews, there are several reviews on the reducing activity of Fe(II)-associated reductants, but these were published more than 20 years ago.[84−88]

This review focuses on assessing recent developments (in the past 15 years) and the current understanding of the redox reactivity of these four types of Fe(II)-associated reductants. The review examines their respective occurrence, reaction kinetics and mechanisms, and common factors affecting their redox reactivity (sections 2−4). Note that the reduction products and reaction pathways of various organic and inorganic compounds are not discussed in detail. These compounds are only treated as chemical probes that have been used to quantify the reactivity of different Fe(II) species. The role of Fe(II) species in zerovalent iron technology is reviewed in section 4.3. The diverse range of reductive reactivity reported for different


https://doi.org/10.1021/acs.chemrev.0c01286
Chem. Rev. 2021, 121, 8161−8233

**Table 1. Summary of Conditions and Results from Studies That Have Investigated Contaminant Reduction by Fe(II)−Organic Ligands**

| [Fe(II)] mM | Ligands | Ligand Conc | Fe(II)−Ligand Conc | pH | Contaminants | Products | $k_{obs}$ or second-order rate constant $k$ | Half-lives | ref |
|---|---|---|---|---|---|---|---|---|---|
| N/A[a] | porphyrins | N/A | $2.75 \times 10^{-4}$ M | N/A | nitrobenzene | aniline | 9.9 to $8 \times 10^3$ $M^{-1}$ $s^{-1}$, 4 to $58 \times 10^4$ $M^{-2}$ $s^{-1}$ | N/A | 1977[179] |
| N/A | porphyrin | N/A | 2 to 50 $\mu$M | 7, 10 | polyhalogenated methanes and ethanes | cysteine, perchloroethylene | $1 \times 10^{-1}$ to $6.1 \times 10^2$ $M^{-1}$ $s^{-1}$ | N/A | 1998[183] |
| 0.001−0.06 | citrate, nitrilotriacetate, oxalate, 1,10-phenanthroline, salicylate, tartrate | 5 to 1000 $\mu$M | N/A | 4.0 to 5.5 | Cr(VI) | Cr(III) | 0 to $3.7 \times 10^7$ $M^{-1}$ $s^{-1}$ | N/A | 1998[174] |
| 0.5 | acetate, malonate, oxalate, citrate, iminodiacetic acid, disodium nitrilotriacetate, disodium ethylenediaminetetraacetate, trimethylenediamine-N,N,N′,N′-tetraacetic acid | 0.5 to 200 mM | N/A | 2.1 to 8.9 | oxamyl and related oxime carbamate pesticides | N/A | $1.66 \times 10^{-7}$ to $2.49 \times 10^{-3}$ $s^{-1}$ | $2.78 \times 10^2$ to $4.18 \times 10^6$ s | 2002[147] |
| 0.5−1 | catechol- and thiol-containing organic ligands | 0.5 to 74 mM | N/A | 4.05 to 8.99 | 4-chloronitrobenzene | 4-chloroaniline | $<1.4 \times 10^{-8}$ to $>5.3 \times 10^{-2}$ $s^{-1}$ | 13.08 to $4.95 \times 10^7$ s | 2006[60] |
| 0.5 | catechol- and thiol-containing organic ligands | 1 to 50 mM | N/A | 5.01 to 8.43 | hexahydro-1,3,5-trinitro-1,3,5-triazine | formaldehyde | $<2.5 \times 10^{-8}$ to $>2.6 \times 10^{-1}$ $s^{-1}$ | 2.67 to $2.77 \times 10^7$ s | 2007[173] |
| 0.5 | organic ligands with catechol or organothiol Lewis base groups | 1 to 50 mM | N/A | 6.49 to 9.25 | polyhalogenated alkanes | acetaldehyde | $1.22 \times 10^{-7}$ to $8.22 \times 10^{-2}$ $s^{-1}$ | 8.43 to $5.68 \times 10^6$ s | 2007[151] |
| 0.2−0.5 | tiron | 5 to 10 mM | N/A | 5.05 to 6 | carbadox | carbadox-N4 | $1.50 \times 10^{-6}$ to $9.58 \times 10^{-4}$ $s^{-1}$ | $7.20 \times 10^2$ to $4.62 \times 10^5$ s | 2013[62] |
| 0.5 | tiron | 10 mM | N/A | 7 | isoxazoles | $\beta$-aminoenone analogs | $3.06 \times 10^{-5}$ to $>3.47 \times 10^{-1}$ $s^{-1}$ | 3.60 to $2.27 \times 10^4$ s | 2018[176] |
| 0.46−93 | surface water DOM | 0.84 to 1.44 mMC | N/A | 7.61 to 7.85 | pentachloronitrobenzene | pentachloroaniline | $1.67 \times 10^{-3}$ to $2.17 \times 10^{-2}$ $s^{-1}$ | 31.2 to $4.16 \times 10^2$ s | 2007[185] |
| 0.38−0.81 | pore water DOM | 1.24 to 3.22 mMC | N/A | 7.65 to 7.77 | pentachloronitrobenzene | pentachloroaniline | $6.39 \times 10^{-6}$ to $1.90 \times 10^{-4}$ $s^{-1}$ | $3.67 \times 10^3$ to $1.08 \times 10^5$ s | 2009[185] |
| 0.5 | cysteine, thioglycolic acid | 1 to 50 mM | N/A | 6 to 9 | nitroaromatic compounds | corresponding aniline | $1.81 \times 10^{-8}$ to $>2.31 \times 10^{-2}$ $s^{-1}$ | 30 to $3.83 \times 10^7$ s | 2008[61] |
| 0.2 | fulvic acids | 10 mg-C/L | N/A | 4 to 6 | Cr(VI) | Cr(III) | $9.67 \times 10^{-5}$ to $1.06 \times 10^{-2}$ $s^{-1}$ | 65.4 to $7.17 \times 10^3$ s | 2009[187] |
| 0.2−2 | hydroxamate siderophore | 0.5 to 50 mM | N/A | 6 to 9 | 4-chloronitrobenzene | 4-chloroaniline | $<1.00 \times 10^{-6}$ to $1.57 \times 10^{-1}$ $s^{-1}$ | 4.41 to $6.93 \times 10^5$ s | 2009[172] |
| 0.5 | ascorbic acid, caffeic acid | 0.5 to 10 mM | N/A | 5.8 to 7.6 | 2,4-dinitrotoluene | 2-amino-4-nitrotoluene, 4-amino-2-nitrotoluene | 0 to $1.26 \times 10^{-5}$ $s^{-1}$ | $>5.50 \times 10^4$ s | 2010[189] |

[a]N/A = not reported.



https://doi.org/10.1021/acs.chemrev.0c01286
Chem. Rev. 2021, 121, 8161−8233

**Table 2. Summary of Conditions and Results from Studies That Have Investigated Contaminant Reduction by Structural Fe(II)**

| Minerals | Loading | pH | Contaminants | Major products | $k$ (L $h^{-1}$ $g^{-1}$ if not specified) | ref |
|---|---|---|---|---|---|---|
| **Magnetite** | | | | | | |
| Magnetite | 25 g/L | 6~10 | $CCl_4$ (CT) | $CHCl_3$ and CO | $7.0 \times 10^{-6}$ −$1.1 \times 10^{-4}$ L/($m^2$ h) | 2004[192] |
| Magnetite | 1~10 g/L | 7 | $CCl_4$ | $CHCl_3$ and CO | 0.025−0.139 | 2007[193] |
| Magnetite | 45.5 g/L | 7 | Perchloroethene (PCE) | Chloride | $1.85 \times 10^{-4}$ | 2002[194] |
| Magnetite | 45.5 g/L | 7 | Trichloroethene (TCE) | Chloride | $2.33 \times 10^{-4}$ | 2002[194] |
| Magnetite | 45.5 g/L | 7 | Cis-DCE | Chloride | $1.69 \times 10^{-4}$ | 2002[194] |
| Magnetite | 45.5 g/L | 7 | Vinyl chloride (VC) | Chloride | $1.77 \times 10^{-4}$ | 2002[194] |
| Magnetite | 1 g/L | 7.2 | 3-Cl-nitrobenzene | 3-Cl-nitroaniline | $3.4 \times 10^{-5}$ − 0.74 | 2009[195] |
| Magnetite | 1 g/L | 7.2 | Nitrobenzene | Nitroaniline | $5.4 \times 10^{-6}$ − 0.57 | 2009[195] |
| Magnetite | 1 g/L | 7.2 | 2-methyl-nitrobenzene | 2-methyl-nitroaniline | $1.6 \times 10^{-6}$ − 0.43 | 2009[195] |
| Magnetite | 60 g/L | 3~7 | Cr(VI) | Cr(III) | 0.58−2.25 mol/($m^2$s) | 1996[196] |
| Magnetite | 20 g/L | 7 | Cr(VI) | Cr(III) | N/A | 1996[70] |
| Magnetite | 10 g/L | 4~10 | Cr(VI) | Cr(III) | N/A | 2014[197] |
| Magnetite | 1.89 mg/L | 6.8 | Cr(VI) | Cr(III) | N/A | 2015[198] |
| Magnetite | N/A | 7.2 | Hg(II) | Hg(0) | N/A | 2013[199] |
| Titanomagnetite | 0.1 g/L | 3, 5, 7 | $NpO_2^+$ | Np(IV) | N/A | 2016[200] |
| Titanomagnetite | 0.043 g/L | 8 | Tc(VII) | Tc(IV) | 0.795 | 2012[201] |
| Titanomagnetite | 76.4 g/L | 7 | Tc(VII) | Tc(IV) | 0.0578 $\mu$M $day^{-1}$ | 2014[202] |
| Titanomagnetite | 76.4 g/L | 7 | Tc(VII) | Tc(IV) | 0.139 $\mu$M $day^{-1}$ | 2014[202] |
| Titanomagnetite | 43.3 g/L | 7 | Tc(VII) | Tc(IV) | 9.899 $\mu$M $day^{-1}$ | 2014[202] |
| Magnetite | N/A | N/A | U(VI) | U(IV) | N/A | 2005[203] |
| **Iron sulfides** | | | | | | |
| FeS | 200 g/L | 6.5 | $CCl_4$ | N/A | 41.5 $day^{-1}$ | 1997[204] |
| FeS | 10 g/L | 8.3 | $CCl_4$ | Chloroform (CF) | $6.39 \times 10^{-2}$ | 2000[205] |
| FeS | 44 g/L | 7.8 | $CCl_4$ | | 0.358 | 2003[206] |
| FeS | 33 g/L | 7.5 | $CCl_4$ | CF | 1.24−1.59 $h^{-1}$ | 2009[207] |
| FeS | 33 g/L | 7.5 | $CCl_4$ | CF | 1.24−1.59 $h^{-1}$ | 2009[207] |
| FeS | 3 mM | 7 and 8 | $CCl_4$ | CF | N/A | 2016[208] |
| FeS | 5~100 g/L | 7.1~9.5 | Hexachloroethane (HCA) | PCE, PCA | 0.0603−3.21 $h^{-1}$ | 1998[209] |
| FeS | 10 g/L | 8.3 | HCA | PCE and PCA | $1.78 \times 10^{-4}$ | 2000[205] |
| FeS | 10 g/L | 8.3 | HCA | PCE | 0.0752 $h^{-1}$ | 2003[210] |
| FeS | 10 g/L | 8.3 | 1,1-dichloroethane (11-DCA) | N/A | N/A | 2000[205] |
| FeS | 10 g/L | 8.3 | 1,1-dichloroethane (12-DCA) | N/A | N/A | 2000[205] |
| FeS | 10 g/L | 8.3 | Perchloroethene (PCE) | Acetylene, cis-DCE and TCE | $6.68 \times 10^{-7}$ | 1999[211] |
| FeS | 10 g/L | 8.3 | PCE | Acetylene, TCE, 1,1-dichloroethylene (1,1-DCE) | $2.2 \times 10^{-6}$ − $9.4 \times 10^{-4}$ $h^{-1}$ | 2007[212] |
| FeS | 10 g/L | 8.3 | PCE | Acetylene, TCE, 1,1-DCE | $4.78 \times 10^{-4}$ − $8.86 \times 10^{-3}$ $h^{-1}$ | 2007[213] |
| FeS | 10 g/L | 7,8,9 | PCE | cis-DCE, TCE, ethene | $6.3 \times 10^{-5}$ − $1.21 \times 10^{-3}$ L/$m^2$/d | 2007[214] |
| FeS | 40 g/L | 7.68 | PCE | N/A | $6.4 \times 10^{-4}$ $h^{-1}$ | 2013[215] |
| FeS | 40 g/L | 7.68 | PCE | N/A | $1.4 \times 10^{-4}$ $h^{-1}$ | 2013[215] |
| FeS | 4.17 g/L | 5~12 | PCE | TCE, DCE, t-DCE, VC | 0−1.4091 $h^{-1}$ | 2015[216] |
| FeS | 10 g/L | 8.3 | Pentachloroethane (PCA) | PCE and TCE | $9.23 \times 10^{-4}$ | 2000[205] |
| FeS | 10 g/L | 8.3 | TCE | Acetylene, cis-DCE and VC | $2.0 \times 10^{-6}$ | 1999[211] |
| FeS | 10 g/L | 7.3~9.3 | TCE | Acetylene, cis-DCE, VC | $4.1 \times 10^{-4}$ − $1.62 \times 10^{-3}$ $h^{-1}$ | 2001[217] |
| FeS | 10 g/L | 8.3 | TCE | Acetylene, cis-DCE, 1,1-DCE | 0-($2.2 \pm 0.1$) × $10^{-3}$ $h^{-1}$ | 2007[212] |
| FeS | 10 g/L | 8.3 | TCE | Acetylene, cis-DCE, 1,1-DCE | $1.43 \times 10^{-4}$ − $1.98 \times 10^{-2}$ $h^{-1}$ | 2007[213] |
| FeS | 10 g/L | 8,9 | TCE | cis-DCE, vinyl chloride, ethene | (1.61−6.4) × $10^{-4}$ L/$m^2$/d | 2007[214] |
| FeS | 20 g/L | 5.4~8.3 | TCE | cis-DCE, 1,1-DCE, vinyl chloride | 0.02−0.751 $M^{-1}$ $d^{-1}$ | 2010[218] |
| FeS | 40 g/L | 7.68 | TCE | N/A | $4.9 \times 10^{-6}$ $h^{-1}$ | 2013[215] |
| FeS | 40 g/L | 7.68 | TCE | N/A | $1.1 \times 10^{-6}$ $h^{-1}$ | 2013[215] |



https://doi.org/10.1021/acs.chemrev.0c01286
Chem. Rev. 2021, 121, 8161−8233

**Table 2. continued**

| Minerals | Loading | pH | Contaminants | Major products | $k$ (L $h^{-1}$ $g^{-1}$ if not specified) | ref |
|---|---|---|---|---|---|---|
| FeS | 10 g/L | 8.3 | 1,1,2,2-tetrachloroethanes | TCE, cis-DCE, trans-DCE, acetylene | $2.16 \times 10^{-5}$ | 2000[205] |
| FeS | 10 g/L | 8.3 | 1,1,1,2-tetrachloroethanes | 11-DCE | $5.08 \times 10^{-5}$ | 2000[205] |
| FeS | 10 g/L | 8.3 | 1,1,1-trichloroethanes | 11-DCA | $1.63 \times 10^{-5}$ | 2000[205] |
| FeS | 10 g/L | 8.3 | 1,1,2-trichloroethanes | 11-DCE, VC | N/A | 2000[205] |
| FeS | 33 g/L | 7.5 | 1,1,1-trichloroethanes | 1,1,1-TCA, 1,1-DCA, ethylene | 0.0375 $h^{-1}$ | 2009[207] |
| FeS | 10 g/L | 8.3 | Tribromomethane | Dibromomethane | 0.129 | 2000[205] |
| FeS | 10 g/L | 5, 7, 8 | Cr(VI) | Cr(III) | N/A | 1997[204] |
| FeS | 0.6∼1.2 g/L | 5 and 7 | Cr(VI) | Cr(III) | N/A | 2004[219] |
| FeS | 1 g/L | 6, 7, 8 | Hg(II) | Hg(0) | N/A | 2014[220] |
| FeS | 273∼397 mM | 4.4, 6.3 | Se(VI) | Se(0) | N/A | 2008[221] |
| FeS | 5 g/L | 5∼11 | U(VI) | U(IV) | N/A | 2012[222] |
| **Green rust** | | | | | | |
| GR($SO_4$) | NR | 8 | $CCl_4$ | $CHCl_3$, $C_2Cl_6$ | $(0.0003-2.18) \times 10^{-5}$ $s^{-1}$ | 1999[223] |
| GR($SO_4$) | 5 g/L | 7.6 | $CCl_4$ | Chloroform, methane | $1.7 \times 10^{-5}$ $s^{-1}$ | 2003[224] |
| GR(Cl) | 1.5 g/L | 7.2 | $CCl_4$ | $CHCl_3$ | $5.4 \times 10^{-2}$ | 2005[225] |
| GR(Cl) | 10 g/L | 8 | $CCl_4$ | $CHCl_3$ | $6.23 \times 10^{-3}$ $Lm^{-2}$ $h^{-1}$ | 2010[226] |
| GR($SO_4$) | | 8 | $CCl_4$ | CO, HCOOH | $6.5 \times 10^{-2} - 0.47$ $h^{-1}$ | 2012[227] |
| GR($SO_4$) | 7 g/L | 7 | cis-DCE | $C_2H_2$, $C_2H_4$, $C_2H_6$ | $3.524 \times 10^{-3}$ | 2002[228] |
| GR($SO_4$) | 0.0037 M | 7.75 | cis-DCE | Ethylene, acetylene | 0.0424 $day^{-1}$ | 2012[229] |
| GR($SO_4$) | 7 g/L | 7 | PCE | $C_2H_2$, $C_2H_4$ | $9.464 \times 10^{-3}$ | 2002[228] |
| GR(Cl) | 10 g/L | 8 | PCE | Acetylene, ethylene, TCE | $5.6 \times 10^{-6}$ $Lm^{-2}$ $d^{-1}$ | 2009[230] |
| GR($SO_4$) | 10 g/L | 8 | PCE | Acetylene, ethylene | N/A | 2009[230] |
| GR($SO_4$) | 7 g/L | 7 | TCE | $C_2H_2$, $C_2H_4$ | $5.357 \times 10^{-3}$ | 2002[228] |
| GR(Cl) | 10 g/L | 8 | TCE | Acetylene, ethylene, cis-DCE | $2.92 \times 10^{-5}$ $Lm^{-2}$ $d^{-1}$ | 2009[230] |
| GR($SO_4$) | 10 g/L | 8 | TCE | Acetylene, ethylene | N/A | 2009[230] |
| GR($SO_4$) | 7 g/L | 7 | VC | $C_2H_4$, $C_2H_6$ | $5.595 \times 10^{-3}$ | 2002[228] |
| GR($SO_4$) | 0.0037 M | 7.75 | VC | Ethylene, ethane | 0.192 $day^{-1}$ | 2012[229] |
| GR($SO_4$) | 5 g/L | N/A | PCA | PCE, TCE | N/A | 2004[231] |
| GR($CO_3$) | 2.4 g/L | 7.5 | Trichloronitromethane | Methylamine | 55.2 or 32.5 $h^{-1}$ | 2007[232] |
| GR($SO_4$), GR($CO_3$) | 0.5∼2 g/L | 7 | Hexahydro-1,3,5-trinitro-1,3,5-triazine | HCHO, $N_2O$, $NH_4^+$, 1,3-dinitro-5-nitroso-1,3,5-triazacychlohexane, 1,3,5-trinitroso-1,3,5-triazacyclohexane | $0.22-0.24$ $M^{-1}$ $s^{-1}$ | 2008[233] |
| GR($SO_4$) | N/A | 7 | Nitrite | $NH_4^+$ | N/A | 1994[234] |
| GR($SO_4$) | N/A | 8.25 | Nitrate | $NH_4^+$ | $(0.047-1.48) \times 10^{-5}$ $s^{-1}$ | 1996[69] |
| GR(Cl) | N/A | N/A | Nitrate | $NH_4^+$ | $2.0 \times 10^{-5}$ $s^{-1}$ | 2001[235] |
| GR($CO_3$) | N/A | 7.5∼10.5 | Nitrate | $NH_4^+$ | $(2.4-4.3) \times 10^{-6}$ $s^{-1}$ | 2014[236] |
| GR($CO_3$) | 1.7 g/L | 7.5 | Nitrite | NO, $N_2O$, $N_2$ | N/A | 2014[237] |
| GR($SO_4$) | 5 g/L | N/A | Ag(I), Au(III), Cu(II), Hg(II) | Ag(0), Au(0), Cu(0), Hg(0) | N/A | 2003[238] |
| GR($SO_4$), GR(Cl) | N/A | 8∼10.1 | Cr(VI) | Cr(III) | N/A | 2000[239] |
| GR($CO_3$) | 0.25 g/L | 7 | Cr(VI) | Cr(III) | $(1.2-11.2) \times 10^{-3}$ $s^{-1}$ | 2001[240] |
| GR(Cl) | 0.125∼0.5 g/L | 7 | Cr(VI) | Cr(III) | 36.288−263.52 | 2003[241] |
| GR($CO_3$) | 0.125∼0.5 g/L | 7 | Cr(VI) | Cr(III) | 55.296−172.08 | 2003[241] |
| GR($CO_3$) | 0.125∼0.5 g/L | 7 | Cr(VI) | Cr(III) | 17.568−130.32 | 2003 |
| GR | N/A | 3.8∼11 | Se(VI) | Se(0), Se(IV) | $(0.75-1.68) \times 10^{-2}$ $h^{-1}$ | 1997[242] |
| **Iron-containing Clay** | | | | | | |
| Smectite | N/A | 7.5 | Nitrobenzene (NB) | Aniline | N/A | 2001[243] |
| Nontronite | 5 g/L | 7.5 | Nitroaromatic compounds | 4-acetyl aniline | N/A | 2003[244] |
| Reduced Nontronite | 2.5 g/L | 7.5 | 2-acetylnitrobenzene | 2-acetylnitroaniline | 0.248−0.76 | 2006[245] |
| Reduced Nontronite | 2.5 g/L | 7.5 | 4-acetylnitrobenzene | 4-acetylnitroaniline | 0.4−3 | 2006[245] |


https://doi.org/10.1021/acs.chemrev.0c01286
Chem. Rev. 2021, 121, 8161−8233

**Table 2. continued**

| Minerals | Loading | pH | Contaminants | Major products | $k$ (L $h^{-1}$ $g^{-1}$ if not specified) | ref |
|---|---|---|---|---|---|---|
| Reduced ferruginous smectite (RWa-R) | 2.5 g/L | 8.5 | $CCl_3CN$ | $CHCl_2CN$ | 0.35 $h^{-1}$ | 2003[246] |
| RWa-R | 2.5 g/L | 8.5 | $CCl_3NO_2$ | $CHCl_2NO_2$ | 4.7 $h^{-1}$ | 2003[246] |
| RWa-R | 2.5 g/L | 8.5 | $CCl_3CHCl_2$ | $CCl_3{=}CCl_2$ | 5.5 $h^{-1}$ | 2003[246] |
| RWa-R | 2.5 g/L | 8.5 | $CHCl_2CHCl_2$ | $CCl_2{=}CHCl$ | 0.16 $h^{-1}$ | 2003[246] |
| RWa-R | 2.5 g/L | 8.5 | $CCl_3CH_3$ | N/A | 0.37 $h^{-1}$ | 2003[246] |
| RWa-R | 2.5 g/L | 8.5 | $CCl_3CCl_3$ | N/A | 0.39 $h^{-1}$ | 2003[246] |
| RWa-R | 2.5 g/L | 8.5 | $CCl_4$ | N/A | 0.07 $h^{-1}$ | 2003[246] |
| Sediment with Magnetite | N/A | N/A | Cis-DCE | Acetylene | 0.31−2.29 $year^{-1}$ | 2004[247] |
| Sediment with Magnetite | N/A | N/A | 1,1-DCE | Acetylene | 1.37 $year^{-1}$ 1.37 $year^{-1}$ | 2004[247] |
| Clay | N/A | ~2.4 | Cr(VI) | Cr(III) | | 2000[248] |
| Montmorillonite | 0.73 g/L | 7.3 | Cr(VI) | Cr(III) | 1.28 $M^{-1}$ $min^{-1}$ | 2017[249] |
| Nontronite | 0.14 g/L | 7.3 | Cr(VI) | Cr(III) | 449 $M^{-1}$ $min^{-1}$ | 2017[249] |

Fe(II) species under various reaction conditions is then compared in section 4.4, together with challenges associated with this comparison. We further review how Fe(II) species are used by Fe(II)-oxidizing microorganisms as an electron and energy source (section 5) and the importance of Fe(II) species to biogeochemical processes, such as nutrient and carbon cycling (section 6). The generation of highly oxidizing reactive oxygen species (ROS) by different Fe(II) species under natural and engineered environmental systems is then examined in section 7. The instruments and methodologies employed for the characterization and understanding of these systems are also described in section 8. Finally, conclusions and priorities for future search are provided.

## 2. AQUEOUS FE(II)

### 2.1. Generation of Fe(II)

It is well-known that Fe(II) can form abiotically during the reduction of different iron(III) (oxyhydr)oxides by organic and inorganic compounds (e.g., sulfide and phenolic substances).[89−92] In the reductive dissolution, surface Fe(III) is reduced to Fe(II) and the detachment of iron becomes more energetically favorable due to the weaker bonds between the reduced iron and its neighboring irons. Therefore, the generated Fe(II) is readily released into the solution. The reaction rate of abiotic reductive dissolution can be accelerated in the presence of ligand-reducing pairs, such as oxalate and ascorbate.[93] This is because the formed, for instance, Fe(II)-oxalate, complexes have lower reduction potentials than that of Fe(II) alone, which favors the release of Fe(II) into the aqueous phase. It also turns out that the presence of a small amount of Fe(II) can significantly promote the ligand-assisted dissolution of Fe(III) (oxyhydr)oxides.[94−96] In a series of early work by Werner Stumm's group, inner-sphere type B ternary surface complexes (i.e., ligands bridge the oxide and Fe(II)) were believed to form in the dissolution process.[89,94,97] These complexes might facilitate electron transfer from the Fe(II) to structural Fe(III) to form sorbed Fe(II) which detaches more easily from the oxide surface. The rate-limiting step was reportedly the detachment of iron sites from oxide surfaces.

Dissimilatory iron(III)-reducing microorganisms (DIRB) are known to reduce a variety of Fe(III) (oxyhydr)oxides including ferrihydrite, goethite, lepidocrocite, hematite, and magnetite[40−42,98] as well as different Fe(III)−ligand complexes.[43−45] Different microorganisms, such as *Shewanella* spp.[99] and *Geobacter* spp.,[100] have demonstrated this capability in almost every anoxic environment. Due to the poorly soluble nature of Fe(III) (oxyhydr)oxides, *four* mechanisms have been identified regarding how DIRB transfer electrons to a poorly soluble Fe(III) (oxyhydr)oxide as the terminal electron acceptor (reviewed in refs 101 and 102): (i) through direct contact of the redox-active compounds inside cell membranes with the oxide;[98,103,104] (ii) through protein "nanowires" including pili and flagella to conduct electrons between the cell and the oxide;[105,106] (iii) through chelating ligands (e.g. siderophores such as catecholates, NTA, EDTA, humic acids) that can form strong complexes with ferric ions and promote their solubilization (this enables much faster electron transfer to soluble Fe(III) complexes as opposed to insoluble oxide surfaces);[107−110] and (iv) through electron shuttles, such as quinones, humic substances, phenazines, flavins, and potentially even conductive nanoparticles[111−114] which can shuttle electrons between bacteria and the oxide.[115−118] Long-term microbial reduction of Fe(III) minerals may be inhibited by Fe(II) accumulation, which can be alleviated by chelating ligands that complex with Fe(II) and, hence, prevent Fe(II) from accumulating on the mineral surfaces.[119−122] It is important to note that many organic compounds can serve as both ligands and electron shuttles.[115−118]

The photochemically mediated production of Fe(II) is also important when iron(III) (oxyhydr)oxides are the dominant ferric species of iron present, with the photolysis of chromophoric Fe(III)−NOM surface complexes recognized to induce the reductive dissolution of iron(III) (oxyhydr)oxides with concomitant formation of Fe(II).[3,89,123−126] This reductive dissolution process has been suggested to be primarily associated with ligand to metal charge-transfer (LMCT) processes occurring in Fe(III) surface complexes in a manner similar to that reported for the light-mediated dissolution of iron(III) (oxyhydr)oxides with adsorbed carboxylic acids such as citrate and oxalate,[127,128] though there is now evidence that superoxides generated on photolysis of NOM may also induce the reductive dissolution of iron(III) (oxyhydr)oxides.[129−131]


https://doi.org/10.1021/acs.chemrev.0c01286
Chem. Rev. 2021, 121, 8161−8233

**Table 3. Summary of Conditions and Results from Studies That Have Investigated Contaminant Reduction by Fe(II)-Treated Minerals**

| Minerals | Loading | Fe(II) ($\mu$M) | pH | Contaminants | Major Products | $k$ (L $h^{-1}g^{-1}$ if not specified) | ref |
|---|---|---|---|---|---|---|---|
| **Iron oxides** | | | | | | | |
| Goethite | 5 g/L | 0~3 mM | 4.11~8.22 | $CCl_4$ | Chloroform | 0−4.3 $day^{-1}$ | 2000[357] |
| Goethite | 25 $m^2$/L | 1 mM | 7.2 | $CCl_4$ | $CHCl_3$, formate, CO | 0.016 $h^{-1}$ | 2002[137] |
| Goethite | 6.9 g/L | 1.02 mM | 6.8 | $CCl_4$ | N/A | 0.1298 | 2003[206] |
| Goethite | 25.6 $m^2$/L | 0.2~3 mM | 7~8.0 | $CCl_4$ | $C_2HCl_3$ | 0.036−1.175 $h^{-1}$ | 2004[358] |
| Goethite | 3.1~5.7 | 1.4~1.5 mM | 7.0~7.2 | $CCl_4$ | Chloroform | 0.019−0.028 $h^{-1}$ | 2005[359] |
| Goethite | 4 g/L | 0~1.5 mM | 8 | $CCl_4$ | N/A | N/A | 2007[360] |
| Goethite | 25 $m^2$/L | 1 mM | 7.2 | $CHBrCl_2$ | $CHBrCl_2$, formate, CO | 0.0013 $h^{-1}$ | 2002[137] |
| Goethite | 25 $m^2$/L | 1 mM | 7.2 | $CHBr_2Cl$ | Formate, CO | 0.0029 $h^{-1}$ | 2002[137] |
| Goethite | 25 $m^2$/L | 1 mM | 7.2 | $CHBr_3$ | $CH_2Br_2Cl_2$, formate, CO | 0.0048 $h^{-1}$ | 2002[137] |
| Goethite | 25 $m^2$/L | 1 mM | 7.2 | $CFBr_3$ | N/A | 0.506 $h^{-1}$ | 2002[137] |
| Goethite | 25 $m^2$/L | 1 mM | 7.2 | $CBrCl_3$ | N/A | 3.577 $h^{-1}$ | 2002[137] |
| Goethite | 25 $m^2$/L | 1 mM | 7.2 | $CBr_2Cl_2$ | $CHBrCl_2$, formate, CO | 11.296 $h^{-1}$ | 2002[137] |
| Goethite | 25 $m^2$/L | 1.24 mM | 7.2 | 4-chloronitrobenzene | 4-chloroaniline | 1.9 $h^{-1}$ $m^{-2}$L | 2004[361] |
| Goethite | 0.65 g/L | 1 mM | 7 | 4-chloronitrobenzene | 4-chloroaniline; nitromethane | 1.48~5.26 | 2006[362] |
| Goethite | 5 mM | 1 mM | 7 | 4-chloronitrobenzene | 4-chloroaniline | $10 \times 10^{-3.74} - 1$ $h^{-1}$ L $m^{-2}$ | 2016[363] |
| Goethite | 0.325 g/L | 1 mM | 7 | 4-chloronitrobenzene | N/A | 0.001−0.0125 | 2016[364] |
| Goethite | 0.55 g/L | 387 $\mu$M | 6.6 | p-cyanonitrobenzene | Hydroxylamine | 1.489 | 2008[365] |
| Goethite | 25 $m^2$/L | 1 mM | 7.2 | HCE | N/A | 0.0501 $h^{-1}$ | 2002[137] |
| Goethite | 25 $m^2$/L | 1.24 mM | 7.2 | HCA | $CCl_4$ | $9.1 \times 10^{-4}$ $h^{-1}$ $m^{-2}$ L | 2004[361] |
| Goethite | 4.0 g/L | 3.0 mM | 6.0 | 2-nitrophenol | N/A | 0.059 $min^{-1}$ | 2013[366] |
| Goethite | 20 $m^2$/L | 4.4~4.6 mM | 6 and 7 | Nitrobenzene | Aniline | $4.5 \times 10^{-3} - 3.86$ $h^{-1}$ | 2013[367] |
| Goethite | 0.65 g/L | 1.0 mM | 6.5~7.8 | Trifluralin | Many products | 0.55−10.24 | 2003[368] |
| Goethite | 48 $m^2$/L | 0.5 mM | 7.4 | Oxamyl | Oxamyl oxime, and *N*,*N*-dimethyl-1-cyanoformamide | 0.0845 | 2003[369] |
| Goethite | 100 mg/L | 0.527 mM | 7.18 | Pentachloronitrobenzene | | | 2004[370] |
| Goethite | 0.8 g/L | 1 mM | 7.5 | Trichloronitromethane, Trichloroacetonitrile, Ttrichloroacetaldehdye hydrate | Nitromethane, Dichloroacetonitrile, trichloroacetamide, Dichloroacetaldehyde, Chloroform | 0.00019−8.05 $h^{-1}$ | 2005[371] |
| Goethite | 11.2 $m^2$/L | 1.5 mM | 7.22 | TNT | Many products | 16.56 $h^{-1}$ | 1999[136] |
| Goethite | 5.4 g/L | 2 mM | 7 | As(III) | As(V) | N/A | 2010[372] |
| Goethite | | | 2.7~6 | $PuO_2$ | Pu(III) | N/A | 2011[373] |
| Goethite | 394 $m^2$/L | 0.6~4.0 $mmol^{-1}$ | 6.8 | U(VI) | U(IV) | N/A | 2005[374] |
| Goethite | 1.5~3.0 g/L | 0.12~0.23 $\mu$M | 7 | Tc(VII) | Tc(IV) | 5.33−10.67 | 2009[346] |
| Hematite | 3.6 g/L | 1.5 mM | 7.2 | $CCl_4$ | $CHCl_3$ | 0.001 $h^{-1}$ | 2005[359] |
| Hematite | 25 $m^2$/L | 1.04 mM | 7.2 | HCA | $C_2Cl_4$ | $1.5 \times 10^{-4}$ | 2004[361] |
| Hematite | 0.53 g/L | 160 $\mu$M | 7.5 | U(VI) | U(IV) | 2.26 | 1999[375] |
| Hematite | 0.53 g/L | 20 $\mu$M | 7.5 | U(VI) | U(IV) | 0.17 | 1999[375] |
| Hematite | 0.53 g/L | 2 $\mu$M | 7.5 | U(VI) | U(IV) | 0.0158 | 1999[375] |
| Hematite | 0.53 g/L | 160 $\mu$M | 6 | U(VI) | U(IV) | 0.0396 | 1999[375] |



https://doi.org/10.1021/acs.chemrev.0c01286
Chem. Rev. 2021, 121, 8161−8233

**Table 3. continued**

| Minerals | Loading | Fe(II) ($\mu$M) | pH | Contaminants | Major Products | $k$ (L $h^{-1}g^{-1}$ if not specified) | ref |
|---|---|---|---|---|---|---|---|
| Hematite | 0.53 g/L | 160 $\mu$M | 7.5 | U(VI) | U(IV) | 2.72 | 1999[375] |
| Hematite | 62.5 mM | 0.6 mM | 6.8 | U(VI) | U(IV) | N/A | 2005[374] |
| Hematite | 1 mM | 0.1 mM | 6.8 | U(VI) | U(IV) | N/A | 2008[376] |
| Hematite | 4.5~9.0 g/L | 0.1~0.23 $\mu$M | 4.5~9 | Tc(VII) | Tc(IV) | $8.89 \times 10^{-5} - 3.56$ | 2009[346] |
| Hydrous ferric oxide | 1 mM as Fe (III) | 0.1 cmM | 6.8 | U(VI) | U(IV) | N/A | 2008[376] |
| Hydrous ferric oxide | 2.5 mM | 261~817 $\mu$M | 6.8 | Nitrite | $N_2O$ | $6.07 \times 10^{-6} - 4.59 \times 10^{-5}$ | 2009[377] |
| Lepidocrocite | 25 $m^2$/L | 1.14 mM | 7.2 | Hexachloroethane | $CCl_4$ | $1.8 \times 10^{-4}$ $h^{-1}$ $m^{-2}$ L | 2004[361] |
| Lepidocrocite | 25 $m^2$/L | 1.14 mM | 7.2 | 4-chloronitrobenzene | 4-chloroaniline | 1.3 $h^{-1}$ $m^{-2}$ L | 2004[361] |
| Lepidocrocite | 2.8 g/L | 1.9 mM | 7.2 | $CCl_4$ | $CHCl_3$ | $6.9 \times 10^{-3}$ $h^{-1}$ | 2005[359] |
| Lepidocrocite | 0.24 g/L | 200 $\mu$M | 8 | Nitrite | $N_2O$ | N/A | 1991[378] |
| Magnetite | 2.6 g/L | 1.8 mM | 7.3 | $CCl_4$ | Chloroform | 0.245 $h^{-1}$ | 2005[359] |
| Magnetite | 0.063 g/g | 42.6 mM | 7 | cis-DCE | Chloride | 0.28 $d^{-1}$ | 2002[194] |
| Magnetite | 0.063 g/g | 42.6 mM | 7 | VC | Chloride | 0.35 $d^{-1}$ | 2002[194] |
| Magnetite | 11.2 $m^2$/L | 1.5 mM | 7 | 4-nitroacetophenone | N/A | 56.64 $h^{-1}$ | 1995[265] |
| Magnetite | 1 g/L | 3 mM | 7.2 | Nitrobenzene | Analine | 12 | 2009[64] |
| Magnetite | 1 g/L | 0.1~10 mM | 7 | Hexahydro-1,3,5-trinitro-1,3,5-triazine | 1,3-dinitro-5-nitroso-1,3,5-triazacyclohexane, 1,3-dinitroso-5-nitro-1,3,5-triazacyclohexane, 1,3,5-trinitroso-1,3,5-triazacyclohexane | $3.0 \times 10^{-4} - 0.1$ | 2004[138] |
| Magnetite | 0.8 g/L | 1 mM | 7.5 | Trichloronitromethane, Trichloroacetonitrile, Ttrichloroacetaldehdye hydrate, | Nitromethane, Dichloroacetonitrile, trichloroacetamide, Dichloroacetaldehyde, Chloroform | 0.00019−8.05 $h^{-1}$ | 2005[371] |
| Magnetite | 142.9 g/L | 0.295 mM | | Tc(VII) | Tc(IV) | $1.86 \times 10^{-5}$ | 1996[379] |
| **Other Minerals** | | | | | | | |
| $\alpha$-AlOOH | 5 g/L | 0.107 mM | 7 | Tc(VII) | Tc(IV) | 0.009 $h^{-1}$ | 2008[380] |
| $\alpha$-$Al_2O_3$ | 3 g/L | 0.097 mM | 7 | Tc(VII) | Tc(IV) | 0.04 $h^{-1}$ | 2008[380] |
| $\gamma$-$Al_2O_3$ | 14 $m^2$/L | 1 mM | 8 | Substituted nitrobenzene | 4-chloroaniline | NR | 1995[265] |
| $\gamma$-$Al_2O_3$ | 4.0 g/L | 0.5 mM | 5.5~7 | 2-nitrophenol | N/A | 0.096 | 2009[381] |
| $\gamma$-$Al_2O_3$ | 901 $m^2$/L | 0.5 mM | 2~7.4 | Oxamyl | N/A | 0.0001−0.4 $h^{-1}$ | 2003[369] |
| FeS | 4.0 g/L | 2.3 mM | 7.2 | $CCl_4$ | $CHCl_3$ | 0.6075 | 2005[359] |
| FeS | 0.6 g/L | 1.4 mM | 7.2 | $CCl_4$ | $CHCl_3$ | 0.105 | 2005[359] |
| FeS | 1.3 g/L | 0.97 mM | 7.1 | $CCl_4$ | $CHCl_3$ | $3.08 \times 10^{-4}$ | 2005[359] |
| FeS | 25 $m^2$/L | 1 mM | 7.2 | 4-chloronitrobenzene | 4-chlorophenyl hydroxylamine | 17 $h^{-1}$ $m^{-2}$ L | 2004[361] |
| $FeS_2$ | 25 $m^2$/L | 1 mM | 7.2 | 4-chloronitrobenzene | N/A | $8.9 \times 10^{-2}$ $h^{-1}$ $m^{-2}$ L | 2004[361] |
| FeS | 25 $m^2$/L | 1 mM | 7.2 | HCA | 4-chlorophenyl hydroxylamine | $1.6 \times 10^{-2}$ $h^{-1}$ $m^{-2}$ L | 2004[361] |
| $FeS_2$ | 25 $m^2$/L | 1 mM | 7.2 | HCA | N/A | $1.6 \times 10^{-2}$ $h^{-1}$ $m^{-2}$ L | 2004[361] |
| $FeS_2$ | 0.084 g/g | 42.6 mM | 8 | PCE; TCE; cis-DCE; VC | TCE, $C_2H_2$, $C_2H_4$, PCE; cis-DCE, $C_2H_2$, $C_2H_4$; $C_2H_2$, $C_2H_4$; $C_2H_2$, $C_2H_4$. | 0.185−1.71 $day^{-1}$ | 2002[194] |
| $FeCO_3$ | 25 $m^2$/L | 1 mM | 7.2 | 4-chloronitrobenzene | N/A | $8.8 \times 10^{-5}$ $h^{-1}$ $m^{-2}$ L | 2004[361] |



https://doi.org/10.1021/acs.chemrev.0c01286
Chem. Rev. 2021, 121, 8161−8233

**Table 3. continued**

| Minerals | Loading | Fe(II) ($\mu$M) | pH | Contaminants | Major Products | $k$ (L $h^{-1}g^{-1}$ if not specified) | ref |
|---|---|---|---|---|---|---|---|
| $FeCO_3$ | 25 $m^2$/L | 1 mM | 7.2 | HCA | N/A | $1.7 \times 10^{-5}$ $h^{-1}$ $m^{-2}$ L | 2004[361] |
| Green rust | 25 $m^2$/L | 1 mM | 7.2 | HCA | 4-chlorophenyl hydroxylamine | $7.5 \times 10^{-3}$ $h^{-1}$ $m^{-2}$ L | 2004[361] |
| $SiO_2$ | 50 g/L | 0.5 mM | 7.4 | Oxamyl | NR | 0.01−4 $h^{-1}$ | 2003[369] |
| $TiO_2$ | 0∼15 g/L | 100∼500 $\mu$M | 2∼9 | 4-chloronitrobenzene | 4-chloronitroaniline, hydroxylamine | $10 \times 10^{-7} - 4.0 \times 10^{-3}$ | 2008[73] |
| $TiO_2$ | 4.0 g/L | 0.5 mM | 5.5∼7 | 2-nitrophenol | N/A | 1.1865 | 2009[381] |
| $TiO_2$ | 4.0 g/L | 3.0 mM | 6 | 2-nitrophenol | N/A | 0.011−0.023 $min^{-1}$ | 2013[382] |
| $TiO_2$ | 198 $m^2$/L | 0.5 mM | 2∼7.4 | Oxamyl | N/A | 0.0001−2.2 $h^{-1}$ | 2003[369] |
| $TiO_2$ | 0∼15 g/L | 100∼500 $\mu$M | 2∼9 | Oxamyl | Oxamyl oxime, N,N-dimethyl-1-cyanoformamide | $1.0 \times 10^{-6} - 1.0 \times 10^{-3}$ $s^{-1}$ | 2008[73] |
| **Clay minerals** | | | | | | | |
| Calcite | 2.3∼2.6 g/L | 0.06 and 0.4 mM | 7 | Se(IV) | Se(0) | N/A | 2010[383] |
| Kaoline | 4.0 g/L | 3.0 mM | 6 | 2-nitrophenol | N/A | 0.01 | 2013[366] |
| Kaolinite | 0∼200 $m^2$/L | 0.5 mM | 7.4 | Oxamyl | N/A | 0.01−0.11 $h^{-1}$ | 2003[369] |
| Kaolinite | | 1 mM | 8 | Substituted nitrobenzene | | | 1995[265] |
| Montmorillonite | 10 g/L | 500 $\mu$M | 6∼8 | 4-chloronitrobenzene | 4-Cl-nitrosobenzene, 4-Cl-aniline | $7.71 \times 10^{-6} - 1.35 \times 10^{-2}$ $min^{-1}$ | 2000 |
| Montmorillonite | 20 g/L | 5 mM | 7.2 | $Se(IV)O_3^-$ | Se(0) | N/A | 2007[384] |
| Montmorillonite | 4.5 g/L | 0.69 and 0.77 mM | 6.1∼8.5 | U(VI) | U(IV) | N/A | 2010[385] |
| Montmorillonite | 9 g/L | 10∼150 $\mu$M | 8.6 | Tc(VII) | N/A | N/A | 2017[345] |
| Montmorillonite (SWy-2) | 5 g/L | 2∼20 mM | 8 | TCE, PCE | Acetylene, ethane, ethane | N/A | 2019[282] |
| Nontronite (SWa-1) | 8.2 g/L | | 7.5 | 4-acetyl nitrobenzene | 4-acetyl aniline | | 2003[244] |
| Nontronite | 0.8 g/L | 263∼1780 $\mu$mol/g | 5.5∼8.5 | Tc(VII) | Tc(IV) | N/A | 2009[386] |



https://doi.org/10.1021/acs.chemrev.0c01286
Chem. Rev. 2021, 121, 8161−8233

Depending on the environmental conditions (pH, presence of NOM, bicarbonate, phosphate, or sulfide), the produced Fe(II) is present as free dissolved Fe(II), Fe(II)−NOM complexes, inorganically complexed Fe(II), or surface-sorbed Fe(II), or it can precipitate as Fe(II) minerals such as siderite ($FeCO_3$), vivianite ($Fe_3(PO_4)_2$), or Fe-sulfides (FeS and $FeS_2$). Depending on the rate of reduction, the total amount of Fe present, and the ratio of Fe(II) to the remaining solid-phase Fe(III), the formation of mixed-valent Fe(II)−Fe(III) minerals such as magnetite, green rusts, and Fe-phosphates is also possible.[132−134] In all cases, the resulting Fe(II)-bearing phases not only are involved in abiotic Fe(II)-associated reductive processes but also can be used by Fe(II)-oxidizing microorganisms as electron and energy sources.[102]

### 2.2. Reactivity of Aqueous Fe(II)

The reduction of a substance by Fe(II) involves the loss of an electron from Fe(II) and the subsequent gain of an electron by the substance being reduced. This results in the oxidation of Fe(II) to Fe(III). The transfer of electrons between species determines the oxidation−reduction potential of the solution or suspension and is often simply referred to as the redox potential. The redox potential is generally measured in millivolts against a reference electrode, with low or negative values indicative of a tendency for the solution/suspension to lose electrons.[135] Mathematically the process is defined by the Nernst equation whereby the redox potential of the system ($E_h$) is a function of a standard redox potential ($E^0$) and the activities of the reduced and oxidized ionic species at 25 °C and 1 atm. For example, for Fe-based systems, the redox potential of the system is defined as

$$E_h = E^0 - 2.3\frac{RT}{nF}\log\frac{[Fe^{2+}]}{[Fe^{3+}]} \quad (1)$$

The lower the redox potential of a solution or suspension containing Fe(II), the greater the ability for a substance, such as an organic pollutant, to be reduced. In the process of reduction by Fe(II), the pollutant may become less toxic and/or easier to degrade in subsequent treatment processes;[136−139] therefore, this is a useful natural attenuation process that can occur in the environment or be exploited as an engineered treatment process.

Understanding what processes increase the rate of contaminant reduction is therefore the same as understanding what processes drive Fe(II) oxidation. There have been a vast array of studies that have investigated aqueous Fe(II) oxidation rates by oxygen,[140−144] whereby the general rate can be simplified by the following rate law (eq 2).

$$-\frac{d[Fe(II)]}{dt} = k'[Fe(II)][O_2] \quad (2)$$

While minor differences in the overall rate constant ($k'$) have been reported from study to study, some of which have been investigated under differing values of oxygen partial pressure, there is a general consensus that the rate is highly pH-dependent due to the different hydrolyzed Fe(II) species present as a function of pH such that, as the pH of a solution increases and the hydrolysis of hexaquo $Fe^{2+}$ to $Fe(OH)^+$ and then $Fe(OH)_2$ occurs, the overall rate of Fe(II) oxidation increases dramatically.[145] Under circumneutral pH conditions, however, $Fe^{2+}$ is the dominant aqueous Fe(II) species and, from what we know about the rate of Fe(II) oxidation by oxygen, $Fe^{2+}$ oxidation is extremely slow in the absence of any oxide surface with which $Fe^{2+}$ can interact to alter its effective speciation.[146] As such, even though Nernstian conditions may be satisfied such that pollutant reduction is "thermodynamically" possible under circumneutral pH conditions, the rate of $Fe^{2+}$ oxidation is known to be extremely slow. Indeed, the 2002 study by Strathmann and Stone demonstrates this.[147] In that study, even though reduction kinetics showed a good relationship with the calculated redox potential, the kinetic rate constants determined appeared to "flat-line" at approximately pH 6.5 and below due to the much slower rate of pollutant reduction in the presence of the dominant $Fe^{2+}$ species at these pH values. Of course, the complexation of Fe(II) by certain inorganic ligands may alter this trend, and again, the 2002 study by Strathmann and Stone[147] demonstrates the dramatic increase in the reducibility of certain pesticides in the presence of particular inorganic ligands, namely fluoride, carbonate, and phosphate, highlighting the importance of Fe(II) speciation to the kinetics of pollutant reduction processes. These particular inorganic ligands have also been shown to have a pronounced impact on Fe(II) oxidation kinetics,[148] again illustrating the link between Fe(II) oxidation and pollutant reduction kinetics.

## 3. IRON(II) COMPLEXED BY ORGANIC LIGANDS

Fe(II)−ligand complexes play an indispensable role in the fate of contaminants, particularly in groundwater, soils, and sediments, where both abiotic and microbial reduction of contaminants can occur. Dissolved Fe(II) and natural organic ligands commonly coexist in reducing environments, are usually more reactive under circumneutral conditions, and can significantly affect the fate and transformation of aquatic contaminants.[60,61,147,149−151] Dissolved Fe(II) associated with small organic ligands are important not only due to their environmental relevance but also because of their simpler structures and properties than NOM which makes them useful probes for molecular-scale factors that determine Fe(II) redox reactivity in different systems.[80] Fe(II)−organic ligand complexes may also bind with NOM on soil mineral surfaces, forming potent reductants for contaminants in soil.[152]

Although certain inorganic ligands including fluoride, carbonate, and phosphate render Fe(II) a good reductant to degrade pesticides,[149] many contaminants including nitro- and halogenated compounds show negligible or limited reactivity in solutions containing inorganic salts of Fe(II) (e.g., $[Fe(NH_3)_6]^{2+}$, $FeCl_2$, and $FeSO_4$).[84,85,100] The lack of reactivity is due to the relatively higher redox potential of inorganic Fe(II) salts compared to those complexed by organics. The reason for this will be discussed in further detail in section 3.2; this section will largely focus on interactions of Fe(II) with organic ligands. Readers are also referred to an excellent review on the reduction of organic contaminants by Fe(II)−ligand complexes.[80]

### 3.1. Environmental Relevance of Fe(II)−Ligand Complexes

NOM is generated from two main sources: the decomposition of dead animals and plants and the excretion of extracellular products from microorganisms and plants.[153] During biogeochemical decomposition processes, organic substances with reduced functional groups, such as hydroquinones and thiols, can be generated in substantial abundance in anoxic environments.[61] For example, the concentration of organic thiols can be up to 17 $\mu$M within dissolved organic matter (DOM) in aquatic systems.[154] NOM consists of large and complex structures with an array of functional groups, forming complexes with ferrous iron mainly through their numerous oxygen-, nitrogen-, and sulfur-containing functional groups by a sharing of electron density with the Fe(II) ion center.


https://doi.org/10.1021/acs.chemrev.0c01286
Chem. Rev. 2021, 121, 8161−8233

It is now recognized that reduced functional groups in NOM can induce the abiotic reduction of Fe(III) with resultant formation of Fe(II) species with the rate and extent of reduction dependent on the electron-donating capacity of the NOM.[155] The reduction of Fe(III) in the dark occurs because of hydroquinone-like moieties in NOM with the Fe(III) reduction rate remaining invariant with change in pH. The oxidation rate of Fe(II) in the dark is influenced by its interaction with $O_2$ and increases as pH increases.[156] Light can also dramatically influence the rates of both Fe(III) reduction and Fe(II) oxidation in the presence of NOM with Fe(III) reduction driven particularly by LMCT processes while Fe(II) oxidation is influenced by the photochemical formation of semiquinone radicals which are effective Fe(II) oxidants.[157,158] These light-mediated processes influence the bioavailability of iron to phytoplankton[159] with this impact particularly important in marine systems where the bioavailability of iron is recognized to exert a major influence on algal growth in high nutrient low carbon surface waters.[160] The photochemical reduction of Fe(III) to Fe(II) results in diurnal cycles of Fe(II) in surface waters with maxima occurring at peak sunlight intensity.[161,162]

Low molecular weight organic ligands exist in natural environments originating from the decay of more complex organic materials and excretion from plants and microorganisms.[80] For example, small organic ligands, such as oxalic acid and formic acid, can be found at concentrations ranging from 25 to 1000 $\mu$M in forest soils and from 5 to 174 $\mu$M in soil solutions.[163] Additionally, siderophores are secreted by microorganisms such as bacteria and fungi, often for the specific purpose of iron acquisition.[165,166] They are among the strongest Fe-chelating agents found in nature, capable of forming strong octahedral complexes with iron, including 1:1 hexadentate complexes such as with desferrioxamine B (DFOB).[167] Concentrations of siderophores in most natural systems are relatively low,[168] while higher levels may be detected in microenvironments.[169]

In some instances, small molecules with Fe(III)-reducing ability may be released by aquatic plants, apparently both to enhance Fe supply and to induce an allelopathic effect on other organisms. For example, seasonally persistent blooms of *Ulvaria obscura var. blyttii* have been well reported in recent decades with the synthesis and release of dopamine by this organism regarded to suppress and inhibit the growth of other organisms competing for limited resources. Sun et al.[170] showed that high concentrations of $H_2O_2$ accumulate over time due to the direct oxidation of dopamine and dopamine-induced generation of 5,6-dihydroxyindole, especially in the presence of elements such as iron, calcium, and magnesium. They suggested that iron mobilization induced by dopamine may favor the persistent blooms of *Ulvaria obscura var. blyttii* or even the whole community through iron increase within the bloom region.[170]

Overall, the simultaneous occurrence of dissolved Fe(II) and natural organic ligands is common in the reducing conditions of suboxic and anoxic aquatic environments.[134,135] Studies have shown the importance of the interactions between Fe(II) and natural organic ligands due to their electron-donating characteristics, which are capable of enhancing the redox activity of Fe(II) and facilitating the in situ reductive transformation of contaminants.[80] Highly stable multidentate complexes can form between Fe(II) ions and ligands, e.g., five-membered ring complexes.[171] As discussed above, microorganisms can also release siderophores into the extracellular environment to aid in the transport of iron across cell membranes with this process also recognized to occur in anoxic and suboxic environments.[167]

### 3.2. Reactivity of Fe(II)−Ligand Complexes

In the presence of organic ligands that can form strong complexes with transition metals, the water molecules bonded to the Fe(II) or Fe(III) cation will be replaced by the organic ligands at one or more of the water positions, leading to a significant change in Fe(II) and Fe(III) speciation. Because Fe(II) hydrolysis states and protonation of hydroxyl ligands are strongly pH-dependent, both pH and ligand concentration are primary parameters that affect Fe(II) or Fe(III) speciation with organic ligands. For example, in solutions containing Fe(II) and tiron (4,5-dihydroxy-1,3-benzenedisulfonic acid), various Fe(II) species (Fe(II), $FeOH^+$, $Fe(OH)_2^0$, $Fe(OH)_3^-$, $FeHL^-$, $FeL^{2-}$, and $FeL_2^{6-}$) (where $L^{4-}$ represents the fully deprotonated tiron) can form. As the pH increases from 4.0 to 9.0, the total Fe(II) concentration remains constant while the concentrations of these Fe(II) complexes increase to different extents and then decrease (Figure 1).

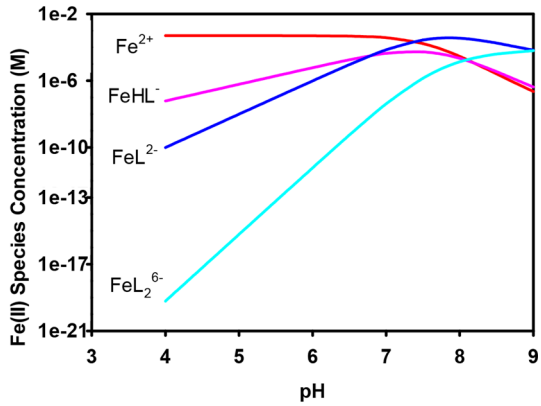


**Figure 1.** Effect of pH on $Fe^{II}$ speciation in solutions containing 0.5 mM $Fe^{II}$ and 10 mM tiron. The concentrations of various $Fe^{II}$ species were calculated by MINIQL+ 4.6. Reprinted with permission from ref 63. Copyright 2016 American Chemical Society.

A few studies have demonstrated that the rate of reduction of reducible organic compounds by individual Fe(II)−organic ligand complexes follows a linear free energy relationship with the one-electron redox potential $E_H^0$ of the corresponding Fe(II)/Fe(III) redox couple under standard conditions (i.e., the $E_H^0$ value is the primary parameter in predicting the reductive reactivity of the Fe(II) species).[36,60,61] The standard redox potential of each Fe(II)/Fe(III) redox couple can be defined using the following relationship.

$$E_H^0 = 0.77 - \frac{RT}{F} \ln\left(\frac{K_{Fe^{III}L}}{K_{Fe^{II}L}}\right) \quad (3)$$

where 0.77 V (vs normal hydrogen electrode, NHE) is the value of $E_H^0$ for the Fe(III)/Fe(II) half reaction under standard conditions, $R$ is the universal gas constant, $T$ is the temperature in degrees Kelvin, $F$ is the Faraday constant, and $K_{Fe(II)L}$ and $K_{Fe(III)L}$ are the equilibrium constants for Fe(II) and Fe(III) complexation with a ligand L, respectively. According to eq 3, ligands that form much stronger complexes with Fe(III) than with Fe(II) will lead to a much lower $E_H^0$ for the Fe(II) complex−Fe(III) complex redox pair, yielding a stronger reductant. As a result of their lower $E_H^0$, Fe(II) complexes with ligands


https://doi.org/10.1021/acs.chemrev.0c01286
Chem. Rev. 2021, 121, 8161−8233

possessing catechol, hydroxamate, and thiol functional groups have gained the most attention because of their higher redox reactivity than Fe(II) complexes with other organic ligands such as carboxylates.[60,147,149] $E_H^0$ values for redox couples associated with Fe(II)−ligand complexes are provided in Figure 2. The low

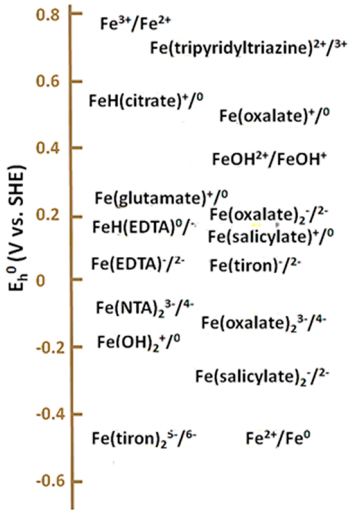


**Figure 2.** Standard one-electron redox potentials ($E_H^0$) for the Fe(III)/Fe(II) redox couples associated with various Fe(II)−organic ligand complexes. Modified with permission from ref 80. Copyright 2011 American Chemical Society.

redox potentials of Fe(II) complexes with catecholate, hydroxamate, and thiol ligands have been linked to their high reductive redox reactivity toward an array of organic contaminants in anoxic aqueous solution.[60,61,151,172,173]

Fe(II) has six inner-sphere coordination sites with a lower number of occupied sites on Fe(II) leading to more positions available for the Fe(II) to complex with other ligands and/or chemical probes. The availability of inner-sphere coordination positions of Fe(II) that are capable of bonding with the Lewis base donor groups within certain chemical probes has been demonstrated to increase the rate of reduction of certain oxime carbamate pesticides.[147] For instance, Fe(II) complexed by carboxylates and phenolates generally enhances the reduction of toxic Cr(VI) to less toxic Cr(III), because a ternary Fe(II)−ligand−Cr(VI) complex forms thereby allowing inner- or outer-sphere electron transfer to occur within the complex.[174] Similarly, carboxylate and aminocarboxylate ligands enhanced the reduction of oxime carbamate pesticides by Fe(II) through enabling both a lower redox potential of the reductant and the formation of inner-sphere complexes with the pesticides.[147] However, experiments have also demonstrated that inner-sphere coordination is not necessary to achieve the reduction of organic contaminants by Fe(II)−organic ligands because Fe(II) complexes with EDTA or $CN^-$ with all six coordination sites saturated have shown enhanced rates of reduction relative to aqueous Fe(II) species.[175]

When examining the influence of Fe(II) species in solutions containing both Fe(II) and tiron on the observed rate constants ($k_{obs}$) for the reduction of nitroaromatic compounds, a strong correlation between the measured $k_{obs}$ values of 4-chloronitrobenzene and the concentration of $FeL_2^{6-}$ is observed (Figure 3), indicating that $FeL_2^{6-}$ is the dominant reductant. The high reactivity of $FeL_2^{6-}$ has been explained based on its lower $E_H^0$ than those of other Fe(II)−tiron complexes (Figure 2).[60]

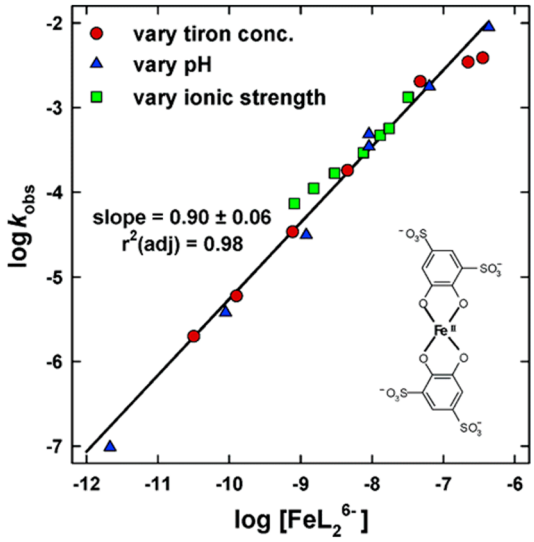


**Figure 3.** Linear correlation of log $k_{obs}$ of 4-chloronitrobenzene reduction vs concentration of $FeL_2^{6-}$, and the structure of $FeL_2^{6-}$. Line represents linear regression of three data sets, including the variations in total tiron concentration, pH, and ionic strength. Reprinted with permission from ref 60. Copyright 2006 American Chemical Society.

The above mechanisms are further expanded in recent studies on the degradation of organic contaminants containing nitrogen−oxygen bonds including aromatic N-oxides, isoxazoles such as sulfamethoxazole, and hydroxylamines in the presence of Fe(II)−tiron.[62,63,176,177] The authors found that several types of complexation between contaminants and Fe(II)-tiron can increase the reaction rates to different extents, with stronger complexation yielding much faster reductive reactivity.[62,63,176] One example is an inner-sphere 5-membered ring complex between Fe(II)-tiron and carbadox, which facilitates electron transfer from $FeL_2^{6-}$ to carbadox to make the reaction 276 times faster.[62,63] Complex formation between Fe(II)-tiron complex and the aromatic N-oxides prior to electron transfer might be the rate-limiting step.[62,63] Another example is an increase in the reductive reactivity of four isoxazoles from 16- to >155-fold upon the formation of different inner-sphere six-membered ring complexes with Fe(II)-tiron.[176] In the case where inner-sphere complexation with Fe(II)-tiron is inhibited due to steric hindrance, as occurs in the case of sulfamethoxazole, the reaction proceeds at a similar rate to that without any added tiron.[176]

The ability of Fe(II)−ligand complexes to reduce organic compounds also means they can act as an electron-transfer mediator. As an example, Fe(II)−porphyrin complexes can rapidly reduce a number of organic functional groups at room temperature, including olefins, acetylenes,[178] alkyl halides, quinones, and nitro and nitroso compounds.[179−182] Correspondingly, Fe(II)−porphyrin can act as an electron-transfer mediator to promote reduction of polyhalogenated methanes and ethanes by bulk reductants such as cysteine in homogeneous aqueous solution.[183,184] The proposed reaction mechanism for the mediated reduction includes outer-sphere electron transfer from the bulk reductant to the polyhalogenated methane or ethane through the mediator.

The reduction of contaminants in the presence of dissolved Fe(II) can be accelerated, inhibited, or not affected by the presence of NOM, and the reported reactivity of Fe(II)−NOM toward contaminants is sometimes contradictory[185−187] due to


https://doi.org/10.1021/acs.chemrev.0c01286
Chem. Rev. 2021, 121, 8161−8233

multiple factors such as different NOM sources, structure, content, and target contaminant type, as well as differing experimental methodologies. For instance, carboxylate, catecholate, and thiol moieties in NOM can form complexes with Fe(III), lowering the $E_H^0$ of the resultant iron-NOM system, thereby rendering the contaminant reduction more favorable.[60,61,147] As demonstrated by eq 3, strong Fe(III) binding functional groups are found to enhance reduction while strong Fe(II) binding functional groups retard reduction.[174] NOM can (and generally does) have both Fe(III) and Fe(II) stabilizing groups, and the amounts of each can vary greatly from site to site such that simple generalizations about how NOM affects the reductive reactivity of Fe(II) cannot be made. Moreover, NOM may inhibit the formation of iron colloids and consequently the formation of surface-complexed Fe(II), leading to slower reductive transformation in Fe(II)−DOM media.[186]

Generally, anything that can alter the relative speciation of Fe(II) and Fe(III) and, therefore, can impact the resultant redox potential of the system according to eqs 1 and 3 will impact the reductive reactivity of Fe(II)−ligand complexes. The most important parameters, in addition to the functional groups present on NOM, are pH and the total concentrations of Fe(II), the complexing ligand, and the target compound. Table 1 summarizes measured reduction kinetics of various contaminants by different Fe(II)−ligand complexes under different conditions. In summary, $k_{obs}$ is found to be positively correlated with Fe(II) concentration, ligand concentration, and pH, but it decreases with increasing concentration of the contaminant. Chen et al.[62] investigated carbadox reduction by the Fe(II)−tiron complex with varying concentrations of carbadox, Fe(II), and tiron and varying pH conditions. The results indicated that an increase in Fe(II) concentration led to an increase in $k_{obs}$ for carbadox reduction at pH 5.90. When the pH increased from 5.05 to 6.00 with the carbadox, Fe(II), and tiron concentrations fixed, the values of $k_{obs}$ increased 3 orders of magnitude. At pH > 7.00, the reaction was too fast to be monitored.

Given the diverse chemical structures and a large number of available ligands, developing quantitative tools for the reactivity of different organic chemicals by soluble Fe(II) complexes has been limited to narrowly defined, relatively homogeneous families of reactants (e.g., dechlorination of alkyl halides). A recent study, however, attempts to approach this challenge by comparing two approaches: classical QSARs based on molecular descriptors, e.g., $E_{LUMO}$ (energy of the lowest-unoccupied molecular orbital), and emerging machine learning algorithms based on different chemical representations, e.g., molecular fingerprints.[188] Based on the obtained reduction kinetics of 60 diverse chemicals toward one Fe(II)−ligand complex as the model reductant under a wide range of solution conditions, the authors observed a similar prediction performance of the models developed by the two approaches (Figure 4). The major difference between these two approaches is that the classical QSARs are only applicable to structurally similar chemicals, including nitroaromatic compounds, aliphatic nitro-compounds, aromatic N-oxides, isoxazoles, polyhalogenated alkanes, and other miscellaneous chemicals under fixed conditions, whereas the machine learning model covers the reduction rates of all classes of chemicals and changing conditions.

In many natural settings where naturally occurring Fe is abundant, Fe can exist in multiple states that may not be favorable toward reduction. For example, Fe(II) may form complexes with other organic ligands to shield it from reacting with oxidants, as illustrated by NOM inhibiting reduction of

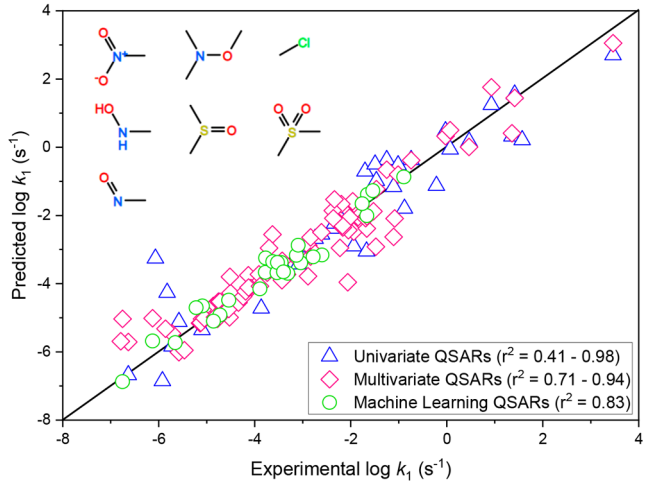


**Figure 4.** Plot of experimental log $k_1$ (first-order rate constants) against predicted values from the conventional QSARs and the machine learning model. Reprinted with permission from ref 188. Copyright 2021 Elsevier.

contaminants by competing with other ligands such as tiron for complexation with Fe(II).[189] Similarly, hydrophobic extractable DOM from rainwater, a complex mixture of hydrophobic ligands, was observed to significantly slow abiotic Fe(II) oxidation by $O_2$ in seawater.[190] In addition, anionic oxygen-containing ligands such as carboxylic acids and hydroxylated organic compounds can facilitate Fe(II) oxidation with the consequent reduction of Fe(III) minerals in saltmarsh sediments and pore waters. These oxygen containing ligands can "pump" electron density from oxygen to Fe(II) to enhance the basicity of the Fe(II) atom and stabilize the formed Fe(III), allowing Fe(III)−ligand complexes to exist even under highly reducing conditions.[191] As a result, the highly reducing nature of sediments would presumably allow Fe(III) (oxyhydr)oxides to exist only near the sediment−water interface, where most active redox chemistry occurs.

## 4. SOLID PHASE FE(II)

### 4.1. Structural Fe(II)

Minerals containing structural Fe(II) play an important role in controlling heterogeneous redox reactions in anoxic environments.[196] Many mineral phases contain structural Fe(II), such as magnetite,[65,195] green rusts,[69,235,237] iron sulfides,[209,211] and clay minerals.[245] As such, these Fe(II) containing minerals are able to reduce various pollutants, including carbon tetrachloride, nitroaromatics, pesticides, polyhalogenated compounds, nitrate, nitrite, Cr(VI), and Tc(VII) (refer to Table 2), often at significant rates. Specific minerals containing structural Fe(II) are examined in the following sections, and readers are referred to an excellent recent review by Usman et al. on the synthesis, properties, and environmental applications of magnetite and green rust for additional information.[79] We focus on magnetite, green rusts, mackinawite, and iron-containing clay minerals as the representative structural Fe(II) below mainly because of their high reactivity toward pollutants and, as such, their potential applicability.

**4.1.1. Magnetite.** Magnetite ($Fe_3O_4$) is a common mixed-valent iron oxide mineral.[2] Magnetite can form through the reduction of Fe(III) (oxyhydr)oxides biotically by dissimilatory iron(III)-reducing bacteria[192,250] or abiotically from the reaction


https://doi.org/10.1021/acs.chemrev.0c01286
Chem. Rev. 2021, 121, 8161−8233

of aqueous Fe(II) with Fe(III) containing minerals,[251,252] by corrosion of zerovalent iron systems,[59,253] and by the oxidation of ferrous minerals and iron metal from both natural and anthropogenic sources.[254−256] Magnetite can also be formed intracellularly by magnetotactic bacteria.[257]

Numerous studies have explored the reductive reactivity of magnetite toward both inorganic and organic contaminants, including organic contaminants such as nitrobenzene,[64,195] carbon tetrachloride ($CCl_4$),[192,193] and *cis*-dichloroethene (*cis*-DCE),[64,247] inorganic contaminants such as Cr(VI)[70,197,258] and Hg(II),[199,259] and radionuclides such as U(VI),[65] the details of which are shown in Table 2. More specifically, structural Fe(II) in magnetite has been shown to donate electrons[193] to induce dechlorination of the chlorinated ethylenes PCE, TCE, cis-DCE, and VC with rate constants ranging from 0.185 to 0.254 $d^{-1}$ at pH 7.[194] Cr(VI) is also found to undergo reduction to Cr(III) in the presence of magnetite at different pH values.[196] These reactions are often modeled based on solid-state diffusion of Fe(II) from the bulk to the surface of magnetite with the diffusion of Fe(II) in the crystalline matrix the rate-limiting step.[193,260−263] However, a recent study discovered that even stoichiometric magnetite does not reduce PCE and TCE, and only the addition of high concentrations of aqueous Fe(II), likely forming $Fe(OH)_2$ precipitate, can lead to PCE and TCE reduction.[264]

Magnetite is able to reduce carbon tetrachloride in the absence of added Fe(II).[192] However, some studies reported that without the addition of $Fe(II)_{aq}$, magnetite exhibited almost no ability to induce the reduction of 4-chloronitrobenzene[265] and hexahydro-1,3,5-trinitro-1,3,5-triazine,[138] even though the reaction is thermodynamically favorable. This difference in the magnetite reactivity might result from their different Fe(II) contents because the structural Fe(II) is more oxidized in the previous study.[265] Indeed, the Fe(II)/Fe(III) ratio in magnetite (eq 4) has been convincingly demonstrated to greatly impact its physicochemical properties such as redox potential and conductivity.[261,266,267] For additional details regarding how to obtain the redox potential of magnetite, see section 8.9. When examining the impact of magnetite stoichiometry on contaminant reduction rates,[64,195] the reduction of nitrobenzene by a nonstoichiometric magnetite ($R = 0.31$) is 5 orders of magnitude smaller than that of a stoichiometric magnetite ($R = 0.5$).[195] The pertinent ratio $R$ can be expressed as

$$R = \frac{Fe^{II}}{Fe^{III}} = \frac{Fe^{II}(Oct)}{Fe^{III}(Oct) + Fe^{III}(Tet)} \quad (4)$$

where $Fe^{II}(Oct)$ and $Fe^{III}(Oct)$ are the amounts of Fe(II) and Fe(III) in the octahedral sublattice (B sites) of magnetite and $Fe^{III}(Tet)$ is the amount of Fe(III) occupying the tetrahedral sublattice (A sites). Not surprisingly, this ratio can vary from the surface to the interior of a magnetite particle. For example, the formation of an oxidized layer on magnetite is found to diminish its reductive reactivity as this reduces the active Fe(II) content available at magnetite surfaces and also inhibits electron transfer between structural Fe(II) and the aqueous interface. Indeed, fresh magnetite can readily reduce Cr(VI) to Cr(III), while the Cr-reducing capacity of maghemite-coated magnetite is greatly reduced.[70] Similarly, the reductive reactivity toward Cr(VI) decreased by a factor of 4 when magnetite was allowed to age in air for 18 months, resulting in some of the magnetite being oxidized to maghemite.[196]

Particle size is another important parameter influencing the reductive reactivity of magnetite. Nanosized (9 nm) magnetite shows higher reactivity toward carbon tetrachloride than larger nanoparticles (80 nm), most likely a result of the higher available reactive surface area and the ability for Fe(II) to diffuse more readily to the surface of magnetite, although the effect of quantum confinement cannot be ignored.[193] Additionally, the redox potential of magnetite increases with smaller particle sizes.[268] Similarly the aggregation state of magnetite affects its reductive reactivity, with smaller aggregates imparting the highest reactivity.[193]

pH can also significantly affect the reductive reactivity of magnetite. It has been shown that a stepwise increase in pH from 6 to 10 steadily enhances the degradation rate of carbon tetrachloride by magnetite, which is attributed to the greater electron density of the deprotonated surface sites at higher pH.[192] pH and ionic strength also influence magnetite reactivity by affecting particle aggregation.[193]

Cationic substitution is common in magnetite. Natural magnetites can contain Al, Mn, Ti, and/or Zn, all of which can affect R (i.e., the Fe(II):Fe(III) ratio) and therefore the redox reactivity.[2] Ti(IV) is a prominent example which, through solid−solution exchange, leads to mixed composition phases such as titanomagnetite. Cationic substitutions can affect R and thereby also increase the redox potential of magnetite. This is because each substituent Ti(IV) cation in titanomagnetite eliminates two Fe(III) cations with the first being replaced and the second being eliminated by reduction to Fe(II) for a net charge balance in the unit cell.[269] This yields a rapid rise in R to values well above those found in stoichiometric magnetite ($R = 0.5$),[200] conceptually enhancing its redox reactivity. However, Ti substitution for Fe can have multiple effects. For instance, Latta et al. (2013) found that the reduction of U(VI) by titanomagnetite was indeed controlled by the initial bulk Fe(II)/Fe(III) ratio,[270] but the reduction of U(VI) to U(IV) only occurred at $R > 0.4$, consistent with previous studies which demonstrate that the $R$ value directly controls the redox potential of magnetite.[270,271] In addition, the presence of Ti was also found to influence the final reduced $U^{IV}$ speciation, resulting in the formation of uraninite by pure magnetite, relative to U(IV) with the bidendate U-O2-U bridges in the presence of Ti-doped magnetites.[270] Other researchers have shown the influence of Ti content on the adsorption of contaminants. For example, Wylie et al. (2016) reported that increasing the Ti concentration in magnetite resulted in higher adsorption of neptunium at pH 3 under anaerobic conditions, likely due to binding of Np to Ti−O sites, as opposed to Fe−O sites.[200] As is the case for magnetite, factors influencing the reactivity of titanomagnetite beyond $R$ include particle surface area to volume ratio and solution pH.[200,201,270,202]

In addition to the presence of Fe(II) within its structure, magnetite can also undergo reaction with aqueous Fe(II), although no secondary mineralization to other oxides such as goethite and hematite occurs.[64,252] This has been shown to result in an increase in structural Fe(II) content,[272] although the extent to which this occurs is limited by the initial stoichiometry of magnetite. Upon reaction with magnetite, the Fe(II) was oxidized to form a magnetite layer and no sorbed or precipitated Fe(II) phase was observed.[64] The injected electrons from Fe(II) into magnetite localize as $^{oct}Fe^{2+}-Fe^{3+}$ pairs.[64] Magnetite particles with a higher Fe(III) content relative to Fe(II) take up more Fe(II) until stoichiometric magnetite forms, whereby any further aqueous Fe(II) uptake is limited.[64] Aqueous Fe(II)


https://doi.org/10.1021/acs.chemrev.0c01286
Chem. Rev. 2021, 121, 8161−8233

can therefore effectively "recharge" or "boost" the reductive reactivity of magnetite toward environmental contaminants by increasing the Fe(II):Fe(III) ratio of nonstoichiometric magnetite,[64] with quinones of likely importance to the generation of aqueous Fe(II) in natural environments.[273] As such, the presence of an active reductant such as aqueous Fe(II) that can "recharge" magnetite is deemed to be more important for contaminant reduction than the presence of magnetite itself in the environment.[64] Parallel to the reaction of aqueous Fe(II) with Fe(III) (oxyhydr)oxides, extensive (i.e., more than 50%) atom exchange is found to occur upon the reaction of aqueous Fe(II) with magnetite, but this is not associated with the transformation of magnetite or alteration of octahedral vs tetrahedral iron site ratios, and the *R* value does not affect the rate and extent of the atom exchange.[274] In the same study, iron atom diffusion, in addition to bulk electron conduction, is proposed as a possible mechanism to explain the rapid rates of Fe atom exchange.[274] Finally, different from the effect of cation substitution on magnetite redox reactivity, Co substitution does not seem to affect the rate and extent of atom exchange between aqueous Fe(II) and magnetite.[274]

**4.1.2. Green Rusts.** Green rusts (GRs) are mixed Fe(II)−Fe(III) layered double hydroxides (LDH) with a sjögrenite-pyroaurite-like structure, whereby anions in the background electrolyte are intercalated into the structure with water molecules in the interlayers between brucite-like layers of $Fe(OH)_2$. The general formula of GRs is $[Fe^{II}_{(1-x)}Fe^{III}_x(OH)_2]^{x+}[(x/n)\ A^{n-}\cdot(m/n)H_2O]^{x-}$, where $x$ is the $Fe^{III}/Fe_{tot}$ ratio and $A^{n-}$ represents intercalated anions (e.g., $Cl^-$, $SO_4^{2-}$, or $CO_3^{2-}$).[275,581] GRs can result from different sources, such as corrosion products in steel and iron pipes,[276,277] reduction products of iron (oxyhydr)oxides by dissimilatory iron(III)-reducing bacteria (DIRB),[278] and oxidation products of zerovalent iron in engineered systems,[279] from the reaction of aqueous Fe(II)- with Fe(III)-containing minerals[280−282] and as natural products in a gleysol,[283] an acid mine drainage,[284] and a stratified lake.[285] The nature of GRs is dependent on the incorporated anions and can be categorized into two types distinguishable from their X-ray diffraction (XRD) patterns due to differential stacking.[286] Green rust 1 (GR1), with a rhombohedral unit cell, contains planar anions, such as chloride or bromide, while green rust 2 (GR2), with a hexagonal cell, contains tetrahedral anions, such as sulfate.[286]

Because of high contents of Fe(II), GRs have been used to reduce different organic and inorganic contaminants by serving as a powerful electron donor,[66,287−289] with examples of the various studies shown in Table 2, such as the reduction of carbon tetrachloride,[225,226] 4-chloronitrobenzene,[281] methane and ethane,[225] PCE,[42,230] TCE,[42,230] chromate,[240] nitrate,[236] and nitrite.[237,290] Many studies have confirmed the contribution of structural Fe(II), as opposed to aqueous Fe(II), toward the reduction reaction.[291] For example, studies of the interaction between $GR2(SO_4)$ and chromate have shown that chromate first substitutes for sulfate in the interlayer and then undergoes reduction by Fe(II).[292] Nonpolar molecules such as carbon tetrachloride, however, might not be able to penetrate the interlayers of GR; thus, its reduction only occurs on external surface sites.[223] Readers are referred to other reviews for additional information on the synthesis methods and environmental application of green rust.[79,293]

Similar to magnetite and titanomagnetite, the reactivity of green rusts can be affected by the ratio of Fe(II)/Fe(III).[79,294] With increasing Fe(II)/Fe(III) ratio, the reductive reactivity of nitrate by GR(Cl) increases due to an increase in the reduction capacity.[235] In addition, different interlayer anions can complex with various contaminants in different ways and influence the energy of the Fe(II) species,[66] thus affecting the reactivity of GRs. For instance, the reactivity of GR(Cl) is approximately six times higher than that of $GR(SO_4)$ when reducing nitrate, which is due to the ease of exchange of chloride for nitrate and a high content of Fe(II) in the octahedral layers of GR, both of which favor the reduction of nitrate at the reactive surfaces.[235,295] There are, however, contrasting results in the literature regarding the influence of the interlayer cation (i.e., chloride, carbonate, sulfate) on the reductive reactivity by GRs for other contaminants such as U(VI).[66] This difference in reactivity might be related to whether or not the contaminant of interest can enter the interlayer,[66] with further research required to confirm this hypothesis.

Solution conditions can greatly affect reactivity. It has been shown that the reductive reactivity of GRs increased with increasing pH,[291,296] which could be related to its lower redox potential at higher pH.[287] GRs can convert to more stable iron (oxyhydr)oxides, such as goethite, magnetite, and lepidocrocite after the reduction,[242,291,296] with pH influencing the transformation products. It has been shown that $GR(SO_4)$ transforms to magnetite when pH > 9 and to goethite when pH < 8 when $GR(SO_4)$ was used to reduce selenate ions, which could also affect its reduction capacity.[296] Trace metal ions can also affect the reactivity of green rusts.[224,231] For example, the addition of Ag(I) or Cu(II) leads to a significant increase in the reduction rates of halogenated ethane.[231] This is related to a galvanic-like cell that forms when green rusts (anode) are combined with submicron-sized particles of Ag(0)/Cu(0) (resulting from the reduction of Ag(I) or Cu(II) by green rusts)[224,231] which are then able to promote the reduction of halogenated ethanes. The presence of anions such as phosphate and silicate can further decrease the reductive reactivity of green rust, due to the loss of structural Fe(II) in green rust associated with the formation of vivianite or surface saturation of lateral sites.[233,296] In addition, the presence of coexisting anions can influence the oxidation products of green rust,[297−299] although more research is needed to identify these transformation products to obtain a better understanding of the underlying reaction mechanisms between green rust and reducible contaminants.

**4.1.3. Mackinawite.** Mackinawite ($Fe_{1+x}S$, where $0 < x < 0.07$, hereafter referred to as FeS), an iron monosulfide, possesses a tetragonal lattice structure with Fe atoms linked in a tetrahedral coordination to four equidistant sulfur atoms.[210,300] The formation of FeS has been observed in various reducing environments, such as reducing freshwater and marine systems, the surface of anoxic clay soils, and eutrophic estuaries.[301−304] Mackinawite is produced primarily through sulfide and soluble iron species chemically and biologically[209,210,305−307] and is considered a transient iron sulfide species,[83,304] an important precursor to the formation of the more thermodynamically stable iron sulfide minerals, such as pyrite and greigite ($Fe_3S_4$).[208,331] Mackinawite has been shown to reduce a large number of contaminants, including carbon tetrachloride,[207] hexachloroethane (HCA),[209] PCE,[216] r-hexachlorocylohexane (lindane),[308] TCE,[218] tribromomethane,[211] Cr(VI),[204] and U(VI).[222] The details of the reaction rates and different products are listed in Table 2. For instance, the rate of transformation of PCE to acetylene is faster than that to TCE.[211] For the reduction of U(VI), although $UO_2$ is regarded the most thermodynamically stable form, partially reduced species (i.e.,


https://doi.org/10.1021/acs.chemrev.0c01286
Chem. Rev. 2021, 121, 8161−8233

$U_3O_8$ and $U_4O_9$) are often reported.[309−311] The synthesis and applications of iron sulfides for various pollutant removals have been reviewed.[312−314] Readers are referred to two reviews for additional information on the chemistry (e.g., structure, composition, and solubility) of FeS.[83,315]

The reactivity of iron sulfide minerals may be associated with either Fe(II) or sulfide,[207,212,220,310,319,331] both of which can provide electrons to reduce chemicals. However, different reduction mechanisms have been reported even for the same chemical probe. Some researchers have suggested that the reduction of U(VI) might result from either Fe(II) or S(-II),[310] while others have proposed the reduction is due to S(-II) instead of Fe(II).[222,319,320] Additionally, the reduction of Cr(VI) by FeS occurs primarily at the FeS surface,[204] while aqueous Fe(II) and S(-II) released from the partial dissolution of FeS can contribute to the reactivity by either surface or solution reaction.[219] Further research is needed to examine the relative contribtuion of these potential reductants.

The physicochemical properties of FeS influence its reductive reactivity. FeS is a metallic conductor with delocalized Fe 3*d* electrons,[321] which is thought to partially explain its effectiveness as a reductant.[210,322] This is why the orientation of FeS layers perpendicular to the iron surface is found to enhance the reductive reactivity.[217,323] The particle size of FeS also influences its reactivity, with nanosize FeS shown to be more reactive than macrosize FeS, due to a higher surface area and more available reactive sites.[324] Indeed, one reason that freeze-dried FeS is less reactive than nonfreeze-dried FeS[218,325] is attributed to particle aggregation during the drying process, which increases its particle size and lowers its reactivity.[218,325] Many polymeric stabilizers (e.g., carboxymethyl cellulose) have been employed to stabilize FeS to improve its reactivity.[317,318,326] In addition, nanosize FeS containing various structural flaws[300,327] contributes to a higher reactivity compared with macrosize FeS. The surface of FeS is more hydrophobic than pyrite,[328] favoring the adsorption of TCE; thus, the rapid transformation of FeS to pyrite greatly decreases the rate of TCE degradation.[218]

The transformation of FeS before and during reactions can also affect its reactivity. As mentioned above, FeS is metastable and can be transformed to other more stable iron sulfides (e.g., $Fe_3S_4$, $FeS_2$) or iron oxides by various oxidants.[218,222] FeS is also prone to oxygenation with the resultant formation of lepidocrocite, elemental sulfur, and surface-located hydroxyl radicals.[329] Freeze-drying of mackinawite also results in less reactive FeS due to the transformation of FeS to greigite and pyrite during the freezing process,[218] both of which are less reactive than mackinawite.[194,330] FeS reaction with various contaminants could also result in its transformation to products such as greigite and ferrihydrite.[208,331] Understanding the transformation products of FeS can be utilized to regenerate FeS, which would greatly improve engineered remediation systems.

Solution pH is also known to affect the reductive reactivity of iron sulfides, with contrasting results observed, warranting further research. For instance, the reductive dechlorination of hexachloroethane,[209] carbon tetrachloride,[208] cis-1,2,-dichloroethylene,[325] and TCE[218] was significantly enhanced as the pH increased,[209] whereas the reduction of U(VI) decreased with increasing pH (5.99−10.17).[316] Both iron sulfide particles and contaminants should be taken into account when discussing the pH effect. Solution pH affects the surface charge of mackinawite ($pH_{pzc}$ = 2.9[332]) and the hydrolysis of contaminants, which would influence the interactions between them (electrostatic effects). Surface reactive Fe(II) species formed at different pH might also be different.[209] However, what specific surface species form and how they are related to the reaction rate deserve further research. The formation of a passivation layer on the FeS surface at high pH might also lower the reduction rate.[219] Another possibility is that electron transfer is faster at higher pH.[333] More studies are needed to determine the impact of pH on mackinawite reductive reactivity.

The presence of inorganic/organic constituents can also affect the reductive reactivity of iron(II) sulfide minerals. Hard metal ions (e.g., Cr(III) and Mn(II)) have been shown to decrease the dechlorination rates by FeS through the formation of surface hydroxide precipitates that inhibit electron transfer between FeS and hexachloroethane.[210] However, intermediate/soft metal ions enhance its reductive reactivity by increasing the release of Fe(II) and the formation of reactive $Fe(OH)_2$ or forming metal substituted FeS (eq 5) or coprecipitated sulfides (eq 6) (e.g., M = Co and Ni), which have more favorable electrical properties.[210]

$$FeS(s) + xM^{2+} \rightleftharpoons [Fe_{1-x}, M_x]S(s) + xFe^{2+} \quad (5)$$

$$FeS(s) + (1 - x)M^{2+} \rightleftharpoons [Fe_x, M_{1-x}]S(s) + (1 - x)Fe^{2+} \quad (6)$$

Organic ligands with a strong affinity for FeS surfaces may also affect its reactivity by inhibiting surface electron-transfer reactions. For example, Butler et al. showed that the addition of cysteine and methionine inhibited the rate of TCE reductive dechlorination by FeS because the adsorption of the thiol and sulfide functional groups to the FeS surface inhibited electron transfer.[209] On the other hand, the addition of 2,2′-bipyridine and 1,10-phenanthrolene resulted in enhanced degradation of hexachloroethane, which was attributed to the participation of delocalized $\pi^*$ molecular orbitals in the electron-transfer reaction.[209] The addition of citrate enhanced the reductive reactivity of FeS, likely due to the inhibition of the passivation layer on the FeS surface or the formation of surface reactive groups facilitating the reaction.[324]

**4.1.4. Iron-Containing Clay Minerals.** Iron-containing clay minerals are ubiquitous in the environment and may form via natural or synthetic processes.[334−337] Structural Fe(III), particularly dioctahedral coordinated Fe(III), in clay minerals can be reduced to form structural Fe(II)[334,338] by microorganisms,[134] surface Fe(II),[281] or chemical reductants such as dithionite.[134,243,244] Several factors can influence the rate and extent of structural Fe reduction in clay minerals including the type of microorganisms and clay minerals used, temperature, solution chemistry, and the presence of electron shuttles such as anthraquinone 2,6-disulfonate.[122,339,340] For instance, the distribution of Fe(II) in chemically reduced clay minerals follows a "pseudo random" model (i.e., the generated Fe(II) tends to be far from other generated Fe(II)),[51] initially forming Fe(II)−Fe(III) pairs instead of Fe(II)−Fe(II) pairs;[52] whereas the biological reduction of clay minerals initially occurs at edge sites (moving front model),[52] with Fe(II)−Fe(III) pairs created only at the interface between the Fe(II) and Fe(III) domains with the reduction front moving inward as the reduction continues.[334] Depending on the types of reduction, the reduction mechanisms differ, resulting in different mineral structures and hence reactivity.[341−343] In these minerals, redox active Fe(II) exists as either structural Fe(II) or surface-associated Fe(II) (the latter will be discussed in detail in section


https://doi.org/10.1021/acs.chemrev.0c01286
Chem. Rev. 2021, 121, 8161−8233

4.2.3). Reduced clay minerals have been used to reduce different organic and inorganic contaminants, including carbon tetrachloride,[139] nitroaromatic compounds,[244,245] Cr(VI),[249,344,345] technetium,[346] and U(VI)[347,348] (Table 2).

Various Fe(II) species generated in reduced clay minerals, including structural Fe(II), edge complexed Fe(II), and exchanged Fe(II),[244,346] influence the reactivity of clay minerals. Compared with edge-complexed and exchanged Fe(II), structural Fe(II) has been shown to be the predominant reactive species in clay minerals.[244,139,343,346] For structural Fe(II), abiotically reduced Fe-rich clay minerals contain two distinct Fe(II) sites (dioctahedral and trioctahedral Fe(II) species)[53] each with different reactivity, resulting in biphasic reduction kinetics (fast initially followed by slow kinetics), while abiotically reduced Fe-poor clay minerals only contain one reactive site, exhibiting pseudo-first-order reaction kinetics instead.[139,343]

The total Fe content of clay minerals is known to influence electron-transfer pathways. For instance, the reduction of Cr(VI) by Fe-rich nontronite is faster than that by Fe-poor montmorillonite.[249] Part of this behavior may be related to the availability of electron-transfer percolation pathways through the clay mineral structure which become limited under low total Fe contents, as well as by site-blocking substitutions.[349,350] Fe content also affects the availability of exposed Fe sites at the edges of clay sheets and electron exchange reactions that can occur there by interactions with sorbed Fe(II).[351,352] The ratio of Fe(II)/Fe(total) for both Fe-poor and Fe-rich clay minerals, as is the case for other structural Fe(II)-containing minerals, can also significantly affect the reductive reactivity. The higher the value of Fe(II)/Fe(total), the higher the reductive reactivity,[249] because of the lower standard redox potential of the mineral.

The presence of ligands, such as citrate, has also been shown to inhibit the reduction of Cr(VI) by structural Fe(II) in nontronite (NAu-2), with the effect of this explained in terms of competitive sorption between citrate and Cr(VI) for surface sites.[353] Most revealing, however, is that the reduction rates of contaminants by structural Fe(II) are not influenced by pH.[139,346] This is a significant point of difference between the redox reactivity of structural Fe(II) species and surface sorbed Fe(II). Nevertheless, while Cr(VI) reduction by Fe-poor clay minerals exhibits a pH-independent effect, the reduction of Cr(VI) by Fe-rich clay minerals is found to increase as pH decreases.[249] Further research is needed to elucidate the different pH effects.

Finally, the nature of the exchanged cations can also affect the redox reactivity of structural Fe(II) in layered clay minerals. For instance, the reductive reactivity of structural Fe(II) in Na-exchanged reduced nontronite (NAu-2) is found to be higher than that in K-exchanged NAu-2.[354,355] This is likely related to the smaller hydration radius of the potassium ion relative to the sodium ion,[347,356] causing interlayers in the clay minerals to collapse and dehydrate in the presence of K relative to Na and, thereby, inhibit electron transfer from structural Fe(II).[347,354]

## 4.2. Surface Sorbed Fe(II)

**4.2.1. Fe(II)-Treated Iron(III) (Oxyhydr)oxides.** Iron (oxyhydr)oxides are important constituents of sediments, soils, and rocks and occur in various crystal structures, sizes, and morphologies.[387,388] Common iron (oxyhr)oxides include goethite ($\alpha$-FeOOH), magnetite ($Fe_3O_4$), hematite ($\alpha$-$Fe_2O_3$), lepidocrocite ($\gamma$-FeOOH), ferroxyhyte ($\delta$-FeOOH), and ferrihydrite ($5Fe_2O_3 \cdot 9H_2O$).[2]

Interactions involving Fe(II) sorbed onto Fe(III) (oxyhydr)-oxides are common in iron-rich humid tropical soils, at plant-root surfaces, in the vadose zone, in marine sediments, and in rice paddy soils where soil wetting and drying can lead to fluctuating redox conditions.[17,389,390] The frequency and magnitude of redox fluctuations are important drivers of the extent of organic carbon cycling in soils[389,390] and sulfur (S) and phosphorus (P) in sediments.[17] For more information of the role of sorbed Fe(II)−Fe(III) (oxyhydr)oxide interactions and other Fe(II)-associated redox processes to biogeochemical processes, readers are referred to section 6.

The most striking impact of surface sorbed Fe(II) (or at least surface-associated Fe(II)—this is further discussed in section 4.2.4)—toward Fe(III) (oxyhydr)oxides is its ability to catalyze the rapid transformation of poorly amorphous forms of Fe(III) (oxyhydr)oxides to those which are more thermodynamically stable and crystalline, as well as causing recrystallization of these more stable forms. The mostly likely first step in this process is now thought to be interfacial electron transfer between sorbed Fe(II) and Fe(III) in the oxide lattice, a process long speculated to be important[391] and first demonstrated to be possible using Mössbauer spectroscopy by Williams and Scherer (2004).[392] This interfacial electron-transfer step is coupled to consequential release of Fe(II) elsewhere from the structure by electron conduction through the lattice, enabling facile recrystallization, as demonstrated by Yanina and Rosso (2008).[393] These observations culminated into the now routinely invoked Fe(II)/Fe(III)-oxide conduction mechanism, such as in the redox-driven conveyor belt model in the study by Handler et al (2009)[394] in which step 3 indicates the key interfacial electron-transfer process (Figure 5). Bulk electron conduction enables

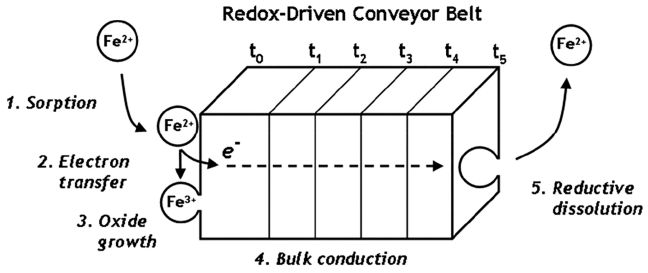


**Figure 5.** Conceptual model for the five steps associated with the redox-driven conveyor belt mechanism. Reprinted with permission from ref 394. Copyright 2009 American Chemical Society.

dissolution of the existing Fe(III) (oxyhydr)oxide coupled to simultaneous precipitation of the same phase (i.e., recrystallization) or a new phase (i.e., transformation). Various aspects of this mechanistic model are discussed further in section 4.2.4.

Characteristic transformations studied under laboratory conditions include the transformation of ferrihydrite to lepidocrocite and/or goethite,[395,396] with the particular mineral formed being dependent on competing mineralization pathways[397] or the presence of anions such as silicate and NOM that can interfere with the Fe(III) nucleation process.[396] It was recently shown that the newly created Fe(III) product resulting from interfacial electron transfer from sorbed Fe(II) to ferrihydrite is the reactive species that leads to nucleation and growth of product oxyhydroxide phases.[398,399] Extensions of this work using Fe-complexing organic acids show that ligands disrupt the formation of stable product minerals by intercepting and sequestering this labile Fe(III) intermediate.[400] In fact,


https://doi.org/10.1021/acs.chemrev.0c01286
Chem. Rev. 2021, 121, 8161−8233

when corrected for the amount of intermediate labile Fe(III) sequestered into organic complexes, the appearance of magnetite as a product was shown to occur when the ratio of sorbed Fe(II) to residual uncomplexed labile Fe(III) was approximately 0.5, the stochiometric ratio in the mixed-valent iron oxide magnetite.[400] The collective findings reinforce the dissolution−reprecipitation mechanism[401] for Fe(II)-catalyzed ferrihydrite transformation to more stable crystalline forms suggested long ago[402] and add to it the importance of interfacial electron transfer as the critical enabling step.

Furthermore, magnetite itself is also reactive with Fe(II), which generally tends to increase its structural Fe(II) content. Importantly, this is associated with a significant degree of Fe atom exchange as observed from Mössbauer spectroscopy.[274] Although consistent with the conduction model, the extent of exchange, and the lack of any effect of cobalt substitution, suggests Fe atom diffusion is an additional mechanistic aspect to explain the rapid rates of Fe atom exchange between aqueous Fe(II) and magnetite.[274] Magnetite stoichiometry has a significant effect on the degree of isotope fractionation, due to the differential degree of octahedral versus tetrahedral iron fractionation occupation.[403] Nevertheless, the $^{56}Fe/^{54}Fe$ equilibrium fractionation factor obtained from the reaction of aqueous Fe(II) with magnetite is similar to that obtained from the transformation of ferrihydrite to magnetite, indicating that kinetic isotope fractionation effects are minimal.[404]

For minerals which are already relatively stable in their environment, Fe(II)-catalyzed recrystallization may be the main source of dynamics with this process resulting in change in the primary particle size or dimension of the original mineral species without significant change in mineralogy,[395,405] although these changes in size may be quite minor.[405,406] Nevertheless, the change in either mineralogy or particle physical characteristics will likely impact the ability of Fe(III) (oxyhydr)oxides to sorb or sequester contaminants in the environment, and indeed, there are a plethora of studies which have investigated the change in contaminant availability associated with the reaction of Fe(II) with iron oxides.[6] Notable studies include the ability of the Fe(II)-catalyzed transformation process to coprecipitate and reduce uranium species into Fe(III) (oxyhydr)oxides, rendering uranium less mobile in the environment as the resultant Fe(III) (oxyhydr)oxide it becomes incorporated into is much less resistant to reductive dissolution.[407] Similarly, the recrystallization of poorly amorphous iron oxides that readily undergo reductive dissolution into more crystalline phases that are more difficult to dissolve in the presence of aqueous Fe(II) has been shown to be an important trapping mechanism for arsenic in the environment.[408] Conversely, other studies have demonstrated that the Fe(II)-activated recrystallization of Cu-, Co-, and Mn-substituted goethite and hematite enhances the release of Cu, Co, and Mn, Ni, and Zn to solution relative to Fe(II)-free controls,[10] with this process a result of continual electron-transfer and atom-exchange processes inducing concurrent dissolution and crystal growth, rather than net reductive dissolution,[409] although the presence of particular coprecipitated species in naturally occurring Fe(III) (oxyhydr)oxides, such as aluminum, can also interfere with the crystal growth process.[410] Additional Fe(II)-catalyzed mineral transformations include iron atom exchange between aqueous Fe(II) and lattice Fe(III) and oxygen isotope exchange between water and structural (singly coordinated) oxygen in goethite and ferrihydrite (please see below for more discussion).[411] For more detailed discussion of Fe(II)-driven stable mineral recrystallization, readers are referred to a comprehensive review by Gorski and Fantle (2017).[412]

As briefly mentioned in section 2.1, in the environment, aqueous Fe(II) is commonly generated by Fe(III)-reducing bacteria, either enzymatically[40,413] or via electron shuttling compounds,[414] with the rate of microbially mediated reductive dissolution of amorphous Fe(III) (oxyhydr)oxides being substantially higher than that of synthetic and naturally crystalline Fe(III) (oxyhydr)oxides.[415,416] Indeed, initial Fe(III) (oxyhydr)oxide bioreduction rates by the *Shewanella* bacterium are positively correlated to the linear free energy of formation of the Fe(III) (oxyhydr)oxide,[417] and more crystalline Fe(III) (oxyhydr)oxides also possess lower available surface areas than their amorphous counterparts resulting in a lower rate of Fe(II) generation per mole of available Fe(III).[418] As such, more stable forms of Fe(III) (oxyhydr)oxides tend to be preserved in the environment relative to those which are less thermodynamically stable, even in highly reducing sediments. While, ironically, this ultimately negatively impacts the ability of Fe(II)-reducing bacteria to couple the oxidation of organic matter to the reduction of Fe(III) (oxyhydr)oxides for energy and growth, it does seem that microbes have developed mechanisms to counter this effect.[419,420] For instance, the organic matter source used by microbes (e.g., lactate) has the effect of retarding the Fe(II)-catalyzed transformation process, which will result in Fe(III) (oxyhydr)oxides that are easier to obtain energy from.[417] Furthermore, the ability of organic matter to retard the Fe(II)-catalyzed transformation process is also favorable for microbes.[781] Another major impact of the presence of Fe(II) sorption onto Fe(III) (oxyhydr)oxides is the enhanced reductive reactivity of sorbed Fe(II) in the presence of iron mineral oxides compared to analogous aqueous Fe(II) solutions alone.[8,67,199,249,423] The most common iron oxides investigated in this regard include goethite, hematite, magnetite, and lepidocrocite, with the details of these studies summarized in Table 3. A common feature of these studies is that the reduction kinetics of Fe(II)−Fe(III) (oxyhydr)oxide systems are found to correlate strongly with the amount of sorbed Fe(II).[357,378]

As discussed in the previous sections, aqueous Fe(II) is known to induce the reduction of contaminants at a much slower rate than Fe(II) complexed with organic ligands or even to certain inorganic ligands such as carbonate or fluoride. From a molecular orbital theory standpoint, when Fe(II) is sorbed or bound to a ligand, the donation of electron density from the ligand to the Fe(II) increases the energy of electron-donating Fe 3*d* orbitals, with bonding to more stable Fe(III) ligands increasing the thermodynamic driving force for electron transfer (and subsequently Fe(II) oxidation or pollutant reduction).[424] Indeed, the stronger the resulting Fe(II)−ligand complex, the lower the redox potential of the system becomes, as indicated in eq 3. A similar argument is invoked to explain why Fe(II) species sorbed onto an Fe(III) (oxyhydr)oxide possess greater reductive reactivity toward contaminants. As has been shown to be the case with Fe(II)−organic ligands, a linear free energy relationship between the redox potential of various aqueous Fe(II)−Fe(III) (oxyhydr)oxide systems and the rate of contaminant reduction has been observed in the presence of a range of iron oxides.[363,425,426] One study has even demonstrated that the use of non-Fe-based mineral oxides as sorbents for Fe(II), such as aluminum oxide, can lower the redox potentials of the system, thereby facilitating faster Fe(II)-mediated reduction.[381]

It has recently been demonstrated, however, that in the presence of an Fe(III) (oxyhydr)oxide, the aqueous Fe(II)


https://doi.org/10.1021/acs.chemrev.0c01286
Chem. Rev. 2021, 121, 8161−8233

species in solution is in thermodynamic equilibrium with the Fe(II) species sorbed to the particle surface and, therefore, possesses the same redox potential or thermodynamic driving force toward oxidation.[425] Indeed, since the amount of Fe(II) sorbed to a particle surface is generally associated with an increase in the aqueous Fe(II) concentration, the contention that surface-sorbed Fe(II) species are better electron donors than aqueous Fe(II) species is not easily confirmed purely from a strong correlation between the amount of sorbed Fe(II) and an increase in contaminant reduction rate. Also, the observation that contaminant reduction in the presence of an Fe(II)−Fe(III) (oxyhydr)oxide can dramatically shut down when aqueous Fe(II) is removed suggests that aqueous Fe(II) may, in fact, be playing an essential role in contaminant reduction in aqueous Fe(II) and Fe(III) (oxyhydr)oxide systems in addition to sorbed Fe(II) species.[392] A similar result has been obtained showing that both the sorbed Fe(II) on ferrihydrite and Fe(II) in the aqueous phase were involved in $O_2$ reduction reactions.[427] It has been speculated that the effect of aqueous Fe(II) is a result of redox equilibrium between aqueous Fe(II) and surface-bound Fe(II).[425]

Counting of the total number of electrons transferred during Fe(II) oxidation and relating this to the amount of sorbed and aqueous Fe(II), however, has demonstrated that the amount of Fe(II) that is readily oxidized upon application of an oxidizing current is isolated to the amount of Fe(II) sorbed to the Fe(III) (oxyhydr)oxide of interest and not the aqueous Fe(II) fraction.[428] Indeed, when the sorbed fraction was lowered but the amount of aqueous Fe(II) was maintained by decreasing the amount of Fe(III) (oxyhydr)oxide present in suspension, the amount of Fe(II) that was oxidized became negligible. This demonstrates that, even though the aqueous Fe(II) species is in equilibrium with the sorbed Fe(II)−Fe(III) (oxyhydr)oxide species present, this does not imply that both Fe(II) species are able to be oxidized, and therefore reduce contaminants, at the same rate. Gorski et al. has further developed a rationale for the faster reaction kinetics of sorbed Fe(II) relative to aqueous Fe(II) despite their equivalent redox potentials,[423] proposing the oxide surface facilitates more rapid electron transfer by either complexing with the contaminant to make it more reactive or enabling a two-electron transfer which is not possible with aqueous Fe(II).[423] Alternatively, aqueous Fe(II) is often oxidized to aqueous Fe(III) complexes or a metastable iron oxide such as ferrihydrite, while sorbed Fe(II) is oxidized to an oxide phase that resembles the existing stable oxide (except magnetite).[373,430] Thermodynamically stable iron oxides have more negative Gibbs free energies than metastable iron oxides; therefore, the formation of stable iron oxides is more thermodynamically favorable. Detailed mechanisms by which Fe(II) interacts with Fe-based mineral oxides as a reductant will be discussed further in section 4.2.4.

Note that when the molar concentrations of aqueous Fe(II):Fe(III) oxyhydroxide are roughly equivalent (or higher) and the pH of the solution is circumneutral, a mixed-valent Fe(II)−Fe(III) species may form as the reaction product following the sorption of aqueous Fe(II) onto an Fe(III) oxyhydroxide.[280,397] The rate of formation, however, is controlled by the solubility of the initial Fe(III) oxyhydroxide phase, with more soluble/less stable solid Fe(III) phases being more susceptible to transformation.[280,397] Under such conditions, the sorbed Fe(II) species becomes incorporated into the final reaction product (i.e., becomes structural Fe(II)). To prevent any unnecessary repetition, these particular cases of sorbed Fe(II)−Fe(III) (oxyhydr)oxide/mineral interactions are not discussed in this section, and readers are instead directed to the section on structural Fe(II) species (section 4.1 above).

As shown in Table 3, contaminants reduced by sorbed Fe(II) on iron oxides include $CCl_4$,[137,206,357,359] chlorinated alkanes,[137,357,431] substituted nitroaromatics,[138,265] nitrogen−oxygen containing compounds,[177] pesticides,[368] Cr(VI),[174,432,433] nitrite,[378] Tc(VII),[379] and U(VI).[375] Regardless of the type of iron oxides employed, the products of organic and inorganic contaminants are similar, and dehalogenation reactions are common. For example, the reduction of $CCl_4$ proceeds via a hydrogenolysis reaction to form chloroform.[357,359] It should be noted, however, that the reductive reactivity differs substantially for Fe(II) sorbed onto iron oxides, even for the same type of iron oxide and the same contaminant.[137,206,357,358] How key environmental factors influence the reductive reactivity of sorbed Fe(II) is discussed below, with the major parameters investigated being pH,[137,265,357] dissolved Fe(II) concentration,[137,357] Fe(II) surface species,[74,370,375,431,434] physiochemical properties of iron oxides,[8,193,369] and the presence of cosolutes such as metal ions and NOM. More details are listed in Table 3.

*4.2.1.1. Effect of Structural and Physiochemical Properties of Iron Oxides.* Sorbed Fe(II) on less crystalline iron oxides including ferrihydrite and lepidocrocite is almost always more reactive than that on more crystalline iron oxides including goethite and hematite. The standard redox potential values for $Fe^{2+}$−Fe(III) (oxyhydr)oxide couples have been calculated to be 0.768 V for goethite, 0.769 V for hematite, 0.846 V for lepidocrocite, 0.937 V for ferrihydrite, and 1.067 V for magnetite.[423,425] Based on these $E_H$ values, the different redox reactivities of Fe(II)−Fe(III) (oxyhydr)oxide couples have been well explained by a linear free energy relationship between the logarithm of the surface-area-normalized rate constant ($k_{SA}$) values and $E_H$ and pH values (Figure 6):[425]

$$\log(k_{SA}) = -E_H/0.059\ \text{V} - \text{pH} + 3.42 \quad (7)$$

Note that ferrihydrite and lepidocrocite are not thermodynamically stable because they can transform to more stable phases, but their standard redox potential values are a good approximation over the reaction time frame.[423] It is also worth mentioning that the above equation was obtained for nitrobenzene reduction where log $k_{SA}$ values depend on one electron and one proton transfer prior to/during the rate-limiting step. When different elementary reactions and rate-limiting steps are involved in the reduction of other compounds, as already observed in the literature,[136,137,265,357,375] different linear free energy relationships are expected which warrant further study.

The particle size and aggregation state of iron oxides have a strong influence on their redox reactivity. Nanoparticles generally react faster than their bulk counterparts, which is attributable to their larger reactive surface area to volume ratios and higher surface energies resulting in more reactive sites. Smaller particles also tend to be better hydrated and have higher solubility, so they can more easily undergo Fe(II)-catalyzed reductive dissolution.[435] For additional size-effects on the reactivity of nano iron oxides, such as quantum confinement, surface restructuring, and surface curvature, readers are referred to a review by Waychunas et al.[436] In a similar manner to that in which particle size strongly impacts the reductive reactivity in Fe(II)−Fe (oxyhydr)oxide systems, strong aggregation effects also reduce their reactive performance in aqueous environments. For instance, while the reductive degradation of nitrobenzene by


https://doi.org/10.1021/acs.chemrev.0c01286
Chem. Rev. 2021, 121, 8161−8233

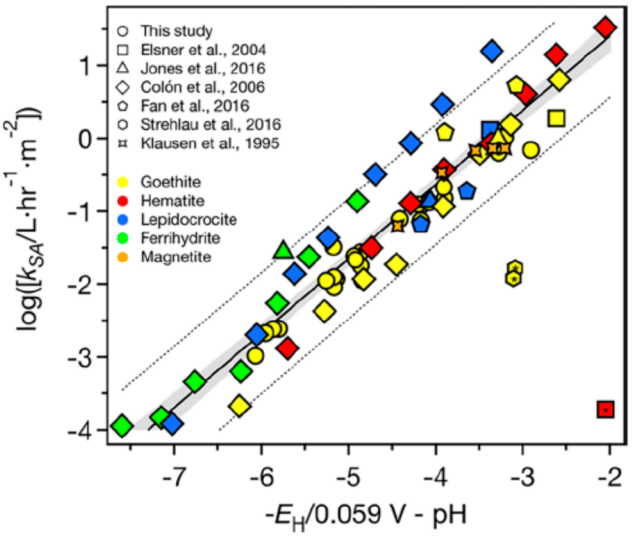


**Figure 6.** Linear free energy relationship between $\log(k_{SA})$ and $E_H$ and pH for the reduction of nitrobenzene by Fe(II) in the presence of goethite, hematite, lepidocrocite, ferrihydrite, and magnetite. Some of the scatter in the figure has been explained by variations in the buffer type and concentrations. Reprinted with permission from ref 425. Copyright 2018 American Chemical Society.

goethite nanorods is higher in relation to goethite microrods on a mass normalized basis,[437] given the tendency for these nanoparticles to aggregate, the reductive reactivity of the goethite nanoparticles was lower than that of the larger particles when rates were normalized to the BET specific surface area. This surface area-normalization approach also raises concern about assessing the size-effect on nanoparticle activity based on primary surface area.[437] The aggregation of goethite particles results in a decrease in the degradation rate of carbon tetrachloride, due to the decrease in the surface available sites and the accessibility of sorbed Fe(II) to contaminants.[357] Commonly used organic buffers such as MOPs, HEPES, and TEA have been shown to enhance the aggregation state of iron oxide nanoparticles and reduce the reductive reactivity of these systems.[438] Another important consideration is the higher redox potential of Fe(II)-nanogoethite suspensions than that of their microgoethite counterparts at equal Fe(II)−Fe(III) loadings, because of the higher solubility of nanogoethite suspensions to lead to more dissolved Fe(III) in solution.[363] The least soluble minerals tend to have the highest rates of contaminant reduction when rates are normalized to the available surface area.[363,426] These minerals, however, also tend to have low reactive surface areas, and therefore, their raw contaminant degradation rates may not reflect such a recognizable trend based on surface area or mineral species type alone.

Al-substitution in iron oxides has been demonstrated to decrease the rate of reductive dissolution of the oxides[439−441] and hinder the recrystallization of ferrihydrite because Al is redox-inactive.[442,443] Indeed, Al- or Ni-substitution inhibits Fe atom exchange between aqueous Fe(II) and goethite and Al-, Cr-, or Sn-substitution into goethite and hematite, although in some cases enhancing the conductivity of iron oxides significantly hinders the Fe(II)-facilitated mineral recrystallization and hence release of Ni and Zn from the corresponding Ni- or Zn-substituted iron oxides. Unfortunately, there are only speculated reasons for these observations, such as Al or Zn physically blocking Fe sites or directing electron flow, forming a coating during the oxide dissolution, or inhibiting bulk electron conduction.[410,444] Nevertheless, the reduction or recrystallization reaction mechanisms involved are not considered to change (see section 4.2.4 for a detailed discussion of the mechanisms). Also, Al-substitution (up to approximately 10%) of goethite still does not prevent electron transfer from the sorbed Fe(II) to goethite, although the newly formed goethite differs from the bulk goethite in complex ways that have yet to be resolved.[444] The above observation leads to speculation that electron transfer might not be the rate-limiting step in the decreased atom exchange reaction; rather, release of the reduced Fe(II) from the oxide surface might have contributed to the inhibited atom exchange.[444]

The exposed facets of an iron oxide can also strongly affect the reductive reactivity of sorbed Fe(II). It is known that single crystals possess symmetrical and periodical characteristics with various facets exposed on the surface dependent on their different atomic arrangements. Facet-specific reactivity of iron oxides in geochemical and biogeochemical processes has broadly significant implications for understanding iron chemistry in environmental processes and remediation strategies.[445] For instance, Chun et al. reported that, compared to a non-Fe(II) control, original goethite crystals were approximately 55% longer after reaction with Fe(II) while the width remained constant resulting in the loss of the (021) facets of goethite during reaction with Fe(II). This may decrease the reductive reactivity of the Fe(II)−goethite suspension over time.[362] Yanina and Rosso showed that the differences in the surface structures between (001) basal and (hk0) facets of hematite provide an electrostatic potential bias that governs the net flow of conduction electrons resulting from sorption and interfacial electron transfer with Fe(II).[393]

The sorption of Fe(II) to iron oxides is strongly facet-specific, thus affecting reductive reactivity. For example, Taylor et al. showed that the sorption of Fe(II) onto hematite is selectively enriched on the basal (001) surface,[446] agreeing well with previous studies.[447] More importantly, many facet-specific studies have focused on developing optimized particle shapes that maximize the Fe(II)/Fe(III) redox potential and its impact on the transformation of toxic heavy metal ions[448] or the degradation of recalcitrant micropollutants.[449] For instance, hematite (110) facets show better chromium(VI) ion adsorption performance because bidentate binuclear complexes form which favor a higher adsorption capacity than monodentate mononuclear configurations which dominate the (001) facet.[450] Conversely, hematite (001) facets favor reductive dissolution in relation to (012) as the bidentate mononuclear iron−ascorbate complexes that form on the (001) facet predispose that facet to more efficient interfacial charge transfer than the monodentate mononuclear configurations on (012) facets.[451] These facet-dependent molecular configurations have a strong influence on the degradation of toxic organic pesticides. For example, the degradation rate constant of alachlor via the bidentate mononuclear complexes that form on hematite (001) is reportedly 2.6-fold greater than the monodentate mononuclear configurations on hematite (012).[452] Recently, Rosso's group also demonstrated that the hematite (001) facet favors the degradation of organics relative to the hematite (012) facet. They pointed out that facet-specific differences appear to be less dependent upon simple aerial cation site density and, instead, are more dependent on their extent of undercoordination.[453] These structure−reactivity correlations of iron oxides result in significant implications for understanding complex processes


https://doi.org/10.1021/acs.chemrev.0c01286
Chem. Rev. 2021, 121, 8161−8233

such as atom exchange, charge transfer, as well as energy exchange at solid−water interfaces in addition to pollutant remediation. These processes are discussed in more detail further on.

Finally, the importance of defects at the iron oxide/Fe(II) interface cannot be overstated. By creation of higher energy sites such as the emergence of dislocations at the surface, step edges, kinks, vacancies, and adatoms, defects can strongly influence reductive reactivity. Probing and characterizing the exact nature of defects has been a great experimental challenge. In a simplified way, iron or oxygen vacancies can be characterized as excess water or hydroxyl groups as compared to the ideal iron oxide formula.[454] Using scanning tunneling microscopy (STM), Eggleston et al. were able to resolve a transient population of individual Fe(III) adatoms on hematite surfaces.[455,456] Likewise, using atomic force microscopy (AFM), defects such as step edges and vicinal faces on goethite could be directly resolved and related to its growth behavior by oxidative adsorption of Fe(II).[457,458] Recently, using nanoscale secondary ion mass spectrometry (NanoSIMS), Taylor et al. showed that Fe(II) adsorption was not only facet-dependent but highly anticorrelated with defective growth pit regions of hematite surfaces.[446] Conversely, the adsorption of Fe(II) on goethite microrods was selective for grain boundaries, as observed by atom probe tomography (APT).[459] This highlights the importance of determining defect types and their relationships to sorption. Computational chemistry calculations have shown that electron transfer between sorbed Fe(II) and iron oxides is inhibited on structurally perfect surfaces but facilitated by adsorption into vacancies.[460,461] Notini et al. provided the first experimental proof of this showing surface defects facilitate electron transfer between Fe(II) and goethite.[454] However, whether the defect content consequently influences the reductive degradation of contaminants by the sorbed Fe(II)/goethite system is not clear, warranting further research.

*4.2.1.2. Effect of Solution Conditions.* Besides structural and physicochemical properties of minerals, solution conditions also affect the reactivity of sorbed Fe(II),[462] among which solution pH is critical. The common pH range of interest for natural systems is 5 to 7.5.[369] Reductive reactivity is typically enhanced as the initial Fe(II) concentration increases because this allows more Fe(II) to adsorb.[265,371] When the pH is lower than 5, there is a negligible amount of Fe(II) sorbed to the mineral surface, resulting in low reductive reactivity. Above pH 7.5, Fe(II) precipitates, such as $Fe(OH)_2(s)$, $FeCO_3$, or green rust, tend to form.[369] Typically reaction rates increase as pH increases,[265,357] as the change in pH impacts other parameters. First, as pH increases more, Fe(II) is sorbed which enhances reactivity.[265] Second, higher pH values result in much lower amounts of dissolved Fe(III) in equilibrium with the Fe(III) minerals, lowering the redox potential.[431] Third, pH affects the types of sorbed Fe(II) species formed.[74,375] For instance, Zhang et al. (1992) studied the adsorption of Fe(II) onto lepidocrocite and reported that there is more than one type of Fe(II) surface species formed, with the Fe(II) monohydroxo surface complex ($\equiv Fe^{III}OFe^{II}OH$) being the dominant species and ($\equiv Fe^{III}OFe^{II})^+$ being the minor species.[463] A later study employing surface complexation modeling (SCM) to fit the adsorption of Fe(II) onto an iron oxide was able to fit these two stable surface Fe(II) complexes using eqs 8 and 9 (Figure 7).[74,375]

$$\equiv Fe^{III}OH + Fe^{2+} \rightleftharpoons \equiv(Fe^{III}OFe^{II})^+ + H^+ \quad (8)$$

$$\equiv Fe^{III}OH + Fe^{2+} + H_2O \rightleftharpoons \equiv Fe^{III}OFe^{II}OH^0 + 2H^+ \quad (9)$$

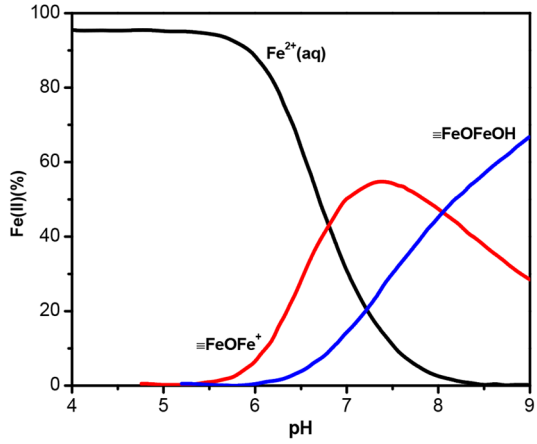


**Figure 7.** Calculated distribution of surface-bound Fe(II) species on nanoparticulate hematite. Reprinted with permission from ref 375. Copyright 1999 Elsevier.

Strong correlations have been observed between the proportion of sorbed Fe(II) present as the hydrolyzed $\equiv Fe^{III}OFe^{II}OH$ species and the rate of 4-chloronitrobenzene[74] or uranium(VI)[375] reduction. However, recent studies have shown that if such complexes do indeed form, they do not exist for long due to interfacial electron transfer with the underlying Fe(III) within the oxide.[392,464] While an added complexity for macroscopic models, ultimately the rate of interfacial electron transfer with the surface is related to the reactivity of the complex toward reduction. The type of electron-transfer mechanisms also affects the structure of the formed iron oxides, as inner-sphere electron-transfer mechanisms yield smaller particle sizes than outer-sphere electron-transfer mechanisms.[465] This is because the electron-transfer mechanisms may affect the hydrolysis and precipitation of Fe(III).[466] This is discussed in further detail in the following section.

The amount of aqueous Fe(II) affects the reactivity of sorbed Fe(II) in different ways. At low Fe(II) concentrations, an increase in Fe(II) concentration leads to more sorbed Fe(II), mostly at surface defects, which facilitates interfacial electron transfer between aqueous Fe(II) and lattice Fe(III) and yields faster reductive reactivity. At high Fe(II) concentrations, sorbed Fe(II) increasingly interacts with structurally ordered surface sites and then goes beyond surface saturation. Under these conditions, there is less interfacial electron transfer and lower surface potential such that the redox reactivity and atom exchange between aqueous Fe(II) and the oxide are both inhibited.[435] Pre-exposure of goethite to Fe(II) leads to the accumulation of a passivation layer of sorbed Fe(II) which inhibits further electron transfer between Fe(II) and goethite, although acid/buffer extraction or oxidation can remove this layer of Fe(II) and restore electron transfer.[467] Please see section 4.2.4 for a detailed discussion of the involved mechanisms.

When there is enough aqueous Fe(II) to regenerate sorbed Fe(II) that has been consumed in contaminant reduction, increasing oxide concentration also enhances reductive reactivity. Nevertheless, when the equilibrium concentration of aqueous Fe(II) was small (≤4 $\mu$M), increasing goethite concentration would decrease the reductive reactivity due to the


https://doi.org/10.1021/acs.chemrev.0c01286
Chem. Rev. 2021, 121, 8161−8233

inhibition of the regeneration of sorbed Fe(II),[357] indicating that besides the amount of Fe(II) sorbed, the density of sorbed Fe(II) can also affect reductive reactivity.

The synergistic effects of transition metals on the reductive reactivity of Fe(II)-treated iron oxides has been investigated. Co(II), Ni(II), and Zn(II) inhibit the reductive reactivity, probably due to the competitive adsorption between these metal ions and Fe(II).[358] Conversely, Cu(II) significantly enhances the reductive reactivity because Cu(II) is reduced to $Cu_2O$ by Fe(II) which is able to act as an additional reductant toward chlorinated hydrocarbons.[358]

NOM can be adsorbed on mineral oxides through electrostatic interactions, hydrogen bonding, ligand exchange, and hydrophobic interactions,[468,469] which would influence the reactivity of sorbed Fe(II).[462] The reduction rates of p-cyanonitrobenzene (pCNB) by Fe(II)-goethite were found to differ when Fe(II) and Suwannee river humic acid (SRHA) were equilibrated in different orders with goethite.[365] Overall, oxidation by and/or the complexation of the surface-sorbed Fe(II) with NOM inhibited electron transfer between chemical probes and sorbed Fe(II) to decrease the reductive reactivity and capacity.[364,365] However, increased molecular weight and amounts of nitrogen, carbon, and aromaticity of NOM were found to enhance the reductive degradation rate of the model contaminant, while increased aliphaticity and carboxyl and oxygen content were shown to decrease the rate of reduction.[364] Interestingly, another study discovered that organic matter (OM) with a high carboxyl content results in faster electron transfer and transformation of ferrihydrite to goethite relative to carboxyl-poor OM sources.[470] This suggests that certain OM types preferentially direct electrons through the iron oxide structure while others direct electrons toward a target contaminant when available.

Regarding Fe(II)-catalyzed mineral transformation, OM coprecipitated with or adsorbed onto ferrihydrite inhibited ferrihydrite transformation to more crystalline iron oxides.[471] In contrast to complete transformation to goethite or hematite in the absence of OM, there was no secondary mineral transformation of ferrihydrite because of the sorption of the OM onto the oxide surface and reduced Fe atom exchange. Nevertheless, the OM-ferrihydrite particles still underwent recrystallization resulting in increased particle crystallinity and subtle changes in particle size or particle aggregation, and both electron transfer and Fe atom exchange between aqueous Fe(II) and ferrihydrite also still occur in the presence of OM. The presence of 4 mM bicarbonate, 1 mM silicate, 10 mM NOM, and even 0.5 mM phosphate did not inhibit electron transfer between aqueous Fe(II) and goethite whereas the presence of a large concentration (1 mM) of phospholipids, biomolecules in cell membranes that form bi- and multilayers on mineral surfaces, did. Sorbed phosphate also did not inhibit Fe atom exchange.[394,444] On the other hand, when using carbonate as a pH buffer, the amount of $Fe^{2+}$ sorbed on different iron oxides decreases due to the blocking of available reactive sites; as such, significantly lower reactivity is observed.[472] Moreover, high, natural concentrations of Si prevented the Fe(II)-catalyzed transformation of ferrihydrite, jarosite, lepidocrocite, and schwertmannite due to recrystallization to more crystalline phases being inhibited.[396]

**4.2.2. Fe(II)-Treated Noniron Oxides.** Compared with iron oxides, relatively few studies have examined the reductive reactivity of Fe(II) sorbed onto other metal oxides (Table 3), possibly because of their less reactive nature for environmental applications. Nevertheless, noniron oxides are still able to significantly enhance the reductive reactivity of Fe(II) relative to Fe(II) alone, with most studies focusing on aluminum oxides, titanium dioxide, and silicon dioxide.[369,381,432] For instance, the aforementioned minerals can increase Cr(VI) reduction by Fe(II) in the order of $\alpha$-FeOOH $\approx$ $\gamma$-FeOOH $\gg$ $SiO_2$ $\gg$ $Al_2O_3$.[432] Similar results were obtained in another study in the order $\alpha$-FeOOH $\gg$ $TiO_2$ $\gg$ $SiO_2$.[8] Conversely, Strathmann et al.[369] studied the reductive reactivity of 12 different metal (hydr)oxides and aluminosilicate minerals treated with Fe(II) and reported a different order of the metal oxides in regard to the reduction of oxime carbamate pesticides by Fe(II).[369] Further research is however needed to fully elucidate the effects of mineral surfaces and physicochemical properties on Fe(II) reactivity. For nonconducting metal oxides (e.g., $\alpha$-$Al_2O_3$), the formation of secondary minerals (e.g., nanogoethite) by sorbed Fe(II) could enhance its reactivity,[465] likely due to the newly formed nanogoethite providing additional surface reactive sites and/or surface reactive sites with a higher reactivity.

As occurs with iron oxides, the nature of the Fe(II) species formed on noniron oxide surfaces can likely affect their reductive reactivity. Nano et al. employed surface complexation modeling to study the reductive reactivity of Fe(II)-treated $TiO_2$ and found that the reactivity was positively related to the hydrolyzed Fe(II) species ($\equiv TiOFe^{II}OH^0$),[73] which is similar to the reactive species formed on iron oxides. However, Li et al. used both electrochemical techniques and surface complexation modeling to investigate the reductive reactivity of 2-nitrophenol by Fe(II)-treated $TiO_2$ and, instead, showed that $\equiv TiOFe^+$ is the reactive species.[381] It is clear that the nature of the Fe(II) species that forms on noniron and iron oxide surfaces is a particular area that warrants further research. In the process of attempting to probe the nature of surface sorbed Fe(II) species, it would be worthwhile to clarify whether or not sorption through inner-sphere processes is required to achieve enhanced reactivity and to obtain more information on the stability of the surface-associated Fe(II) species.[473]

NOM can also affect the reductive reactivity of Fe(II) in the presence of noniron minerals, similar to their iron-counterparts. For instance, Zhu et al. found that DOM increased the reactivity of Fe(II)-treated $TiO_2$ when the DOM concentration was low (0∼10 mgC/L) but decreased the reactivity when the DOM concentration was high (10∼100 mgC/L) which, the authors believed, was due to the change of the amount of Fe(II) sorbed on $TiO_2$ at varying DOM concentrations.[382] Overall, Fe(II)-treated noniron oxides are much less studied and are less well understood compared to Fe(II)-treated iron oxides which, given the abundance of noniron oxides in the environment, warrants further investigation.

**4.2.3. Fe(II)-Treated Iron-Containing Clay Minerals.** Fe(II)-treated clay minerals are indispensable in the environment for natural or enhanced attenuation of pollutants at contaminated sites. At pH values less than 6.0, Fe(II) is mainly sorbed to negatively charged basal planes via ion exchange while at higher pH values additional Fe(II) is sorbed to edge-OH groups via cation complexation.[474] Significant electron transfer between the sorbed Fe(II) and lattice Fe(III) is enabled in the latter case, with the more sorbed, the greater the reduced state of the clay (for more information see the discussion at the end of this section).[474] When clay minerals have been prereduced, the addition of aqueous Fe(II) will result in less Fe(II) sorption due to the formation of reactive Fe(II) mineral precipitates such as $Fe(OH)_2$. As shown in Table 3, Fe(II) associated with clay


https://doi.org/10.1021/acs.chemrev.0c01286
Chem. Rev. 2021, 121, 8161−8233

minerals has been used to reduce a wide range of organic and inorganic contaminants, including substituted nitrobenzene,[244,475] chlorinated compounds,[282] Se(VI),[384] U(VI),[385] and Cr(VI).[432] However, structural Fe(II) in clay minerals or clay minerals with a low Fe(II) concentration cannot reduce chlorinated solvents, and only when higher amounts are added such that surface $Fe(OH)_2$ minerals are able to form can PCE and TCE be reduced.[282] Sorbed Fe(II) on clay minerals is much less reactive than sorbed Fe(II) on Fe(III) (oxyhydr)oxides, despite their structural similarities (such as close Fe−Fe distances). This is mainly due to lower electron mobilities in clay minerals associated with their higher internal reorganization energy and weaker electron coupling.[352]

The Fe content in clay minerals affects their reductive reactivity with a higher Fe content leading to more electrons transferred between aqueous Fe(II) and lattice Fe(III) to form more mixed surface precipitates.[282] These electrons would otherwise engage in contaminant reduction. Also, the clay mineral Fe content influences the Fe(II)/Fe(total) ratio of the reactive Fe-containing precipitate(s), which are mixed Fe(II)−Fe(III) precipitates for clay mineral SWy-2 but $Fe(OH)_2$ for an Fe-free clay mineral with the latter proposed to be the reactive Fe(II) species instead of structural Fe(II) in regard to chlorinated alkane reduction.[282] Because of the different surface precipitates formed, Entwistle et al. reported that the reactivity toward contaminant reduction decreased with increasing clay mineral Fe content.[282] Several studies have characterized the secondary Fe(II)−Fe(III) precipitates formed in Fe(II)-treated clay minerals, including ferrihydrite,[476,477] magnetite,[476,478] lepidocrocite,[476,478,479] green rust or green rust-like,[281,477] and nikischerite (a Fe/Al-layered double hydroxide).[480,481] However, the role of these secondary precipitates in the reduction process is unclear. While some studies did not observe much impact of these secondary precipitates on the partitioning or speciation of contaminants,[476] others proposed that they play an important role,[281,385] or even the dominant role, in the reduction process.[282] In the case of chlorinated solvents, these can only be reduced by $Fe(OH)_2$ precipitates with the reactivity of the precipitates, surprisingly, not dependent on the underlying mineral.[282] Future research is still needed to understand the effect of key Fe-containing clay minerals properties (e.g., Fe content) on the reactivity of the resulting precipitates.

Similar to iron (oxyhydr)oxides (section 4.2.1), pH can largely affect the amount of Fe(II) sorbed and the types of Fe(II) surface species formed on clay minerals.[476] 96% of the total sorbed U(VI) was reduced by Fe(II)-montmorillonite at pH 8.5, while the reduction significantly decreased at lower pH (pH 6.1) as the amount of sorbed Fe(II) decreased.[385] As mentioned earlier, there are mainly two types of surface sorbed Fe(II) species on clay minerals: one is Fe(II) complexed by surface hydroxyl groups at the edge surfaces, and the other is Fe(II) bound by ion exchange at the basal siloxane surfaces with the latter believed to have a minor contribution to contaminant reduction.[244] The former can readily undergo electron exchange with Fe(III) in octahedral sheets, whereas the latter cannot because of the longer electron-transfer distances necessary to span the tetrahedral siloxane sheets.[351,352] The adsorption of Fe(II) on montmorillonite was mainly in the interlayer region via cation exchange when pH < 7.5, whereas it was on the edge sites via surface complexation when pH > 7.5.[482] Schultz et al. demonstrated that the concentration of $FeOH^+$ increased as pH increased above 7.5 and $FeOH^+$ is the dominant reductive species in Fe(II)-treated montmorillonite.[475] The reaction time between Fe(II) and smectites can also influence its reductive reactivity.

Hofstetter et al. reported a lower reactivity of sorbed Fe(II) on nontronite at longer equilibrium times (2-week), but the underlying mechanism is unclear.[245] It is likely that the dissolution of the clay mineral over time leads to an increase of Fe(III) content in the intermediate product (green rusts) with the result that the redox potential of Fe(II)-treated smectite increases thereby yielding lower reactivity.[281]

In addition to reaction with external contaminants, sorbed Fe(II) on Fe-containing clay minerals, especially Fe(II) complexed to edge-OH groups and, to a much less extent, Fe(II) sorbed to basal planes, has been demonstrated to undergo interfacial electron transfer, whereby the sorbed Fe(II) is oxidized to form lepidocrocite when the clay mineral is nontronite.[474] When low Fe-containing clay minerals are reduced by Fe(II), electrons are transferred through the basal plane rather than edge-OH sites, allowing electrons to access the Fe atoms throughout the structure.[477] The injected electrons from Fe(II) preferentially reduce cis-octahedral Fe(III) and become delocalized in structural Fe(III) with fast electron hopping rates.[479] However, the same authors discovered that there is a limit to the extent of reduction beyond which more Fe(II) cannot induce further clay reduction. Interestingly, this incomplete reduction under high Fe(II) contents has also been observed in other chemical or microbial reduction of clays with possible reasons including (1) less hydroxyl groups upon reduction to impose charge balance limitations, (2) more sorbed Fe(II) to physically block the reactive sites, (3) oxidation products of the sorbed Fe(II) to passivate the surface, and (4) lower redox potential of the redox couple as more Fe(II) is sorbed.[479,483,484]

Although Fe in clay minerals is thought to be more stable and sterically protected than in Fe (oxyhydr)oxides, Fe atom exchange still occurs in both directions between aqueous Fe(II) and structural Fe,[485] likely following the same mechanism as detailed in section 4.2.4. This Fe atom exchange is also independent of where Fe(II) is sorbed, with 5−20% of structural Fe able to undergo exchange.[485] However, the same authors discovered that the presence of silicate sheets can stabilize the Fe-containing octahedral sheets to limit the extent of Fe atom exchange whereas the presence of tetrahedral Fe may have the opposite effect.

#### 4.2.4. Reaction Mechanisms of Fe(II)-Treated Minerals.

As mentioned above, the resulting redox potential of Fe(II)-treated mineral oxide systems is one of the main factors impacting their reactivity.[381,425,431,486,487] This enhancement has been attributed to the effect of O-donor atoms coordinating with the sorbed Fe(II) on the surface, similar to that which occurs during aqueous Fe(II) oxidation.[488] As such, the reductive reactivity of the surface-associated Fe(II) species will be affected by the degree of Fe(II) hydrolysis or species formed.

In order to explore Fe(II) speciation on the surfaces of metal oxides and their reductive reaction mechanisms, surface complexation modeling (SCM) is commonly applied, where the amounts of Fe(II) sorbed at different pH values were measured in order to study speciation at the mineral surfaces.[73,74,375,381,489] As mentioned earlier, based on SCM, two stable surface sorbed Fe(II) species ($(\equiv Fe^{III}OFe^{II})^+$ and $\equiv Fe^{III}OFe^{II}OH$) are formed on iron oxide surfaces,[74,375] with $Fe^{III}OFe^{II}OH$ being the dominant reactive species in the reduction of 4-chloronitrobenzene[74] and uranium(VI).[375] However, the relevance of SCM when the underlying mineral


https://doi.org/10.1021/acs.chemrev.0c01286
Chem. Rev. 2021, 121, 8161−8233

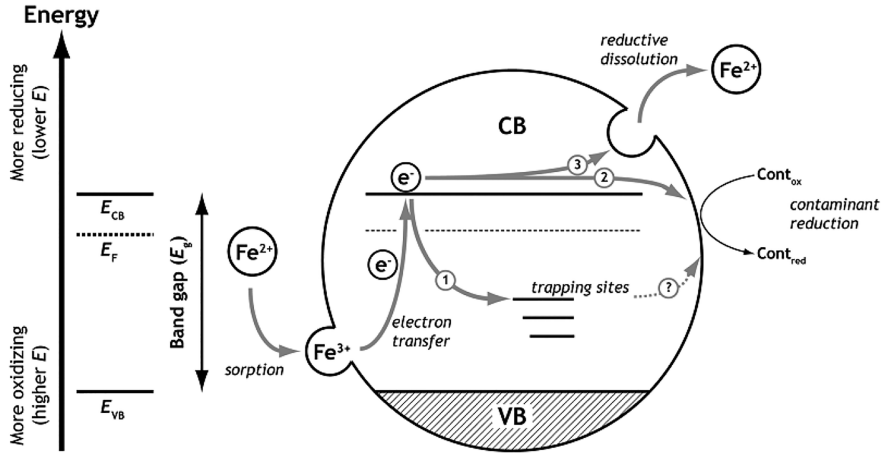


**Figure 8.** Conceptual schematic representation of how aqueous Fe(II) interacts with iron (oxyhydr)oxides in contaminant reduction. Reprinted with permission from ref 491. Copyright 2011 American Chemical Society.

is an iron oxide is unresolved because the complexity of interfacial electron exchange dominates the reactive behavior in these systems. For additional details regarding surface complexation modeling, see section 8.10.

Despite the fact that reduction rates of contaminants are typically well correlated with hydrolyzed sorbed Fe(II) species, many studies have questioned whether reactive enhancement is attributed to higher electron density of sorbed Fe(II) in relation to aqueous Fe(II) species. For instance, stable sorbed Fe(II) complexes are not experimentally observed on the surfaces of iron oxides under low concentrations of aqueous Fe(II) because of ultrafast electron transfer between the sorbed Fe(II) species and the iron oxide[392,464] or, likewise, Fe(III)-containing clay minerals.[479,490] Instead, a stable, sorbed Fe(II) phase, likely a mixture of sorbed Fe(II) and $Fe(OH)_2$ precipitates, only formed on iron oxide surfaces under high aqueous Fe(II) concentrations.[464] Isotope exchange experiments indicate that, upon the addition of $^{57}Fe(II)$ into an $^{56}Fe(III)$ (oxyhydr)oxide suspension, there is oxidation of $^{57}Fe(II)$ to $^{57}Fe(III)$ with the $^{57}Fe(III)$ phase being similar to the underlying oxide with some unresolved differences. With $^{56}Fe$ invisible to Mössbauer spectroscopy, the differences before and after reaction with Fe(II) are easily distinguished.[392,431,464]

The regeneration of sorbed Fe(II) species (limited by either the release of the resultant surface Fe(II) species from the solid following electron transfer or the rate of sorption to a new surface site) is suggested to be the rate-limiting step in reduction by Fe(II)-treated iron oxides.[138,265,357] Recently, $TiO_2$ was found to significantly enhance the surface-mediated reductive reactivity of Fe(II)/goethite due to interparticle electron transfer.[8] This further invokes the question of whether the sorbed Fe(II) species needs to be complexed through an inner- or outer-sphere binding mode on iron oxide surfaces.

Despite the above traditional view of how Fe(II) sorbs onto Fe(III) (oxyhydr)oxides, given the clear importance of the participation of the solid itself as a sink and source of electron density, it is likely more useful to view the interfacial reaction system from the perspective of band theory for semiconductors (Figure 8).[491] In this model, iron oxide particles can be regarded as semiconductors, where electrons are transferred to the bulk particles from sorbed Fe(II), effectively doping the semiconductor with additional electrons. In the model, Fe(II) adsorbs onto iron (oxyhydr)oxides and becomes oxidized by the solid, with electrons transferred into the conduction band. Conduction electrons have three fates: (a) trapping in localized states in the band gap; (b) participating as mobile charge carriers in reactions with redox-active aqueous compounds; and (c) converting interfacial Fe(III) to Fe(II) yielding reductive dissolution. Through this mechanism, the sorbed Fe(II) can both alter the surface potential and participate in redox reactions occurring at the most electrochemically favorable sites at the oxide/water interface.[435]

This new model was enabled by Yanina and Rosso's 2008 landmark study that provided the first experimental proof of the critical role of electron transport through the solid in interfacial redox reactivity.[393] That study was the first to show that the interaction of Fe(II) with specific facets of iron oxides involved coupled interfacial electron exchange reactions linking one facet to another. Detailed AFM imaging of each facet type along with in situ single-facet potentiometry showed that electrochemical potential gradients exist between structurally distinct facets and create electric fields across crystallites that can drive conduction currents. These currents are, in turn, supplied by interfacial electron exchange reactions with Fe(II). For example, the interactions of Fe(II) with (001) basal facets and (hk0) edge facets were shown to be quite different only when these facet types were connected on the same hematite crystallite, creating an electric potential bias driving interfacial electron exchange currents. These facet-specific biases yield reductive dissolution and oxidative growth processes interlinked by bulk conduction.

Since that time, a great deal of experimental and computational molecular advances have helped to validate the conduction model. For instance, Rosso's group combined iron isotopic labeling and atom probe tomography (APT) techniques to show, for the first time, the distribution of iron resulting from the autocatalytic interaction of Fe(II) with the hematite (001) facet.[492] The images unambiguously provide direct evidence for $^{57}Fe(II)$ oxidative adsorption and growth on the hematite (001) surface and a net oxidative adsorption of 3.2−4.3 $^{57}Fe$ atoms $nm^{-2}$ on average. Later on, they directly visualized the iron atom exchange between Fe(II) and goethite microrods using isotope tracers and three-dimensional APT.[459] The findings yielded an unprecedented view into the spatial and temporal properties of Fe(II)-catalyzed recrystallization at the atomic scale, demonstrating the heterogeneity of the exchange front but nonetheless establishing further microscopic evidence supporting the


https://doi.org/10.1021/acs.chemrev.0c01286
Chem. Rev. 2021, 121, 8161−8233

conduction model. Recently, their study using isotope tracers and NanoSIMS provided visual evidence consistent with that of Yanina and Rosso showing that Fe(II) preferred to adsorb onto hematite basal (001) surfaces relative to edge (012) facets.[446] The findings provide insights into the facet-specific reactivity of iron oxides which are important in the biogeochemical and geochemical cycling of iron in environmental processes and environmental remediation strategies.

Rosso's group has also put forward some of the most atomistically detailed and comprehensive theoretical simulations of the conduction model to date. Conduction in iron(III) (oxyhydr)oxides is based on thermally activated site-to-site hopping of electron and hole small polaronic charge carriers.[493,494] The adsorption and interfacial electron-transfer processes for Fe(II) onto various facets of hematite and goethite and Fe-rich 2:1 phyllosilicate minerals have been explicitly modeled in numerous studies that lay out the thermodynamics and kinetics of these processes in quantitative detail.[495−501] This includes treatment not only for individual charge carriers (i.e., in the limit of infinite dilution) but also for their collective dynamics, which provides a lattice-specific view of percolation networks for collective conduction and the role of site-blocking impurities.[350,502] In their most recent simulation study, a novel hybrid/reactive molecular simulation was laid out for Fe(II) interaction with goethite that established operative dimensionality for conduction path lengths in the near-surface of individual goethite crystallites. The simulations quantitatively showed that room temperature thermal energy is sufficient to promote the conduction model mechanism of iron atom exchange via short intrasurface conduction pathways of 1−2 nm, at a rate of $10^{-5}$ Fe $s^{-1}$ $cm^{-2}$ and confirmed that defects represented in the form of surface roughness greatly accelerate the process.[503] The conduction model introduced by Yanina and Rosso in 2008[393] therefore appears to be highly relevant to redox transformations of environmental contaminants on the basis of Fe(II)/iron oxide systems, if not more generally when the mineral substrate is electrically semiconducting.

The conduction model has highlighted how dynamic and reactive the traditionally viewed "sorbed Fe(II)" is. It has also been successfully utilized to explain a number of processes including (1) the near complete Fe atom exchange between aqueous Fe(II) and goethite within 30 days or 5−25% Fe atom exchange between Fe(II) and hematite of different sizes, both with no substantial differences observed in the mineral phase, average particle size, crystallinity, or redox reactivity after the exchange;[394,406,435] (2) Fe(II)-catalyzed growth of hematite on the hematite (001) surface following preferential Fe(II) adsorption;[504] and (3) roughly three-times the extent of iron-isotope exchange with goethite than oxygen-isotope exchange in the Fe(II)−goethite interaction but complete oxygen-isotope exchange in the case of Fe(II)-ferrihydrite.[411] Even at pH 5 where there is negligible sorption of Fe(II) and, hence, less likelihood of forming an inner-sphere Fe(II) surface complex, there is still some Fe atom exchange between aqueous Fe(II) and micro- or nanogoethite.[406]

### 4.3. Zero-Valent Iron

Iron in the zero valence state ($Fe^0$) does not occur naturally among terrestrial materials (except for an occasional meteorite). However, anthropogenic occurrences of $Fe^0$ in the environment are common due to the widespread use of ferruginous metals (in pipes, bridges, etc.), and these materials interact with the environment through biogeochemical processes that are mediated by Fe(II) and Fe(III). Over the last ∼25 years, another prominent role of $Fe^0$ in the environment has emerged: the use of fine-grained, $Fe^0$-containing materials for water treatment, especially remediation of contaminated groundwater. The materials used in these applications are usually termed zerovalent iron (ZVI), but the grains always are coated with iron (oxyhydr)oxide minerals and often contain significant impurities (e.g., scrap cast iron contains several percent elemental carbon).

Since the first field-scale applications of ZVI in groundwater remediation (in the 1990s), some variations on this technology have become standard engineering practice and many innovative variations have been proposed. In addition, the academic literature on environmental applications of ZVI has become very large with many aspects of this technology studied extensively. Some of the best of this work has used ZVI as a model system to characterize other, more general and/or fundamental, aspects of iron reactivity in environmental systems. In fact, there are multiple examples where research undertaken using ZVI has led to advances in environmental chemistry with implications well beyond its application in specific remediation technologies.[505]

Aspects of ZVI applications for water treatment and/or remediation have been reviewed many times,[59,506−508] so for the purposes of this review, just three aspects will be addressed: (a) corrosion of ZVI as a source of Fe(II), (b) the role of iron (oxyhydr)oxides as mediator of redox processes at the ZVI/water interface, and (c) the kinetics of probe-contaminant reactions with ZVI relative to other Fe(II)-containing minerals. The latter issue (c) will be discussed in section 4.4, and the former two issues (a and b) will be discussed together, here, because they are closely related.

The primary reactions involved in corrosion of ZVI under aquatic conditions are summarized in Figure 9. Reactions

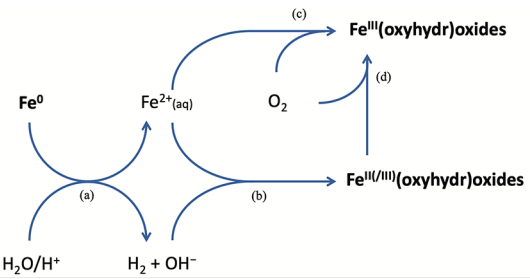


**Figure 9.** Major chemical reactions contributing to subsurface conditions after addition of ZVI (shown generically as $Fe^0$). (a) Corrosion of $Fe^0$; (b) and (c) precipitation of Fe(II) and Fe(III) (oxyhydr)oxides; (d) transformation of Fe (oxyhydr)oxides. Solid phases are shown in bold. Revised with permission from ref 509. Copyright 2015 Elsevier.

involving contaminants are not shown because they usually are not stoichiometrically significant and, from the perspective of iron chemistry, they serve mainly as oxidants to drive additional reactions analogous to a, c, and d.

From a biogeochemical perspective, the primary effect of the reactions in Figure 9 is to generate Fe(II) and raise the pH, which, in turn, form $Fe^{II/III}$ oxides that become authigenic colloids, coatings, crusts, etc. When ZVI is deployed as an in situ permeable reactive barrier (PRB),[510] the above processes play out along the groundwater flow path. This results in a complex (and, at least initially, dynamic) system of spatially distributed zones, divided by more or less sharp interfaces and linked


https://doi.org/10.1021/acs.chemrev.0c01286
Chem. Rev. 2021, 121, 8161−8233

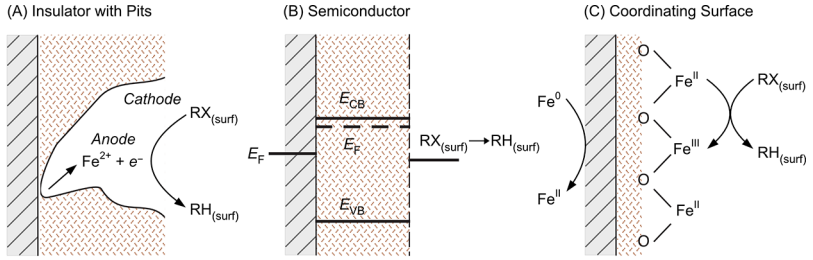


**Figure 10.** Conceptual models for how the layer of iron oxides at the ZVI/water interface might mediate reduction of contaminants such as organohalides (RX to RH): (A) "direct" coupling of dechlorination with oxidative dissolution of $Fe^0$ within a pit or other defect; (b) charge transfer through (semi)conductive oxides to RX at the oxide/water interface; and (C) dechlorination at reducing surface sites where Fe(II) from oxidative dissolution of $Fe^0$ has readsorbed at the oxide surface. $E_F$, $E_{CB}$, and $E_{VB}$ refer to the Fermi, conduction band, and valence band energies, respectively. Note: the gray zone indicates zerovalent iron, while the brownish zone indicates iron oxides. Revised with permission from ref 517. Copyright 1998 American Chemical Society.

through a variety of biogeochemical gradients. The complexity of this system has long been anticipated,[511] but only a few studies have characterized this at the field scale (e.g., using cores taken diagonally through a permeable reactive barrier (PRB)).[512−514]

While the ZVI-containing zone of a PRB usually exhibits elevated Fe(II), $H_2$, and pH, these changes are not commonly observed in groundwater that has moved more than a few meters down-gradient. Even in field applications of nanosized ZVI (nZVI), which is engineered for mobility so that it can be emplaced by injection, the direct impacts of reactions involving ZVI do not extend very far down-gradient. In fact, recent field studies of nZVI for remediation of groundwater contaminated with chlorinated solvents (e.g., TCE) have placed more emphasis on biodegradation of the contaminants, where the main role of ZVI is to provide labile Fe and $H_2$, which can stimulate microbiology down-gradient.[515,516]

The majority of laboratory research on the reactivity of ZVI with contaminants has focused on micron-scale effects at the surface of ZVI particles suspended in well mixed batch reactors. At this scale, the fundamental issue of greatest significance is how electrons from oxidation of $Fe^0$ are able to reduce contaminants in solution despite the intervening "passive film" composed of iron oxides, sulfides, carbonates, and other precipitates. The main options for this were classified in a three-part conceptual model by Scherer et al. using reduction of a generic alkyl halide (RX) as a prototypical contaminant (Figure 10).[517]

The possibility that contaminant reduction occurs by direct electron transfer from $Fe^0$ within pits, crevices, or equivalent defects in the passive film (Figure 10A) has received relatively little attention. However, direct spectroscopic evidence for this hypothesis was obtained at very high RX concentrations,[518] and recent studies have implied that pitting plays a significant role in increased contaminant reduction rates during passive film breakdown.[519] The semiconductor hypothesis (Figure 10B) is supported by specific evidence of photoeffects on contaminant reduction in batch reactors.[520] The coordinating surface model is supported by many studies that have used surface complexation modeling to interpret the effects of competing ligands on contaminant reduction rates.[521,522] However, some aspects of this interpretation might require revision to accommodate recent advances in understanding the nature of Fe(II) surface sites on iron minerals, which is described above in section 4.2.4.

### 4.4. Comparison of the Reactivity of Different Solid Fe(II) Species

It is challenging to compare the reactivity of all Fe(II) species on an equal footing since most studies examine reactivity under highly variable conditions. Only a few studies have compared the reductive reactivity of a large range of different Fe(II) species. The comparison of the reductive reactivity of sorbed Fe(II) species on various minerals has been reported in some studies.[8,346,369] For instance, the reduction of Tc(VII) by surface sorbed Fe(II) on iron(III) (oxyhydr)oxides is much faster than that by sorbed Fe(II) on the surface of different phyllosilicates.[346] The degradation of *cis*-DCE by different Fe(II) species was reported to follow the order of GR(Cl) ≫ GR($SO_4$) > Fe(OH)$_2$ > mackinawite = magnetite,[523] which is similar to other reported results.[194,228] The degradation of chlorinated solvents by different Fe(II) species has been summarized by He et al. (2015) with the order of disordered FeS > FeS > ZVI > $FeS_2$ > sorbed Fe(II) > green rust = magnetite > biotite = vermiculite.[524]

The qualitative comparisons summarized above were based on observed rates of (probe) contaminant reduction, usually expressed as pseudo-first-order rate constants ($k_{obs}$) or the corresponding half-lives ($t_{1/2}$). Of course, these comparisons are only valid under a set of otherwise equivalent conditions (e.g., equal dose of the Fe(II) mineral phases that act as the reductants). To allow quantitative comparisons of rate data across more varied conditions, a variety of normalizations have proven to be useful. The now standard formulation uses terms and units originally popularized for studies of contaminant reduction by ZVI.[525] In that formulation, $k_{obs}$ is normalized by the mass concentration of reduction to obtain $k_M$ (L $g^{-1}$ $min^{-1}$) and by the surface area concentration to obtain $k_{SA}$ (L $m^{-2}$ $min^{-1}$). Alternatively, $k_{SA} = k_M/a_s$, where $a_s$ is the specific surface area of the solid-phase reductant (usually determined by BET gas adsorption measurements). This formulation and terminology have been adopted to describe the kinetics of the contaminant reaction with a wide range of heterogeneous reductants, including iron oxides.[194,361,425,426,526] One way that this formulation has been extended is by plotting log $k_{SA}$ vs log $k_M$, which has proven useful for comparing reactivity among contaminants, among reductants, and across a variety of other operational variables.[508,527−529] Note that the reactivity of iron modified forms or their composite minerals is beyond the scope of this review, but readers are referred to several reviews on this topic.[508,530−533]

For the purposes of this review, we have summarized the kinetic data compiled in Tables 2 and 3 and ref 426 in Figure 11,


https://doi.org/10.1021/acs.chemrev.0c01286
Chem. Rev. 2021, 121, 8161−8233

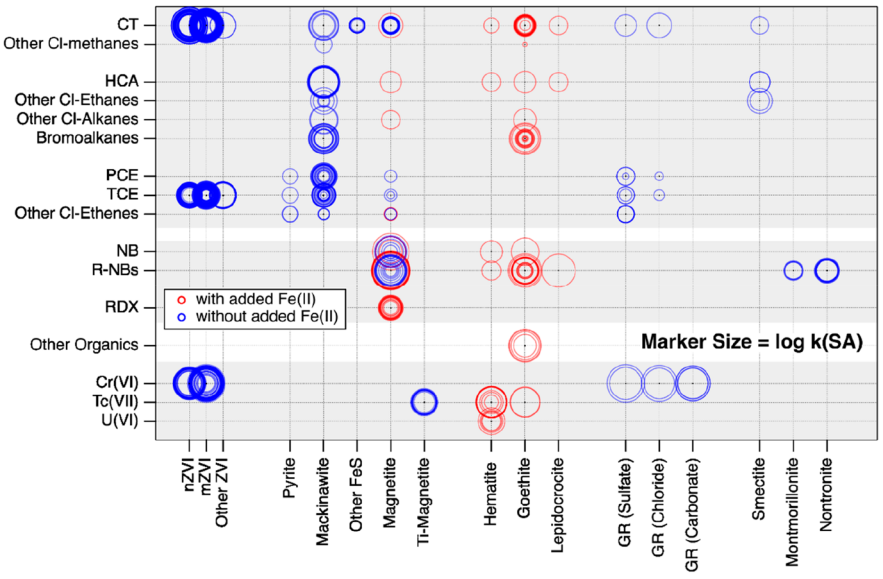


**Figure 11.** Bubble plot of surface-normalized reduction rate constants (log $k_{SA}$) of different chemical compounds by various reducing Fe(II) species. CT, carbon tetrachloride; HCA, hexachloroethane; PCE, perchloroethene; TCE, trichloroethene; NB, nitrobenzene; and RDX, hexahydro-1,3,5-trinitro-1,3,5-triazine. Literature data used in this plot are from Tables 2 and 3 and ref 426.

which emphasizes the distribution of experimental results across classes of contaminants (*y*-axis categories) and iron-based reductants (*x*-axis categories). The size of the circles in Figure 11 is proportional to log $k_{SA}$, and the circle color distinguishes data from experiments without (blue) and with (red) added aqueous Fe(II). The circle colors are partially transparent, so darker color indicates overlapping data. Note that the data from Tables 2 and 3 for iron minerals should be relatively comprehensive, but the source used for the ZVI data includes only the three contaminants shown,[426] and many data for other contaminants are available. Also, note that the analogue to Figure 11 using $k_M$ (not shown) instead of $k_{SA}$ is qualitatively similar but the circle sizes are less consistent for each contaminant−reductant combination.

Several significant conclusions can be drawn from Figure 11. Without added Fe(II) (blue markers), only ZVI and minerals containing Fe(II) reduce any of the contaminants shown. Conversely, the minerals containing only Fe(III) reduce contaminants only when Fe(II) is added. Magnetite is an intermediate case, consistent with its mixed valence of iron, but note that magnetite with added Fe(II) consistently gives larger $k_{SA}$ than magnetite without added Fe(II). Rates of contaminant reduction by ZVI are consistently fast, but $k_{SA}$ is more variable for the iron oxides and sulfides. This difference might be due to greater sensitivity of the latter to other factors such as pH, Fe(II) concentration, oxide mineral surface coatings, etc. Clearly, there are many nodes in Figure 11 that lack markers, but it is difficult to determine which of these are because no reaction was observed (e.g., because the relatively unreactive chlorinated ethenes only give measurable dechlorination with the most reactive oxides) and which are because the experiments are yet to be reported.

In addition to the rate of contaminant reduction, another measure of the reactivity of Fe(II)-containing solid phases is their *capacity* for reduction. Reductive capacity is an operationally defined concept because it is strongly dependent on the strength of the oxidant(s), the availability of the oxidant to react with the reductant phase (e.g., if there are mass transport limitations), and the contact time (relative to the time required for complete reaction). With respect to Fe(II)-containing minerals, the reductive capacity concept has been most thoroughly investigated in a series of papers by Lee and Batchelor.[534,535] They used their assay to investigate the reductive capacity of different reductants for Cr(VI) and PCE and found that it decreased in the order GR($SO_4$) > magnetite > pyrite > biotite > montmorillonite > vermiculite, which is directly proportional to the Fe(II) content.[534] They also found that the reductive capacities of iron(II)-bearing phyllosilicates were 1 to 3 orders of magnitude less than those of iron sulfides.[535] Recently, the related concepts of efficiency and selectivity have received a great deal of attention in the literature on ZVI,[536] but how this aspect applies to Fe(II)-associated minerals is not yet well developed.

Rates and capacities of contaminant reduction are related to the redox potential ($E_h$) of the system in various ways. The most widely studied involves attempts to obtain correlations between reduction rate constants ($k_{obs}$, $k_M$, or $k_{SA}$) and measured or calculated (from thermodynamic data) values of $E_h$ for the reducing system. Early efforts to do this were marginally successful,[537] but the demand for practical tools for assessing the potential for reduction at field sites has persisted.[538] Recently, strong correlations have been obtained with data from laboratory model systems, such as those found between $k_{SA}$ for nitrobenzene reduction and pe + pH as the descriptor variable,[425] and between $k_{SA}$ for 4-chloronitrobenzene, 2-chloroacetophenone, and carbon tetrachloride using $E_h$ in the presence of electron-transfer mediators.[426] More recently, redox potentials measured with electron-transfer mediators have been shown to be effective at describing $k_M$ for carbon tetrachloride dechlorination in suspensions of aquifer materials from a diverse range of field sites.[539]


https://doi.org/10.1021/acs.chemrev.0c01286
Chem. Rev. 2021, 121, 8161−8233

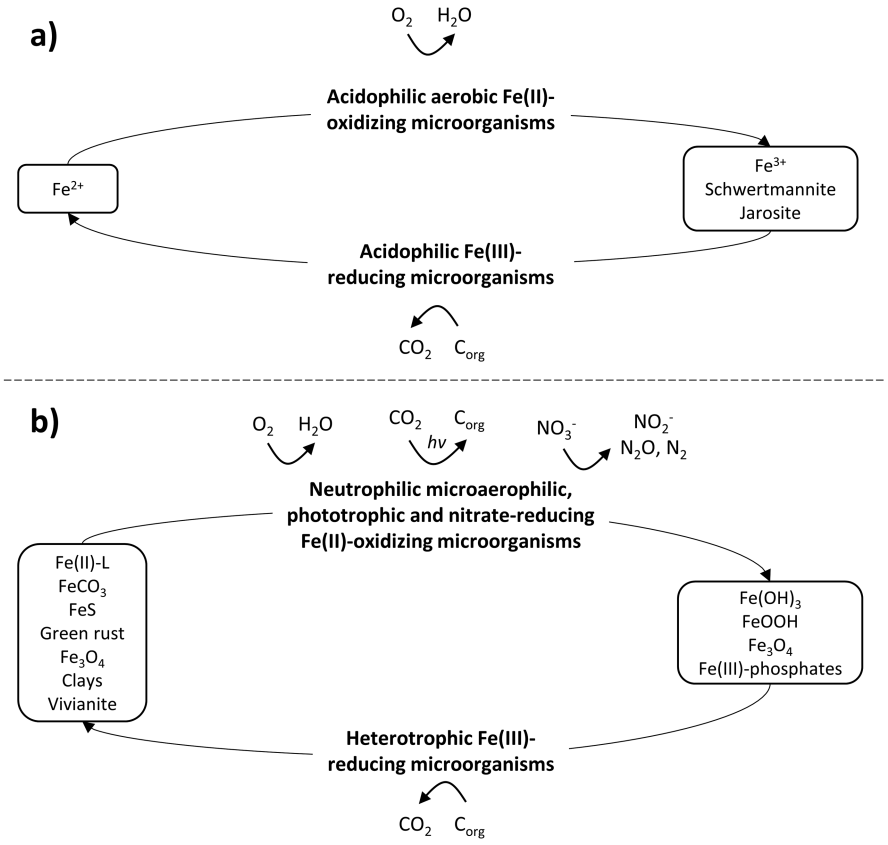


**Figure 12.** Redox cycling of Fe as mediated by (a) acidophilic and (b) neutrophilic microorganisms. Different Fe(II) and Fe(III) species are listed to emphasize the diversity of reactants and products involved in these reactions.

## 5. MICROBIAL PROCESSES RELATED TO FE(II) REDOX CHEMISTRY

### 5.1. Fe(II)-Oxidizing Microorganisms: Acidophilic and Neutrophilic (Microaerophilic, Nitrate-Reducing, and Phototrophic) Fe(II) Oxidizers (FeOx)

The first intensively studied microorganisms capable of performing Fe(II) oxidation were the aerobic acidophilic FeOx (e.g., *Acidithiobacillus* sp.)[862,863] due to their recognized prevalence in metal-polluted environments such as acid mine drainages (pH < 5). These microorganisms couple the oxidation of dissolved $Fe^{2+}$ (which is kinetically stable at low pH under oxic conditions) to the reduction of $O_2$ as an electron acceptor (Figure 12).[540]

In the past 30 years, a diversity of microorganisms capable of catalyzing Fe(II) oxidation at circumneutral pH has been discovered. At neutral pH, Fe(II) oxidation can be coupled by microorganisms to the (a) reduction of $O_2$, (b) reduction of oxidized N-species including nitrate and nitrite, and (c) photosynthetic reduction of $CO_2$ (Figure 12).[102] These reactions are catalyzed by microaerophilic, nitrate-reducing, and phototrophic FeOx, respectively. Microaerophilic and nitrate-reducing FeOx uses Fe(II) as both an electron and energy source, while phototrophic FeOx gains energy from light and uses Fe(II) only as an electron source for $CO_2$ fixation.

Microaerophilic FeOx typically grows in environments with opposing gradients of $Fe^{2+}$ and $O_2$, such as those present in stratified water columns or near the sediment−water interface.[541−543] These microorganisms have become famous due to their striking structures of twisted stalks, sheaths, and dreads associated with Fe(III) minerals.[544] The proposed mechanistic $Fe^{2+}$ oxidation model starts with dissolved $Fe^{2+}$ being taken up into the cell, then oxidized and released together with the characteristic organics of twisted stalks, sheaths, and dreads forming organo-mineral associations.[544] These unique structures are thought to play multiple roles to help the cells to avoid mineral encrustation (and death), to help maintain the optimal position along the $O_2$-$Fe^{2+}$ gradients, and potentially to be used to supplement the transmembrane proton gradient.[419,542]

About 25 years ago, it was suggested that microorganisms can couple the oxidation of Fe(II) to the reduction of nitrate and fixation of $CO_2$ under anoxic conditions.[545] However, early isolates of proposed nitrate-reducing Fe(II) oxidizers (NRFeOx) are more likely to be heterotrophic (oxidizing organic carbon) nitrate reducers that produce reactive N-species (including nitrite), which then oxidize Fe(II) abiotically in a process termed chemodenitrification.[546−548] To date, only a few examples of "true" NRFeOX are known in which oxidation of Fe(II) is enzymatically coupled to nitrate reduction under autotrophic growth conditions, including the archetype enrichment culture KS that is dominated by the NRFeOx *Gallionellaceae* species with flanking communities of heterotrophic nitrate reducers.[549−551] Attempts to isolate the primary Fe(II)-oxidizer—the *Gallionellaceae* sp.—into a pure culture have been unsuccessful, possibly because metabolic activities of the flanking communities are needed to detoxify reactive nitrogen species produced by the *Gallionellaceae* sp. during Fe(II) oxidation.

Photoautotrophic FeOx has been found in many anoxic surface habitats that have a supply of reduced iron and are influenced by daylight.[548] These organisms have also been


https://doi.org/10.1021/acs.chemrev.0c01286
Chem. Rev. 2021, 121, 8161−8233

suggested to have played a major role in Fe(II) oxidation and the deposition of banded iron formations in ancient Fe(II)-rich oceans.[552,553] With their amazing metabolism, they have the capability to produce Fe(III) minerals from Fe(II) under anoxic conditions by simply transferring the reducing equivalents to $CO_2$ in the absence of classical electron acceptors such as $O_2$ or nitrate. The isolated photoautotrophic FeOx generally belong to three microbial classes: the purple sulfur bacteria (Gammaproteobacteria), purple nonsulfur bacteria (Alphaproteobacteria), and green sulfur bacteria (Chlorobia).[410]

### 5.2. Microbial Oxidation of Dissolved Inorganic $Fe^{2+}$

Microbial oxidation of dissolved inorganic $Fe^{2+}$ is particularly important at low pH because the abiotic oxidation rate of $Fe^{2+}$ is extremely slow under this condition,[554] with the exception of systems that contain high HCl concentrations that favor abiotic oxidation by $O_2$, especially at elevated temperatures.[555] The rapid aerobic oxidation of $Fe^{2+}$ by acidophilic FeOx is considered to be the main driver for generation of acid mine drainages. The produced $Fe^{3+}$ is the main oxidant for pyrite, leading to the release of $H^+$ and of pyrite-associated toxic metals (e.g., As, Cu, Ni) along with copious deposits of Fe(III) (oxyhydr)oxides and other Fe minerals (e.g., schwertmannite, jarosite) with devastating effects to the ecosystem.[540,556]

At neutral pH, dissolved inorganic $Fe^{2+}$ is stable under anoxic conditions but is rapidly oxidized to poorly soluble Fe(III) (oxyhydr)oxides under oxic conditions. Microaerophilic FeOx thrive at the oxic-anoxic interfaces where opposing gradients of $Fe^{2+}$ and $O_2$ exist. Cultivation methods for these bacteria are thus principally based on air-exposed gradient tubes or plates—using FeS or $Fe^0$ as the base—in order to establish $Fe^{2+}$–$O_2$ interfaces.[558] Fe(II) oxidation at these interfaces reflects the combined influence of both biotic and abiotic pathways. Kinetic constraints suggest that microaerophilic FeOx can only outcompete abiotic Fe(II) oxidation when the $O_2$ concentration is <50 $\mu$M.[557] Another constraint is the presence of Fe(III) (oxyhydr)oxides, which can catalyze heterogeneous abiotic Fe(II) oxidation.[558] Estimates suggest that microaerophilic FeOx contribute to 10–90% of the total oxidized Fe(II) at these interfaces, with higher microbial contributions relative to abiotic oxidation observed with lower $O_2$ concentrations and pH values.[541,559,560]

In anoxic environments, both NRFeOx and photoautotrophic FeOx can oxidize dissolved $Fe^{2+}$. The formed products consist of mixtures of ferrihydrite, Fe-phosphates, green rust, magnetite, goethite, and lepidocrocite depending on the geochemical conditions (e.g., pH, carbonate, phosphate, and presence of humic acids), with generally higher crystallinity with longer incubation time.[561,562]

### 5.3. Microbial Oxidation of Fe(II)–Ligand Complexes

As discussed previously, Fe(II) is present not only as dissolved free $Fe^{2+}$ in the environment but also associated with NOM (or OM in general) as Fe(II)–NOM or Fe(II)–OM complexes.[441,563] In two recent studies the microbial oxidation of Fe(II)–OM complexes has been investigated. In the first study, Peng et al. (2018) showed that the heterotrophic nitrate-reducing strain *Acidovorax*. sp. BoFeN1 can oxidize Fe(II)–OM complexes (Fe(II)-citrate, Fe(II)-EDTA, and also Fe(II) complexed with humic and fulvic acids), but only in the presence of easily bioavailable organic matter (e.g., acetate) and dissolved $Fe^{2+}$.[861] The reaction network is complex even in this relatively simple laboratory culture: electrons from acetate are channeled to fuel enzymatic nitrate reduction, leading to the production of reactive nitrite that abiotically oxidizes the Fe(II)–OM complexes. Why the initial presence of dissolved $Fe^{2+}$ is required for the oxidation of Fe(II)–OM complexes is still unclear. It is thought that Fe(III) mineral encrustation of the cells leads to differing inhibition of enzyme activities for the inner membrane nitrate reductase (produces nitrite) versus the periplasmic nitrite reductase (converts nitrite to less reactive N species), which then affects the amount of nitrite released into the solution that can then oxidize the Fe(II)–OM complexes. This is an illustrative example of how a complex reaction network initiated by environmentally relevant microorganisms ultimately leads to the oxidation of Fe(II)–OM complexes. Whether truly autotrophic NRFeOx such as the aforementioned enrichment culture KS can oxidize Fe(II)–OM complexes directly remains to be clarified in future studies.

In the second study, Peng et al. (2019) studied the photoautotrophic FeOx *Rhodopseudomonas palustris* TIE-1 for its capability to oxidize Fe(II)–OM complexes.[563] For all complexes studied (Fe(II)-citrate, -EDTA, -humic and -fulvic acid) the OM stimulated Fe(II) oxidation compared to oxidation of free $Fe^{2+}$. Additionally, it was found that the oxidation products, the Fe(III)-phases, were nearly all present as Fe(III) colloids in the 3–200 nm size range. These processes may be of great importance in open ocean environments where Fe(III)–OM complexes represent the main fraction of dissolved Fe present,[564] although the link between these laboratory studies to natural environments remains to be elucidated in the future.

### 5.4. Microbial Oxidation of Fe(II)-Containing Minerals

Besides dissolved $Fe^{2+}$ and Fe(II)–ligand complexes, microorganisms can also oxidize various Fe(II)-containing minerals such as vivianite, siderite, mackinawite, pyrite, clays, reduced goethite, magnetite, and green rust. In most cases, the enzymatic pathways, in particular the extracellular electron-transfer pathways from the Fe(II)-containing solid into the cells, are unknown. Furthermore, in contrast to studies in abiotic systems, there is often no distinction made between microbial oxidation of surface sorbed Fe(II) and structural Fe(II).

Vivianite was shown to be oxidized by the heterotrophic nitrate-reducing strain *Acidovorax*. sp. BoFeN1.[132] The oxidation is thought to proceed abiotically via the secretion of reactive nitrite to the extracellular space, which oxidizes vivianite to poorly crystalline Fe(III) phosphates over 14 days. Whether true enzymatic oxidation of vivianite is also possible needs to be determined in future studies.

Several photoautotrophic FeOx were shown to be able to oxidize the relatively soluble siderite, mackinawite, and green rust minerals but not the poorly soluble pyrite and vivianite.[565,566] Heterotrophic nitrate-reducing bacteria can also oxidize green rust.[566−568] An enrichment culture of NRFeOx bacteria was suggested to be able to oxidize abiogenic siderite and biogenic magnetite, as well as the surface sorbed Fe(II) on microbially reduced Fe(III) mineral goethite and soils.[569] The products of Fe(II) oxidation are typically poorly crystalline Fe(III) oxyhydroxides (ferrihydrite with traces of goethite by slow Fe(II)-induced transformation of the ferrihydrite). In a few cases, the formation of magnetite has also been reported.[568,570]

Pyrite has been shown to be oxidized by acidophilic FeOx and neutrophilic Fe(II)- and S-oxidizing microorganisms. Acidophilic FeOx oxidizes pyrite via cell attachment and the localized production of $Fe^{3+}$, which is the main chemical oxidant of pyrite.[571] At neutral pH, pyrite oxidation can be accelerated by


https://doi.org/10.1021/acs.chemrev.0c01286
Chem. Rev. 2021, 121, 8161−8233

Table 4. Summary of Conditions and Results from Various Studies That Have Investigated Microbial Fe(II) Oxidation[a]

| Microorganisms | Fe(II) form and concentration | Incubation parameters | Light flux/carbon/$O_2$ | Cells/mL | Max Fe(II) oxidation rate (mM/day) | Fe(II) oxidation products | References |
|---|---|---|---|---|---|---|---|
| **Phototrophic FeOx** | | | **Light flux** | | | | |
| *Chlorobium ferrooxidans* KoFox (in coculture with *Geospirillum* KoFum) | 4.7 mM $Fe^{2+}$ | 24 °C | | | 1.6 | Fh, Go, Lp | Kappler (2004)[565] |
| | 40 mM FeS | 24 °C | | | 2.0 | Fh, Go, Lp | Kappler (2004)[565] |
| | 2−4 mM $Fe^{2+}$ | 5−30 °C, pH 5−8 | 50−2,300 lx | | 0.5−2.2 | | Hegler (2008)[582] |
| | 3−4 mM $Fe^{2+}$ | 20 °C, 0−2 mM Si | 25−1,300 lx | | 0.6−0.8 w/o Si, 0.9−1.3 w Si | Fh, Lp | Gauger (2016)[586] |
| *Rhodobacter ferrooxidans* SW2 | 4.7 mM $Fe^{2+}$ | 16−18 °C | | | 0.5 | Fh, Go, Lp | Kappler (2004)[565] |
| | 40 mM FeS | 16−18 °C | | | 1.4 | Fh, Go, Lp | Kappler (2004)[565] |
| | 2−4 mM $Fe^{2+}$ | 5−30 °C, pH 5−8 | 50−2,300 lx | $2 \times 10^8 - 1 \times 10^9$ | 0.2−0.7 | | Hegler (2008)[582] |
| | 0.2−30 mM $Fe^{2+}$ | 20 °C | 650 lx | | 0.2−2.5 | | Hegler (2008)[582] |
| | 6 mM Fe(II)−GR | 20 °C | 600 lx | | 0.5−1.3 | Fh, Go | Han (2020)[566] |
| *Thiodictyon* F4 | 4.7 mM $Fe^{2+}$ | 24 °C | | | 0.9 | Fh, Go, Lp | Kappler (2004)[565] |
| | 40 mM FeS | 24 °C | | | 2.0 | Fh, Go, Lp | Kappler (2004)[565] |
| | 2−4 mM $Fe^{2+}$ | 5−30 °C, pH 5−8 | 50−2,300 lx | | 0.6−4.5 | | Hegler (2008)[582] |
| *Chlorobium* strain N1 | 10 mM $Fe^{2+}$ | 20 °C, salinity = 23 | 380 lx | $3 \times 10^7 - 7 \times 10^8$ | 0.8 | Fh | Laufer (2017) |
| | 10 mM $Fe^{2+}$ | 7−45 °C, pH 6−9.1, salinity = 1.6−50 | 46−1,270 lx | | 0.1−0.7 | Fh | Laufer (2017) |
| *Rhodovulum iodosum* | 10 mM $Fe^{2+}$ | 20 °C | | | 0.5 | Fh | Straub (1999) |
| | 0.4−4.1 mM $Fe^{2+}$ | 26 °C | 600 lx | $2 \times 10^7 - 2 \times 10^8$ | 0.2−1.3 | Fh, Go, Lp | Wu (2014) |
| | 4.1 mM $Fe^{2+}$ | 26 °C | 150−1,000 lx | $2 \times 10^7 - 2 \times 10^8$ | 0.9−1.4 | Fh, Go, Lp | Wu (2014) |
| *Rhodopseudomonas palustris* TIE-1 | 4.5 mM $Fe^{2+}$ | 30 °C | | $2 \times 10^7 - 2 \times 10^8$ | 0.4 | Fh, Go, Mg | Jiao (2005)[570] |
| | 10 mM $Fe^{2+}$ | 20 °C | 550 lx | $\sim 4 \times 10^7$ | 0.2 | Mostly colloids <200 nm | Peng (2019) |
| | 10 mM Fe(II)−humic acid | 20 °C | 550 lx | $\sim 4 \times 10^7$ | 0.5 | | Peng (2019) |
| | 10 mM Fe(II)−fulvic acid | 20 °C | 550 lx | $\sim 4 \times 10^7$ | 1.1 | | Peng (2019) |
| | 10 mM Fe(II)−citrate | 20 °C | 550 lx | $\sim 4 \times 10^7$ | 2.4 | | Peng (2019) |
| | 10 mM Fe(II)−EDTA | 20 °C | 550 lx | $\sim 4 \times 10^7$ | 3.0 | | Peng (2019) |
| | 6 mM Fe(II)−GR | 20 °C | 600 lx | | 0.3 | Fh, Go | Han (2020)[566] |
| | | | **OVERALL RANGE** | | **0.1−4.5** | | |
| **NRFeOx** | | | **Carbon** | | | | |



https://doi.org/10.1021/acs.chemrev.0c01286
Chem. Rev. 2021, 121, 8161−8233

Table 4. continued

| Microorganisms | Fe(II) form and concentration | Incubation parameters | Light flux/carbon/$O_2$ | Cells/mL | Max Fe(II) oxidation rate (mM/day) | Fe(II) oxidation products | References |
|---|---|---|---|---|---|---|---|
| Enrichment culture KS | 8−10 mM $Fe^{2+}$ | 28 °C, 4 mM $NO_3^-$ | 22 mM $HCO_3^-$ | | 3 | | Straub (1996)[545] |
| | | | | $1 \times 10^5 - 2 \times 10^7$ | 3.5 | Fh | Nordhoff (2017)[587] |
| | | | | $4 \times 10^4 - 2 \times 10^6$ | 2 | | Tominski (2018) |
| | | 28 °C, 4 mM $NO_3^-$ | 5 mM acetate | $1 \times 10^5 - 1 \times 10^8$ | 2 | Fh | Nordhoff (2017)[587] |
| | | | | $6 \times 10^4 - 3 \times 10^7$ | 1.2 | | Tominski (2018) |
| Enrichment culture | 10 mM $Fe^{2+}$ ($FeSO_4$) | 30 °C, 2.5−6 mM $NO_3^-$ | 30 mM $HCO_3^-$ | | 3.8 | HCl-extractable Fe(III) | Weber (2001)[569] |
| | 20 mM synthetic $FeCO_3$ | | | | 2.8 | | Weber (2001)[569] |
| | 20 mM bio-$FeCO_3$ | | | | 0.2 | | Weber (2001)[569] |
| | 5−8 mM Fe(II) in reduced subsoils | | | | 1.7−1.8 | | Weber (2001)[569] |
| | 2 mM Fe(II) in reduced goethite | | | | 0.6 | | Weber (2001)[569] |
| | 6 mM Fe(II) in bio-$Fe_3O_4$ | | | | 0.8 | | Weber (2001)[569] |
| | | | **OVERALL RANGE** | | **0.2−3.5** | | |
| **Microaerophilic FeOX** | | | **$O_2$** | | | | |
| Enrichment cultures, *Gallionella* or *Zetaproteobacteria* sp. | <2.5 mM $Fe^{2+}$, decreasing with height | Gradient tubes, 20 °C | <300 μM, increasing with height | | 4.8 | | Lueder (2018)[558] |
| Enrichment culture, *Sideroxydans* sp. | 0.6−0.8 mM $Fe^{2+}$ | Miniaturized microcosms, 25 °C | 1 μM | $1 \times 10^6 - 4 \times 10^6$ | 0.3 | Fh | Maisch (2019)[559] |
| | | | 5 μM | $1 \times 10^6 - 5 \times 10^6$ | 0.4 | Fh | Maisch (2019)[559] |
| | | | 10 μM | $2 \times 10^6 - 5 \times 10^6$ | 0.7 | Fh | Maisch (2019)[559] |
| | | | 20 μM | $2 \times 10^6 - 5 \times 10^6$ | 1.4 | Fh | Maisch (2019)[559] |
| | | | 30 μM | $2 \times 10^6 - 5 \times 10^6$ | 2.2 | Fh | Maisch (2019)[559] |
| *Sideroxydans lithotrophicus* ES-1 | 0.1 mM $Fe^{2+}$ | Culture cell, 20−23 °C | 9−10 μM | $2 \times 10^7$ | 4.3−5.0 | | Druschel (2008)[557] |
| | | | 15−16 μM | $2 \times 10^7$ | 7.0−9.1 | | Druschel (2008)[557] |
| | | | 25 μM | $2 \times 10^7$ | 3.4−5.5 | | Druschel (2008)[557] |
| | | | 45−50 μM | $2 \times 10^7$ | 3.3−5.5 | | Druschel (2008)[557] |



https://doi.org/10.1021/acs.chemrev.0c01286
Chem. Rev. 2021, 121, 8161−8233

Table 4. continued

| Microorganisms | Fe(II) form and concentration | Incubation parameters | Light flux/carbon/$O_2$ | Cells/mL | Max Fe(II) oxidation rate (mM/day) | Fe(II) oxidation products | References |
|---|---|---|---|---|---|---|---|
| | | | OVERALL RANGE | | 0.3–9.1 | | |
| Heterotrophic $NO_3^-$-reducers | | | | | | | |
| *Acidovorax* sp. BoFeN1 | 2 mM $Fe^{2+}$ | 30 °C, 5 mM $NO_3^-$ | 2 mM acetate | | 1.0 | Fh, Go | Kappler (2005) |
| | 4 mM $Fe^{2+}$ | | 2 mM acetate | | 1.2 | Fh, Go | Kappler (2005) |
| | | | 1 mM acetate | | 0.8 | Fh, Go | Kappler (2005) |
| | | | 0 mM acetate | | 0.1 | Fh, Go | Kappler (2005) |
| | 3 mM $Fe^{2+}$ | 30 °C, 10 mM $NO_3^-$ | 5 mM acetate | | 1.2 | Fe-phosphates | Miot (2009)[132] |
| | 5.5 mM $Fe^{2+}$ | 28 °C, 10 mM $NO_3^-$ | 5 mM acetate | $5 \times 10^7 - 8 \times 10^8$ | 5.5 | | Muehe (2009)[606] |
| | 3 mM $Fe^{2+}$ | 26 °C, 3 mM $NO_3^-$, pH 6.3–7.7, 0–3 mM $HCO_3^-$, 0–3 mM $HPO_4^-$, 0–3 mM humic aid | 0.3 mM acetate | $5 \times 10^7 - 4 \times 10^8$ | 0.1–5.0 | Lp, Go, Fe-phosphates | Larese-Casanova (2010)[561] |
| | 7 mM $Fe^{2+}$ | 28 °C, 10 mM $NO_3^-$ | 5 mM acetate | $5 \times 10^6$ | 2.3–3.5 | | Klueglein (2013)[546] |
| | 8 mM $Fe^{2+}$ | 28 °C, 10 mM $NO_3^-$ | 5 mM acetate | | 2.7 | Go | Klueglein (2014)[547] |
| | 3 mM $Fe^{2+}$ | 28 °C, 10 mM $NO_3^-$ | 5 mM acetate | $4–7 \times 10^8$ | 4.6–11.0 | | Peng (2018)[861] |
| | 3 mM Fe(II)–citrate | w. or w/o free $Fe^{2+}$ | | $4–7 \times 10^8$ | 2.6 w/o $Fe^{2+}$, 16.3–21.6 w $Fe^{2+}$ | | Peng (2018)[861] |
| | 3 mM Fe(II)–EDTA | w. or w/o free $Fe^{2+}$ | | $4–7 \times 10^8$ | 1.4–1.9 w/o $Fe^{2+}$, 8.9 w $Fe^{2+}$ | | Peng (2018)[861] |
| | 3 mM Fe(II)–fulvic acid | w. or w/o free $Fe^{2+}$ | | $4–7 \times 10^8$ | 0.5 w/o $Fe^{2+}$, 3.6 w $Fe^{2+}$ | | Peng (2018)[861] |
| | 3 mM Fe(II)–humic acid | w. or w/o free $Fe^{2+}$ | | $4–7 \times 10^8$ | <0.24 w/o $Fe^{2+}$, 3.1 w $Fe^{2+}$ | | Peng (2018)[861] |
| | | | OVERALL RANGE | | 0.1–21.6 | | |

[a]Experiments were performed at circumneutral pH unless otherwise stated.



https://doi.org/10.1021/acs.chemrev.0c01286
Chem. Rev. 2021, 121, 8161–8233

microbes under oxic conditions, releasing sulfate to the solution while Fe(III) is sequestered as a thin coating layer on the surfaces of the original pyrite minerals.[572] Pyrite (and FeS) oxidation can also be coupled to the reduction of nitrate in anoxic environments.[573,574] These reactions are catalyzed by *T. denitrificans*, representatives of the *Acidovorax* and *Geothrix* genera, and a *Marinobacter*-related isolate.[573,575,576] The involvement of direct enzymatic Fe(II) oxidation in nitrate-dependent pyrite oxidation is unclear. Sulfate was found to be released to the solution in multiple studies, but dissolved Fe was either not measured or cannot be accurately determined due to the catalytic oxidation of pyrite during acidic extraction in the presence of microbially produced nitrite.[577] Trace amounts of elemental sulfur in experimental setups could also contribute to the amount of sulfate released to the solution, complicating mass balance calculations associated with nitrate-dependent pyrite oxidation.[578]

Lastly, NRFeOx has been shown to oxidize Fe(II) in clays (e.g., illite,[579] smectites,[864] biotite[580] coupled to nitrate reduction, although a contribution of nitrite or Fe(III) as the responsible (abiotic) oxidant can also not be ruled out.

### 5.5. Controls on Microbial Fe(II) Oxidation Rates

Microbial Fe(II) oxidation rates are dependent on several interconnecting factors including the mechanism of oxidation (enzymatic vs chemically mediated), incubation parameters (pH, temperature, medium composition), cell numbers, substrate availability (e.g., $Fe^{2+}$, $O_2$, $NO_3^-$, organic carbon), aqueous $Fe^{2+}$ complexation, light flux (for photoautotrophic FeOx), mineral particle size, solubility and accessibility (for solid-phase Fe(II) oxidation), and of course, the specific microbial species itself. Here we highlight several studies in which one or more of these factors were systematically varied so as to allow direct and meaningful comparisons (Table 4).

The Fe(II) oxidation dynamics of three species of photoautotrophic FeOx: (a) Rhodobacter ferrooxidans strain SW2 (purple nonsulfur bacteria), (b) Thiodictyon sp. strain F4 (purple sulfur bacteria), and (c) Chlorobium ferrooxidans strain KoFox (green sulfur bacteria) in coculture with Geospirillum strain KoFum, were determined through culturing-based approaches.[565] These three cultures were chosen because they represent three different, distinct phylogenetic groups within photoautotrophic FeOx. In the presence of 4.7 mM dissolved $Fe^{2+}$, strain KoFox exhibited the highest maximum Fe(II) oxidation rates (1.6 mM/day), followed by strain F4 (0.9 mM/day) and SW2 (0.5 mM/day). The three species exhibited different periods of lag phase (7−10 days), but in all cases, dissolved $Fe^{2+}$ was completely oxidized within 20 days. In the presence of 40 mM FeS mineral, these species exhibited slightly higher Fe(II) oxidation rates (1.4−2.0 mM/day) compared to the oxidation of dissolved $Fe^{2+}$. Nonetheless, the rates in these two sets of experiments were comparable to one another, even though the concentration of the supplied FeS was about 10× higher than dissolved $Fe^{2+}$. This suggests that the photoautotrophic FeOx were dependent on the dissolved $Fe^{2+}$ generated by FeS dissolution rather than being capable of oxidizing the mineral themselves. This is supported by the lack of Fe(II) oxidation for poorly soluble minerals such as vivianite, pyrite, and magnetite in the same study. In another study, strain SW2 and *Rhodopseudomonas palustris* TIE-1 were also shown to oxidize 6 mM Fe(II)-GR (in green rusts) at a rate of 0.3−1.3 mM/day.[566] This rate is comparable to the oxidation rates measured for dissolved $Fe^{2+}$ for the respective species in previous studies (Table 4).

The same three species of photoautotrophic FeOx (SW2, F4, and KoFox) have been utilized to understand their Fe(II) oxidation rates as a function of pH, temperature, $Fe^{2+}$ concentrations, and light flux.[582] For pH, temperature, and $Fe^{2+}$ concentrations, the Fe(II) oxidation rate was found to follow a typical biological profile, i.e. having a middle optimum with lower to zero values on both sides of the optimum. The pH and temperature profiles were fitted to the cardinal temperature pH model (CTPM model),[583] yielding a range of pH (6.5−6.9) and temperature (23−26 °C) values for optimal Fe(II) oxidation (0.7−2.5 mM/day), with the exact values depending on the species. Within the tested range of 0.2−30 mM $Fe^{2+}$, the fastest Fe(II) oxidation rate was observed at 8 mM dissolved $Fe^{2+}$ for SW2 (2.5 mM/day), while $Fe^{2+}$ concentrations were not varied for the other two bacteria. Interestingly, Fe(II) oxidation by SW2 still occurs even at 30 mM $Fe^{2+}$ albeit at slower rates (0.5 mM/day), suggesting that some photoautotrophic FeOx are well-adapted to extreme Fe(II) concentrations. In terms of light flux, the Fe(II) oxidation rate increases with increasing light flux until the rate remains constant above a certain light flux threshold, indicating saturation of the photon-accepting sites of the enzymes. This profile can be described using Michaelis−Menten kinetics (eq 10):

$$V = \frac{V_{max} I}{K_M + I} \tag{10}$$

where $V$ = oxidation rate, $V_{max}$ = maximum oxidation rate, $I$ = light intensity, and $K_M$ = light intensity at which the oxidation rate equals 50% of $V_{max}$. To date, the highest measured Fe(II) oxidation rate by a photoautotrophic FeOx is 4.5 mM/day by strain F4 at 2,300 lx. The same approaches detailed in this study were used to describe the dependence of Fe(II) oxidation rates on pH, temperature, $Fe^{2+}$ concentrations, light flux, and/or salinity for other photoautotrophic FeOx.[584,585]

In addition to the aforementioned factors, microbial Fe(II) oxidation rates by photoautotrophic FeOx are also affected by the presence of other elements and complexing agents in the growth medium. The presence of Si likely contributed to higher cell tolerance toward elevated Fe(II) concentration, resulting in the increase of the rate of Fe(II) oxidation by strain KoFox by up to 2-fold, which is relevant for estimates of Fe(II) oxidation rates in the Si-rich Archean ocean.[586] Organic matter complexation was found to increase the rate of Fe(II) oxidation by up to 20-fold for *Rhodopseudomonas palustris* TIE-1.[563] It is thought that OM complexation may have decreased the energy barrier associated with the binding of Fe(II) and/or subsequent oxidation of Fe(II) by the Fe(II)-oxidizing enzyme—leading to faster rates—although further studies are needed to confirm the proposed mechanism(s).

The Fe(II) oxidation rates of an NRFeOx enrichment culture were investigated in the presence of different forms of Fe(II) (dissolved $Fe^{2+}$ as $FeSO_4$, synthetic $FeCO_3$, biogenic $FeCO_3$ and magnetite, surface-sorbed Fe(II) on microbially reduced goethite and soils).[569] Recalculation of the maximum Fe(II) oxidation rates from the presented data set yielded a range of 0.2−3.8 mM/day, with the highest rates measured in the following order: $Fe^{2+}$ > synthetic $FeCO_3$ > reduced soils > biomagnetite > reduced goethite > bio-$FeCO_3$. However, the initial Fe(II) contents (ranging from 2 mM for reduced goethite to 20 mM for $FeCO_3$) as well as the nitrate concentrations (2.5−


https://doi.org/10.1021/acs.chemrev.0c01286
Chem. Rev. 2021, 121, 8161−8233

6 mM) varied between treatments, thus complicating direct comparisons. Interestingly, the oxidation rate for synthetic $FeCO_3$ is significantly faster than bio-$FeCO_3$ (both supplied at 20 mM with nitrate = 5−6 mM), most likely as a result of variation in surface areas and particle sizes. Recent studies on the NRFeOx enrichment culture KS have highlighted the importance of organic carbon to the rate of Fe(II) oxidation. In the presence of 8−10 mM $Fe^{2+}$, the Fe(II) oxidation rates were faster under autotrophic conditions (2.0−3.5 mM/day) compared to mixotrophic conditions (1.2−2.0 mM/day in the presence of 5 mM acetate).[545,587,588] Under autotrophic conditions, the primary Fe(II)-oxidizing and $CO_2$-fixing *Gallionellaceae* sp. outcompetes the other heterotrophic nitrate-reducing strain present in the mixed culture. Under mixotrophic conditions, the community shifted to higher proportions of heterotrophic nitrate reducers, leading to slower rates of Fe(II) oxidation.[557] As mentioned previously, the rates of Fe(II) oxidation for microaerophilic FeOx reflect combined biological and abiotic oxidation, with higher microbial contributions at lower $O_2$ concentrations and pH values. The measured rates ranged from 0.3 to 9.1 mM/day,[557−559] which are overall higher than the rates exhibited by NRFeOx and photoautotrophic FeOx. These estimates were derived from cultures with typically micromolar levels of $Fe^{2+}$ as opposed to millimolar levels in batch cultures of NRFeOx and photoautotrophic FeOx, indicating that higher Fe(II) oxidation rates are generally expected from microaerophilic FeOx in environments with low $O_2$. Recent studies have shown that microaerophilic NRFeOx and photoautotrophic FeOx can coexist in the same redox zones in sediments, challenging the classical notion that they live in separate redox zones expected from thermodynamic constraints.[589,645] Determining the relative contribution of different types of FeOx to Fe(II) oxidation will be crucial to understanding Fe biogeochemistry in suboxic−anoxic environments.

Heterotrophic nitrate-reducing bacteria can oxidize Fe(II) indirectly through the production of reactive nitrite which reacts rapidly (abiotically) with Fe(II) via chemodenitrification. As shown in Table 4, strain BoFeN1 (the most studied bacteria with this metabolism) exhibited even higher maximum Fe(II) oxidation rates (up to 21.6 mM/day, typically < 5.5 mM/day) than microaerophilic FeOx. Heterotrophic nitrate-reducing bacteria also exist in the NRFeOx enrichment culture KS, but nitrite never accumulated to high concentrations in that mixed culture. Nitrite was detectable only when the heterotrophic nitrate-reducing bacteria were isolated into pure cultures. Therefore, the environmental significance of biologically mediated Fe(II) oxidation via nitrite is a subject of ongoing debate.[587]

### 5.6. Fe Redox Cycling Involving Fe(II)-Oxidizing and Fe(III)-Reducing Microorganisms

Very recently, it has been demonstrated that microorganisms can reduce and oxidize mixed-valent (Fe(II)- and Fe(III)-containing) minerals such as magnetite in alternating redox cycles (under alternating reducing and oxidizing conditions) using these minerals as biogeobatteries.[590] Specifically, it has been shown that both phototrophic FeOx as well as NRFeOx can extract electrons from magnetite oxidizing some of the magnetite-Fe(II) to Fe(III), while Fe(III)-reducing microorganisms (*Shewanella, Geobacter*) are able to dump electrons during their metabolism on the same magnetite particles, thus rereducing some of the Fe(III) to Fe(II). The rates and extent of these processes depend on the magnetite particle size.[591] Magnetite particles have also been shown to enhance interspecies electron transfer in various lab and natural environments with particularly important implications for the rate of anaerobic pollutant degradation and methane formation.[592−601] However, the extent to which redox Fe cycling occurred in the magnetite in those studies has not been evaluated.

Recent work has highlighted the importance of cryptic cycles of Fe, in which Fe(II) or Fe(III) concentrations appear to be at steady-state even as intense redox cycling occurs at small spatial scales.[602] For example, continuous oxidation of Fe(II)−OM complex by phototrophic FeOx coupled to rapid abiotic rereduction of the produced Fe(III)−OM complex by photochemistry can sustain a low and steady-state dissolved $Fe^{2+}$ concentration.[603] Intense redox cycling of Fe, despite low overall Fe concentrations, was also demonstrated to be coupled by phototrophic and microaerophilic Fe(II) oxidizers to anaerobic Fe(III) reducers in the water column of a stratified lake.[604,605] Thus, one single atom of Fe that is being continuously (re)cycled increases the overall energy available to microbial populations. Fe-based remediation designs that incorporate the possibility of cryptic cycles may eventually lead to more rapid and efficient pollutant removal.

## 6. BIOGEOCHEMICAL PROCESSES INVOLVING FORMATION AND REACTIVITY OF FE(II)

The frequency and magnitude of redox fluctuations are important drivers of organic carbon and nutrient cycling in soils[389,390] and sediments.[17] The more frequent and rapid these fluctuations are, the more dynamic these systems are in terms of Fe-associated organic carbon mineralization and P, N, and S availability due to the preferential formation of poorly crystalline Fe(III) (oxyhydr)oxide species under such varying oxygen conditions.

Additionally, the onset of anoxic conditions in natural waters typically results in a dramatic increase in the concentration of Fe(II) with this phenomenon a major water quality concern in stratified lakes where reductive dissolution of Fe(III) minerals in benthic sediments and subsequent accumulation of Fe(II) in anoxic hypolimnetic waters may result in severe quality issues in domestic supplies if these waters enter reticulation systems. In oxic surface waters, light- and superoxide-mediated reductive dissolution of iron oxides and the subsequent formation of bioavailable Fe(II) may induce the growth of phytoplankton either because of the corelease of major nutrients such as phosphorus (as is the case in many freshwaters) or because of the increased bioavailability of iron, a micronutrient recognized to limit organism growth in coastal and open oceans.

In the previous sections, specific consideration has been given to the redox chemistry of soluble Fe(II) complexes, sorbed Fe(II), and structural Fe(II) from different perspectives. In this section, we briefly describe the biogeochemical cycling of nutrients associated with Fe in various soils, sediments, and natural waters and introduce some of the biogeochemical implications of Fe(II) formation. Some of these effects are related to aqueous Fe(II) (as is the case for formation of bioavailable Fe in oceanic surface waters) while others are related to solid-phase Fe(II) (as is the case for Fe(II)-mediated transformation of iron oxides and the reduction of contaminants or key nutrients in sediments). It is important to appreciate, however, that the examples presented only represent some of the environments in which these reactions can occur and that these


https://doi.org/10.1021/acs.chemrev.0c01286
Chem. Rev. 2021, 121, 8161−8233

reactions are essentially ubiquitous in all pedological and aquatic environments considering iron is the second most abundant metallic element in the earth's crust.[607]

### 6.1. Biogeochemical Cycling Associated with Fe in Soils

In soils the reduction of Fe (oxyhydr)oxides to produce Fe(II) is almost exclusively driven by microbial catalysis.[40] In fact, anaerobic respiration coupled to Fe (oxyhydr)oxide reduction is the primary terminal electron-accepting process, accounting for 40 to 60% of the ecosystem respiration in arctic permafrost soils.[608] This can have important implications to the fate of the large amounts of organic carbon stored in Arctic soils.[608] Indeed, thermodynamics predicts that Fe (oxyhydr)oxide reduction may out-compete methanogenesis under anaerobic conditions, potentially serving as a means to suppress methanogenesis into the future.[608] While the complexities of the Fe cycle to greenhouse gas emissions, particularly from arctic soils, are difficult to predict, this is something to look out for in the future.

Remarkably, direct contact between microbes and Fe (oxyhydr)oxides is not necessary to induce the reduction of Fe(III),[40] with this process able to occur at a distance through the release of electron shuttling compounds or chelators or the production of conductive nanowires by microbes.[106] For example, Fe (oxyhydr)oxide reduction in upland soils is driven by organic matter exudates from root plants, ultimately derived by photosynthesis, with these exudates able to shuttle electrons from microbes to Fe (oxyhydr)oxides. The resultant reduced aqueous Fe(II) species is then able to be transported away from the rhizosphere and into the neighboring environment, resulting in some very striking color contrasts between rhizospheres and inter-rhizosphere microsites.[609]

Due to depth-dependent concentrations of oxygen diffusion, solid Fe speciation is found to change with depth, with more rapid Fe cycling in the shallow horizons of upland soils resulting in Fe (oxyhydr)oxides that are more reactive and therefore able to undergo more rapid reduction, while more stable crystalline species are found at depth.[610] This is associated with the persistence of Fe(II) at depth, facilitating Fe(II)-catalyzed Fe (oxyhydr)oxide transformations to those which are more crystalline, or the formation of reactive structural Fe(II) minerals such as green rust and magnetite.[283,611]

The presence of reactive Fe mineral surfaces of low crystallinity in arctic and boreal peat soils has been found to effectively compete with biological phosphate sequestration processes, thereby acting as a powerful regulator of nutrients in these sensitive ecosystems.[612] This potentially restricts plant growth and the sequestration of $CO_2$ from the atmosphere,[612] but it may also result in Fe minerals acting as important reservoirs for phosphate in these P-limited systems.[612] It will be interesting to observe the dominant impact of Fe(II) on P availability in these sensitive systems over time as a result of climate change, particularly as evapotranspiration and water table fluctuations are predicted to become more extreme.

Wet tropical soils, which are often dominated by iron-rich clays and oxides, provide one of the most dynamic natural soil environments to study Fe-associated redox fluctuations, with these fluctuations readily driven by these soils' high biological oxygen demand, moisture, temperature, and abundance of labile carbon.[390] As such, these soils in particular are widely studied to determine the impact of Fe redox chemistry on soil organic carbon in general. Indeed, tropical soils have revealed some amazing findings in relation to the impact of Fe redox chemistry on soil carbon cycling. Fluctuating redox conditions encourage the oxidation of soil carbon to $CO_2$ due to the generation of ROS following abiotic Fe(II) oxidation in conjunction with anaerobic metabolism,[613,614] and indeed, Fe-rich soils are often reported to have high rates of $CO_2$ and $NO_x$ emissions.[615]

Nevertheless, over time, iron oxide crystallinity increases, associated with Fe(II)-catalyzed transformation processes,[614,616,617] and this makes the Fe (oxyhydr)oxides within these soils less prone to reductive dissolution, providing a degree of protection against soil carbon mineralization to $CO_2$. Similarly, the formation of Fe−soil organic matter (SOM) aggregates with soil minerals such as clays, again aided by the presence of Fe(II) (through a process of Fe(II) oxidation and SOM coprecipitation), is known to make soil organic carbon more resistant to oxidation and degradation (i.e., more stable) over time.[614,618,619] Fe(III) (oxyhydr)oxides are traditionally thought to aid in the persistence of organic matter in soils as sorption of SOM onto, or coprecipitation of SOM with, Fe (oxyhydr)oxides makes them less susceptible to mineralization, and recent studies broadly confirm this finding. However, the more wide ranging impacts of iron redox chemistry make this correlation less than perfect.[614] Overall, the production of Fe-SOM aggregates via Fe(II) oxidation will initially increase $CO_2$ production in the short term because of a pulse of hydroxyl radicals generation; however, over time, the Fe−SOM aggregates protect SOM from oxidation, resulting in a net decrease in C mineralization.[614] In relation to the cycling of nutrients, such as nitrogen, the anaerobic oxidation of ammonium to nitrite, nitrate, or dinitrogen has been observed in wetland soils under Fe(III)-reducing conditions.[620] The relative importance of abiotic or biotic processes involved in the coupled oxidation of ammonia and reduction of Fe(III) minerals, as well as their ecological effects under field conditions, however, is an area that still requires further clarification.[621] In paddy soils, microbial and abiotic reduction processes are associated with the release of trace amounts of nitrous oxide and nitrogen gas.[622−624] While this is highly undesirable as it results in losses of nitrogen from the soil (and therefore low fertilizer efficiency) as well as the release of potent greenhouse gases (notable $N_2O$), under conditions where oxygen may form, such as at the roots of rice plants, the ability for nitrification to occur, associated with the formation of iron oxides, counters much of this loss.[622] Much of the cycling of N with iron in soils is associated with microbial activity, although N cycling in highly dynamic redox environments is likely to be related to carbon cycling and the ferrous Fe redox wheel both abiotically and biotically.[621] Indeed, a recent study has shown that the abiotic production of $N_2O$ coupled to Fe(II) oxidation can be important in soils containing elevated Fe(II) and SOM concentrations.[623]

An important impact of the formation of Fe(II) and its subsequent interaction with Fe (oxyhydr)oxides that also needs to be acknowledged here is the ability of Fe(II)−Fe (oxyhydr)-oxides to induce the natural attenuation of pollutants in ground waters and soil. Contaminants able to undergo Fe(II)−Fe (oxyhydr)oxide interactions include chlorinated organics and a host of redox active inorganic contaminants such as arsenic and uranium. Readers are referred to the review by Borch et al. (2010) for more information on these important Fe(II)−Fe (oxyhydr)oxide interactions in soils,[6] in addition to section 4.2.1 of this review.


https://doi.org/10.1021/acs.chemrev.0c01286
Chem. Rev. 2021, 121, 8161−8233

Table 5. Summary of the Reported Work on Fe(II) Species-Associated Fenton-Type Reactions

| Fe(II) species | Oxidant | Model Compounds | Reactivity | Reactive Species | ref |
|---|---|---|---|---|---|
| **Fe(II)** | | | | | |
| Fe(II) | $H_2O_2$ | formate | pH-dependent | •OH | 2008[701] |
| Fe(II) | $H_2O_2$ | phenol | 100% removal in 5 min | •OH | 2011[702] |
| Fe(II) | $H_2O_2$ | dimethyl sulfoxide (DMSO), *tert*-Butyl alcohol | | Fe(IV), •OH | 2014[658] |
| Fe(II) in acid mine drainage (AMD) | $O_2$ | *p*-aminobenzenesulfonamide | 19.3% removal in 4 h | •OH | 2017[697] |
| **Fe(II)−ligand complexes** | | | | | |
| Fe(II)−hydroxylamine | $H_2O_2$ | benzoic acid | *p*-hydroxybenzoic acid was formed | •OH | 2011[673] |
| Fe(II)−ascorbate | $O_2$ | rhodamine B | 39.5% removal in 6 h | •OH | 2016[676] |
| Fe(II)−fulvic acid | $H_2O_2$ | | | •OH | 2013[637] |
| **Structural Fe(II)** | | | | | |
| Magnetite | $H_2O_2$ | polycyclic aromatic hydrocarbons (PAHs) | 90% removal | •OH | 2012[680] |
| Magnetite−ascorbate | $H_2O_2$ | Alachlor | 62.6% removal | •OH | 2020[681] |
| Mackinawite | $O_2$ | benzoic acid | | $•OH_{ads}$ | 2020[329] |
| **Surface-sorbed Fe(II)** | | | | | |
| Fe(II)−nZVI | $O_2$ | malonate | | •OH | 2004[691] |
| Fe(II)−nZVI/ferrihydrite/lepidocrocite | $O_2$ | formate | | •OH | 2016[692] |
| Fe(II)−hematite (001) facets | $H_2O_2$ | rhodamine B | 47% removal | •OH | 2016[449] |
| Fe(II)−hematite (110) facets | $H_2O_2$ | rhodamine B | 90% removal | •OH | 2016[449] |
| Fe(II) in aquifer sediment | $O_2$ | As(III) | As(III) was oxidized to As(V) | •OH | 2016[696] |
| Fe(II) in soil and sediment | $O_2$ | phenol | adsorbed Fe(II) and structural Fe(II) predominantly contributed to •OH formation | •OH | 2020[695] |

### 6.2. Biogeochemical Cycling of Carbon and Other Nutrients Associated with Fe in Sediments

Field studies have demonstrated how the upper few centimeters of lake and estuarine river sediments are impacted by fluctuating redox conditions that control the concentrations and speciation of iron, sulfur, and phosphorus in the overlying waters and associated pore waters,[17] with this layer highly enriched in poorly crystalline, reactive iron oxyhydroxides.[625] Such oxides, when resuspended in the water column, may then become a source of bioavailable iron to primary producers.[625] This occurs via the reduction of iron(III) minerals in the sediments through dissimilatory Fe(III) reduction, whereby microbes couple this process to organic carbon oxidation[40] over time-scales ranging from hours to days to years. The Fe(II) released from Fe(III) mineral reduction may precipitate as a sulfide mineral in the presence of sufficient sulfide concentrations,[17,191] precipitate as a mixed Fe(II)−Fe(III) mineral such as green rust or magnetite,[285,626] or diffuse upward and undergo oxidation by oxygen, nitrate, or manganese oxides.[627] This process results in an iron-enriched layer just above the sediment "redox" boundary (or oxygen penetration depth).[625]

In addition to the release of Fe(II), any species associated with the iron oxides may be released into the water column. Phosphorus is one of the most significant species able to be released from Fe (oxyhydr)oxides as it is a major limiting nutrient for the formation of harmful algal blooms (HAB).[628] Even when external inputs of P are low, the rapid reduction and release of P trapped in iron oxides from sediments can lead to eutrophication of environmental waters.[629] The resultant decay of the excess organic matter produced (in the form of algae) is able to strip these waters of oxygen leading to deadly fish kills, as well as toxic levels of sulfide.[17] Considering that many estuarine waters are highly productive, this is of particular ecological concern. Interestingly, the release of P from Fe (oxyhydr)oxide sediments is actually enhanced during HAB,[630] predominately due to the rise in anoxic conditions that further enhance Fe (oxyhydr)oxide dissolution to Fe(II)[631] but also due to the desorption of phosphate from Fe (oxyhydr)oxide surfaces as the pH increases, resulting in conditions which prolong the lifespan of the bloom.[632]

In relation to nitrogen, the production of Fe(II) from the dissolution of Fe (oxyhydr)oxides in lake sediments and its subsequent oxidation have been shown to drive dissimilatory nitrate reduction to ammonium while reducing denitrification.[633] Field and culture studies have also demonstrated that there is a complex interaction between abiotic and biotic Fe(II) oxidation processes in relation to nitrogen oxide reduction[634] and that ephemeral Fe(II)−Fe(III) minerals such as green rust are likely to be important drivers of nitrate reduction in sediments in addition to nitrate reducing bacteria.[69] This further strengthens the importance of Fe-cycling and the production of Fe(II) toward the biogeochemical cycling of key nutrients in sediments.[635]

Following the release of Fe(II) and the return of oxic conditions, the oxidation of reduced iron in environmental water bodies and sediments can result in the production of reaction oxygen species (ROS)[636−638] which are capable of inducing oxidative damage to fish.[639] However, while the impact of Fe (oxyhydr)oxide reduction and the subsequent release of nutrients and Fe(II) may be highly detrimental for most environmental water bodies in relation to the formation of HAB and ROS, at the mouth of large marine water bodies, this process becomes an important source of nutrients in otherwise nutrient deficient seawaters, as discussed in the following section.


https://doi.org/10.1021/acs.chemrev.0c01286
Chem. Rev. 2021, 121, 8161−8233

### 6.3. Biogeochemical Cycling of Carbon and Other Nutrients Associated with Fe(II) Formation in the Oceans

Iron redox chemistry has played an important role in the evolution of Earth. In the anoxic early oceans, iron would have been present principally in Fe(II) form and thus would have been substantially more bioavailable. Indeed, the fact that iron exists in a number of proteins today, despite the passage of time and the rise of an oxygenated atmosphere that has vastly reduced the solubility of iron, indicates that iron was once much more accessible to early biological systems.[640] However, as a result of the low solubility of oxidized iron in the absence of ligands at neutral pH, iron acquisition poses a problem for organisms in the oxidized oceans of today.[641] To overcome this, most prokaryotes produce siderophores, which have an extremely high affinity for iron.[642] As discussed earlier, siderophores form soluble ferric chelates that are taken up by the cells via high affinity receptors. In the euphotic zone of oceans, these ferric siderophore complexes are also able to undergo photolysis,[46,47,643] or reduction by photoproduced superoxide,[644] further increasing the bioavailability of iron through the formation of Fe(II).

The availability of iron in the ocean has a huge impact on the production of phytoplankton, which underpins the global carbon cycle.[160] Considering that the ocean is one of the world's largest sinks for carbon dioxide, various experiments have been conducted around the world to assess if "iron seeding" of the oceans can reduce global $CO_2$ levels.[646−648] Much controversy exists as to the wisdom of such an engineered approach given the complex nature of iron redox chemistry and the potential for unaccounted reactions that may have undesirable side-effects.[648,649]

## 7. FE(II)-ASSOCIATED OXIDATION PROCESSES

### 7.1. Fenton Type Reactions

In 1894, Henry J. Fenton found that tartaric acid was oxidized by a combination of $Fe^{2+}$ salts and $H_2O_2$ and concluded that $H_2O_2$ was activated by $Fe^{2+}$.[650] Since then, the Fenton reaction has become one of the most important reactions in environmental remediation due to its ability to generate powerful oxidants that can facilitate so-called advanced oxidation processes (AOPs), capable of oxidizing a large array of environmental contaminants (examples in Table 5). In 1932, Bray and Gorin reported that the ferryl ion (Fe(IV)) was involved in the Fenton reaction (Bray−Gorin mechanism).[651] Then in 1934, Haber and Weiss proposed that Fe(II) was oxidized by $H_2O_2$ to produce hydroxyl radicals and hydroxyl ions, and the Haber−Weiss iron redox cycle was thus established.[652] Fe(II) can decompose $H_2O_2$ via a competitive outer-sphere one-electron transfer to produce hydroxyl radicals with its redox cycle shown in eqs 11 and 12 and via an inner-sphere two-electron oxidation through O-atom transfer to produce high valent iron species (eq 13). Nevertheless, hydroxyl radials are often referred to as the reactive species in the Fenton reaction in the majority of the modern literature,[653,654] although recent studies demonstrate that high valent iron species, i.e., the Bray−Gorin mechanism, may play a significant role in Fenton reactions under certain conditions, such as circumneutral pH.[655−658] Because Fenton type reactions have been comprehensively reviewed in the recent literature,[659−663] we intend to be brief in this section and only summarize how Fe(II)−ligand complexes, structural Fe(II), and sorbed Fe(II) are involved in Fenton type reactions.

$$Fe(II) + H_2O_2 \rightarrow Fe(III) + {}^{\bullet}OH + OH^- \quad (11)$$

$$Fe(III) + H_2O_2 \rightarrow Fe(II) + HO_2^{\bullet} + H^+ \quad (12)$$

$$Fe(II) + H_2O_2 \rightarrow Fe(IV)\ (e.g., Fe^{IV}O^{2+}) + H_2O \quad (13)$$

While debate on the mechanism continues, this has not affected their widespread applications in environmental sciences, geosciences, biology, and engineering.[664−666] In particular, the development of ligand-mediated Fenton type reactions is a rapidly growing field in the engineering field due to its ability to extend the working pH range relative to conventional aqueous-based Fenton reactions and prevent ferric precipitation which would otherwise diminish the efficiency of pollutant removal through loss of iron.[660,661] Various studies have investigated the use of Fe(II) ligands to activate molecular oxygen or hydrogen peroxide to generate hydroxyl radicals and oxidize organic organics.[659,660,667−671] Some of these ligands are also reductants that can accelerate iron redox cycling and enhance the reaction rate.[672] For instance, the addition of hydroxylamine facilitates the reduction of Fe(III) to Fe(II), maintaining a steady concentration of Fe(II) and increasing the reactivity of the system.[673] However, hydroxylamine is toxic to humans, limiting its applicability, so ligands such as ascorbate have been applied to AOPs instead.[674,675] Fe(II)-ascorbate complexes have been used to activate molecular oxygen, producing hydroxyl radicals that efficiently degrade rhodamine B.[676] Reducing ligands, however, can also consume the produced hydroxyl radicals,[677] and therefore, determination of the optimum dose is important. The reaction rate of various Fe(II) complexes with $H_2O_2$ differs, with the following trend in reactivity observed: ethylenediamine-N,N′-diacetic acid (EDDA) > ethylenediaminetetraacetic acid (EDTA) > diethylenetriaminepenta-acetic acid (DTPA) > nitrilotriacetic acid (NTA),[669] consistent with the rate of $H_2O_2$ decomposition being strongly correlated with the stability constant of the Fe(III)−ligand complex formed.[678] The presence of iron complexing agents also appears to influence the nature of the oxidant formed, with a nonhydroxyl radical oxidant produced at circumneutral pH in the absence of ligands but hydroxyl radicals generated if a complexing agent is present.[638] NOM has also been shown to induce the formation of hydroxyl radicals upon the reaction of the Fe(II)−NOM complex with $H_2O_2$ at circumneutral pH, with an estimated $^{\bullet}OH$ production rate of 37 $nM{\cdot}h^{-1}$ under conditions typical of coastal waters.[637]

Structural Fe(II) in iron-containing minerals can also initiate Fenton type reactions. The reactivity of many Fe(II)-containing minerals to initiate a Fenton process has been shown to be strongly correlated with Fe(II) content.[660,679] A major representative structural Fe(II)-containing mineral is magnetite. Previous studies have demonstrated that 90% of polycyclic aromatic hydrocarbons (PAHs) can be oxidized by hydroxyl radicals generated when mixing magnetite and hydrogen peroxide.[680] Similarly, ascorbate-coated magnetite can efficiently decompose hydrogen peroxide to produce hydroxyl radicals to oxidize alachlor.[681] Some studies report that Fe(II) surface sites on magnetite (heterogeneous Fenton reactions) instead of released aqueous Fe(II) from magnetite (homogeneous Fenton reactions) play the dominant role in decomposing $H_2O_2$,[682] while other studies suggest the release of Fe(II) from magnetite under acid conditions reacts with $H_2O_2$.[683] Further research is hence needed to elucidate the relative contribution of heterogeneous vs homogeneous Fenton reactions for magnetite


https://doi.org/10.1021/acs.chemrev.0c01286
Chem. Rev. 2021, 121, 8161−8233

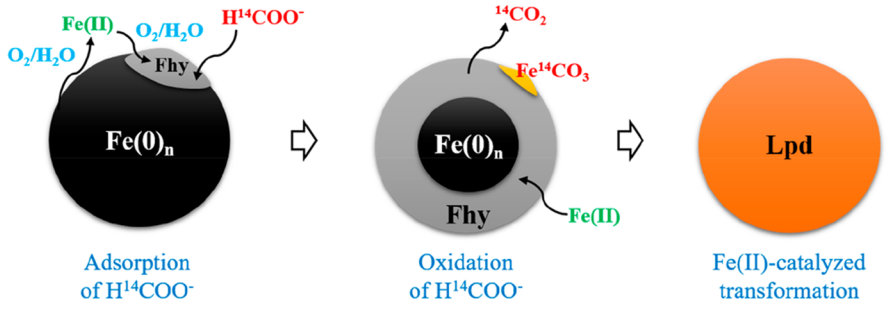


**Figure 13.** Investigation of formate oxidation by nZVI-mediated generation of Fe(II) and $H_2O_2$ indicates that oxidation was effective only after formation of iron oxides at the nZVI surface which acted as sorbing sites for the target organic compound. Interestingly, Fenton-mediated formate oxidation continued long after the nZVI had been consumed. Reprinted with permission from ref 692. Copyright 2016 American Chemical Society.

**Table 6. Summary of the Reported Work on the Activation of Peroxydisulfate (PDS) and Peroxymonosulfate (PMS) by Fe(II) Species**

| Fe(II) species | Persulfate | Contaminant | Reactivity | Reactive Species | ref |
|---|---|---|---|---|---|
| **Fe(II)** | | | | | |
| Fe(II) | PDS | trichloroethylene (TCE) | 95% removal | proposed $SO_4^{\bullet-}$ | 2004[703] |
| Fe(II) | PMS | 2-chlorobiphenyl (2-CB) | 90% removal | $SO_4^{\bullet-}$and $^{\bullet}OH$ | 2009[704] |
| Fe(II) | PDS | diuron | maximum: 80% | $SO_4^{\bullet-}$ | 2011[705] |
| Fe(II) | PDS | methyl phenyl sulfoxide (PMSO) | decreased in the first 2 min, and then leveled off | Fe(IV) | 2018[706] |
| Fe(II) | PDS | trimethoprim | 73.4% removal in 4 h | | 2018[164] |
| Fe(II) | PDS | acetaminophen | fast reaction in first 3 min | $SO_4^{\bullet-}$and $^{\bullet}OH$ | 2019[707] |
| Fe(II) | PDS | PMSO, dimethyl sulfoxide, *p*-nitrobenzoic acid (*p*-NBA), and benzoic acid (BA) | | Fe(IV), $SO_4^{\bullet-}$ and $^{\bullet}OH$ | 2020[708] |
| Fe(II) | PDS | antibiotic resistant microbes (ARMs) | 99.9% removal in 2 h | Fe(IV) and $SO_4^{\bullet-}$ | 2020[709] |
| Fe(II) | PDS | p-arsanilic acid | 99% removal in 10 min | | |
| **Fe(II)−ligand complexes** | | | | | |
| Fe(II)−citric acid | PDS | TCE | 100% removal in 20 min | proposed $SO_4^{\bullet-}$ | 2004[710] |
| Fe(II)−citric acid | PMS | 2-CB | 74% removal in 4 h | $SO_4^{\bullet-}$and $^{\bullet}OH$ | 2009[704] |
| Fe(II)−citric acid | PDS | trichloroethylene | 100% removal in 60 min | $SO_4^{\bullet-}$, $^{\bullet}OH$, and $O_2^{\bullet-}$ | 2014[711] |
| Fe(II)−citric acid; -EDTA; -EDDS | PDS | sulfamethoxazole | 74.7% removal in 240 min | $SO_4^{\bullet-}$ and $^{\bullet}OH$ | 2014[712] |
| Fe(II)−citric acid; -oxalic acid; Fe(II)−tartaric acid; -EDDS | PDS | aniline | oxalic acid and tartaric acid are more effective | $SO_4^{\bullet-}$ and $^{\bullet}OH$ | 2015[713] |
| Fe(II)−oxalate acid; -citric acid; -nitrilotriacetic; -EDTA; -pyrophosphate; -tetrapolyphosphate | PDS | PMSO | decreased in 90 min | Fe(IV) and/or $SO_4^{\bullet-}$ | 2019[714] |
| **Structural Fe(II)** | | | | | |
| FeS; pyrite | PDS | 2,4-dinitrotoluene | 91% removal in 300 min | proposed $SO_4^{\bullet-}$ | 2011[715] |
| Magnetite | PDS | 2,4,4′-trichlorobiphenyl | 90% removal in 4 h | $O_2^{\bullet-}$ and $SO_4^{\bullet-}$ | 2013[716] |
| FeS | PDS | *p*-chloroaniline | $k_{obs}$: 0.0144 $min^{-1}$ | $SO_4^{\bullet-}$ and $^{\bullet}OH$ | 2018[717] |
| Titanomagnetite | PDS | atrazine | $k_{obs}$: 2.7 × $10^{-2}$ $min^{-1}$ | Fe(IV), Fe(V), $SO_4^{\bullet-}$, and $^{\bullet}OH$ | 2020[718] |
| Pyrite | PDS | atrazine | 70% decrease in 10 min | $SO_4^{\bullet-}$, $^{\bullet}OH$, and $O_2^{\bullet-}$ | 2020[719] |
| **Surface-sorbed Fe(II)** | | | | | |
| Magnetite, hematite, goethite, $MnO_2$ | PDS | diesel | 36% removal in 12h | N/A | 2010[720] |

under different conditions. To enhance the reactivity of magnetite in Fenton reactions, ZVI/magnetite composites have been synthesized to favor electron transfer from ZVI to magnetite to generate structural Fe(II) to maintain the reactivity.[684] Some chelating ligands (e.g., oxalate, EDTA, citrate, and succinate) have also been shown to enhance the degradation rate of contaminants by magnetite/$H_2O_2$, due to the involvement of homogeneous Fenton reactions.[685] Moreover, the replacement of Fe(II) with $Co^{2+}$ and $Mn^{2+}$ at octahedral sites in magnetite has been shown to enhance the reactivity of magnetite.[682]

In addition to participating in Fenton reactions, structural Fe(II)-containing minerals can be oxidized by oxygen to form reactive oxygen species (ROS). For instance, under acidic conditions, hydrogen peroxide is produced from the reduction of molecular oxygen by Fe(II) within pyrite, which is then able to decompose forming hydroxyl radicals.[686,687] The reaction mechanism between pyrite and oxygen, however, is still not well


https://doi.org/10.1021/acs.chemrev.0c01286
Chem. Rev. 2021, 121, 8161−8233

understood.[688] Similar effects to those observed for pyrite have also recently been reported for mackinawite (FeS).[689] However, some studies have reported that, during the oxygenation of FeS, the surface-localized oxidant generates a suite of products upon reaction with benzoic acid which are very different from those produced by the reaction with solution-phase hydroxyl radicals, indicating homogeneous hydroxyl radicals are not the main oxidant in the reaction process.[329] Further research is needed to elucidate the exact cause of these differences.

Fe(II) sorbed to solid surfaces can also initiate heterogeneous Fenton reactions to catalyze the generation of highly oxidizing ROS which, in turn, indirectly degrade environmental pollutants. In oxic conditions, Fe(II) generated upon the oxidation of nZVI reacts with $H_2O_2$ produced from nZVI-mediated reduction of oxygen, with the hydroxyl radicals formed capable of oxidizing a wide range of contaminants.[690,691] Interestingly, more recent work by He et al.[692] suggests that the initial formation of ferrihydrite on the nZVI is the prerequisite for the oxidation of target organics, which also promotes the adsorption of the organics (Figure 13). Of relevance to this observation, sorbed Fe(II) on different iron oxide facets demonstrates different $H_2O_2$ decomposition efficiencies, with Fe(II) bound to hematite (110) facets exhibiting a higher degradation rate than the (001) counterpart.[449,693,694]

Iron redox processes can occur under oxic conditions in natural systems as a result of Fenton type reactions, opening up additional pathways for pollutant degradation.[695,696] That is, in addition to the direct reduction reactions described in the previous sections, the Fenton type reactions enable Fe(II) and Fe(II)-associated species to indirectly degrade pollutants by reacting with other environmental oxidants to produce more powerful oxidants capable of degrading a much wider range of contaminants. In environmental processes, different Fe(II)-containing materials have been reported to contribute to ROS generation to degrade contaminants. As an example, Tong et al. demonstrated that oxygenation of subsurface sediments at different depths and the generated hydroxyl radicals are predominantly a result of the reduction of oxygen by Fe(II) within the sediments.[696] Based on a similar mechanism, oxygenation of Fe(II) in acid mine drainage (AMD) can produce hydroxyl radials to degrade *p*-aminobenzenesulfonamide.[697] Xie et al. recently revealed that both surface-sorbed Fe(II) and structural Fe(II) were the predominant contributors to the production of hydroxyl radicals during the oxygenation of different natural sediments for phenol degradation.[695]

It is worth mentioning that iron(III) oxides and oxyhydroxides alone are able to directly decompose hydrogen peroxide in heterogeneous Fenton reactions, generating hydroxyl radicals sustained by ongoing autocatalytic regeneration of Fe(II).[665] While the rate of hydrogen peroxide-mediated reduction of Fe(III) within iron(III) oxyhydroxides is slow, there are many methods to facilitate more rapid production of Fe(II) and subsequent generation of hydroxyl radicals. For instance, the addition of hydroxylamine promotes the reduction of Fe(III) on the surface of goethite generating hydroxyl radicals to degrade a herbicide.[698] More details on the utilization of iron(III) oxides and oxyhydroxides in heterogeneous Fenton type reactions can be found in previous reviews.[699,700]

### 7.2. Persulfate Activation by Fe(II) Species

Sulfate radical-based advanced oxidation processes (SR-AOPs) have attracted increasing attention in the past decades in treating contaminated water and soil. Peroxymonosulfate (PMS, $HSO_5^-$) and peroxydisulfate (PDS, $S_2O_8^{2-}$) are common sources of sulfate radicals in SR-AOPs. Compared with traditional $^{\bullet}OH$-based AOPs, SR-AOPs have unique advantages because $SO_4^{\bullet-}$ (a) has a high redox potential ($E^0(SO_4^{\bullet-}/SO_4^{2-})$ = 2.6−3.1 V vs NHE); (b) has a long half-life (30−40 $\mu$s); (c) works within a relatively wide pH range; and (d) has a low cost of storage and transportation.[721,722]

Different methods have been employed to activate persulfates,[722−724] among which Fe(II) species have been shown to be effective (Table 6) with the reaction mechanisms summarized below:

$$HSO_5^- + Fe(II) \rightarrow SO_4^{\bullet-} + OH^- + Fe(III) \quad (14)$$

[704]

$$S_2O_8^{2-} + Fe(II) \rightarrow SO_4^{\bullet-} + SO_4^{2-} + Fe(III) \quad (15)$$

[711]

$$SO_4^{\bullet-} + Fe(II) \rightarrow SO_4^{2-} + Fe(III) \quad (16)$$

[704]

Increasing Fe(II) concentration often enhances the performance of persulfates. However, too much Fe(II) decreases the reactivity of persulfates owing to the quenching reaction between Fe(II) and sulfate radicals (eq 16).[703,705,725] The optimum ratio of Fe(II)/PMS in the degradation of PCBs is reportedly 1:1;[704] therefore, an efficient strategy is to gradually add Fe(II) of a low concentration to improve the degradation of contaminants by $SO_4^{\bullet-}$.[703] The oxidation rates of contaminants in Fe(II)/PDS systems decrease with increasing pH, likely due to the strong precipitation of iron and the self-decomposition of PDS under higher pH conditions.[726]

It has been long recognized that free radicals ($SO_4^{\bullet-}$ and $^{\bullet}OH$) are the dominant reactive species in the activation of persulfates by Fe(II), but this idea has been challenged in recent studies. By employing an interesting chemical probe (methyl phenyl sulfoxide (PMSO)), Wang et al. (2018) demonstrated that in Fe(II)−PDS systems, a high valent iron−oxo species (Fe(IV)) was the dominant reactive species under acidic conditions.[706,727] This is because sulfoxides such as PMSO can be oxidized to form corresponding sulfones (e.g., methyl phenyl sulfone ($PMSO_2$)) by high valent iron−oxo species, which is different from the products (biphenyl compounds) of PMSO when oxidized by $SO_4^{\bullet-}$ or $^{\bullet}OH$.[714,727,728] However, Dong et al. (2020) argued that the generation of Fe(IV) does not necessarily rule out the possibility of the production of free radicals, and they demonstrated that both Fe(IV) and free radicals ($SO_4^{\bullet-}$ and $HO^{\bullet}$) have contributed to the reactivity in Fe(II)−PDS systems,[708] with further research required to understand the mechanism.

In order to overcome the inefficiency of Fe(II)/persulfate due to iron precipitation under high pH conditions, many ligands have been employed to stabilize Fe(II).[704,710] For instance, citric acid enhances the degradation of TEC by Fe(II)−PDS.[710] Polycarboxylates (e.g., oxalate and citrate) exhibit better performance than aminocarboxylate and polyphosphate ligands because the former (a) have higher reactivity in PDS activation, (b) have lower steric hindrance, and (c) can enhance Fe(II)/Fe(III) cycling.[714] The ratio of ligand: Fe(II) can influence the


https://doi.org/10.1021/acs.chemrev.0c01286
Chem. Rev. 2021, 121, 8161−8233

reactivity because of the formation of different aqueous Fe(II)−ligand complexes which show various reaction rates with persulfates[714] as well as affecting the availability of Fe(II).[710] However, too much ligand may inhibit the reactivity through the formation of hexacoordinated iron complexes that constrains the availability of the iron center for peroxymonosulfate attachment.[704] In addition, the ratio of ligand/Fe(II) affects the types of reactive species generated. For example, Wang et al. showed that the yield of PMSO2 decreased as the ratio of ligand/Fe(II) increased in Fe(II)/ligand/PDS systems, suggesting that the reactive species changed from Fe(IV) (eq 17) to $SO_4^{\bullet-}$ (eq 15).[714] However, what induced this change is not well understood and requires further research.

$$S_2O_8^{2-} + Fe(II) + H_2O \rightarrow 2SO_4^{2-} + Fe^{IV}O^{2+} + 2H^+ \quad (17)$$

In addition to Fe(II) and Fe(II)−ligand complexes in homogeneous activation processes, structural Fe(II) in mixed-valent iron oxides in heterogeneous activation processes has also been employed in SR−AOPs. Magnetite can activate PDS to effectively degrade 2,4,4′-trichlorobiphenyl under neutral pH with superoxide radicals ($O_2^{\bullet-}$) and $SO_4^{\bullet-}$ involved in the reaction.[716] Although $O_2^{\bullet-}$ (eq 18) is a mild oxidant, it plays a critical role in inducing the generation of $SO_4^{\bullet-}$ (eq 19). ZVI is able to activate persulfate for the removal of contaminants, which is mainly attributable to the released aqueous Fe(II) species and the surface iron (oxyhydr)oxide layer on ZVI.[729,730] The transformation products of ZVI (e.g., magnetite) in ZVI/persulfate systems can continue to activate persulfate to remove residual contaminants.[730] FeS has also been shown to effectively activate persulfates to degrade various contaminants.[715,717,731] In addition to the roles of Fe(II) mentioned above, S(-II) in iron sulfides such as mackinawite can induce the regeneration of Fe(II) from Fe(III), which further enhances the reactivity.[717] Moreover, since the high valent iron−oxo species were discovered in Fe(II) species−persulfate systems in 2018,[706] more and more papers have proved the essential roles of Fe(IV) and Fe(V) in SR−AOPs. For instance, both free radicals ($SO_4^{\bullet-}$ and $^{\bullet}OH$) and nonradicals (Fe(IV) and Fe(V)) are observed to be involved in the activation of PDS by a natural titanomagnetite.[718] Therefore, the mechanisms reported in earlier papers should be re-evaluated for a potential involvement of the high valent iron−oxo species.

$$Fe(II) + O_2 \rightarrow O_2^{\bullet-} + Fe(III) \quad (18)$$

$$S_2O_8^{2-} + O_2^{\bullet-} \rightarrow SO_4^{2-} + SO_4^{\bullet-} + O_2 \quad (19)$$

There are very few studies on the utilization of sorbed Fe(II) on metal oxides to activate persulfates. Do et al. (2010) examined the effect of four metal oxides (goethite, hematite, magnetite, and manganese oxide (pyrolusite)) on the activation of PDS by Fe(II) and found that the manganese oxide is the most effective due to a high amount of Fe(II) sorbed at low pH.[720] However, the mechanism is not well discussed, warranting further research. In addition, compared with iron oxides, manganese oxides themselves are reportedly more effective in the activation of PDS and PMS.[421] Therefore, it is difficult to conclude if the reactivity enhancement in that study is due to the manganese oxide or sorbed Fe(II) on the manganese oxide, or both. More research is needed to elucidate the mechanisms.

## 8. METHODOLOGIES

Thanks to considerable advances in spectroscopic and microscopic analyses, Fe(II)-associated reductants in the environment are now much better understood than they were decades ago. In addition to classic batch kinetic experiments and conventional wet extraction techniques, a number of techniques are available to characterize mineral composition and transformation, including X-ray diffraction (XRD), Mössbauer spectroscopy, X-ray photoelectron spectroscopy (XPS), X-ray adsorption spectroscopy including X-ray absorption near edge (XANES) and extended X-ray absorption fine structure (EXAFS) spectroscopy, (cryo-)transmission electron microscopy (TEM), and scanning electron microscopy-energy dispersive X-ray spectroscopy (SEM-EDX).[437] In addition, surface complexation modeling,[489] kinetic modeling,[149] and computational methods[271,352,496] have aided in a better understanding of these systems. In the sections below, we focus on reviewing the applications of these techniques in understanding Fe redox chemistry without going into detail about how each technique works.

### 8.1. Classic Batch Kinetic Experiments

To quantify the reductive reactivity of Fe(II)-associated reductants, batch kinetic experiments are usually performed in anoxic chambers with different organic or inorganic compounds as the probe compounds. The probe compounds are often easily reducible, such as 4-chloronitrobenzene and hexachloroethane. The effect of a range of factors on the rate and extent of reduction is typically studied including the initial concentration of Fe(II), mineral loading or ligand concentration, ionic strength, and pH. Rate constants for the reductive reactivity ($k$) are usually calculated based on pseudo-first-order kinetics (eq 20):

$$\ln\left(\frac{C}{C_0}\right) = -k_{obs}t \quad (20)$$

where $k_{obs}$ is the pseudo-first-order rate constant, $C$ is the concentration of a chemical probe after a certain reaction time ($t$), and $C_0$ is the initial chemical probe concentration.

Author: Besides pseudo-first-order rate constants, other common response variables include $k_{SA}$ and $k_M$,[426,536] as shown in section 4.4. While batch experiments are able to provide information about the relative reactivity of Fe(II)-associated reductants, results from these studies highly depend on the experimental conditions used.[732] Quantitative structure activity relationships (QSARs), also referred to as linear free energy relationships (LFERs), are one important predictive tool to probe the influence of structural differences of classes of compounds (e.g., chlorinated methanes and nitroaromatic compounds) on reactivity.[733] Descriptor variables such as one-electron reduction potentials ($E^1$)[60,182] and $E_{LUMO}$ (energy of the lowest-unoccupied molecular orbital)[734] have been employed as predictors for nitroaromatic compounds. For example, the reductive reactivity of nitroaromatics by Fe(II)−tiron is related to the one-electron reduction potential of nitroaromatics.[60] Linear free energy relationships have also been reported between the second-order rate constants and either $-E_H/0.059$ V − pH for sorbed Fe(II) onto iron (oxyhydr)-oxides[425] or $E_H^0$ for Fe(II)−ligand complexes.[80] However, few QSARs have been reported for Fe(II)-associated reductants, mainly because of complexities in the structural and surface-


https://doi.org/10.1021/acs.chemrev.0c01286
Chem. Rev. 2021, 121, 8161−8233

associated reductants and a lack of suitable descriptors to correlate with the reactivity.

### 8.2. Wet Chemical Extraction

Wet chemical extraction is often conducted to study reactive Fe(II) surface complexes on iron (oxyhydr)oxide surfaces.[392] For example, wet chemical extraction can be performed to determine the bulk stoichiometry of magnetite, with the Fe(II) and total Fe concentration determined using an Fe(II)-specific colorimetric agent such as phenanthroline, while total Fe concentrations can also be measured using inductively coupled plasma−optical emission spectrometry/mass spectrometry (ICP-OES/OES).[201] Based on wet chemical extraction, Gorski et al. demonstrated that the uptake of Fe(II) by magnetite was controlled by the initial Fe(II) content, confirming the stoichiometry of the magnetite particles after complete dissolution in acid.[64]

Wet chemical extraction can provide indirect evidence of the transformation of Fe(II) sorbed onto iron (oxyhydr)oxides. Two terms that are widely used in the literature should however be clearly defined. One is "sorbed" Fe(II), which is the difference between the Fe(II) extracted by 0.5 N HCl within 20 h and that recovered after filtration through 0.2 $\mu$m filters. The other is "fixed" Fe(II), which is the difference between the Fe(II) extracted by 3 N HCl in 7 d and that extracted by 0.5 N HCl in 20 h.[735] Based on these two parameters, previous research showed an incomplete recovery of Fe(II) when it is sorbed onto iron (oxyhydr)oxides, and this has been used to suggest the formation of new mixed-valent iron phases on the surface of the original iron (oxyhydr)oxides.[735−737]

Wet chemical extraction has also been employed to distinguish Fe(II) sorbed to basal planes—extracted by 1 M $CaCl_2$—from Fe(II) sorbed to edge OH-groups—extracted by 1 M $NaH_2PO_4$—of clay minerals.[474] For instance, only a small amount of Fe(II) was recovered using $CaCl_2$ for sorbed Fe(II) on a clay mineral at pH 7.5, while more Fe(II) was recovered by using $NaH_2PO_4$, indicating the majority of Fe(II) was sorbed to edge OH-groups.[474]

Wet chemical acidic extraction is not able to accurately determine the ratio of Fe(II)/Fe(III) when Fe(III) can react with contaminants during the extraction procedure. For example, there is a redox reaction between Fe(III) and Tc(IV) at low pH,[201] which limits the application of the acidic extraction method to study the reduction of Tc(IV) by titanomagnetite. Additionally, Fe(II) reacts rapidly with $O_2$ at acidic pH in the presence of high HCl concentrations (e.g., 6 M HCl), particularly at elevated temperatures (e.g., 70 °C) as sometimes used during acid extractions.[420] The presence of reactive N-species (e.g., nitrite) is also problematic because they can oxidize Fe(II) at acidic pH during extraction,[408] but this can be circumvented by adding sulfamic acid, a compound that reacts with nitrite and prevents the oxidation of Fe(II) by the nitrite during acidification.[738] The presence of sulfide could also cause the reduction of ferrihydrite, resulting in the overestimation of the extracted Fe(II) concentration by a factor of 2, which could be used as a correction factor to calculate the amount of excess Fe(II).[739]

### 8.3. X-ray Diffraction (XRD)

X-ray diffraction is an indispensable tool for identification and characterization of various iron(III) (oxyhydr)oxide phases.[740] XRD can be used to identify the transformation products of iron (oxyhydr)oxides after reaction with Fe(II) in the presence or absence of contaminants. For example, Pedersen et al. used XRD to examine the transformation of iron (oxyhydr)oxides induced by the presence of different concentrations of Fe(II) and showed that new peaks ($2\theta$) at 2∼16° and 2∼25° formed on ferrihydrite (Figure 14), suggesting the formation of lepidocrocite and goethite.[395] The transformation is complete within two days. However, no new phases were observed for other iron (oxyhydr)oxides including goethite, hematite, and lepidocrocite. Note that the XRD diffraction patterns of various iron oxides or sulfides can be found in previous papers.[79,741,742]

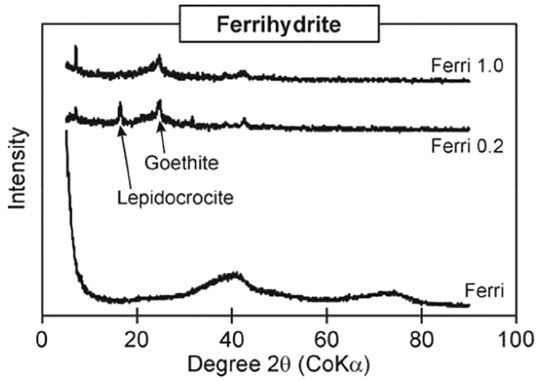


**Figure 14.** XRD of ferrihydrite reacting with 0, 0.2, and 1.0 mM Fe(II). Reprinted with permission from ref 395. Copyright 2005 Elsevier.

XRD can also be used to determine the ratio of Fe(II)/Fe(III) of mixed-valent iron oxides. Previous studies have shown that the unit-length decreases when magnetite is oxidized and there is a positive relationship between the unit-cell length and the stoichiometry of magnetite regardless of its size.[743] However, Pearce et al. observed a correlation between the unit-cell parameter and the ratio of Fe(II)/Fe(III) (R) in titanomagnetite and obtained an equation called "the Master Curve" (eq 21) based on the Hill−Langmuir function.[269] This equation has been used to calculate the change in R in titanomagnetite before and after Tc(VII) reduction.[201]

$$R = 0.89598/\left(\frac{0.1989}{(\alpha - 8.3344)} - 1\right)^{1/1.1988} \quad (21)$$

where $\alpha$ is the cell parameter in angstroms.

The particle size of Fe(II)-containing minerals such as magnetite can also be estimated from the broadening of the characteristic peaks during XRD analysis by applying the Scherrer formula (eq 22).[193]

$$d_{XRD} = \frac{K\lambda}{b\cos\theta} \quad (22)$$

where $K$ is the shape factor, $\lambda$ is the X-ray wavelength, $b$ is the corrected line broadening at half of the maximum intensity (fwhm), and $\theta$ is the Bragg angle. For example, Vikesland et al. relied on XRD to determine the diameter of magnetite particles to be 21.2 nm when using its (110) peak, which was larger than that obtained by TEM data.[193] The authors believed that this is due to more extensive processing of XRD samples and some larger particles being omitted from TEM analysis.

The main limitation of XRD is that it is not suitable for the analysis of poorly crystalline minerals or for determining the relative proportion of each mineral present in a mixture, particularly those containing poorly crystalline species. How-


https://doi.org/10.1021/acs.chemrev.0c01286
Chem. Rev. 2021, 121, 8161−8233

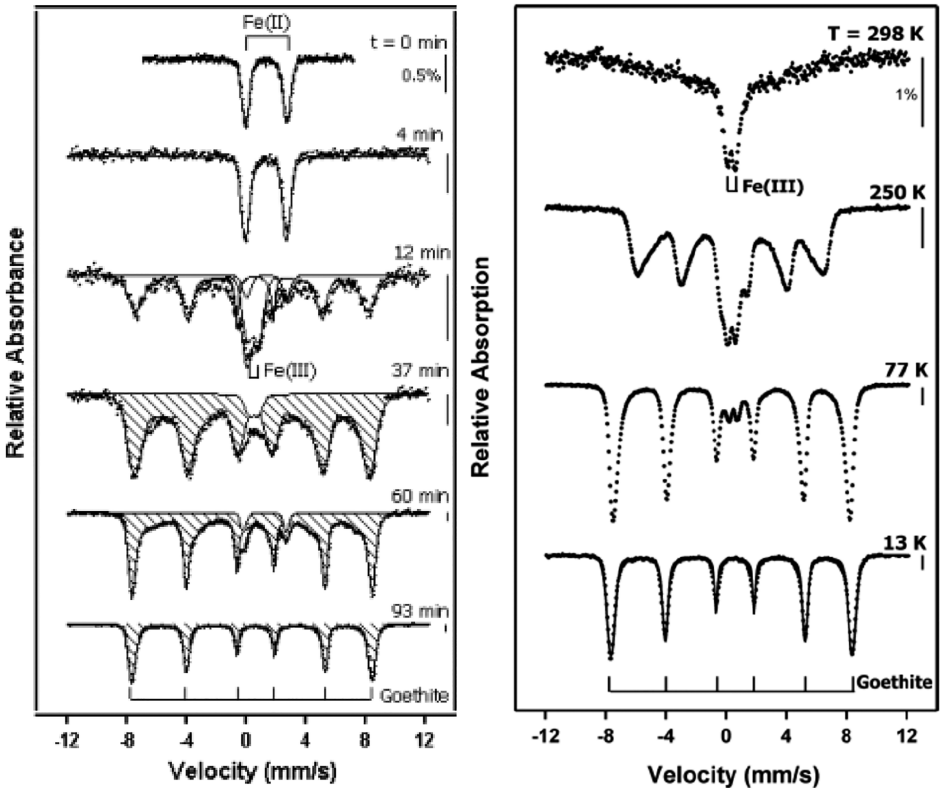


**Figure 15.** Left: Mössbauer spectra of $^{57}$Fe(II) adsorbed on $\alpha$-$Al_2O_3$ and of $^{57}$Fe(II) reacted with nitrobenzene on $\alpha$-$Al_2O_3$. Right: Temperature profile of the Mössbauer spectra of goethite formed during the reduction of nitrobenzene by Fe(II) in the presence of $\alpha$-$Al_2O_3$. Reprinted with permission from ref 465. Copyright 2010 American Chemical Society.

ever, this property can be utilized to differentiate the crystallinity of products formed during the redox reactions of Fe(II) species.

### 8.4. Mössbauer Spectroscopy

Mössbauer spectroscopy is a powerful technique to investigate the redox chemistry of iron in the environment because it is only sensitive to Fe. Center shift, quadrupole splitting distribution, and magnetic hyperfine field are three important parameters in a Mössbauer spectrum.[392,744] Among all iron isotopes, Mössbauer spectroscopy can only detect $^{57}$Fe and, as such, the use of $^{57}$Fe and a Mössbauer invisible Fe isotope, such as $^{56}$Fe, can be exploited to track and identify the degree and rate of electron transfer and atom exchange between aqueous Fe(II) and Fe(III) (oxyhydr)oxides or Fe(III)-bearing clay minerals, as has been done in many studies.[392,437,464,479] For example, Mössbauer spectra have been collected for sorbed $^{57}$Fe(II) on mineral oxides ($Al_2O_3$, $TiO_2$, and iron oxides),[392] and the results showed that an Fe(II) phase formed on $Al_2O_3$ and $TiO_2$, while an Fe(III) phase was the major species on the iron oxide surface, indicating electron transfer between $^{57}$Fe(II) and the underlying $^{56}$Fe(III) (oxyhydr)oxide had occurred. Gorski et al. exchanged isotopically normal magnetite with aqueous $^{56}$Fe(II) and observed a decreased concentration of $^{57}$Fe in the magnetite structure, suggesting Fe atom exchange between the two phases.[274] Mössbauer parameters for some Fe(II) bearing minerals can be referred to previous papers.[79,745−747]

Mössbauer spectroscopy can also be used to characterize different iron mineral structures and Fe(II) phases.[64,282,392,444] For instance, aqueous Fe(II), Fe(II) sorbed onto Al- and Ti-oxides through inner-sphere complexation, and $Fe(OH)_2$ precipitates are distinguishable based on Mössbauer spectra.[465] Mössbauer spectra of the reaction products of $^{57}$Fe(II) with $^{56}$Fe-goethite (nanorods and microrods) showed nearly identical ferric iron sextets, and model fitting parameters for the 13-K spectra indicated the formation of goethite.[437] It has also been reported that the spectrum of sorbed $^{57}$Fe(II) on a filtered $\alpha$-$Al_2O_3$ was almost a symmetrical doublet with the model parameters consistent with those of Fe(II) in high spin configuration and an octahedral coordination (CS = 1.31 mm/s, QS = 2.76 mm/s) (Figure 15, left). After the addition of nitrobenzene, Fe(II) was oxidized to Fe(III) with products evident after 37 min.[465] It is worth noting that Mössbauer spectra are often collected under different temperatures, from room temperature to as low as 4.2 K. This is to take advantage of the size-dependent superparamagnetism of Fe (oxyhydr)oxides; that is, particles cannot overcome thermal excitation to lose magnetic order at low temperature so they show increasing magnetically ordered absorption patterns with decreasing temperature (Figure 15, right).[465] The peaks of octahedral and tetrahedral Fe(III) sites in clay minerals are also different in Mössbauer spectra.[479]

Another application of Mössbauer spectroscopy is to determine magnetite and maghemite stoichiometry, by comparing the relative areas of the $^{Oct,Tet}Fe^{3+}$ and $^{Oct}Fe^{2.5+}$ peaks for large magnetite particles.[743,748] For nanomagnetite, Gorski et al. used Mössbauer spectra collected at 140 K to determine its stoichiometry with the values obtained in good agreement with those obtained via acid dissolution.[743]

One limitation of Mössbauer data is that structural Fe(II) versus sorbed Fe(II) or Fe(II) complexed with ligands or cis- versus trans-octahedral Fe(II) sites are indistinguishable.[464,479] Mössbauer spectra alone are also not sufficient to identify iron


https://doi.org/10.1021/acs.chemrev.0c01286
Chem. Rev. 2021, 121, 8161−8233

mineral phases such as goethite, ferrihydrite, lepidocrocite, green rust, and vivianite.[282,479,749]

### 8.5. X-ray Photoelectron Spectroscopy (XPS)

XPS has become an invaluable surface-sensitive analytical tool for the identification and characterization of near surface properties and the reactivity of a wide range of minerals. For the electron energies that are commonly used in XPS, the attenuation lengths are about 1−10 monolayers for emission angles normal to the surface.[750] XPS is often employed to identify the composition and valence changes of iron species, which are useful in probing the mechanism of mineral dissolution,[751] changes in Fe oxidation state in catalysts,[752,753] and sorption reactions at the mineral/water interface.[754] XPS spectra of various iron oxides or sulfides can be found in previous papers.[750,755,756]

XPS has been used in studying reactions involving Fe(II) for different purposes. XPS spectra can help quantify the relative abundance of Fe(II) and Fe(III) on the surface of iron oxides as the peak positions of the Fe $2p_{1/2}$ and Fe $2p_{3/2}$ orbitals are sensitive to the oxidation state.[750] An important step in XPS data analysis for this purpose is the selection and preparation of standard materials. Appropriate curve fitting processes are also essential in obtaining the accurate ratio of Fe(II)/Fe(III), with further details regarding this approach described in a previous study.[757]

XPS has been employed to understand C speciation on the surface of iron mineral−organic matter complexes. The binding energies at 284.6, 286.2, 287.6, and 289.1 eV were assigned to C−C, C−O−C, C═O, and COOH, respectively.[758] For instance, Adhikari et al. studied microbial reduction of ferrihydrite−Elliot humic acid and found that the components of C−C on the ferrihydrite surface increased from 38.5 to 49.4% to 49.6∼68.5%, which is contributed by the binding of the biomass and biomolecules of *Shewanella putrefaciens* CN32.[579] XPS survey spectra can be further used to calculate the C/Fe molar ratio for iron oxide−organic matter complexes. Many studies showed that the C/Fe ratio of iron oxide−organic matter complexes based on XPS was higher than that of the bulk coprecipitate, indicating the accumulation of organic matter on iron oxide surfaces.[759]

XPS can also be used to investigate changes in the nature of surface-located inorganic elements, such as arsenic and uranium. The products of the reaction of U(VI) with magnetite have been investigated by XPS.[203] The relative surface concentrations can be obtained by fitting the U 4f photoelectron peaks, and a shift or broadening of the U 4f peaks to lower binding energies suggests U(VI) is reduced to a lower oxidation state.[203] Based on previous studies,[760,761] the As $3d_{5/2}$ peaks for As(III) and As(V) can be distinguished by their distinct binding energy ranges of 44.0∼45.5 eV and 45.2∼46.8 eV, respectively.[762]

The main limitations of XPS are that it can only detect surface Fe species and that samples must be dried for analysis, which may alter the hydrated mineral surfaces.[392] Note that the analysis of XPS spectra on the distribution of different valent elements in many previous studies might not be accurate, as already summarized.[763,764] Thus, caution should be taken to interpret XPS data.

### 8.6. X-ray Absorption Spectroscopy (XAS)

XAS relies on the generation of powerful X-ray light beams using the synchrotron accelerator technology[765] and has been employed extensively to determine the valence state of an element and the bonding environment of an atom. X-ray absorption near edge structure spectroscopy (XANES) and extended X-ray absorption fine structure spectroscopy (EXAFS) can help quantify the speciation changes for Fe(II)-associated reductants. XANES spectra can provide detailed insight into the oxidation state and local coordination environment of Fe atoms,[766] while EXAFS spectra can provide information on the coordination environment, nearest neighboring elements, etc.[767] The fundamentals and applications of XAS have been well documented elsewhere.[79,767,768]

XANES can be used to explore the oxidation state of iron and its coordination environment. Compared to Mössbauer spectroscopy, the Fe K-edge is sensitive to even small amounts of iron because hard X-rays measure the bulk signal.[769] Wilke et al. (2001) have shown that the centroid position and the integrated intensity of Fe K pre-edge can be used to obtain the Fe oxidation state and coordination number.[766] The average pre-edge centroid positions for $Fe^{2+}$ and $Fe^{3+}$ are 1.4 ± 0.1 eV apart, so the average pre-edge position for mixed Fe(II)−Fe(III) compounds is between these two positions. If the site geometry is known for both Fe(II) and Fe(III), the Fe(II)/Fe(III) ratio can be accurately determined with an error of ±10 mol%. With this approach, Wilke et al. successfully determined the Fe(II)/Fe(III) ratios in 12 Fe minerals;[766] Guerbois et al. quantified the evolution of the total Fe(II) during the reduction of nitrite by biogenic hydroxycarbonate green rusts.[237]

Fe K-edge EXAFS spectroscopy provides distinct spectra for different iron (oxyhydr)oxides, such as akaganeite, ferric oxyhydroxycarbonate, ferrihydrite, goethite, green rusts, lepidocrocite, mackinawite, maghemite, magnetite, siderite, and white rust ($Fe(OH)_2$), and clay minerals such as montmorillanite and nontronite.[237,281,770,771] The obtained spectra can help characterize these mineral phases by comparing to reference standard spectra. For instance, it has been employed to examine the Fe(II)-catalyzed transformation products of ferrihydrite, schwertmannite, jarosite, and lepidocrocite,[396,428] the formation of chloride-green rust upon interactions of Fe(II) with smectites,[281] and the reaction products of biogenic hydroxycarbonate green rusts with nitrite.[237] Additionally, Budi et al. have utilized linear combination fitting (LCF) to qualitatively analyze XANES spectra of a natural magnetite based on different standard minerals, and they found that natural magnetite consisted of 98% $Fe_2O_3$ and 2% FeO.[772]

XAS can also be relied on in identifying the product of the reduction of other metals by Fe(II) species. By comparing with the XANES spectra of three Tc species of different oxidation states, Yalcintas et al. observed the reduction of sorbed Tc(VII) to Tc(IV) by magnetite or mackinawite and the Tc(IV) is structurally incorporated into the magnetite.[773] The same authors then obtained the EXAFS spectra of the Tc-magnetite samples and noticed chemically different Tc species, such as Tc coordinating with 6 oxygen atoms forming the corners of a $TcO_6$ octahdron, which is linked to neighboring $FeO_6$ octahedra and tetradra, or Tc substituting for octahedral Fe. Wylie et al. employed EXAFS to investigate the reduction of neptunium ions by titanomagnetite and confirmed the reduction of Np(V) to Np(IV), and there was no $NpO_2$ precipitation.[200] Bond and Fendorf studied the reduction of chromate by green rust, and the obtained XANES spectra revealed a strong partition of the reduced Cr(III) into the formed solid ferric hydroxides such as lepidocrocite.[241] When Fe(III) (oxyhydr)oxides undergo microbial reduction to form magnetite, the XAS data cannot distinguish whether the coexisting As(III) is chemically bonded to magnetite or simply adsorbed to the magnetite surface,


https://doi.org/10.1021/acs.chemrev.0c01286
Chem. Rev. 2021, 121, 8161−8233

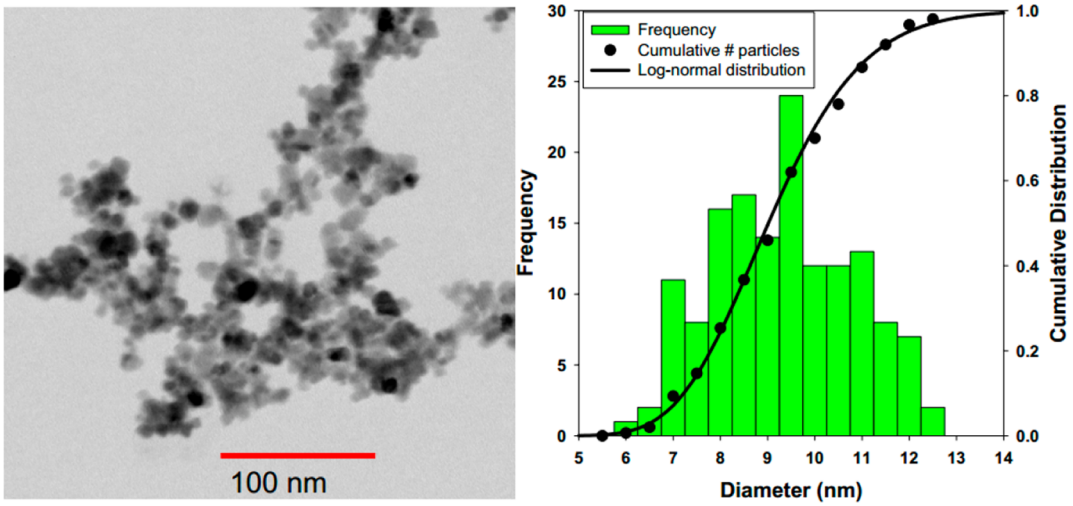


**Figure 16.** TEM images of magnetite (left) and histogram of the particle size distribution ($n$ = 150 particles). Reprinted with permission from ref 193. Copyright 2007 American Chemical Society.

whereas the XAS data confirms the incorporation of the coexisting As(V) into the formed magnetite upon the microbial reduction of ferrihydrite.[774]

While XAS is an extremely powerful technique for the measurement of aqueous Fe(II)−mineral interactions, the main drawback of this technique is that access to such facilities is difficult with less than 100 XAS instruments available worldwide.[775] There are also rigorous safety requirements associated with this technique because of its use of X-rays. It is also difficult to distinguish between solid phases with slightly different atomic distances.[200,776]

### 8.7. Fourier Transform Infrared Spectroscopy (FTIR)

FTIR is a useful technology for reaction monitoring and characterization of iron containing products.[422,777] Compared with XAS or Mössbauer spectroscopy, there are some advantages to the use of FTIR spectroscopy, including low cost, ease of access, minimal safety precautions, and simple interpretation of spectra. FTIR spectroscopy has been demonstrated to be a suitable technique for the identification and basic characterization of a range of iron oxides.[733,778−781] The absorption bands of Fe(III) (oxyhydr)oxides in the fingerprint region (400−1500 $cm^{-1}$) are associated with Fe−O and Fe−OH lattice vibrations and bends. For example, two strong FTIR peaks can be observed at approximately 570 and 390 $cm^{-1}$ for magnetite.[782] The absorption bands of goethite are at approximately 890 and 795 $cm^{-1}$ due to O−H bending,[783] while lepidocrocite demonstrates absorption peaks at 1150, 1020, and 750 $cm^{-1}$ due to O−H bending.[783]

IR has been used to characterize the phase change of iron oxides. The IR absorbance intensity has been shown to be linearly correlated with the amount of specific iron oxides; thus, it can be used to quantify the relative proportion of iron oxides present in a mixture.[780,779] Xiao et al. used FTIR spectroscopy to study the Fe(II)-catalyzed transformation of a poorly crystalline Fe(III) oxyhydroxide at circumneutral pH to more crystalline Fe(III) (oxyhydr)oxides such as goethite, lepidocrocite, and magnetite, with the results found to be comparable to those obtained using XAS.[780]

Another usage of FTIR is to identify the structural Fe(II) arrangements in smectites. For example, the absorption band at 884 $cm^{-1}$ indicates AlFe(III)−OH entities for an unaltered Wyonming montmorillonite (0% Fe(II)/total Fe). This band disappeared for reduced Wyoming montmorillonite (75% Fe(II)/total Fe) and reappeared with reoxidation (40% Fe(II)/total Fe), indicating iron remained in the smectite lattice during the reaction.[53]

However, the size and shape of iron oxides might influence the IR spectra characterization of iron oxides.[784] Therefore, care is required in order to obtain accurate information, such as appropriate calibration standards, well-mixed suspensions, and so on.[780]

### 8.8. Transmission Electron Microscopy (TEM) and Scanning Electron Microscopy (SEM)

The size, morphology, and structure of iron oxides are usually examined by two common electron microscope techniques—SEM and TEM. These imaging techniques provide details of the micron and nanoscale structures of these minerals. SEM can provide information on topology (i.e., pseudo 3D) while TEM provides insight into aspects such as crystallinity.[79]

Particle size can be determined from SEM and TEM images. For example, by applying image analysis software, TEM images have been used to ascertain that the median diameter of magnetite nanoparticles in a particular study was 9.2 ± 1.2 nm (Figure 16).[193] Handler et al. showed that the size of a microgoethite did not change before and after reaction with Fe(II).[406] However, recent studies demonstrated that the shape of goethite particles became wider and shorter upon exposure to Fe(II),[405,785] so future investigation is needed to understand the discrepancy between these studies. In addition, SEM images revealed that nanoscale particles formed dense aggregates on the order of several microns in diameter. The clear formation of particle aggregates in solution raises questions regarding the use of primary particle surface area as a basis for assessing nanoscale size-effects in iron oxide suspensions at circumneutral pH.[437] Besides SEM and TEM, the size distribution of iron oxides and iron oxide−NOM particles can be obtained using other techniques,[786] such as flow-field flow fractionation ICP-MS, dynamic light scattering, and nanoparticle tracking analysis, which will not be elaborated here.

TEM images can be used to observe the phase change of iron oxides. For example, Chun et al. obtained histograms of the length of nanogoethite particles after reaction with 4-chloronitrobenzene using TEM and found that the particles did not change in width but exhibited increased roughness at the


https://doi.org/10.1021/acs.chemrev.0c01286
Chem. Rev. 2021, 121, 8161−8233

particle tips, indicating the growth of the particles along the *c*-axis.[362] HRTEM images of nanogoethite before and after reaction with Fe(II) at pH 7.5 for 30 days, including imaging through rod widths and along the long-axis of the rods, showed no detectable difference in the crystallinity of nanogoethite before and after reaction with Fe(II) (Figure 17).[406]

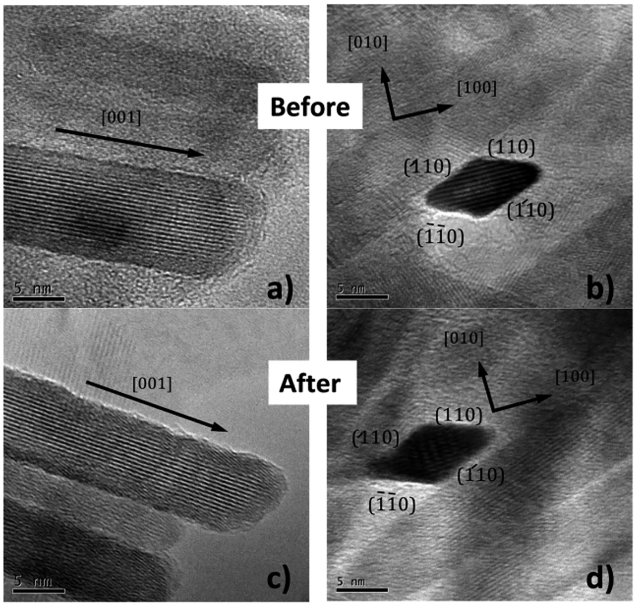


**Figure 17.** HRTEM images of nanogoethite before (a, b) and after (c, d) a 30 day atom exchange reaction with Fe(II) at pH 7.5. Reprinted with permission from ref 406. Copyright 2014 American Chemical Society.

We can also rely on TEM images to determine the nature of reduction products for some inorganic contaminants.[787−789] For example, HRTEM images of the sample of U(VI) reduction by pyrite showed a distinct lattice fringe (*d*-spacing of 3.16 Å), indicating a unique phase different from the pyrite formed.[311] In addition, the selected area electron diffraction (SAED) pattern suggests that besides a strong *d*-spacing of ∼3.16 Å, additional spacings of ∼1.67 and ∼1.98 Å also exist, which agree with the values reported for $U_4O_9$, $UO_2$, $U_3O_8$, and $U_3O_7$ and confirm the reduction of U(VI).[311]

Cryo-TEM/SEM images can further inform the reductive reactivity of Fe(II) species in complex systems.[364,438,790] Conventional TEM/SEM is only suitable for dry samples, but cryo-TEM/SEM is capable of examining the in situ aggregation state of iron oxides at specific reaction times in complex systems, which represents the actual solution condition. For example, Vindedahl et al. showed that the addition of 4-chloronitrobenzene and its degradation process have no effect on the aggregation state of nanogoethite,[791] which is different from a previous study likely because of differences in nanogoethite storage.[438] In situ images of aggregates allow for a direct determination of fractal dimension ($D_f$), a parameter that is related to the compactness, accessibility, and surface area of aggregates. Therefore, the physical structure of aggregates can be linked directly to their reactivity.[792−794]

### 8.9. Electrochemical Methods

A wide range of electrochemical methods have been used to characterize redox reactions involving Fe(II). The most conventional approach involves voltammetry performed on stable, aqueous complexes of iron Fe(II)/Fe(III) that form reversible redox couples at a working electrode made with an inert material such as platinum or glassy carbon. Environmentally relevant examples of this type of work include fundamental studies of the redox properties of iron siderophores and porphyrins.[795,796] This is one of the methods used to determine standard potentials for redox couples such as those shown in Figure 2.

Many Fe redox couples involve species of Fe(III) that are not truly dissolved but are nano- or colloidal particles that are sufficiently labile to give a useful, if not ideal, electrode response. Satisfactory agreement between measured and calculated potentials has been reported in several older studies using freshly precipitated minerals.[797−799] A more recent and thorough evaluation of this was performed on systems containing Fe(II) and several Fe(III) (oxyhyr)oxides (goethite, lepidocrocite, nanosized ferric oxide hydrate, and hydrous ferric oxide) by comparing the pH dependence of potentials measured with a conventional Pt electrode to potentials calculated from detailed equilibrium speciation calculations.[431] The agreement was good for the two poorly crystalline oxides but less satisfactory for goethite and lepidocrocite.

As the particles involved in such redox couples become larger and/or more crystalline, the electrode response becomes more complex and difficult to interpret.[800,801] One complicating factor is deposition of particles onto the electrode, which can appear to enhance the working electrode response[797] but can also coat the electrode with a new phase that fundamentally changes the nature of the working electrode. The latter effect was clearly demonstrated in a study of potentiometry on suspensions of nanoparticles containing $Fe^0$ (nZVI), where the dependence of the measured potential on concentration of nZVI was nonlinear in a manner that suggested surface site saturation.[802] Another system where the electrode response of borderline dissolved species has been controversial involves freshly formed FeS clusters and/or colloids under iron-rich, sulfidic conditions.[803,804]

The above-mentioned electrochemical studies were focused on *direct* interactions between redox-active solutes and the working electrode surface, but these interactions are weak in many systems of environmental interest, which results in potential measurements that are unstable, irreproducible, and/or inaccurate. A flexible way to alleviate this issue is by adding soluble electron-transfer mediators (ETMs) that form a reversible redox couple that facilitates electron-transfer between the analyte species and the electrode. The principles of this approach, and its applications to characterization of redox-active iron minerals, were reviewed by Sander et al. (2015).[800] The characteristics that they propose for selection of recommended ETMs include the following: well-defined standard reduction potentials and electron and proton-transfer stoichiometries, solubility and stability in aqueous solutions over the experimental pH range, and reversible interactions of the mediator with the mineral and the working electrode.

The most straightforward application of ETMs to iron mineral characterization is for the improvement of potential measurements. Once the mineral has equilibrated with the ETM, the resulting potential can be measured by potentiometry, where the working electrode response is mainly due to the ETM, or calculated from the speciation of the ETM obtained by spectrophotometry. The latter involves the measured speciation of ETMs, the Nernst equation, and literature values of the standard reduction potential and $pK_a$ values for the ETM couple


https://doi.org/10.1021/acs.chemrev.0c01286
Chem. Rev. 2021, 121, 8161−8233

species. Examples of this analysis can be found in recent work by Fan et al., where spectrophotometric analysis of ETMs was used to measure reduction potentials of various iron minerals in the presence of aqueous Fe(II).[426] The spectrophotometric data for one ETM, anthraquinone disulfonate (AQDS), before and after exposure to the mineral suspensions, is shown in Figure 18. A

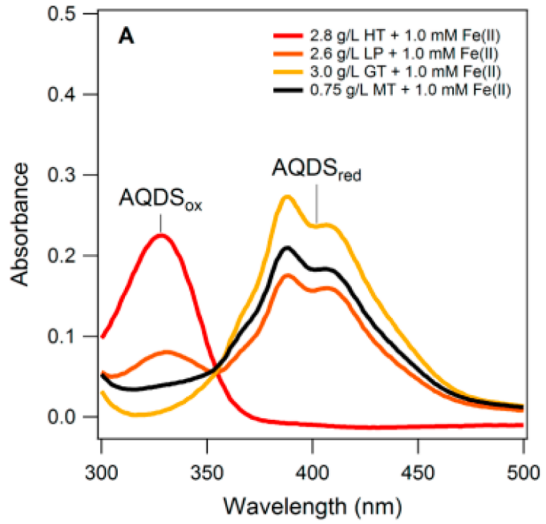


**Figure 18.** Spectrophotometric determination of the speciation of an electron-transfer mediator (AQDS) upon exposure to iron oxides in the presence of aqueous Fe(II). HT, LP, GT, and MT refer to hematite, lepidocrocite, goethite, and magnetite, respectively. Reprinted with permission from ref 426. Copyright 2016 American Chemical Society.

Beer's Law calculation with these data was used to obtain the concentrations of oxidized and reduced forms of AQDS ([$AQDS_{ox}$] and [$AQDS_{red}$]), and these data were used in the Nernst equation (eq 23) to calculate the apparent potential of the mineral suspension ($E_{AQDS}$)

$$E_{AQDS} = E^0 + \frac{RT}{2F}\ln([H^+]^2 + K_{r1}[H^+] + K_{r1}K_{r2}) + \frac{RT}{2F}\ln\left(\frac{[AQDS_{ox}]}{[AQDS_{red}]}\right) \quad (23)$$

where $E^0$ is the standard reduction potential of the AQDS, $R$ is the gas constant, $T$ is the temperature, $F$ is the Faraday constant.

The potentiometric and spectrophotometric methods of analyzing ETM speciation in mediated potentiometry can be complementary, as demonstrated by a few studies that have compared the results obtained both ways.[281,426,486] An advantage of the spectrophotometric method is confirmation that ETM loss by irreversible side-reactions is negligible, but a disadvantage is the interference caused by naturally colored waters. The converse applies to potentiometric analysis of ETMs, which is part of the reason that this method was used in a recent study demonstrating the approach's application to characterization of redox conditions in suspensions of aquifer sediments.[539]

The other major application of ETMs is for the determination of oxidation or reduction capacity. In contrast to potential measurements, capacity measurements are made by amperometry. Protocols for the use of ETMs to measure the redox capacity of mineral suspensions have recently been developed under the names mediated electrochemical reduction (MER) and mediated electrochemical oxidation (MEO).[800] Examples

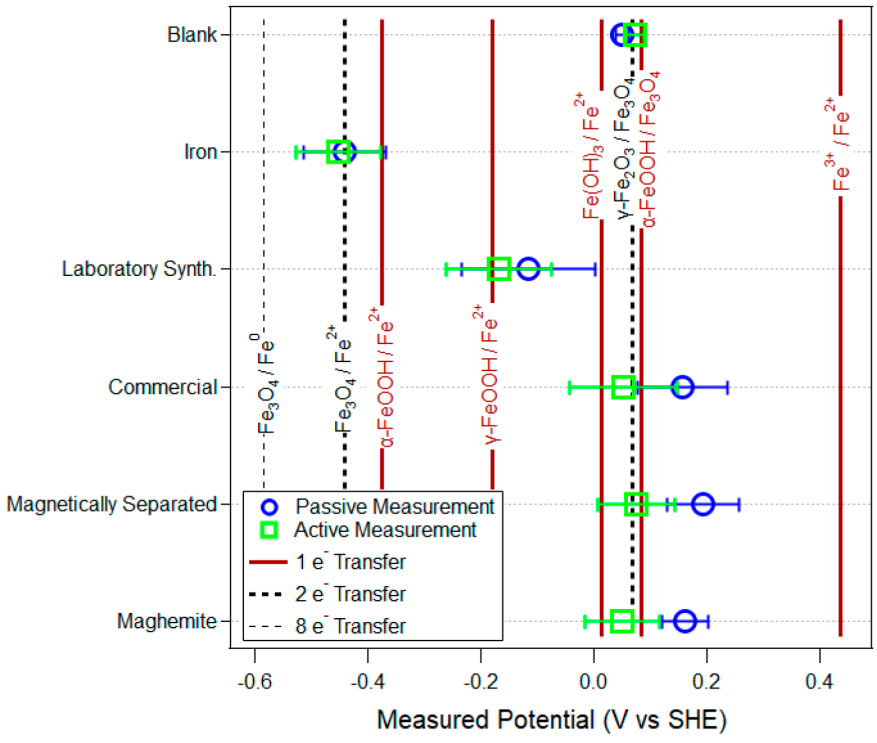


**Figure 19.** Comparison of potential measured on PDEs made with magnetite of various types [passive (open circuit potential) and active (linear sweep voltammetry)] vs potential calculated for Fe(III) (oxyhydr)oxide/Fe(II) redox couples at pH 8.4. Adapted with permission from ref 815. Copyright 2019 American Chemical Society.



https://doi.org/10.1021/acs.chemrev.0c01286
Chem. Rev. 2021, 121, 8161−8233

of the application of MER/MEO to studies of redox processes involving iron minerals include pyrite, siderite, Illite, Fe-bearing smectites, ferrihydrite, and goethite.[428,732,805−807] A preliminary summary of this work on ETM-based mineral characterization was included in a review by Niu et al.,[801] but the most thorough and definitive description of the method and its uses is in Sander et al. (2015).[800]

As noted above, some conditions cause sufficient deposition of suspended particles to significantly modify the working electrode surface. Rather than try to prevent this, some studies use this to advantage by deliberate, controlled deposition of the analyte material as a thin-film onto a base electrode of inert material (usually a Pt or GC polished disk, but other base materials can be used, such as conductive glass). An example of this approach is to a coat mineral slurry on a GC working electrode to study the electrochemical behavior of sorbed Fe(II).[366,381]

Another way to deliberately make iron oxides into an electrode is by packing the material into a cavity in an otherwise conventional disk electrode. The two main versions of this are called cavity microelectrodes (CMEs)[808] and powder disk electrodes (PDEs), but only the latter has been used to study redox reactions of environmentally relevant iron-based materials. The majority of this work has been focused on characterization of ZVI,[195,527,802,809−814] but the method and some of the results have been applied to iron oxides.[195,426,815] A particularly relevant example is shown in Figure 19, where potentials measured with PDEs made with magnetite of various types were used to show that the effective potential of most environmental materials is significantly more positive than theoretical or pure magnetite.

While all of the above approaches to electrochemical measurements with iron oxides utilize particles as they exist in detrital environments (soils, sediments, dusts, etc.), a few studies have utilized electrodes made from a solid of single or polycrystalline iron oxide. The main advantage of this approach is that it enables the use of advanced methods, such as electrochemical impedance spectroscopy[816−819] and electrochemical force microscopy.[393,820] However, this approach is less flexible in the types of materials that it can accommodate, and almost all of the work to date has been done on hematite.

### 8.10. Surface Complexation Modeling (SCM)

SCM was originally developed to describe surface charges and ion adsorption to the surface of mineral oxides,[821] but it has been widely used to describe sorption processes in geochemistry over the past several decades.[821−823] For a comprehensive overview of SCM, refer to Goldberg (1995),[824] Venema et al. (1996),[822] and Groenenberg et al. (2014).[825] Compared with traditional adsorption models, such as the distribution coefficient ($K_d$) and Langmuir and Freundlich models, SCM enables a description of the effect of solution chemistry (e.g., pH and ionic strength) on the binding of aqueous solutes to the surface of minerals.[826] Such modeling requires an understanding of the nature of the adsorbed species and the acid−base chemistry of these species and a knowledge of the stability constants of all surface species. As an example, equilibrium reactions and constants for surface species for adsorption of Fe(II) onto $TiO_2$ suspensions are listed in Table 7.

A number of computer software programs have been used for SCM including FITEQL,[827] Visual Minteq,[828] PHREEQC,[829] MINEQL+,[830] GRFIT,[831] and ECOSAT.[832] The surface charge properties are described with common approaches including the constant capacitance model (CCM),[833] the double diffuse layer model (DLM),[73,834,835] the triple layer model (TLM),[736] and the charge distribution model.[836] As discussed earlier, Silvester et al. used CCM to describe the adsorption of Fe(II) onto iron(III) (oxyhydr)oxides and were able to deduce the suspension redox potential, which agreed well with the experimental redox potential values.[431] DLM was proposed by Stumm and co-workers[837,838] and has been widely used in binary systems to study sorption of metal ions or ligands onto metal oxides.[839,840] The DLM has been utilized to examine surface species when Fe(II) is sorbed to iron (oxyhydr)oxides. Previous work has investigated the reduction of organic and inorganic compounds by a mixture of Fe(II) and iron oxides and found that the reaction rates were proportional to the concentration of $\equiv Fe^{III}OFe^{II}OH^0$ species.[74] The reactivity of surface sorbed Fe(II) has also been shown to be affected by the degree of hydrolysis.[431] In all these models, sorbed Fe(II) is assumed to form a monodentate surface complex, i.e., $\equiv Fe^{III}OFe^{II}OH^0$ and/or $\equiv Fe^{III}OFe^{II}O^-$ (refer to section 4.2.1.2 for more discussion). Unlike previous papers using monodentate binding of Fe(II) onto surfaces of iron oxide,[73,74,375,431,463,736] Hiemstra and van Riemsdijk (2007) turned to the charge distribution model by including multidentate adsorption complexes to improve the surface complexation modeling of Fe(II) adsorption.[836] They showed that the sorption of Fe(II) onto lepidocrocite can only occur if electron transfer from Fe(II) to Fe(III) is included, while for goethite and amorphous ferric hydroxide, Fe(II) adsorption occurs with or without electron transfer.

Although the SCM approach can suggest hypothetical reactive surface species that are responsible for reduction from a macroscopic kinetic perspective, there are some concerns. For example, in Fe(II)/$TiO_2$ systems, some researchers have found that the hydrolyzed Fe(II) surface complex (i.e., $\equiv TiOFe^{II}OH^0$) is the reductive species,[73] while others believed that $\equiv TiOFe^+$ is the reductive species when they combined modeling with electrochemical methods.[381] Recently, it was reported that the amount of $\equiv Fe^{III}OFe^{II}OH$ was maintained almost the same in the presence of phthalic acid, yet the reductive reactivity significantly decreased, most likely because of the competitive adsorption of phthalate physically blocking the reactive sites.[489] Therefore, macroscopic modeling alone is not able to identify the exact microscopic surface species that is responsible for contaminant reduction. In light of the conduction model described in section 4.2.4, future work

**Table 7. Equilibrium Reactions and Constants for Surface Species[73]**

| Aqueous reactions | log K |
|---|---|
| $H_2O \leftrightharpoons OH^- + H^+$ | −14.00 |
| $Fe^{2+} + H_2O \leftrightharpoons FeOH^+ + H^+$ | −9.40 |
| $Fe^{2+} + 2H_2O \leftrightharpoons Fe(OH)_2^0 + 2H^+$ | −20.49 |
| $Fe^{2+} + 3H_2O \leftrightharpoons Fe(OH)_3^- + 3H^+$ | −28.99 |
| $Fe^{2+} + 4H_2O \leftrightharpoons Fe(OH)_4^{2-} + 4H^+$ | −45.99 |
| Surface reactions | |
| Surface site density, $N$ (sites nm$^{-2}$) | 2.5 |
| $\equiv TiOH + H^+ \leftrightharpoons \equiv TiOH_2^+$ | 3.9 |
| $\equiv TiOH + H_2O \leftrightharpoons \equiv TiO^- + H^+$ | −8.7 |
| $\equiv TiOH + Fe^{2+} \leftrightharpoons \equiv TiOFe^+ + H^+$ | −2.87 |
| $\equiv TiOH + Fe^{2+} + H_2O \leftrightharpoons \equiv TiOFeOH^0 + 2H^+$ | −10.92 |


https://doi.org/10.1021/acs.chemrev.0c01286
Chem. Rev. 2021, 121, 8161−8233

should focus on how to incorporate electron transfer into SCM to better model the involved kinetics.

### 8.11. Kinetic Modeling

Kinetic modeling can be used to quantify the changes in species composition over time. However, empirical expressions of this form do not account for the reaction mechanism underpinning the overall process. To be able to model reactions in complex systems, we need to hypothesize reaction sets for simplified model systems. The hypothesized reaction sets and associated rate constants should be validated using experiments in which the concentrations of as many reactants, intermediates, and end products as possible are determined.[841] For example, Boland et al. conducted the first detailed investigation into the kinetics of the Fe(II)-accelerated transformation of ferrihydrite to goethite with the hypothesized reaction set used shown in eqs 24−27.[398,781]

$$Fe^{II} + \text{ferrihydrite} \rightarrow Fe^{II}_{solid-ads} + \text{ferrihydrite*} \quad k_1 \tag{24}$$

$$Fe^{II}_{solid-ads} + \text{ferrihydrite*} \rightarrow \text{Goethite} + Fe^{II} \quad k_2 \tag{25}$$

$$Fe^{II}_{solid-ads} + \text{ferrihydrite*} \rightarrow \text{lepidocrocite} + Fe^{II} \quad k_3 \tag{26}$$

$$Fe^{II}_{solid-ads} + \text{lepidocrocite} \rightarrow \text{Goethite} + Fe^{II} \quad k_4 \tag{27}$$

where ferrihydrite* represents a reactive or "activated" ferrihydrite site.

Kinetic modeling has often been employed to interpret the reactivity of Fe(II)-associated reductants[147,149] using computer software programs such as Kintecus[156,842] and Scientist.[149] The overall reaction rate constant is considered as a weighted sum of the reaction rate constants of each Fe(II) species reacting with the probe contaminants,[147,149] as shown in eq 28. For instance, two soluble Fe(II) complexes ($FeL^0$ and $FeL_2^{2-}$) formed in the presence of malonate (L); when both complexes were considered reactive (Figure 20), there is a good agreement

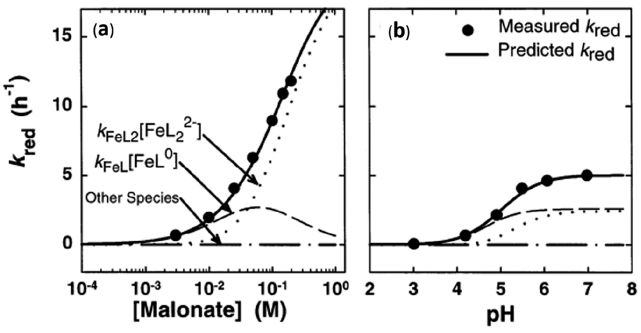


**Figure 20.** Contribution of Fe(II) species to $k_{red}$ in oxamyl reduction in the presence of malonate (L), including: (a) effect of malonate loading and (b) effect of pH. Reprinted with permission from ref 147. Copyright 2002 American Chemical Society.

between the calculated and experimental kinetics.[147] The concentration of $FeL_2^{2-}$ increased with increasing malonate loading and pH, and $FeL_2^{2-}$ was the dominant reactive species at high malonate loading. These results assisted in understanding the contribution of individual Fe(II) species to the overall reactivity.

$$k_{red} = [Fe(II)] \sum_i k_i \alpha_i \tag{28}$$

where $k_{red}$ is the overall reaction rate constant, [Fe(II)] is the total Fe(II) concentration, $k_i$ is the second-order reaction rate constant for Fe(II) species $i$, and $\alpha_i$ is the fractional concentration of $i$.

### 8.12. Quantum Chemical Methods

In recent decades, an increasing number of quantum chemical investigations involving Fe species have been published.[62,63,176,351,352] These studies can be divided into three main types: (1) determining the geometries of aqueous Fe−ligand inner-sphere complexes, (2) investigating the interactions between sorbed Fe(II) and Fe(III) mineral surfaces, and (3) elucidating reaction mechanisms. Calculations typically commence with self-consistent minimization of the total electronic energy by geometry optimization, often with subsequent calculation of vibrational frequencies that can be used to estimate thermochemical contributions to the total energy using statistical mechanical partition functions. Based on the calculated Gibbs free energies of different proposed structures for Fe−ligand complexes, one can then identify the most stable geometry and properties comparable with spectroscopic measurements. Chemical and electronic properties of various mineral surfaces are now also routinely determined using electronic structure codes to help understand reactions occurring on the surfaces such as adsorption and redox processes.[429,460,473] By calculating reaction energy barriers based on the transition state geometries, certain reaction pathways and the rate-limiting steps can be tested and used to explore possible reaction mechanisms.[843−845] For example, Chen et al. has studied various possible structures and geometries of the Fe−tiron complexation intermediates formed in the reduction of pyridine *N*-oxide (PNO).[63] The authors performed tests including changing the number and position of water molecules binding to the Fe center and the initial position of PNO relative to the Fe center. The results showed that in the most probable geometry of the complexation intermediates, the water molecule formed no bridge between the PNO ring and tiron. Hofstetter et al.[846,847] performed density functional theory (DFT) calculations for the reduction of nitroaromatic compounds by Fe(II) bonding to goethite surfaces or Fe(II)−organic ligand, to investigate the influence of aromatic substituents during nitroaromatic reduction and to elucidate the mechanism of N−O bond cleavage. The authors compared the experimental values of the apparent kinetic isotope effect for N−O bond cleavage ($AKIE_N$) to computational $KIE_N$ and obtained similar values which suggest no substituent effect. They also demonstrated the dominant transition-state structures of nitroaromatic reduction intermediates to be substituted *N*,*N*-dihydroxyanilines, suggesting dehydration of *N*,*N*-dihydroxyanilines, i.e., the N−O bond cleavage step, is rate-limiting.

Most modern quantum chemical calculations are based on DFT because of its computational efficiency, because of its versatility to treat molecules, solids, and interfaces on an equal footing, and because of the availability of various well benchmarked formulations of the exchange-correlation functional.[848] The computational cost of calculations using this method is relatively low when compared to traditional exact exchange approaches such as Hartree−Fock but correspondingly does increase when admixtures of exact exchange into the exchange-correlation functional, so-called hybrid functionals, are needed for the sake of computational accuracy. DFT approaches have


https://doi.org/10.1021/acs.chemrev.0c01286
Chem. Rev. 2021, 121, 8161−8233

been widely adopted as a workhorse tool in the field of transition metal chemistry and computational chemistry. The hybrid B3LYP functional is one of the most commonly used classes of approximations for the exchange−correlation functional, which is a highly benchmarked functional based on Becke's three-parameter hybrid functional combined with the Lee−Yang−Parr correlation functional.[849−851] In quantum chemistry codes based on local orbital basis functions, the B3LYP functional combined with the basis set 6-31G(d) has been widely used with good performance.[852] As computing power has increased in recent decades, more accurate methods have become available and more widely used. For example, an increase in the basis set from the double-$\zeta$ basis set 6-31G(d) to the triple-$\zeta$ basis set 6-311+G(d,p) can provide sufficient accuracy especially in calculating more complex systems involving transition metal ions.[853] The major alternatives to these local orbital approaches to DFT are based on planewave basis functions, which while applicable to molecular computations tend to be much more efficient and versatile for solids and interfaces. Planewave DFT has the additional major added advantage of efficient implementation of molecular dynamics simulations for total free energy simulations with DFT-level accuracy.

It is noteworthy that the use of DFT for calculations of iron (oxyhydr)oxide phases requires careful attention to the details of the assumptions employed in order to properly obtain the correct description of their often complex magnetic structures arising from their strongly correlated 3*d* electrons.[752,763] To optimize the computational method, in addition to use of hybrid functionals, alternatively an empirically calibrated Hubbard U term can be added to the generalized gradient approximation (GGA) functional.[854−856] Calculations performed at this so-called GGA+*U* level can recover the correct electronic properties for calculations on models involving Fe.[857,858] Please see sections 4.2.1.1 and 4.2.4 for applications of various kinds of theoretical simulations applied to understanding key interactions between aqueous Fe(II) and iron(III) (oxyhydr)oxides.

Computational calculations remain an essential tool to explore detailed reaction mechanisms and to provide a basis for assisting interpretation of various kinds of experimentally measured values containing molecular-level information. They are also very useful for testing hypotheses pertaining to reaction mechanisms and pathways. Based on certain calculated intermediates and reaction barriers, a specific reaction pathway can sometimes be isolated, tracked, and confirmed.[753,754] However, computational calculations at the quantum mechanical level remain, often, too expensive to evaluate all possible elementary reactions and must be paired with robust physical chemistry intuition to be usefully effective.[859,860] Given the above difficulties, a theory and computational expert is often an essential component for success.

## 9. CONCLUSIONS AND FUTURE WORK

Understanding the redox reactivity of different types of Fe(II) species, including aqueous Fe(II), Fe(II) with ligands, structural Fe(II), and surface sorbed Fe(II) in natural and engineered environments, is important, due to their roles in the fate and transport of various contaminants in the environment, the global cycles of many major and minor elements, environmental remediation technologies, and microbial activity. Despite the progress made in the past 15 years, further research is still needed in several aspects, as detailed below.

Understanding the electron-transfer processes associated with these Fe(II) species can help examine the fate and transport of toxic species in the environment. However, as mentioned earlier, it is still unclear how electrons are transferred from sorbed and structural Fe(II) to contaminants and into microbial cells. Key questions in this field that still remain unanswered include what Fe(II) or composite Fe(II)−Fe(III) species, specifically, are formed on iron mineral surfaces? Is it necessary for Fe(II) to form inner-sphere species to enable electron transfer between Fe(II) and Fe(III), and what is the rate-limiting step in the electron-transfer process? In addition, although mechanisms have been proposed in a few studies to explain the differences in the reactivity of different Fe(II)-associated reductants, a complete understanding of these differences remains elusive. Similarly, the enzymatic mechanism of microbial oxidation of Fe(II)-containing minerals and surface sorbed Fe(II) species remains to be elucidated.

Recent studies have highlighted the importance of cryptic Fe cycling in biogeochemistry, which occurs through a concerted action of Fe(II)-oxidizing and Fe(III)-reducing bacteria or through coupled abiotic and microbially mediated redox reactions. It needs to be determined whether this process is common in the environment or is restricted to a few specialized habitats. Such a process has been shown to be vital in the limitation of energy for microbial life that depends on the availability of continuous redox reactions. Despite limited impacts to the net movement of one Fe atom, if one part of the cycle (e.g., Fe(II) oxidation) is repeatedly coupled to the redox transformation of a molecule (e.g., reduction of a pollutant) without being balanced by other processes, the cryptic Fe cycle can result in an amplifying effect to the transformation of the said molecule. Enormous consequences are therefore expected regarding the extent of biogeochemical cycling of various elements (e.g., C, S, N) and pollutants that are coupled to the cryptic Fe cycle.

In relation to elucidating the reductive transformations of contaminants in the environment, while this has significantly improved in recent decades, we are still far from possessing predictive tools due to the complexity of natural systems. Natural environments contain mixtures of dissolved inorganic $Fe^{2+}$, Fe(II)−NOM complexes, structural Fe(II), and surface sorbed Fe(II) on a diversity of minerals at varying ratios as well as other cosolutes and precipitates. The relative importance of these different Fe(II) species for Fe(II)-mediated redox reactions and microbial Fe(II) oxidation have yet to be determined. Moreover, for most studies involving surface sorbed Fe(II) and structural Fe(II), these are generally only focused on single, well defined iron oxides such as goethite, hematite, magnetite, or lepidocrocite. However, iron (oxyhydr)-oxides typically coexist with other minerals and organic matter in the environment. Understanding how secondary minerals and coexisting ions or organic matter affect the redox chemistry of iron is necessary. Over the past several years, there have been some studies examining the effect of secondary metal oxides and/or organic matter on oxidation,[366,444,771] yet very few studies have investigated the effect of these secondary oxides and/or organic matter on Fe(II)-mediated redox reactions and microbial Fe(II) oxidation.

The utilization of ZVI and Fe(II) bearing minerals in environmental applications has received increasing interest, but further attention should be given to the development of cost-effective methods for improving the reducing reactivity of these iron-based materials in different environments. Systematic research is also needed to improve their stability over a wide


https://doi.org/10.1021/acs.chemrev.0c01286
Chem. Rev. 2021, 121, 8161−8233

range of conditions to expand their possible application in contaminant sequestration and degradation in the environment.

Finally, an increasing volume of data has been generated in the past few decades about the redox reactivity of various Fe(II) species. Instead of employing traditional methods to understand such complex systems, which are inherently limited to well-defined systems including the types of compounds, the types of Fe(II) species, and reaction conditions, machine learning can be a very promising tool to help model these processes.[188] This is because machine learning algorithms have a powerful self-learning ability to identify the influencing factor(s) without the need for complicated chemical knowledge and computational calculations. To build robust machine learning models, it is pivotal to maintain a well-curated, open-access, and comprehensive database on all possible redox chemistry for Fe(II) in the environment.

## AUTHOR INFORMATION


### Corresponding Author

**Huichun Zhang** − *Department of Civil and Environmental Engineering, Case Western Reserve University, Cleveland, Ohio 44106, United States;* orcid.org/0000-0002-5683-5117; Email: hjz13@case.edu

### Authors

**Jianzhi Huang** − *Department of Civil and Environmental Engineering, Case Western Reserve University, Cleveland, Ohio 44106, United States*

**Adele Jones** − *UNSW Water Research Centre, School of Civil and Environmental Engineering, University of New South Wales, Sydney, New South Wales 2052, Australia*

**T. David Waite** − *UNSW Water Research Centre, School of Civil and Environmental Engineering, University of New South Wales, Sydney, New South Wales 2052, Australia;* orcid.org/0000-0002-5411-3233

**Yiling Chen** − *Institute of Environmental and Ecological Engineering, Guangdong University of Technology, Guangzhou 510006, China;* orcid.org/0000-0003-4806-5623

**Xiaopeng Huang** − *Physical Sciences Division, Pacific Northwest National Laboratory, Richland, Washington 99352, United States;* orcid.org/0000-0001-6606-7468

**Kevin M. Rosso** − *Physical Sciences Division, Pacific Northwest National Laboratory, Richland, Washington 99352, United States;* orcid.org/0000-0002-8474-7720

**Andreas Kappler** − *Geomicrobiology, Center for Applied Geosciences, University of Tuebingen, 72076 Tuebingen, Germany;* orcid.org/0000-0002-3558-9500

**Muammar Mansor** − *Geomicrobiology, Center for Applied Geosciences, University of Tuebingen, 72076 Tuebingen, Germany;* orcid.org/0000-0001-7830-650X

**Paul G. Tratnyek** − *School of Public Health, Oregon Health & Science University, Portland, Oregon 97239, United States;* orcid.org/0000-0001-8818-6417

Complete contact information is available at: https://pubs.acs.org/10.1021/acs.chemrev.0c01286


### Notes

The authors declare no competing financial interest.

### Biographies

Jianzhi Huang is a postdoc at the University of Washington studying the properties of interfacial water at hydrophilic surfaces. He received his Ph.D. degree in 2019 from Case Western Reserve University under the guidance of Prof. Huichun Zhang. His research focuses on environmental interfacial chemistry.

Adele Jones is a research associate at the Water Research Center, School of Civil and Environmental Engineering at the University of New South Wales (UNSW), Australia. Her research interests encompass a wide variety of areas including investigations into the reduction of contaminants in the environment by natural Fe(II)−Fe(III) mineral systems and iron nanoparticles. She completed her Ph.D. at UNSW in 2010 entitled "Chemical Transformations of Fe and Al from Acid Sulfate Soils to Coastal Waters"—a project which had a large field-based component. One of the most important findings from this work was that silica and natural organic matter can inhibit Fe(II)-catalyzed Fe(III) mineral transformation processes in the environment. Since the completion of her Ph.D. Adele has been working at UNSW as a research associate, and she also completed a 1-year Postdoctoral Fellowship at the Swiss Federal Institute of Aquatic Science and Technology (EAWAG) funded by the Swiss Government where she employed electrochemistry to study Fe(II)−Fe(III) oxide interactions. Adele has a great passion for the environment and enjoys research which combines fundamental and applied aspects. She is particularly fond of field work.

David Waite is a Scientia Professor in the School of Civil and Environmental Engineering at the University of New South Wales in Sydney, Australia. He served as Director of the UNSW Centre for Water and Waste Technology (now UNSW Water Research Centre) from 1993 to 2006, Head of the School of Civil and Environmental Engineering from 2007 to 2013, and Deputy Dean of the Facuilty of Engineering from 2013 to 2017. Professor Waite currently holds the position of Executive Chairman of the UNSW Centre for Transformational Environmental Technologies (CTET) in Yixing (Jiangsu Province) and is an Associate Editor of the journal Environmental Science & Technology. He was honoured with membership of the US National Academy of Engineering in 2018. Professor Waite's research interests are focussed on the kinetics of metal-mediated redox processes in natural and engineered systems.

Yiling Chen is an associate professor in the Institute of Environmental and Ecological Engineering at Guangdong University of Technology, China. She obtained her Ph.D. degree at Temple University in 2016, where she worked with Prof. Huichun Zhang for her doctoral dissertation on the topic of reduction of organic contaminants. Dr. Chen moved to the University of Minnesota in 2017 as a postdoctoral associate, working with Profs. Raymond Hozalski, Bill Arnold, and John Gulliver, in the field of satellite imaging, photodegradation, and tire derived aggregates. She joined Guangdong University of Technology in 2021. The majority of Dr. Chen's current work focuses on the fate and transformation of organic contaminants based on machine learning and satellite remote sensing.

Xiaopeng Huang gained his Ph.D. degree in Physical Chemistry from Central China Normal University in 2017 under the supervision of Professor Lizhi Zhang and Academician Jincai Zhao. Currently, he is a Post Doctorate Research Associate in Geochemistry Group under the supervision of Laboratory Fellow Kevin M. Rosso at Pacific Northwest National Laboratory. His research interests focus on iron biogeochemical processes and environmental remediation.

Kevin M. Rosso received his first degree in geological sciences from California State Polytechnic University at Pomona, California, USA in 1992 and then completed his M.S. (1994) and Ph.D. (1998) degrees in geochemistry at Virginia Polytechnic and State University in Blacksburg, Virginia, USA. He then joined the staff of Pacific Northwest National Laboratory (PNNL) in Richland, Washington, USA where he


https://doi.org/10.1021/acs.chemrev.0c01286
Chem. Rev. 2021, 121, 8161−8233

is now a Laboratory Fellow and the Associate Director of the Physical Sciences Division for Geochemistry. Having studied diverse molecular interfacial science topics over his career, he is best known for his pioneering research on understanding and predicting rates of electron-transfer reactions between aqueous ions, mineral surfaces, and bacterial enzymes. Prof. Rosso has published a large body of work based on laboratory experimental and molecular computational studies across geochemical, environmental, and materials science topics ranging from the electronic and atomic structure of minerals and their surfaces, electron transfer through cytochromes and metal oxide reduction by microorganisms, iron sulfide oxidation mechanisms, and redox kinetics between various aqueous metal cations, organics, proteins, and mineral surfaces.

Andreas Kappler is a professor for Geomicrobiology at the University of Tuebingen (Germany). He received his M.Sc. in Chemistry and his Ph.D. in Environmental Microbiology from University of Konstanz (Germany) and had postdoc positions at the EAWAG/ETH Zuerich (Swirtzerland) in Environmental Chemistry and at Caltech (USA) in Geobiology. The major focus of his research is the biogeochemical cycling of iron and natural organic matter (NOM) and the consequences for the environmental fate of greenhouse gases, toxic metals (arsenic, cadmium, etc.), and nutrients. Other main research areas are the role of microbial iron oxidation in the deposition of Precambrian Banded Iron Formations, biochar as soil amendment, and carbon/iron cycling in permafrost soils.

Muammar Mansor is a Junior Research Group Leader at the University of Tuebingen (Germany). He received his M.Sc. in Biotechnology and his Ph.D. in Geosciences & Astrobiology from Penn State University (USA) and served as a postdoc in Nanogeomicrobiology at the University of Texas at El Paso (USA). His research focuses on biomineral formation by microbial life, focusing on their roles in biogeochemical cycling, environmental remediation, and ancient biosignatures. Other research areas include the development of new approaches to study nanoparticle-driven processes in the environment and the investigation of pyrite in modern microbial mats.

Paul G. Tratnyek is a Professor at Oregon Health & Science University. He received his Ph.D. from Colorado School of Mines in 1987. His research concerns the physicochemical processes that control the fate and effects of environmental substances, including minerals, metals (for remediation), organics (as contaminants), and nanoparticles (for remediation, as contaminants, and in biomedical applications). Dr. Tratnyek is best known for his work on the degradation of groundwater contaminants with zerovalent metals, but his interests extend to all aspects of contaminant reduction and oxidation (redox) in all aquatic media. Some of his recent work emphasizes the fate/remediation of emerging contaminants (e.g., nanoparticles and 1,2,3-trichloropropane) and next generation energetic compounds (e.g., DNAN). He has given numerous invited presentations on contaminant degradation by iron metal and is a (co)principal organizer of many relevant symposia.

Huichun Zhang is Frank H. Neff Professor in the Department of Civil and Environmental Engineering at Case Western Reserve University (US). She received her B.S. (1994) and M.S. (1997) in environmental chemistry from Nanjing University (China), and her Ph.D. (2004) in Environmental Engineering from Georgia Institute of Technology (US). Her major research interests include interfacial reduction–oxidation processes in complex mixtures and the fate and transformation of emerging organic contaminants in natural and engineered environments. Her recent research areas also include predictive modeling for contaminant reactivity and sorption using both classical models and machine learning tools.

## ACKNOWLEDGMENTS

H.Z. acknowledges the support by the National Science Foundation under Grants CBET-1762691 and CHE-1762686. K.M.R. and X.H. acknowledge support by the U.S. Department of Energy (DOE), Office of Science, Office of Basic Energy Sciences, Chemical Sciences, Geosciences & Biosciences Division through its Geosciences Program at Pacific Northwest National Laboratory (PNNL). P.G.T.'s contributions were funded via NSF grant 1708513 and SERDP grant ER-20-1357. The authors are thankful to Anke Neumann from Newcastle University and Michelle Scherer from University of Iowa for their valuable suggestions.

## REFERENCES

(1) Johnson, K. S.; Gordon, R. M.; Coale, K. H. What Controls Dissolved Iron Concentrations in the World Ocean? *Mar. Chem.* **1997**, *57*, 137–161.
(2) Cornell, R. M.; Schwertmann, U. *The Iron Oxides: Structure, Properties, Reactions, Occurrences and Uses*; Wiley-VCH: Berlin, 2003.
(3) Stumm, W.; Sulzberger, B. The Cycling of Iron in Natural Environments: Considerations Based on Laboratory Studies of Heterogeneous Redox Processes. *Geochim. Cosmochim. Acta* **1992**, *56*, 3233–3257.
(4) Shi, D.; Xu, Y.; Hopkinson, B. M.; Morel, F. M. M. Effect of Ocean Acidification on Iron Availability to Marine Phytoplankton. *Science* **2010**, *327*, 676–679.
(5) Sunda, W. G. Iron and the Carbon Pump. *Science* **2010**, *327*, 654–655.
(6) Borch, T.; Kretzschmar, R.; Kappler, A.; Cappellen, P. V.; Ginder-Vogel, M.; Voegelin, A.; Campbell, K. Biogeochemical Redox Processes and Their Impact on Contaminant Dynamics. *Environ. Sci. Technol.* **2010**, *44*, 15–23.
(7) Dinh, H. T.; Kuever, J.; Mußmann, M.; Hassel, A. W.; Stratmann, M.; Widdel, F. Iron Corrosion by Novel Anaerobic Microorganisms. *Nature* **2004**, *427*, 829–832.
(8) Huang, J.; Dai, Y.; Liu, C.-C.; Zhang, H. Effects of Second Metal Oxides on Surface-Mediated Reduction of Contaminants by Fe(II) with Iron Oxide. *ACS Earth Space Chem.* **2019**, *3*, 680–687.
(9) Cundy, A. B.; Hopkinson, L.; Whitby, R. L. D. Use of Iron-Based Technologies in Contaminated Land and Groundwater Remediation: A Review. *Sci. Total Environ.* **2008**, *400*, 42–51.
(10) Frierdich, A. J.; Catalano, J. G. Fe(II)-Mediated Reduction and Repartitioning of Structurally Incorporated Cu, Co, and Mn in Iron Oxides. *Environ. Sci. Technol.* **2012**, *46*, 11070–11077.
(11) Frierdich, A. J.; Luo, Y.; Catalano, J. G. Trace Element Cycling through Iron Oxide Minerals During Redox-Driven Dynamic Recrystallization. *Geology* **2011**, *39*, 1083–1086.
(12) Shindo, H.; Huang, P. M. Catalytic Effects of Manganese(IV), Iron(III), Aluminum, and Silicon Oxides on the Formation of Phenolic Polymers. *Soil Sci. Soc. Am. J.* **1984**, *48*, 927–934.
(13) Shindo, H. Relative Effectiveness of Short-Range Ordered Mn(IV), Fe(III), Al, and Si Oxides in the Synthesis of Humic Acids from Phenolic Compounds. *Soil Sci. Plant Nutr.* **1992**, *38*, 459–465.
(14) Davis, J. A. Adsorption of Natural Dissolved Organic Matter at the Oxide/Water Interface. *Geochim. Cosmochim. Acta* **1982**, *46*, 2381–2393.
(15) Gu, B.; Schmitt, J.; Chen, Z.; Liang, L.; McCarthy, J. F. Adsorption and Desorption of Natural Organic Matter on Iron Oxide: Mechanisms and Models. *Environ. Sci. Technol.* **1994**, *28*, 38–46.
(16) Kraemer, S. M.; Butler, A.; Borer, P.; Cervini-Silva, J. Siderophores and the Dissolution of Iron-Bearing Minerals in Marine Systems. *Rev. Mineral. Geochem.* **2005**, *59*, 53–84.
(17) Rozan, T. F.; Taillefert, M.; Trouwborst, R. E.; Glazer, B. T.; Ma, S.; Herszage, J.; Valdes, L. M.; Price, K. S.; Luther, G. W., III Iron-Sulfur-Phosphorus Cycling in the Sediments of a Shallow Coastal Bay: Implications for Sediment Nutrient Release and Benthic Macroalgal Blooms. *Limnol. Oceanogr.* **2002**, *47*, 1346–1354.


https://doi.org/10.1021/acs.chemrev.0c01286
*Chem. Rev.* 2021, 121, 8161–8233

(18) Goldich, S. S. A Study in Rock-Weathering. *J. Geol.* **1938**, *46*, 17−58.
(19) Weber, K. A.; Achenbach, L. A.; Coates, J. D. Microorganisms Pumping Iron: Anaerobic Microbial Iron Oxidation and Reduction. *Nat. Rev. Microbiol.* **2006**, *4*, 752−764.
(20) Weiss, W.; Ranke, W. Surface Chemistry and Catalysis on Well-Defined Epitaxial Iron-Oxide Layers. *Prog. Surf. Sci.* **2002**, *70*, 1−151.
(21) Kang, Y.; Ye, X.; Chen, J.; Qi, L.; Diaz, R. E.; Doan-Nguyen, V.; Xing, G.; Kagan, C. R.; Li, J.; Gorte, R. J. Engineering Catalytic Contacts and Thermal Stability: Gold/Iron Oxide Binary Nanocrystal Superlattices for Co Oxidation. *J. Am. Chem. Soc.* **2013**, *135*, 1499−1505.
(22) Cantillo, D.; Baghbanzadeh, M.; Kappe, C. O. In Situ Generated Iron Oxide Nanocrystals as Efficient and Selective Catalysts for the Reduction of Nitroarenes Using a Continuous Flow Method. *Angew. Chem., Int. Ed.* **2012**, *51*, 10190−10193.
(23) Sarin, P.; Snoeyink, V.; Bebee, J.; Kriven, W. M.; Clement, J. Physico-Chemical Characteristics of Corrosion Scales in Old Iron Pipes. *Water Res.* **2001**, *35*, 2961−2969.
(24) Mornet, S.; Vasseur, S.; Grasset, F.; Duguet, E. Magnetic Nanoparticle Design for Medical Diagnosis and Therapy. *J. Mater. Chem.* **2004**, *14*, 2161−2175.
(25) Hradil, D.; Grygar, T.; Hradilová, J.; Bezdička, P. Clay and Iron Oxide Pigments in the History of Painting. *Appl. Clay Sci.* **2003**, *22*, 223−236.
(26) A. Jadhav, S.; Bongiovanni, R.; L. Marchisio, D.; Fontana, D.; Egger, C. Surface Modification of Iron Oxide ($Fe_2O_3$) Pigment Particles with Amino-Functional Polysiloxane for Improved Dispersion Stability and Hydrophobicity. *Pigm. Resin Technol.* **2014**, *43*, 219−227.
(27) Kaushik, A.; Solanki, P. R.; Ansari, A. A.; Sumana, G.; Ahmad, S.; Malhotra, B. D. Iron Oxide-Chitosan Nanobiocomposite for Urea Sensor. *Sens. Actuators, B* **2009**, *138*, 572−580.
(28) Klahr, B. M.; Martinson, A. B.; Hamann, T. W. Photoelectrochemical Investigation of Ultrathin Film Iron Oxide Solar Cells Prepared by Atomic Layer Deposition. *Langmuir* **2011**, *27*, 461−468.
(29) Wu, W. Q.; Xu, Y. F.; Rao, H. S.; Feng, H. L.; Su, C. Y.; Kuang, D. B. Constructing 3D Branched Nanowire Coated Macroporous Metal Oxide Electrodes with Homogeneous or Heterogeneous Compositions for Efficient Solar Cells. *Angew. Chem., Int. Ed.* **2014**, *53*, 4816−4821.
(30) Phenrat, T.; Thongboot, T.; Lowry, G. V. Electromagnetic Induction of Zerovalent Iron (ZVI) Powder and Nanoscale Zerovalent Iron (NZVI) Particles Enhances Dechlorination of Trichloroethylene in Contaminated Groundwater and Soil: Proof of Concept. *Environ. Sci. Technol.* **2016**, *50*, 872−880.
(31) Fu, F.; Dionysiou, D. D.; Liu, H. The Use of Zero-Valent Iron for Groundwater Remediation and Wastewater Treatment: A Review. *J. Hazard. Mater.* **2014**, *267*, 194−205.
(32) Tucek, J.; Kemp, K. C.; Kim, K. S.; Zboril, R. Iron-Oxide-Supported Nanocarbon in Lithium-Ion Batteries, Medical, Catalytic, and Environmental Applications. *ACS Nano* **2014**, *8*, 7571−7612.
(33) Tanaka, S.; Kaneti, Y. V.; Septiani, N. L. W.; Dou, S. X.; Bando, Y.; Hossain, M. S. A.; Kim, J.; Yamauchi, Y. A Review on Iron Oxide-Based Nanoarchitectures for Biomedical, Energy Storage, and Environmental Applications. *Small Methods* **2019**, *3*, 1800512−1800555.
(34) Brundrett, M.; Yan, W.; Velazquez, M. C.; Rao, B.; Jackson, W. A. Abiotic Reduction of Chlorate by Fe(II) Minerals: Implications for Occurrence and Transformation of Oxy-Chlorine Species on Earth and Mars. *ACS Earth Space Chem.* **2019**, *3*, 700−710.
(35) Taylor, K. G.; Konhauser, K. O. Iron in Earth Surface Systems: A Major Player in Chemical and Biological Processes. *Elements* **2011**, *7*, 83−88.
(36) Stumm, W.; Morgan, J. *Aquatic Chemistry*; John Wiley & Sons. Inc.: New York, 1996.
(37) Millero, F. J. Solubility of Fe(III) in Seawater. *Earth Planet. Sci. Lett.* **1998**, *154*, 323−329.
(38) Millero, F. J.; Yao, W.; Aicher, J. The Speciation of Fe(II) and Fe(III) in Natural Waters. *Mar. Chem.* **1995**, *50*, 21−39.
(39) Burns, R. G. Rates and Mechanisms of Chemical Weathering of Ferromagnesian Silicate Minerals on Mars. *Geochim. Cosmochim. Acta* **1993**, *57*, 4555−4574.
(40) Lovley, D. R.; Holmes, D. E.; Nevin, K. P. Dissimilatory Fe(III) and Mn(IV) Reduction. *Adv. Microb. Physiol.* **2004**, *49*, 219−286.
(41) Bosch, J.; Heister, K.; Hofmann, T.; Meckenstock, R. U. Nanosized Iron Oxide Colloids Strongly Enhance Microbial Iron Reduction. *Appl. Environ. Microbiol.* **2010**, *76*, 184−189.
(42) Roden, E. E. Geochemical and Microbiological Controls on Dissimilatory Iron Reduction. *C. R. Geosci.* **2006**, *338*, 456−467.
(43) Balzano, S.; Statham, P.; Pancost, R.; Lloyd, J. Role of Microbial Populations in the Release of Reduced Iron to the Water Column from Marine Aggregates. *Aquat. Microb. Ecol.* **2009**, *54*, 291−303.
(44) Salmon, T. P.; Rose, A. L.; Neilan, B. A.; Waite, T. D. The FeL Model of Iron Acquisition: Nondissociative Reduction of Ferric Complexes in the Marine Environment. *Limnol. Oceanogr.* **2006**, *51*, 1744−1754.
(45) Wang, Z.; Liu, C.; Wang, X.; Marshall, M. J.; Zachara, J. M.; Rosso, K. M.; Dupuis, M.; Fredrickson, J. K.; Heald, S.; Shi, L. Kinetics of Reduction of Fe(III) Complexes by Outer Membrane Cytochromes MtrC and OmcA of *Shewanella Oneidensis* MR-1. *Appl. Environ. Microbiol.* **2008**, *74*, 6746−6755.
(46) Barbeau, K.; Rue, E.; Bruland, K. W.; Butler, A. Photochemical Cycling of Iron in the Surface Ocean Mediated by Microbial Iron(III)-Binding Ligands. *Nature* **2001**, *413*, 409−413.
(47) Amin, S. A.; Green, D. H.; Hart, M. C.; Küpper, F. C.; Sunda, W. G.; Carrano, C. J. Photolysis of Iron−Siderophore Chelates Promotes Bacterial−Algal Mutualism. *Proc. Natl. Acad. Sci. U. S. A.* **2009**, *106*, 17071−17076.
(48) Li, Y.-L.; Vali, H.; Yang, J.; Phelps, T. J.; Zhang, C. L. Reduction of Iron Oxides Enhanced by a Sulfate-Reducing Bacterium and Biogenic $H_2S$. *Geomicrobiol. J.* **2006**, *23*, 103−117.
(49) Stucki, J. W.; Golden, D. C.; Roth, C. B. Preparation and Handling of Dithionite-Reduced Smectite Suspensions. *Clays Clay Miner.* **1984**, *32*, 191−197.
(50) Fialips, C.-I.; Huo, D.; Yan, L.; Wu, J.; Stucki, J. W. Infrared Study of Reduced and Reduced-Reoxidized Ferruginous Smectite. *Clays Clay Miner.* **2002**, *50*, 455−469.
(51) Lear, P. R.; Stucki, J. W. Intervalence Electron Transfer and Magnetic Exchange in Reduced Nontronite. *Clays Clay Miner.* **1987**, *35*, 373−378.
(52) Ribeiro, F. R.; Fabris, J. D.; Kostka, J. E.; Komadel, P.; Stucki, J. W. Comparisons of Structural Iron Reduction in Smectites by Bacteria and Dithionite: II. A Variable-Temperature Mössbauer Spectroscopic Study of Garfield Nontronite. *Pure Appl. Chem.* **2009**, *81*, 1499−1509.
(53) Neumann, A.; Petit, S.; Hofstetter, T. B. Evaluation of Redox-Active Iron Sites in Smectites Using Middle and near Infrared Spectroscopy. *Geochim. Cosmochim. Acta* **2011**, *75*, 2336−2355.
(54) Fredrickson, J. K.; Gorby, Y. A. Environmental Processes Mediated by Iron-Reducing Bacteria. *Curr. Opin. Biotechnol.* **1996**, *7*, 287−294.
(55) Urrutia, M.; Roden, E.; Fredrickson, J.; Zachara, J. Microbial and Surface Chemistry Controls on Reduction of Synthetic Fe(III) Oxide Minerals by the Dissimilatory Iron-Reducing Bacterium Shewanella Alga. *Geomicrobiol. J.* **1998**, *15*, 269−291.
(56) Zachara, J. M.; Kukkadapu, R. K.; Fredrickson, J. K.; Gorby, Y. A.; Smith, S. C. Biomineralization of Poorly Crystalline Fe(III) Oxides by Dissimilatory Metal Reducing Bacteria (DMRB). *Geomicrobiol. J.* **2002**, *19*, 179−207.
(57) Glasauer, S.; Langley, S.; Beveridge, T. J. Intracellular Iron Minerals in a Dissimilatory Iron-Reducing Bacterium. *Science* **2002**, *295*, 117−119.
(58) Vargas, M.; Kashefi, K.; Blunt-Harris, E. L.; Lovley, D. R. Microbiological Evidence for Fe (III) Reduction on Early Earth. *Nature* **1998**, *395*, 65−67.
(59) Sun, Y.; Li, J.; Huang, T.; Guan, X. The Influences of Iron Characteristics, Operating Conditions and Solution Chemistry on Contaminants Removal by Zero-Valent Iron: A Review. *Water Res.* **2016**, *100*, 277−295.
(60) Naka, D.; Kim, D.; Strathmann, T. J. Abiotic Reduction of Nitroaromatic Compounds by Aqueous Iron(II)-Catechol Complexes. *Environ. Sci. Technol.* **2006**, *40*, 3006−3012.


https://doi.org/10.1021/acs.chemrev.0c01286
*Chem. Rev.* 2021, 121, 8161−8233

(61) Naka, D.; Kim, D.; Carbonaro, R. F.; Strathmann, T. J. Abiotic Reduction of Nitroaromatic Contaminants by Iron(II) Complexes with Organothiol Ligands. *Environ. Toxicol. Chem.* **2008**, *27*, 1257−1266.
(62) Chen, Y.; Zhang, H. Complexation Facilitated Reduction of Aromatic N-Oxides by Aqueous $Fe^{II}$−Tiron Complex: Reaction Kinetics and Mechanisms. *Environ. Sci. Technol.* **2013**, *47*, 11023−11031.
(63) Chen, Y.; Dong, H.; Zhang, H. Experimental and Computational Evidence for the Reduction Mechanisms of Aromatic N-Oxides by Aqueous $Fe^{II}$−Tiron Complex. *Environ. Sci. Technol.* **2016**, *50*, 249−258.
(64) Gorski, C. A.; Scherer, M. M. Influence of Magnetite Stoichiometry on $Fe^{II}$ Uptake and Nitrobenzene Reduction. *Environ. Sci. Technol.* **2009**, *43*, 3675−3680.
(65) Latta, D. E.; Gorski, C. A.; Boyanov, M. I.; O'Loughlin, E. J.; Kemner, K. M.; Scherer, M. M. Influence of Magnetite Stoichiometry on $U^{VI}$ Reduction. *Environ. Sci. Technol.* **2012**, *46*, 778−786.
(66) Latta, D.; Boyanov, M.; Kemner, K.; Loughlin, E.; Scherer, M. Reaction of Uranium(VI) with Green Rusts: Effect of Interlayer Anion. *Curr. Inorg. Chem.* **2015**, *5*, 156−168.
(67) Génin, J.-M.; Olowe, A.; Refait, P.; Simon, L. On the Stoichiometry and Pourbaix Diagram of Fe(II)-Fe(III) Hydroxy-Sulphate or Sulphate-Containing Green Rust 2: An Electrochemical and Mössbauer Spectroscopy Study. *Corros. Sci.* **1996**, *38*, 1751−1762.
(68) Grambow, B.; Smailos, E.; Geckeis, H.; Müller, R.; Hentschel, H. Sorption and Reduction of Uranium(VI) on Iron Corrosion Products under Reducing Saline Conditions. *Radiochim. Acta* **1996**, *74*, 149−154.
(69) Hansen, H. C. B.; Koch, C. B.; Nancke-Krogh, H.; Borggaard, O. K.; Sørensen, J. Abiotic Nitrate Reduction to Ammonium: Key Role of Green Rust. *Environ. Sci. Technol.* **1996**, *30*, 2053−2056.
(70) Peterson, M. L.; Brown, G. E.; Parks, G. A. Direct XAFS Evidence for Heterogeneous Redox Reaction at the Aqueous Chromium/Magnetite Interface. *Colloids Surf., A* **1996**, *107*, 77−88.
(71) Zhang, H.; Weber, E. J. Elucidating the Role of Electron Shuttles in Reductive Transformations in Anaerobic Sediments. *Environ. Sci. Technol.* **2009**, *43*, 1042−1048.
(72) Zhang, H.; Weber, E. J. Identifying Indicators of Reactivity for Chemical Reductants in Sediments. *Environ. Sci. Technol.* **2013**, *47*, 6959−6968.
(73) Nano, G. V.; Strathmann, T. J. Application of Surface Complexation Modeling to the Reactivity of Iron(II) with Nitroaromatic and Oxime Carbamate Contaminants in Aqueous $TiO_2$ Suspensions. *J. Colloid Interface Sci.* **2008**, *321*, 350−359.
(74) Charlet, L.; Silvester, E.; Liger, E. N-Compound Reduction and Actinide Immobilisation in Surficial Fluids by Fe(II): The Surface $Fe^{III}OFe^{II}OH°$ Species as Major Reductant. *Chem. Geol.* **1998**, *151*, 85−93.
(75) Bauer, I.; Knölker, H.-J. Iron Catalysis in Organic Synthesis. *Chem. Rev.* **2015**, *115*, 3170−3387.
(76) Wei, D.; Darcel, C. Iron Catalysis in Reduction and Hydrometalation Reactions. *Chem. Rev.* **2019**, *119*, 2550−2610.
(77) Mondal, P.; Anweshan, A.; Purkait, M. K. Green Synthesis and Environmental Application of Iron-Based Nanomaterials and Nanocomposite: A Review. *Chemosphere* **2020**, *259*, 127509.
(78) Zou, Y.; Wang, X.; Khan, A.; Wang, P.; Liu, Y.; Alsaedi, A.; Hayat, T.; Wang, X. Environmental Remediation and Application of Nanoscale Zero-Valent Iron and Its Composites for the Removal of Heavy Metal Ions: A Review. *Environ. Sci. Technol.* **2016**, *50*, 7290−7304.
(79) Usman, M.; Byrne, J. M.; Chaudhary, A.; Orsetti, S.; Hanna, K.; Ruby, C.; Kappler, A.; Haderlein, S. B. Magnetite and Green Rust: Synthesis, Properties, and Environmental Applications of Mixed-Valent Iron Minerals. *Chem. Rev.* **2018**, *118*, 3251−3304.
(80) Strathmann, T. Redox Reactivity of Organically Complexed Iron(II) Species with Aquatic Contaminants. In *Aquatic Redox Chemistry*; Tratnyek, P. G., Grundl, T. J., Haderlein, S. B., Eds.; ACS Symposium Series; American Chemical Society: Washington, DC, 2011; Vol. *1071*, Chapter 14, pp 283−313.
(81) Neumann, A.; Sander, M.; Hofstetter, T. B. Redox Properties of Structural Fe in Smectite Clay Minerals. In *Aquatic Redox Chemistry*; Tratnyek, P. G., Grundl, T. J., Haderlein, S. B., Eds.; ACS Symposium Series; American Chemical Society: Washington, DC, 2011; Vol. *1071*, Chapter 17, pp 361−379.
(82) He, Y.; Su, C.; Wilson, J.; Wilkin, R.; Adair, C.; Lee, T.; Bradley, P.; Ferrey, M. Identification and Characterization Methods for Reactive Minerals Responsible for Natural Attenuation of Chlorinated Organic Compounds in Ground Water. EPA/600/R-09/115; U.S. Environmental Protection Agency Office of Research and Development: Ada, OK, 2009.
(83) Rickard, D.; Luther, G. W. Chemistry of Iron Sulfides. *Chem. Rev.* **2007**, *107*, 514−562.
(84) Lee Wolfe, N.; Macalady, D. L. New Perspectives in Aquatic Redox Chemistry: Abiotic Transformations of Pollutants in Groundwater and Sediments. *J. Contam. Hydrol.* **1992**, *9*, 17−34.
(85) Tsukano, Y. Transformations of Selected Pesticides in Flooded Rice-Field Soil—a Review. *J. Contam. Hydrol.* **1986**, *1*, 47−63.
(86) Macalady, D. L.; Tratnyek, P. G.; Grundl, T. J. Abiotic Reduction Reactions of Anthropogenic Organic Chemicals in Anaerobic Systems: A Critical Review. *J. Contam. Hydrol.* **1986**, *1*, 1−28.
(87) Haderlein, S. B.; Pecher, K. Pollutant Reduction in Heterogeneous Fe(II)-Fe(III) Systems. In *Mineral-Water Interfacial Reactions*; Sparks, D. L., Grundl, T. J., Eds.; ACS Symposium Series; American Chemical Society: Washington, DC, 1999; Vol. *715*, Chapter 17, pp 342−357.
(88) Amonette, J. E. Iron Redox Chemistry of Clays and Oxides: Environmental Application. In *Electrochemical Properties of Clays*; Fitch, A., Eds.; Clay Minerals Society: Aurora, CO, 2002; Vol. *10*, pp 89−147.
(89) Sulzberger, B.; Suter, D.; Siffert, C.; Banwart, S.; Stumm, W. Dissolution of Fe (III)(Hydr) Oxides in Natural Waters; Laboratory Assessment on the Kinetics Controlled by Surface Coordination. *Mar. Chem.* **1989**, *28*, 127−144.
(90) Canfield, D. E. Reactive Iron in Marine Sediments. *Geochim. Cosmochim. Acta* **1989**, *53*, 619−632.
(91) Amirbahman, A.; Sigg, L.; Gunten, U. v. Reductive Dissolution of Fe(III) (Hydr)Oxides by Cysteine: Kinetics and Mechanism. *J. Colloid Interface Sci.* **1997**, *194*, 194−206.
(92) Zhang, H.; Rasamani, K. D.; Zhong, S.; Taujale, S.; Baratta, L. R.; Yang, Z. Dissolution, Adsorption, and Redox Reaction in Ternary Mixtures of Goethite, Aluminum Oxides, and Hydroquinone. *J. Phys. Chem. C* **2019**, *123*, 4371−4379.
(93) Banwart, S.; Davies, S.; Stumm, W. The Role of Oxalate in Accelerating the Reductive Dissolution of Hematite ($\alpha$-$Fe_2O_3$) by Ascorbate. *Colloids Surf.* **1989**, *39*, 303−309.
(94) Suter, D.; Siffert, C.; Sulzberger, B.; Stumm, W. Catalytic Dissoluion of Iron(III)(Hydr)Oxides by Oxalic Acid in the Presence of Fe(II). *Naturwissenschaften* **1988**, *75*, 571−573.
(95) Dhungana, S.; Anthony, C. R.; Hersman, L. E. Ferrihydrite Dissolution by Pyridine-2,6-Bis(Monothiocarboxylic Acid) and Hydrolysis Products. *Geochim. Cosmochim. Acta* **2007**, *71*, 5651−5660.
(96) Jang, J.-H.; Mathur, R.; Liermann, L. J.; Ruebush, S.; Brantley, S. L. An Iron Isotope Signature Related to Electron Transfer between Aqueous Ferrous Iron and Goethite. *Chem. Geol.* **2008**, *250*, 40−48.
(97) Suter, D.; Banwart, S.; Stumm, W. Dissolution of Hydrous Iron(III) Oxides by Reductive Mechanisms. *Langmuir* **1991**, *7*, 809−813.
(98) Lovley, D. R. Microbial Fe (III) Reduction in Subsurface Environments. *FEMS Microbiol. Rev.* **1997**, *20*, 305−313.
(99) Myers, C. R.; Nealson, K. H. Respiration-Linked Proton Translocation Coupled to Anaerobic Reduction of Manganese(IV) and Iron(III) in *Shewanella Putrefaciens* MR-1. *J. Bacteriol.* **1990**, *172*, 6232−6238.
(100) Lovley, D. R.; Phillips, E. J. P. Novel Mode of Microbial Energy Metabolism: Organic Carbon Oxidation Coupled to Dissimilatory Reduction of Iron or Manganese. 1988, *54*, 1472-1480.
(101) Brutinel, E. D.; Gralnick, J. A. Shuttling Happens: Soluble Flavin Mediators of Extracellular Electron Transfer in Shewanella. *Appl. Microbiol. Biotechnol.* **2012**, *93*, 41−48.


https://doi.org/10.1021/acs.chemrev.0c01286
*Chem. Rev.* 2021, 121, 8161−8233

(102) Kappler, A.; Bryce, C.; Mansor, M.; Lueder, U.; Byrne, J. M.; Swanner, E. D. An Evolving View on Biogeochemical Cycling of Iron. *Nat. Rev. Microbiol.* **2021**, *19*, 360.
(103) Lower, S. K.; Hochella, M. F.; Beveridge, T. J. Bacterial Recognition of Mineral Surfaces: Nanoscale Interactions between *Shewanella* and α-FeOOH. *Science* **2001**, *292*, 1360−1363.
(104) Nevin, K. P.; Lovley, D. R. Lack of Production of Electron-Shuttling Compounds or Solubilization of Fe(III) During Reduction of Insoluble Fe(III) Oxide by *Geobacter Metallireducens*. *Appl. Environ. Microbiol.* **2000**, *66*, 2248−2251.
(105) Childers, S. E.; Ciufo, S.; Lovley, D. R. *Geobacter Metallireducens* Accesses Insoluble Fe(III) Oxide by Chemotaxis. *Nature* **2002**, *416*, 767−769.
(106) Reguera, G.; McCarthy, K. D.; Mehta, T.; Nicoll, J. S.; Tuominen, M. T.; Lovley, D. R. Extracellular Electron Transfer Via Microbial Nanowires. *Nature* **2005**, *435*, 1098−1101.
(107) Nevin, K. P.; Lovley, D. R. Mechanisms for Fe(III) Oxide Reduction in Sedimentary Environments. *Geomicrobiol. J.* **2002**, *19*, 141−159.
(108) Lovley, D. R.; Woodward, J. C.; Chapelle, F. H. Rapid Anaerobic Benzene Oxidation with a Variety of Chelated Fe(III) Forms. *Appl. Environ. Microbiol.* **1996**, *62*, 288−291.
(109) Lovley, D. R.; Woodward, J. C.; Chapelle, F. H. Stimulated Anoxic Biodegradation of Aromatic Hydrocarbons Using Fe(III) Ligands. *Nature* **1994**, *370*, 128−131.
(110) Holmén, B. A.; Casey, W. H. Hydroxamate Ligands, Surface Chemistry, and the Mechanism of Ligand-Promoted Dissolution of Goethite [α-FeOOH(s)]. *Geochim. Cosmochim. Acta* **1996**, *60*, 4403−4416.
(111) Hernandez, M. E.; Newman, D. K. Extracellular Electron Transfer. *Cell. Mol. Life Sci.* **2001**, *58*, 1562−1571.
(112) Scherr, K. E., Extracellular electron transfer in *in situ* petroleum hydrocarbon bioremediation. In *Hydrocarbon*; Kutcherov, V., Kolesnikov, A., Eds.; InTech: New York, 2013; pp 161−194.
(113) Watanabe, K.; Manefield, M.; Lee, M.; Kouzuma, A. Electron Shuttles in Biotechnology. *Curr. Opin. Biotechnol.* **2009**, *20*, 633−641.
(114) Zhou, S.; Tang, J.; Yuan, Y.; Yang, G.; Xing, B. $TiO_2$ Nanoparticle-Induced Nanowire Formation Facilitates Extracellular Electron Transfer. *Environ. Sci. Technol. Lett.* **2018**, *5*, 564−570.
(115) Lovley, D. R.; Coates, J. D.; Blunt-Harris, E. L.; Phillips, E. J. P.; Woodward, J. C. Humic Substances as Electron Acceptors for Microbial Respiration. *Nature* **1996**, *382*, 445−448.
(116) Marsili, E.; Baron, D. B.; Shikhare, I. D.; Coursolle, D.; Gralnick, J. A.; Bond, D. R. *Shewanella* Secretes Flavins That Mediate Extracellular Electron Transfer. *Proc. Natl. Acad. Sci. U.S.A.* **2008**, *105*, 3968−3973.
(117) Newman, D. K.; Kolter, R. A Role for Excreted Quinones in Extracellular Electron Transfer. *Nature* **2000**, *405*, 94−97.
(118) von Canstein, H.; Ogawa, J.; Shimizu, S.; Lloyd, J. R. Secretion of Flavins by *Shewanella Species* and Their Role in Extracellular Electron Transfer. *Appl. Environ. Microbiol.* **2008**, *74*, 615−623.
(119) Roden, E. E.; Urrutia, M. M. Ferrous Iron Removal Promotes Microbial Reduction of Crystalline Iron(III) Oxides. *Environ. Sci. Technol.* **1999**, *33*, 1847−1853.
(120) Royer, R. A.; Burgos, W. D.; Fisher, A. S.; Unz, R. F.; Dempsey, B. A. Enhancement of Biological Reduction of Hematite by Electron Shuttling and Fe(II) Complexation. *Environ. Sci. Technol.* **2002**, *36*, 1939−1946.
(121) Urrutia, M. M.; Roden, E. E.; Zachara, J. M. Influence of Aqueous and Solid-Phase Fe(II) Complexants on Microbial Reduction of Crystalline Iron(III) Oxides. *Environ. Sci. Technol.* **1999**, *33*, 4022−4028.
(122) Jaisi, D. P.; Dong, H.; Liu, C. Influence of Biogenic Fe(II) on the Extent of Microbial Reduction of Fe(III) in Clay Minerals Nontronite, Illite, and Chlorite. *Geochim. Cosmochim. Acta* **2007**, *71*, 1145−1158.
(123) Waite, T. D.; Morel, F. M. Photoreductive Dissolution of Colloidal Iron Oxides in Natural Waters. *Environ. Sci. Technol.* **1984**, *18*, 860−868.
(124) Garg, S.; Xing, G.; Waite, T. D. Influence of pH on the Kinetics and Mechanism of Photoreductive Dissolution of Amorphous Iron Oxyhydroxide in the Presence of Natural Organic Matter: Implications to Iron Bioavailability in Surface Waters. *Environ. Sci. Technol.* **2020**, *54*, 6771−6780.
(125) Lueder, U.; Jørgensen, B. B.; Kappler, A.; Schmidt, C. Photochemistry of Iron in Aquatic Environments. *Environ. Sci. Process Impacts* **2020**, *22*, 12−24.
(126) Lueder, U.; Jørgensen, B. B.; Kappler, A.; Schmidt, C. Fe(III) Photoreduction Producing $Fe_{aq}^{2+}$ in Oxic Freshwater Sediment. *Environ. Sci. Technol.* **2020**, *54*, 862−869.
(127) Waite, T. D.; Morel, F. M. M. Photoreductive Dissolution of Colloidal Iron Oxide: Effect of Citrate. *J. Colloid Interface Sci.* **1984**, *102*, 121−137.
(128) Siffert, C.; Sulzberger, B. Light-Induced Dissolution of Hematite in the Presence of Oxalate. A Case Study. *Langmuir* **1991**, *7*, 1627−1634.
(129) Rose, A. L.; Waite, T. D. Predicting Iron Speciation in Coastal Waters from the Kinetics of Sunlight-Mediated Iron Redox Cycling. *Aquat. Sci.* **2003**, *65*, 375−383.
(130) Fujii, M.; Rose, A. L.; Waite, T. D.; Omura, T. Superoxide-Mediated Dissolution of Amorphous Ferric Oxyhydroxide in Seawater. *Environ. Sci. Technol.* **2006**, *40*, 880−887.
(131) Xing, G.; Garg, S.; Waite, T. D. Is Superoxide-Mediated Fe(III) Reduction Important in Sunlit Surface Waters? *Environ. Sci. Technol.* **2019**, *53*, 13179−13190.
(132) Miot, J.; Benzerara, K.; Morin, G.; Bernard, S.; Beyssac, O.; Larquet, E.; Kappler, A.; Guyot, F. Transformation of Vivianite by Anaerobic Nitrate-Reducing Iron-Oxidizing Bacteria. *Geobiology* **2009**, *7*, 373−384.
(133) Zegeye, A.; Mustin, C.; Jorand, F. Bacterial and Iron Oxide Aggregates Mediate Secondary Iron Mineral Formation: Green Rust Versus Magnetite. *Geobiology* **2010**, *8*, 209−222.
(134) Dippon, U.; Schmidt, C.; Behrens, S.; Kappler, A. Secondary Mineral Formation During Ferrihydrite Reduction by *Shewanella Oneidensis* MR-1 Depends on Incubation Vessel Orientation and Resulting Gradients of Cells, $Fe^{2+}$ and Fe Minerals. *Geomicrobiol. J.* **2015**, *32*, 878−889.
(135) Brusseau, M. L.; Chorover, J. Chemical Processes Affecting Contaminant Transport and Fate. In *Environmental and Pollution Science* 3rd ed.; Brusseau, M. L., Pepper, I. L., Gerba, C. P., Eds.; Academic Press, 2019; Chapter 8, pp 113−130.
(136) Hofstetter, T. B.; Heijman, C. G.; Haderlein, S. B.; Holliger, C.; Schwarzenbach, R. P. Complete Reduction of TNT and Other (Poly)Nitroaromatic Compounds under Iron-Reducing Subsurface Conditions. *Environ. Sci. Technol.* **1999**, *33*, 1479−1487.
(137) Pecher, K.; Haderlein, S. B.; Schwarzenbach, R. P. Reduction of Polyhalogenated Methanes by Surface-Bound Fe(II) in Aqueous Suspensions of Iron Oxides. *Environ. Sci. Technol.* **2002**, *36*, 1734−1741.
(138) Gregory, K. B.; Larese-Casanova, P.; Parkin, G. F.; Scherer, M. M. Abiotic Transformation of Hexahydro-1, 3, 5-Trinitro-1, 3, 5-Triazine by $Fe^{II}$ Bound to Magnetite. *Environ. Sci. Technol.* **2004**, *38*, 1408−1414.
(139) Neumann, A.; Hofstetter, T. B.; Skarpeli-Liati, M.; Schwarzenbach, R. P. Reduction of Polychlorinated Ethanes and Carbon Tetrachloride by Structural Fe(II) in Smectites. *Environ. Sci. Technol.* **2009**, *43*, 4082−4089.
(140) Stumm, W.; Lee, G. F. Oxygenation of Ferrous Iron. *Ind. Eng. Chem.* **1961**, *53*, 143−146.
(141) Millero, F. J.; Sotolongo, S.; Izaguirre, M. The Oxidation Kinetics of Fe(II) in Seawater. *Geochim. Cosmochim. Acta* **1987**, *51*, 793−801.
(142) Pham, A. N.; Waite, T. D. Oxygenation of Fe(II) in Natural Waters Revisited: Kinetic Modeling Approaches, Rate Constant Estimation and the Importance of Various Reaction Pathways. *Geochim. Cosmochim. Acta* **2008**, *72*, 3616−3630.
(143) Santana-Casiano, J. M.; González-Dávila, M.; Millero, F. J. The Oxidation of Fe(II) in NaCl−$HCO_3^-$ and Seawater Solutions in the


https://doi.org/10.1021/acs.chemrev.0c01286
*Chem. Rev.* 2021, 121, 8161−8233

Presence of Phthalate and Salicylate Ions: A Kinetic Model. *Mar. Chem.* **2004**, *85*, 27−40.
(144) Kanzaki, Y.; Murakami, T. Rate Law of Fe(II) Oxidation under Low $O_2$ Conditions. *Geochim. Cosmochim. Acta* **2013**, *123*, 338−350.
(145) Rosso, K. M.; Morgan, J. J. Outer-Sphere Electron Transfer Kinetics of Metal Ion Oxidation by Molecular Oxygen. *Geochim. Cosmochim. Acta* **2002**, *66*, 4223−4233.
(146) Jones, A. M.; Griffin, P. J.; Collins, R. N.; Waite, T. D. Ferrous Iron Oxidation under Acidic Conditions−the Effect of Ferric Oxide Surfaces. *Geochim. Cosmochim. Acta* **2014**, *145*, 1−12.
(147) Strathmann, T. J.; Stone, A. T. Reduction of Oxamyl and Related Pesticides by $Fe^{II}$: Influence of Organic Ligands and Natural Organic Matter. *Environ. Sci. Technol.* **2002**, *36*, 5172−5183.
(148) Tamura, H.; Goto, K.; Nagayama, M. Effect of Anions on the Oxygenation of Ferrous Ion in Neutral Solutions. *J. Inorg. Nucl. Chem.* **1976**, *38*, 113−117.
(149) Strathmann, T. J.; Stone, A. T. Reduction of the Pesticides Oxamyl and Methomyl by $Fe^{II}$: Effect of pH and Inorganic Ligands. *Environ. Sci. Technol.* **2002**, *36*, 653−661.
(150) Luther, G. W.; Shellenbarger, P. A.; Brendel, P. J. Dissolved Organic Fe(III) and Fe(II) Complexes in Salt Marsh Porewaters. *Geochim. Cosmochim. Acta* **1996**, *60*, 951−960.
(151) Bussan, A. L.; Strathmann, T. J. Influence of Organic Ligands on the Reduction of Polyhalogenated Alkanes by Iron(II). *Environ. Sci. Technol.* **2007**, *41*, 6740−6747.
(152) Curtis, G. P.; Reinhard, M. Reductive Dehalogenation of Hexachloroethane, Carbon Tetrachloride, and Bromoform by Anthrahydroquinone Disulfonate and Humic Acid. *Environ. Sci. Technol.* **1994**, *28*, 2393−2401.
(153) Kördel, W.; Dassenakis, M.; Lintelmann, J.; Padberg, S. The Importance of Natural Organic Material for Environmental Processes in Waters and Soils (Technical Report). *Pure Appl. Chem.* **1997**, *69*, 1571−1600.
(154) Joe-Wong, C.; Shoenfelt, E.; Hauser, E. J.; Crompton, N.; Myneni, S. C. B. Estimation of Reactive Thiol Concentrations in Dissolved Organic Matter and Bacterial Cell Membranes in Aquatic Systems. *Environ. Sci. Technol.* **2012**, *46*, 9854−9861.
(155) Aeschbacher, M.; Sander, M.; Schwarzenbach, R. P. Novel Electrochemical Approach to Assess the Redox Properties of Humic Substances. *Environ. Sci. Technol.* **2010**, *44*, 87−93.
(156) Garg, S.; Jiang, C.; Waite, T. D. Impact of pH on Iron Redox Transformations in Simulated Freshwaters Containing Natural Organic Matter. *Environ. Sci. Technol.* **2018**, *52*, 13184−13194.
(157) Garg, S.; Jiang, C.; Miller, C. J.; Rose, A. L.; Waite, T. D. Iron Redox Transformations in Continuously Photolyzed Acidic Solutions Containing Natural Organic Matter: Kinetic and Mechanistic Insights. *Environ. Sci. Technol.* **2013**, *47*, 9190−9197.
(158) Garg, S.; Jiang, C.; Waite, T. D. Mechanistic Insights into Iron Redox Transformations in the Presence of Natural Organic Matter: Impact of pH and Light. *Geochim. Cosmochim. Acta* **2015**, *165*, 14−34.
(159) Fujii, M.; Dang, T.; Bligh, M.; Rose, A. L.; Waite, T. Effect of Natural Organic Matter on Iron Uptake by the Freshwater Cyanobacterium Microcystis Aeruginosa. *Environ. Sci. Technol.* **2014**, *48*, 365−374.
(160) Tagliabue, A.; Bowie, A. R.; Boyd, P. W.; Buck, K. N.; Johnson, K. S.; Saito, M. A. The Integral Role of Iron in Ocean Biogeochemistry. *Nature* **2017**, *543*, 51−59.
(161) Johnson, K. S.; Coale, K. H.; Elrod, V. A.; Tindale, N. W. Iron Photochemistry in Seawater from the Equatorial Pacific. *Mar. Chem.* **1994**, *46*, 319−334.
(162) Waite, T. D.; Szymczak, R.; Espey, Q. I.; Furnas, M. J. Diel Variations in Iron Speciation in Northern Australian Shelf Waters. *Mar. Chem.* **1995**, *50*, 79−91.
(163) Fox, T. R.; Comerford, N. B. Low-Molecular-Weight Organic Acids in Selected Forest Soils of the Southeastern USA. *Soil Sci. Soc. Am. J.* **1990**, *54*, 1139−1144.
(164) Wang, S.; Wang, J. Trimethoprim Degradation by Fenton and Fe(II)-Activated Persulfate Processes. *Chemosphere* **2018**, *191*, 97−105.
(165) Neilands, J. Siderophores: Structure and Function of Microbial Iron Transport Compounds. *J. Biol. Chem.* **1995**, *270*, 26723−26726.
(166) Cornelis, P.; Andrews, S. C. *Iron Uptake and Homeostasis in Microorganisms*; Caister Academic Press, 2010.
(167) Hider, R. C.; Kong, X. Chemistry and Biology of Siderophores. *Nat. Prod. Rep.* **2010**, *27*, 637−657.
(168) Kraemer, S. M. Iron Oxide Dissolution and Solubility in the Presence of Siderophores. *Aquat. Sci.* **2004**, *66*, 3−18.
(169) Kalinowski, B. E.; Liermann, L. J.; Givens, S.; Brantley, S. L. Rates of Bacteria-Promoted Solubilization of Fe from Minerals: A Review of Problems and Approaches. *Chem. Geol.* **2000**, *169*, 357−370.
(170) Sun, Y.; Pham, A. N.; Waite, T. D. Effect of Release of Dopamine on Iron Transformations and Reactive Oxygen Species (ROS) Generation under Conditions Typical of Coastal Waters. *Environ. Sci. Process Impacts* **2018**, *20*, 232−244.
(171) Martell, A. E.; Motekaitis, R. J.; Chen, D.; Hancock, R. D.; McManus, D. Selection of New Fe(III)/Fe(II) Chelating Agents as Catalysts for the Oxidation of Hydrogen Sulfide to Sulfur by Air. *Can. J. Chem.* **1996**, *74*, 1872−1879.
(172) Kim, D.; Duckworth, O. W.; Strathmann, T. J. Hydroxamate Siderophore-Promoted Reactions between Iron(II) and Nitroaromatic Groundwater Contaminants. *Geochim. Cosmochim. Acta* **2009**, *73*, 1297−1311.
(173) Kim, D.; Strathmann, T. J. Role of Organically Complexed Iron(II) Species in the Reductive Transformation of Rdx in Anoxic Environments. *Environ. Sci. Technol.* **2007**, *41*, 1257−1264.
(174) Buerge, I. J.; Hug, S. J. Influence of Organic Ligands on Chromium(VI) Reduction by Iron(II). *Environ. Sci. Technol.* **1998**, *32*, 2092−2099.
(175) Strathmann, T. J.; Stone, A. T. Reduction of the Carbamate Pesticides Oxamyl and Methomyl by Dissolved $Fe^{II}$ and $Cu^{I}$. *Environ. Sci. Technol.* **2001**, *35*, 2461−2469.
(176) Chen, Y.; Dong, H.; Zhang, H. Reduction of Isoxazoles Including Sulfamethoxazole by Aqueous $Fe^{II}$−Tiron Complex: Impact of Structures. *Chem. Eng. J.* **2018**, *352*, 501−509.
(177) Li, X.; Chen, Y.; Zhang, H. J. C. E. J. Reduction of Nitrogen-Oxygen Containing Compounds (NOCs) by Surface-Associated Fe(II) and Comparison with Soluble Fe(II) Complexes. *Chem. Eng. J.* **2019**, *370*, 782−791.
(178) Tsutsui, M.; Velapoldi, R. A.; Hoffman, L.; Suzuki, K.; Ferrari, A. Unusual Metalloporphyrins. III. Induced Oxidation of Cobalt(II) and Iron(II) Porphyrins by Unsaturated Hydrocarbons. *J. Am. Chem. Soc.* **1969**, *91*, 3337−3341.
(179) Ong, J. H.; Castro, C. Oxidation of Iron(II) Porphyrins and Hemoproteins by Nitro Aromatics. *J. Am. Chem. Soc.* **1977**, *99*, 6740−6745.
(180) Wade, R. S.; Castro, C. Oxidation of Iron(II) Porphyrins by Alkyl Halides. *J. Am. Chem. Soc.* **1973**, *95*, 226−230.
(181) Wade, R. S.; Havlin, R.; Castro, C. Oxidation of Iron(II) Porphyrins by Organic Molecules. *J. Am. Chem. Soc.* **1969**, *91*, 7530−7530.
(182) Salter-Blanc, A. J.; Bylaska, E. J.; Johnston, H. J.; Tratnyek, P. G. Predicting Reduction Rates of Energetic Nitroaromatic Compounds Using Calculated One-Electron Reduction Potentials. *Environ. Sci. Technol.* **2015**, *49*, 3778−3786.
(183) Perlinger, J. A.; Buschmann, J.; Angst, W.; Schwarzenbach, R. P. Iron Porphyrin and Mercaptojuglone Mediated Reduction of Polyhalogenated Methanes and Ethanes in Homogeneous Aqueous Solution. *Environ. Sci. Technol.* **1998**, *32*, 2431−2437.
(184) Schwarzenbach, R. P.; Stierli, R.; Lanz, K.; Zeyer, J. Quinone and Iron Porphyrin Mediated Reduction of Nitroaromatic Compounds in Homogeneous Aqueous Solution. *Environ. Sci. Technol.* **1990**, *24*, 1566−1574.
(185) Hakala, J. A.; Fimmen, R. L.; Chin, Y.-P.; Agrawal, S. G.; Ward, C. P. Assessment of the Geochemical Reactivity of Fe-DOM Complexes in Wetland Sediment Pore Waters Using a Nitroaromatic Probe Compound. *Geochim. Cosmochim. Acta* **2009**, *73*, 1382−1393.


https://doi.org/10.1021/acs.chemrev.0c01286
*Chem. Rev.* 2021, 121, 8161−8233

(186) Hakala, J. A.; Chin, Y.-P.; Weber, E. J. Influence of Dissolved Organic Matter and Fe(II) on the Abiotic Reduction of Pentachloronitrobenzene. *Environ. Sci. Technol.* **2007**, *41*, 7337−7342.
(187) Agrawal, S. G.; Fimmen, R. L.; Chin, Y.-P. Reduction of Cr(VI) to Cr(III) by Fe(II) in the Presence of Fulvic Acids and in Lacustrine Pore Water. *Chem. Geol.* **2009**, *262*, 328−335.
(188) Gao, Y.; Zhong, S.; Torralba-Sanchez, T. L.; Tratnyek, P. G.; Weber, E. J.; Chen, Y.; Zhang, H. Quantitative Structure Activity Relationships (QSARs) and Machine Learning Models for Abiotic Reduction of Organic Compounds by an Aqueous Fe(II) Complex. *Water Res.* **2021**, *192*, 116843.
(189) Uchimiya, M. Reductive Transformation of 2,4-Dinitrotoluene: Roles of Iron and Natural Organic Matter. *Aquat. Geochem.* **2010**, *16*, 547−562.
(190) Willey, J. D.; Kieber, R. J.; Seaton, P. J.; Miller, C. Rainwater as a Source of Fe(II)-Stabilizing Ligands to Seawater. *Limnol. Oceanogr.* **2008**, *53*, 1678−1684.
(191) Luther, G. W.; Kostka, J. E.; Church, T. M.; Sulzberger, B.; Stumm, W. Seasonal Iron Cycling in the Salt-Marsh Sedimentary Environment: The Importance of Ligand Complexes with Fe(II) and Fe(III) in the Dissolution of Fe(III) Minerals and Pyrite. *Mar. Chem.* **1992**, *40*, 81−103.
(192) Danielsen, K. M.; Hayes, K. F. pH Dependence of Carbon Tetrachloride Reductive Dechlorination by Magnetite. *Environ. Sci. Technol.* **2004**, *38*, 4745−4752.
(193) Vikesland, P. J.; Heathcock, A. M.; Rebodos, R. L.; Makus, K. E. Particle Size and Aggregation Effects on Magnetite Reactivity toward Carbon Tetrachloride. *Environ. Sci. Technol.* **2007**, *41*, 5277−5283.
(194) Lee, W.; Batchelor, B. Abiotic Reductive Dechlorination of Chlorinated Ethylenes by Iron-Bearing Soil Minerals. 1. Pyrite and Magnetite. *Environ. Sci. Technol.* **2002**, *36*, 5147−5154.
(195) Gorski, C. A.; Nurmi, J. T.; Tratnyek, P. G.; Hofstetter, T. B.; Scherer, M. M. Redox Behavior of Magnetite: Implications for Contaminant Reduction. *Environ. Sci. Technol.* **2010**, *44*, 55−60.
(196) White, A. F.; Peterson, M. L. Reduction of Aqueous Transition Metal Species on the Surfaces of Fe(II)-Containing Oxides. *Geochim. Cosmochim. Acta* **1996**, *60*, 3799−3814.
(197) Jiang, W.; Cai, Q.; Xu, W.; Yang, M.; Cai, Y.; Dionysiou, D. D.; O'Shea, K. E. Cr(VI) Adsorption and Reduction by Humic Acid Coated on Magnetite. *Environ. Sci. Technol.* **2014**, *48*, 8078−8085.
(198) Swindle, A. L.; Cozzarelli, I. M.; Elwood Madden, A. S. Using Chromate to Investigate the Impact of Natural Organics on the Surface Reactivity of Nanoparticulate Magnetite. *Environ. Sci. Technol.* **2015**, *49*, 2156−2162.
(199) Pasakarnis, T. S.; Boyanov, M. I.; Kemner, K. M.; Mishra, B.; O'Loughlin, E. J.; Parkin, G.; Scherer, M. M. Influence of Chloride and Fe(II) Content on the Reduction of Hg(II) by Magnetite. *Environ. Sci. Technol.* **2013**, *47*, 6987−6994.
(200) Wylie, E. M.; Olive, D. T.; Powell, B. A. Effects of Titanium Doping in Titanomagnetite on Neptunium Sorption and Speciation. *Environ. Sci. Technol.* **2016**, *50*, 1853−1858.
(201) Liu, J.; Pearce, C. I.; Qafoku, O.; Arenholz, E.; Heald, S. M.; Rosso, K. M. Tc(VII) Reduction Kinetics by Titanomagnetite ($Fe_{3-X}Ti_xO_4$) Nanoparticles. *Geochim. Cosmochim. Acta* **2012**, *92*, 67−81.
(202) Pearce, C. I.; Liu, J.; Baer, D. R.; Qafoku, O.; Heald, S. M.; Arenholz, E.; Grosz, A. E.; McKinley, J. P.; Resch, C. T.; Bowden, M. E. Characterization of Natural Titanomagnetites ($Fe_{3-X}Ti_xO_4$) for Studying Heterogeneous Electron Transfer to Tc(VII) in the Hanford Subsurface. *Geochim. Cosmochim. Acta* **2014**, *128*, 114−127.
(203) Scott, T.; Allen, G.; Heard, P.; Randell, M. Reduction of U(VI) to U(IV) on the Surface of Magnetite. *Geochim. Cosmochim. Acta* **2005**, *69*, 5639−5646.
(204) Patterson, R. R.; Fendorf, S.; Fendorf, M. Reduction of Hexavalent Chromium by Amorphous Iron Sulfide. *Environ. Sci. Technol.* **1997**, *31*, 2039−2044.
(205) Butler, E. C.; Hayes, K. F. Kinetics of the Transformation of Halogenated Aliphatic Compounds by Iron Sulfide. *Environ. Sci. Technol.* **2000**, *34*, 422−429.
(206) Kenneke, J. F.; Weber, E. J. Reductive Dehalogenation of Halomethanes in Iron-and Sulfate-Reducing Sediments. 1. Reactivity Pattern Analysis. *Environ. Sci. Technol.* **2003**, *37*, 713−720.
(207) Choi, J.; Choi, K.; Lee, W. Effects of Transition Metal and Sulfide on the Reductive Dechlorination of Carbon Tetrachloride and 1, 1, 1-Trichloroethane by FeS. *J. Hazard. Mater.* **2009**, *162*, 1151−1158.
(208) Lan, Y.; Butler, E. C. Iron-Sulfide-Associated Products Formed During Reductive Dechlorination of Carbon Tetrachloride. *Environ. Sci. Technol.* **2016**, *50*, 5489−5497.
(209) Butler, E. C.; Hayes, K. F. Effects of Solution Composition and pH on the Reductive Dechlorination of Hexachloroethane by Iron Sulfide. *Environ. Sci. Technol.* **1998**, *32*, 1276−1284.
(210) Jeong, H. Y.; Hayes, K. F. Impact of Transition Metals on Reductive Dechlorination Rate of Hexachloroethane by Mackinawite. *Environ. Sci. Technol.* **2003**, *37*, 4650−4655.
(211) Butler, E. C.; Hayes, K. F. Kinetics of the Transformation of Trichloroethylene and Tetrachloroethylene by Iron Sulfide. *Environ. Sci. Technol.* **1999**, *33*, 2021−2027.
(212) Jeong, H. Y.; Kim, H.; Hayes, K. F. Reductive Dechlorination Pathways of Tetrachloroethylene and Trichloroethylene and Subsequent Transformation of Their Dechlorination Products by Mackinawite (FeS) in the Presence of Metals. *Environ. Sci. Technol.* **2007**, *41*, 7736−7743.
(213) Jeong, H. Y.; Hayes, K. F. Reductive Dechlorination of Tetrachloroethylene and Trichloroethylene by Mackinawite (FeS) in the Presence of Metals: Reaction Rates. *Environ. Sci. Technol.* **2007**, *41*, 6390−6396.
(214) Liang, X.; Dong, Y.; Kuder, T.; Krumholz, L. R.; Philp, R. P.; Butler, E. C. Distinguishing Abiotic and Biotic Transformation of Tetrachloroethylene and Trichloroethylene by Stable Carbon Isotope Fractionation. *Environ. Sci. Technol.* **2007**, *41*, 7094−7100.
(215) Velimirovic, M.; Larsson, P.-O.; Simons, Q.; Bastiaens, L. Reactivity Screening of Microscale Zerovalent Irons and Iron Sulfides Towards Different CAHs under Standardized Experimental Conditions. *J. Hazard. Mater.* **2013**, *252*, 204−212.
(216) Kim, S.; Park, T.; Lee, W. Enhanced Reductive Dechlorination of Tetrachloroethene by Nano-Sized Mackinawite with Cyanocobalamin in a Highly Alkaline Condition. *J. Environ. Manage.* **2015**, *151*, 378−385.
(217) Butler, E. C.; Hayes, K. F. Factors Influencing Rates and Products in the Transformation of Trichloroethylene by Iron Sulfide and Iron Metal. *Environ. Sci. Technol.* **2001**, *35*, 3884−3891.
(218) He, Y. T.; Wilson, J. T.; Wilkin, R. T. Impact of Iron Sulfide Transformation on Trichloroethylene Degradation. *Geochim. Cosmochim. Acta* **2010**, *74*, 2025−2039.
(219) Mullet, M.; Boursiquot, S.; Ehrhardt, J.-J. Removal of Hexavalent Chromium from Solutions by Mackinawite, Tetragonal FeS. *Colloids Surf., A* **2004**, *244*, 77−85.
(220) Bone, S. E.; Bargar, J. R.; Sposito, G. Mackinawite (FeS) Reduces Mercury(II) under Sulfidic Conditions. *Environ. Sci. Technol.* **2014**, *48*, 10681−10689.
(221) Scheinost, A. C.; Charlet, L. Selenite Reduction by Mackinawite, Magnetite and Siderite: XAS Characterization of Nanosized Redox Products. *Environ. Sci. Technol.* **2008**, *42*, 1984−1989.
(222) Hyun, S. P.; Davis, J. A.; Sun, K.; Hayes, K. F. Uranium(VI) Reduction by Iron(II) Monosulfide Mackinawite. *Environ. Sci. Technol.* **2012**, *46*, 3369−3376.
(223) Erbs, M.; Bruun Hansen, H. C.; Olsen, C. E. Reductive Dechlorination of Carbon Tetrachloride Using Iron(II) Iron(III) Hydroxide Sulfate (Green Rust). *Environ. Sci. Technol.* **1999**, *33*, 307−311.
(224) O'Loughlin, E. J.; Kemner, K. M.; Burris, D. R. Effects of $Ag^{I}$, $Au^{III}$, and $Cu^{II}$ on the Reductive Dechlorination of Carbon Tetrachloride by Green Rust. *Environ. Sci. Technol.* **2003**, *37*, 2905−2912.


https://doi.org/10.1021/acs.chemrev.0c01286
*Chem. Rev.* 2021, 121, 8161−8233

(225) Maithreepala, R.; Doong, R.-a. Enhanced Dechlorination of Chlorinated Methanes and Ethenes by Chloride Green Rust in the Presence of Copper(II). *Environ. Sci. Technol.* **2005**, *39*, 4082−4090.
(226) Liang, X.; Butler, E. C. Effects of Natural Organic Matter Model Compounds on the Transformation of Carbon Tetrachloride by Chloride Green Rust. *Water Res.* **2010**, *44*, 2125−2132.
(227) Ayala-Luis, K. B.; Cooper, N. G.; Koch, C. B.; Hansen, H. C. B. Efficient Dechlorination of Carbon Tetrachloride by Hydrophobic Green Rust Intercalated with Dodecanoate Anions. *Environ. Sci. Technol.* **2012**, *46*, 3390−3397.
(228) Lee, W.; Batchelor, B. Abiotic Reductive Dechlorination of Chlorinated Ethylenes by Iron-Bearing Soil Minerals. 2. Green Rust. *Environ. Sci. Technol.* **2002**, *36*, 5348−5354.
(229) Han, Y.-S.; Hyun, S. P.; Jeong, H. Y.; Hayes, K. F. Kinetic Study of *cis*-Dichloroethylene (*cis*-DCE) and Vinyl Chloride (VC) Dechlorination Using Green Rusts Formed under Varying Conditions. *Water Res.* **2012**, *46*, 6339−6350.
(230) Liang, X.; Philp, R. P.; Butler, E. C. Kinetic and Isotope Analyses of Tetrachloroethylene and Trichloroethylene Degradation by Model Fe(II)-Bearing Minerals. *Chemosphere* **2009**, *75*, 63−69.
(231) O'Loughlin, E. J.; Burris, D. R. Reduction of Halogenated Ethanes by Green Rust. *Environ. Toxicol. Chem.* **2004**, *23*, 41−48.
(232) Chun, C. L.; Hozalski, R. M.; Arnold, W. A. Degradation of Disinfection Byproducts by Carbonate Green Rust. *Environ. Sci. Technol.* **2007**, *41*, 1615−1621.
(233) Larese-Casanova, P.; Scherer, M. M. Abiotic Transformation of Hexahydro-1, 3, 5-Trinitro-1, 3, 5-Triazine (RDX) by Green Rusts. *Environ. Sci. Technol.* **2008**, *42*, 3975−3981.
(234) Hansen, H. C. B.; Borggaard, O. K.; Sørensen, J. Evaluation of the Free Energy of Formation of Fe(II)-Fe(III) Hydroxide-Sulphate (Green Rust) and Its Reduction of Nitrite. *Geochim. Cosmochim. Acta* **1994**, *58*, 2599−2608.
(235) Hansen, H. C. B.; Guldberg, S.; Erbs, M.; Koch, C. B. Kinetics of Nitrate Reduction by Green Rusts—Effects of Interlayer Anion and Fe(II): Fe(III) Ratio. *Appl. Clay Sci.* **2001**, *18*, 81−91.
(236) Etique, M.; Zegeye, A.; Grégoire, B.; Carteret, C.; Ruby, C. Nitrate Reduction by Mixed Iron(II-III) Hydroxycarbonate Green Rust in the Presence of Phosphate Anions: The Key Parameters Influencing the Ammonium Selectivity. *Water Res.* **2014**, *62*, 29−39.
(237) Guerbois, D.; Ona-Nguema, G.; Morin, G.; Abdelmoula, M.; Laverman, A. M.; Mouchel, J.-M.; Barthelemy, K.; Maillot, F.; Brest, J. Nitrite Reduction by Biogenic Hydroxycarbonate Green Rusts: Evidence for Hydroxy-Nitrite Green Rust Formation as an Intermediate Reaction Product. *Environ. Sci. Technol.* **2014**, *48*, 4505−4514.
(238) O'Loughlin, E. J.; Kelly, S. D.; Kemner, K. M.; Csencsits, R.; Cook, R. E. Reduction of $Ag^{I}$, $Au^{III}$, $Cu^{II}$, and $Hg^{II}$ by $Fe^{II}/Fe^{III}$ Hydroxysulfate Green Rust. *Chemosphere* **2003**, *53*, 437−446.
(239) Loyaux-Lawniczak, S.; Refait, P.; Ehrhardt, J.-J.; Lecomte, P.; Génin, J.-M. R. Trapping of Cr by Formation of Ferrihydrite During the Reduction of Chromate Ions by Fe(II)-Fe(III) Hydroxysalt Green Rusts. *Environ. Sci. Technol.* **2000**, *34*, 438−443.
(240) Williams, A. G.; Scherer, M. M. Kinetics of Cr(VI) Reduction by Carbonate Green Rust. *Environ. Sci. Technol.* **2001**, *35*, 3488−3494.
(241) Bond, D. L.; Fendorf, S. Kinetics and Structural Constraints of Chromate Reduction by Green Rusts. *Environ. Sci. Technol.* **2003**, *37*, 2750−2757.
(242) Myneni, S.; Tokunaga, T. K.; Brown, G. Abiotic Selenium Redox Transformations in the Presence of Fe(II, III) Oxides. *Science* **1997**, *278*, 1106−1109.
(243) Yan, L.; Bailey, G. W. Sorption and Abiotic Redox Transformation of Nitrobenzene at the Smectite−Water Interface. *J. Colloid Interface Sci.* **2001**, *241*, 142−153.
(244) Hofstetter, T. B.; Schwarzenbach, R. P.; Haderlein, S. B. Reactivity of Fe(II) Species Associated with Clay Minerals. *Environ. Sci. Technol.* **2003**, *37*, 519−528.
(245) Hofstetter, T. B.; Neumann, A.; Schwarzenbach, R. P. Reduction of Nitroaromatic Compounds by Fe(II) Species Associated with Iron-Rich Smectites. *Environ. Sci. Technol.* **2006**, *40*, 235−242.
(246) Cervini-Silva, J. Linear Free-Energy Relationship Analysis of the Fate of Chlorinated 1-and 2-Carbon Compounds by Redox-Manipulated Smectite Clay Minerals. *Environ. Toxicol. Chem.* **2003**, *22*, 2298−2305.
(247) Ferrey, M. L.; Wilkin, R. T.; Ford, R. G.; Wilson, J. T. Nonbiological Removal of cis-Dichloroethylene and 1, 1-Dichloroethylene in Aquifer Sediment Containing Magnetite. *Environ. Sci. Technol.* **2004**, *38*, 1746−1752.
(248) Brigatti, M. F.; Lugli, C.; Cibin, G.; Marcelli, A.; Giuli, G.; Paris, E.; Mottana, A.; Wu, Z. Reduction and Sorption of Chromium by Fe(II)-Bearing Phyllosilicates: Chemical Treatments and X-Ray Absorption Spectroscopy (XAS) Studies. *Clays Clay Miner.* **2000**, *48*, 272−281.
(249) Joe-Wong, C.; Brown, G. E.; Maher, K. Kinetics and Products of Chromium(VI) Reduction by Iron(II/III)-Bearing Clay Minerals. *Environ. Sci. Technol.* **2017**, *51*, 9817−9825.
(250) McCormick, M. L.; Bouwer, E. J.; Adriaens, P. Carbon Tetrachloride Transformation in a Model Iron-Reducing Culture: Relative Kinetics of Biotic and Abiotic Reactions. *Environ. Sci. Technol.* **2002**, *36*, 403−410.
(251) Tronc, E.; Belleville, P.; Jolivet, J. P.; Livage, J. Transformation of Ferric Hydroxide into Spinel by Iron(II) Adsorption. *Langmuir* **1992**, *8*, 313−319.
(252) Jolivet, J.-P.; Tronc, E. Interfacial Electron Transfer in Colloidal Spinel Iron Oxide. Conversion of $Fe_3O_4$-$\gamma Fe_2O_3$ in Aqueous Medium. *J. Colloid Interface Sci.* **1988**, *125*, 688−701.
(253) Huang, Y. H.; Zhang, T. C. Effects of Dissolved Oxygen on Formation of Corrosion Products and Concomitant Oxygen and Nitrate Reduction in Zero-Valent Iron Systems with or without Aqueous $Fe^{2+}$. *Water Res.* **2005**, *39*, 1751−1760.
(254) Stratmann, M.; Bohnenkamp, K.; Engell, H.-J. An Electrochemical Study of Phase-Transitions in Rust Layers. *Corros. Sci.* **1983**, *23*, 969−985.
(255) Lin, J.; Ellaway, M.; Adrien, R. Study of Corrosion Material Accumulated on the Inner Wall of Steel Water Pipe. *Corros. Sci.* **2001**, *43*, 2065−2081.
(256) Sarin, P.; Snoeyink, V.; Bebee, J.; Kriven, W.; Clement, J. Physico-Chemical Characteristics of Corrosion Scales in Old Iron Pipes. *Water Res.* **2001**, *35*, 2961−2969.
(257) Amor, M.; Tharaud, M.; Gélabert, A.; Komeili, A. Single-Cell Determination of Iron Content in Magnetotactic Bacteria: Implications for the Iron Biogeochemical Cycle. *Environ. Microbiol.* **2020**, *22*, 823−831.
(258) Peterson, M. L.; White, A. F.; Brown, G. E.; Parks, G. A. Surface Passivation of Magnetite by Reaction with Aqueous Cr(VI): XAFS and TEM Results. *Environ. Sci. Technol.* **1997**, *31*, 1573−1576.
(259) Wiatrowski, H. A.; Das, S.; Kukkadapu, R.; Ilton, E. S.; Barkay, T.; Yee, N. Reduction of Hg(II) to Hg(0) by Magnetite. *Environ. Sci. Technol.* **2009**, *43*, 5307−5313.
(260) Gallagher, K.; Feitknecht, W.; Mannweiler, U. J. N. Mechanism of Oxidation of Magnetite to $\gamma$-$Fe_2O_3$. *Nature* **1968**, *217*, 1118−1121.
(261) White, A. F.; Peterson, M. L.; Hochella, M. F. Electrochemistry and Dissolution Kinetics of Magnetite and Ilmenite. *Geochim. Cosmochim. Acta* **1994**, *58*, 1859−1875.
(262) Sidhu, P.; Gilkes, R.; Posner, A. J. J. o. I.; Chemistry, N. Mechanism of the Low Temperature Oxidation of Synthetic Magnetites. *J. Inorg. Nucl. Chem.* **1977**, *39*, 1953−1958.
(263) Tang, J.; Myers, M.; Bosnick, K. A.; Brus, L. E. Magnetite $Fe_3O_4$ Nanocrystals: Spectroscopic Observation of Aqueous Oxidation Kinetics. *J. Phys. Chem. B* **2003**, *107*, 7501−7506.
(264) Culpepper, J. D.; Scherer, M. M.; Robinson, T. C.; Neumann, A.; Cwiertny, D.; Latta, D. E. Reduction of PCE and TCE by Magnetite Revisited. *Environ. Sci. Process Impacts* **2018**, *20*, 1340−1349.
(265) Klausen, J.; Troeber, S. P.; Haderlein, S. B.; Schwarzenbach, R. P. Reduction of Substituted Nitrobenzenes by Fe(II) in Aqueous Mineral Suspensions. *Environ. Sci. Technol.* **1995**, *29*, 2396−2404.
(266) Verwey, E.; Haayman, P. Electronic Conductivity and Transition Point of Magnetite ("$Fe_3O_4$"). *Physica* **1941**, *8*, 979−987.


https://doi.org/10.1021/acs.chemrev.0c01286
*Chem. Rev.* 2021, 121, 8161−8233

(267) Itai, R.; Shibuya, M.; Matsumura, T.; Ishi, G. Electrical Resistivity of Magnetite Anodes. *J. Electrochem. Soc.* **1971**, *118*, 1709−1711.
(268) Navrotsky, A.; Ma, C.; Lilova, K.; Birkner, N. Nanophase Transition Metal Oxides Show Large Thermodynamically Driven Shifts in Oxidation-Reduction Equilibria. *Science* **2010**, *330*, 199−201.
(269) Pearce, C. I.; Qafoku, O.; Liu, J.; Arenholz, E.; Heald, S. M.; Kukkadapu, R. K.; Gorski, C. A.; Henderson, C. M. B.; Rosso, K. M. Synthesis and Properties of Titanomagnetite ($Fe_{3-X}Ti_xO_4$) Nanoparticles: A Tunable Solid-State Fe(II/III) Redox System. *J. Colloid Interface Sci.* **2012**, *387*, 24−38.
(270) Latta, D. E.; Pearce, C. I.; Rosso, K. M.; Kemner, K. M.; Boyanov, M. I. Reaction of $U^{VI}$ with Titanium-Substituted Magnetite: Influence of Ti on $U^{IV}$ Speciation. *Environ. Sci. Technol.* **2013**, *47*, 4121−4130.
(271) Skomurski, F. N.; Kerisit, S.; Rosso, K. M. Structure, Charge Distribution, and Electron Hopping Dynamics in Magnetite ($Fe_3O_4$)(1 0 0) Surfaces from First Principles. *Geochim. Cosmochim. Acta* **2010**, *74*, 4234−4248.
(272) Tronc, E.; Jolivet, J.-P.; Lefebvre, J.; Massart, R. Ion Adsorption and Electron Transfer in Spinel-Like Iron Oxide Colloids. *J. Chem. Soc., Faraday Trans. 1* **1984**, *80*, 2619−2629.
(273) Peng, H.; Pearce, C. I.; N'Diaye, A. T.; Zhu, Z.; Ni, J.; Rosso, K. M.; Liu, J. Redistribution of Electron Equivalents between Magnetite and Aqueous $Fe^{2+}$ Induced by a Model Quinone Compound AQDS. *Environ. Sci. Technol.* **2019**, *53*, 1863−1873.
(274) Gorski, C. A.; Handler, R. M.; Beard, B. L.; Pasakarnis, T.; Johnson, C. M.; Scherer, M. M. Fe Atom Exchange between Aqueous $Fe^{2+}$ and Magnetite. *Environ. Sci. Technol.* **2012**, *46*, 12399−12407.
(275) Génin, J.-M. R.; Bourrié, G.; Trolard, F.; Abdelmoula, M.; Jaffrezic, A.; Refait, P.; Maitre, V.; Humbert, B.; Herbillon, A. Thermodynamic Equilibria in Aqueous Suspensions of Synthetic and Natural Fe(II)-Fe(III) Green Rusts: Occurrences of the Mineral in Hydromorphic Soils. *Environ. Sci. Technol.* **1998**, *32*, 1058−1068.
(276) Boucherit, N.; Hugot-Le Goff, A.; Joiret, S. Raman Studies of Corrosion Films Grown on Fe and Fe-6mo in Pitting Conditions. *Corros. Sci.* **1991**, *32*, 497−507.
(277) Świetlik, J.; Raczyk-Stanisławiak, U.; Piszora, P.; Nawrocki, J. Corrosion in Drinking Water Pipes: The Importance of Green Rusts. *Water Res.* **2012**, *46*, 1−10.
(278) Fredrickson, J. K.; Zachara, J. M.; Kennedy, D. W.; Dong, H.; Onstott, T. C.; Hinman, N. W.; Li, S.-m. Biogenic Iron Mineralization Accompanying the Dissimilatory Reduction of Hydrous Ferric Oxide by a Groundwater Bacterium. *Geochim. Cosmochim. Acta* **1998**, *62*, 3239−3257.
(279) Roh, Y.; Lee, S.; Elless, M. Characterization of Corrosion Products in the Permeable Reactive Barriers. *Environ. Geol.* **2000**, *40*, 184−194.
(280) Usman, M.; Hanna, K.; Abdelmoula, M.; Zegeye, A.; Faure, P.; Ruby, C. Formation of Green Rust via Mineralogical Transformation of Ferric Oxides (Ferrihydrite, Goethite and Hematite). *Appl. Clay Sci.* **2012**, *64*, 38−43.
(281) Jones, A. M.; Murphy, C. A.; Waite, T. D.; Collins, R. N. Fe(II) Interactions with Smectites: Temporal Changes in Redox Reactivity and the Formation of Green Rust. *Environ. Sci. Technol.* **2017**, *51*, 12573−12582.
(282) Entwistle, J.; Latta, D. E.; Scherer, M. M.; Neumann, A. Abiotic Degradation of Chlorinated Solvents by Clay Minerals and Fe(II): Evidence for Reactive Mineral Intermediates. *Environ. Sci. Technol.* **2019**, *53*, 14308−14318.
(283) Feder, F.; Trolard, F.; Klingelhöfer, G.; Bourrié, G. In Situ Mössbauer Spectroscopy: Evidence for Green Rust (Fougerite) in a Gleysol and Its Mineralogical Transformations with Time and Depth. *Geochim. Cosmochim. Acta* **2005**, *69*, 4463−4483.
(284) Johnson, C. A.; Freyer, G.; Fabisch, M.; Caraballo, M. A.; Küsel, K.; Hochella, M. F. Observations and Assessment of Iron Oxide and Green Rust Nanoparticles in Metal-Polluted Mine Drainage within a Steep Redox Gradient. *Environ. Chem.* **2014**, *11*, 377−391.
(285) Zegeye, A.; Bonneville, S.; Benning, L. G.; Sturm, A.; Fowle, D. A.; Jones, C.; Canfield, D. E.; Ruby, C.; MacLean, L. C.; Nomosatryo, S. Green Rust Formation Controls Nutrient Availability in a Ferruginous Water Column. *Geology* **2012**, *40*, 599−602.
(286) Génin, J.-M. R.; Refait, P.; Bourrié, G.; Abdelmoula, M.; Trolard, F. Structure and Stability of the Fe(II)−Fe(III) Green Rust "Fougerite" Mineral and Its Potential for Reducing Pollutants in Soil Solutions. *Appl. Geochem.* **2001**, *16*, 559−570.
(287) Ruby, C.; Upadhyay, C.; Géhin, A.; Ona-Nguema, G.; GÉnin, J.-M. R. In Situ Redox Flexibility of $Fe^{II-III}$ Oxyhydroxycarbonate Green Rust and Fougerite. *Environ. Sci. Technol.* **2006**, *40*, 4696−4702.
(288) He, H.; Wu, D.; Wang, Q.; Luo, C.; Duan, N. Sequestration of Hexavalent Chromium by Fe(II)/Fe(III) Hydroxides: Structural Fe(II) Reactivity and $PO_4^{3-}$ Effect. *Chem. Eng. J.* **2016**, *283*, 948−955.
(289) Yin, W.; Ai, J.; Huang, L.-Z.; Tobler, D. J.; B. Hansen, H. C. A Silicate/Glycine Switch to Control the Reactivity of Layered Iron(II)−Iron(III) Hydroxides for Dechlorination of Carbon Tetrachloride. *Environ. Sci. Technol.* **2018**, *52*, 7876−7883.
(290) Refait, P.; Reffass, M.; Landoulsi, J.; Sabot, R.; Jeannin, M. Role of Nitrite Species During the Formation and Transformation of the Fe(II−III) Hydroxycarbonate Green Rust. *Colloids Surf., A* **2014**, *459*, 225−232.
(291) Han, Y.; Huang, J.; Liu, H.; Wu, Y.; Wu, Z.; Zhang, K.; Lu, Q. Abiotic Reduction of P-Chloronitrobenzene by Sulfate Green Rust: Influence Factors, Products and Mechanism. *RSC Adv.* **2020**, *10*, 19247−19253.
(292) Skovbjerg, L. L.; Stipp, S. L. S.; Utsunomiya, S.; Ewing, R. C. The Mechanisms of Reduction of Hexavalent Chromium by Green Rust Sodium Sulphate: Formation of Cr-Goethite. *Geochim. Cosmochim. Acta* **2006**, *70*, 3582−3592.
(293) Bhave, C.; Shejwalkar, S. A Review on the Synthesis and Applications of Green Rust for Environmental Pollutant Remediation. *Int. J. Environ. Sci. Technol.* **2018**, *15*, 1243−1248.
(294) Wander, M. C. F.; Rosso, K. M.; Schoonen, M. A. A. Structure and Charge Hopping Dynamics in Green Rust. *J. Phys. Chem. C* **2007**, *111*, 11414−11423.
(295) Hansen, H.; Koch, C. B. Reduction of Nitrate to Ammonium by Sulphate Green Rust: Activation Energy and Reaction Mechanism. *Clay Miner.* **1998**, *33*, 87−101.
(296) Hayashi, H.; Kanie, K.; Shinoda, K.; Muramatsu, A.; Suzuki, S.; Sasaki, H. pH-Dependence of Selenate Removal from Liquid Phase by Reductive Fe(II)−Fe(III) Hydroxysulfate Compound, Green Rust. *Chemosphere* **2009**, *76*, 638−643.
(297) Feng, X.; Wang, X.; Zhu, M.; Koopal, L. K.; Xu, H.; Wang, Y.; Liu, F. Effects of Phosphate and Silicate on the Transformation of Hydroxycarbonate Green Rust to Ferric Oxyhydroxides. *Geochim. Cosmochim. Acta* **2015**, *171*, 1−14.
(298) Legrand, L.; Mazerolles, L.; Chaussé, A. The Oxidation of Carbonate Green Rust into Ferric Phases:Solid-State Reaction or Transformation via Solution. *Geochim. Cosmochim. Acta* **2004**, *68*, 3497−3507.
(299) Benali, O.; Abdelmoula, M.; Refait, P.; Génin, J.-M. R. Effect of Orthophosphate on the Oxidation Products of Fe(II)-Fe(III) Hydroxycarbonate: The Transformation of Green Rust to Ferrihydrite. *Geochim. Cosmochim. Acta* **2001**, *65*, 1715−1726.
(300) Wolthers, M.; Van der Gaast, S. J.; Rickard, D. J. A. M. The Structure of Disordered Mackinawite. *Am. Mineral.* **2003**, *88*, 2007−2015.
(301) Berner, R. A. Sedimentary Pyrite Formation. *Am. J. Sci.* **1970**, *268*, 1−23.
(302) Morse, J. W.; Millero, F. J.; Cornwell, J. C.; Rickard, D. The Chemistry of the Hydrogen Sulfide and Iron Sulfide Systems in Natural Waters. *Earth-Sci. Rev.* **1987**, *24*, 1−42.
(303) Rickard, D. The Chemistry of Iron Sulphide Formation at Low Temperatures. *Stockholm Contr. Geol.* **1969**, *20*, 67−95.
(304) Kraal, P.; Burton, E. D.; Bush, R. T. Iron Monosulfide Accumulation and Pyrite Formation in Eutrophic Estuarine Sediments. *Geochim. Cosmochim. Acta* **2013**, *122*, 75−88.


https://doi.org/10.1021/acs.chemrev.0c01286
*Chem. Rev.* 2021, 121, 8161−8233

(305) Zhou, J.; Chen, S.; Liu, J.; Frost, R. L. J. C. E. J. Adsorption Kinetic and Species Variation of Arsenic for As(V) Removal by Biologically Mackinawite (FeS). *Chem. Eng. J.* **2018**, *354*, 237−244.
(306) Picard, A.; Gartman, A.; Clarke, D. R.; Girguis, P. R. Sulfate-Reducing Bacteria Influence the Nucleation and Growth of Mackinawite and Greigite. *Geochim. Cosmochim. Acta* **2018**, *220*, 367−384.
(307) Huo, Y.-C.; Li, W.-W.; Chen, C.-B.; Li, C.-X.; Zeng, R.; Lau, T.-C.; Huang, T.-Y. Biogenic FeS Accelerates Reductive Dechlorination of Carbon Tetrachloride by *Shewanella Putrefaciens* CN32. *Enzyme Microb. Technol.* **2016**, *95*, 236−241.
(308) Paknikar, K.; Nagpal, V.; Pethkar, A.; Rajwade, J. Degradation of Lindane from Aqueous Solutions Using Iron Sulfide Nanoparticles Stabilized by Biopolymers. *Sci. Technol. Adv. Mater.* **2005**, *6*, 370−374.
(309) Wersin, P.; Hochella, M. F., Jr; Persson, P.; Redden, G.; Leckie, J. O.; Harris, D. W. Interaction between Aqueous Uranium(VI) and Sulfide Minerals: Spectroscopic Evidence for Sorption and Reduction. *Geochim. Cosmochim. Acta* **1994**, *58*, 2829−2843.
(310) Hua, B.; Deng, B. Reductive Immobilization of Uranium(VI) by Amorphous Iron Sulfide. *Environ. Sci. Technol.* **2008**, *42*, 8703−8708.
(311) Yang, Z.; Kang, M.; Ma, B.; Xie, J.; Chen, F.; Charlet, L.; Liu, C. Inhibition of U(VI) Reduction by Synthetic and Natural Pyrite. *Environ. Sci. Technol.* **2014**, *48*, 10716−10724.
(312) Gong, Y.; Tang, J.; Zhao, D. Application of Iron Sulfide Particles for Groundwater and Soil Remediation: A Review. *Water Res.* **2016**, *89*, 309−320.
(313) Yang, Y.; Chen, T.; Sumona, M.; Gupta, B. S.; Sun, Y.; Hu, Z.; Zhan, X. Utilization of Iron Sulfides for Wastewater Treatment: A Critical Review. *Rev. Environ. Sci. Bio/Technol.* **2017**, *16*, 289−308.
(314) Chen, Y.; Liang, W.; Li, Y.; Wu, Y.; Chen, Y.; Xiao, W.; Zhao, L.; Zhang, J.; Li, H. Modification, Application and Reaction Mechanisms of Nano-Sized Iron Sulfide Particles for Pollutant Removal from Soil and Water: A Review. *Chem. Eng. J.* **2019**, *362*, 144−159.
(315) Vaughan, D. J.; Lennie, A. R. The Iron Sulphide Minerals: Their Chemistry and Role in Nature. *Sci. Prog.* **1991**, 371−388.
(316) Powell, P. E.; Cline, G. R.; Reid, C. P. P.; Szaniszlo, P. J. Occurrence of Hydroxamate Siderophore Iron Chelators in Soils. *Nature* **1980**, *287*, 833−834.
(317) Wu, J.; Wang, X.-B.; Zeng, R. J. Reactivity Enhancement of Iron Sulfide Nanoparticles Stabilized by Sodium Alginate: Taking Cr(VI) Removal as an Example. *J. Hazard. Mater.* **2017**, *333*, 275−284.
(318) Duan, J.; Ji, H.; Zhao, X.; Tian, S.; Liu, X.; Liu, W.; Zhao, D. Immobilization of U(VI) by Stabilized Iron Sulfide Nanoparticles: Water Chemistry Effects, Mechanisms, and Long-Term Stability. *Chem. Eng. J.* **2020**, *393*, 124692−124704.
(319) Veeramani, H.; Scheinost, A. C.; Monsegue, N.; Qafoku, N. P.; Kukkadapu, R.; Newville, M.; Lanzirotti, A.; Pruden, A.; Murayama, M.; Hochella, M. F., Jr Abiotic Reductive Immobilization of U(VI) by Biogenic Mackinawite. *Environ. Sci. Technol.* **2013**, *47*, 2361−2369.
(320) Troyer, L. D.; Tang, Y.; Borch, T. Simultaneous Reduction of Arsenic(V) and Uranium(VI) by Mackinawite: Role of Uranyl Arsenate Precipitate Formation. *Environ. Sci. Technol.* **2014**, *48*, 14326−14334.
(321) Kwon, K. D.; Refson, K.; Bone, S.; Qiao, R.; Yang, W.-l.; Liu, Z.; Sposito, G. Magnetic Ordering in Tetragonal FeS: Evidence for Strong Itinerant Spin Fluctuations. *Phys. Rev. B: Condens. Matter Mater. Phys.* **2011**, *83*, 064402-1−064402-7.
(322) Vaughan, D.; Ridout, M. Mössbauer Studies of Some Sulphide Minerals. *J. Inorg. Nucl. Chem.* **1971**, *33*, 741−746.
(323) Shoesmith, D. W.; Taylor, P.; Bailey, M. G.; Owen, D. G. The Formation of Ferrous Monosulfide Polymorphs During the Corrosion of Iron by Aqueous Hydrogen Sulfide at 21 °C. *J. Electrochem. Soc.* **1980**, *127*, 1007.
(324) Hyun, S. P.; Hayes, K. F. Abiotic Reductive Dechlorination of cis-DCE by Ferrous Monosulfide Mackinawite. *Environ. Sci. Pollut. Res.* **2015**, *22*, 16463−16474.
(325) Ferdelman, T. G.; Church, T. M.; Luther, G. W. Sulfur Enrichment of Humic Substances in a Delaware Salt Marsh Sediment Core. *Geochim. Cosmochim. Acta* **1991**, *55*, 979−988.
(326) Gong, Y.; Liu, Y.; Xiong, Z.; Kaback, D.; Zhao, D. Immobilization of Mercury in Field Soil and Sediment Using Carboxymethyl Cellulose Stabilized Iron Sulfide Nanoparticles. *Nanotechnology* **2012**, *23*, 294007.
(327) Ohfuji, H.; Rickard, D. High Resolution Transmission Electron Microscopic Study of Synthetic Nanocrystalline Mackinawite. *Earth Planet. Sci. Lett.* **2006**, *241*, 227−233.
(328) Park, S.-W.; Kim, S.-K.; Kim, J.-B.; Choi, S.-W.; Inyang, H. I.; Tokunaga, S. Particle Surface Hydrophobicity and the Dechlorination of Chloro-Compounds by Iron Sulfides. *Water, Air, Soil Pollut.: Focus* **2006**, *6*, 97−110.
(329) He, J.; Miller, C. J.; Collins, R. N.; Wang, D.; Waite, T. D. Production of a Surface-Localized Oxidant During Oxygenation of Mackinawite (FeS). *Environ. Sci. Technol.* **2020**, *54*, 1167−1176.
(330) Shao, H.; Butler, E. C. Influence of Soil Minerals on the Rates and Products of Abiotic Transformation of Carbon Tetrachloride in Anaerobic Soils and Sediments. *Environ. Sci. Technol.* **2009**, *43*, 1896−1901.
(331) Lan, Y.; Madden, A. S. E.; Butler, E. C. Transformation of Mackinawite to Greigite by Trichloroethylene and Tetrachloroethylene. *Environ. Sci. Process Impacts* **2016**, *18*, 1266−1273.
(332) Widler, A.; Seward, T. The Adsorption of Gold(I) Hydrosulphide Complexes by Iron Sulphide Surfaces. *Geochim. Cosmochim. Acta* **2002**, *66*, 383−402.
(333) Conway, B. E.; Ku, J. C. H.; Ho, F. C. The Electrochemical Surface Reactivity of Iron Sulfide, $FeS_2$. *J. Colloid Interface Sci.* **1980**, *75*, 357−372.
(334) Komadel, P.; Madejová, J.; Stucki, J. W. Structural Fe(III) Reduction in Smectites. *Appl. Clay Sci.* **2006**, *34*, 88−94.
(335) Stucki, J. W. A Review of the Effects of Iron Redox Cycles on Smectite Properties. *C. R. Geosci.* **2011**, *343*, 199−209.
(336) Stucki, J.; Properties, W. Behaviour of Iron in Clay Minerals. In *Developments in Clay Science*; Bergaya, F., Lagaly, G., Eds.; Elsevier, 2013; Vol. *5*, pp 559−611.
(337) Aoki, S.; Kohyama, N. The Vertical Change in Clay Mineral Composition and Chemical Characteristics of Smectite in Sediment Cores from the Southern Part of the Central Pacific Basin. *Mar. Geol.* **1991**, *98*, 41−49.
(338) Komadel, P.; Lear, P. R.; Stucki, J. W. Reduction and Reoxidation of Nontronite: Extent of Reduction and Reaction Rates. *Clays Clay Miner.* **1990**, *38*, 203−208.
(339) Dong, H.; Jaisi, D. P.; Kim, J.; Zhang, G. Microbe-Clay Mineral Interactions. *Am. Mineral.* **2009**, *94*, 1505−1519.
(340) Zhang, J.; Dong, H.; Liu, D.; Agrawal, A. Microbial Reduction of Fe(III) in Smectite Minerals by Thermophilic Methanogen Methanothermobacter Thermautotrophicus. *Geochim. Cosmochim. Acta* **2013**, *106*, 203−215.
(341) Luan, F.; Gorski, C. A.; Burgos, W. D. Linear Free Energy Relationships for the Biotic and Abiotic Reduction of Nitroaromatic Compounds. *Environ. Sci. Technol.* **2015**, *49*, 3557−3565.
(342) Luan, F.; Liu, Y.; Griffin, A. M.; Gorski, C. A.; Burgos, W. D. Iron(III)-Bearing Clay Minerals Enhance Bioreduction of Nitrobenzene by *Shewanella Putrefaciens* CN32. *Environ. Sci. Technol.* **2015**, *49*, 1418−1426.
(343) Neumann, A.; Hofstetter, T. B.; Lüssi, M.; Cirpka, O. A.; Petit, S.; Schwarzenbach, R. P. Assessing the Redox Reactivity of Structural Iron in Smectites Using Nitroaromatic Compounds as Kinetic Probes. *Environ. Sci. Technol.* **2008**, *42*, 8381−8387.
(344) Brigatti, M. F.; Franchini, G.; Lugli, C.; Medici, L.; Poppi, L.; Turci, E. Interaction between Aqueous Chromium Solutions and Layer Silicates. *Appl. Geochem.* **2000**, *15*, 1307−1316.
(345) Qafoku, O.; Pearce, C. I.; Neumann, A.; Kovarik, L.; Zhu, M.; Ilton, E. S.; Bowden, M. E.; Resch, C. T.; Arey, B. W.; Arenholz, E.; et al. Tc(VII) and Cr(VI) Interaction with Naturally Reduced Ferruginous Smectite from a Redox Transition Zone. *Environ. Sci. Technol.* **2017**, *51*, 9042−9052.
(346) Peretyazhko, T.; Zachara, J. M.; Heald, S. M.; Jeon, B.-H.; Kukkadapu, R. K.; Liu, C.; Moore, D.; Resch, C. T. Heterogeneous


https://doi.org/10.1021/acs.chemrev.0c01286
*Chem. Rev.* 2021, 121, 8161−8233

Reduction of Tc(VII) by Fe(II) at the Solid−Water Interface. *Geochim. Cosmochim. Acta* **2008**, *72*, 1521−1539.
(347) Ilton, E. S.; Haiduc, A.; Moses, C. O.; Heald, S. M.; Elbert, D. C.; Veblen, D. R. Heterogeneous Reduction of Uranyl by Micas: Crystal Chemical and Solution Controls. *Geochim. Cosmochim. Acta* **2004**, *68*, 2417−2435.
(348) Ilton, E. S.; Heald, S. M.; Smith, S. C.; Elbert, D.; Liu, C. Reduction of Uranyl in the Interlayer Region of Low Iron Micas under Anoxic and Aerobic Conditions. *Environ. Sci. Technol.* **2006**, *40*, 5003−5009.
(349) Rosso, K. M.; Ilton, E. S. Charge Transport in Micas: The Kinetics of $Fe^{II/III}$ Electron Transfer in the Octahedral Sheet. *J. Chem. Phys.* **2003**, *119*, 9207−9218.
(350) Rosso, K. M.; Ilton, E. S. Effects of Compositional Defects on Small Polaron Hopping in Micas. *J. Chem. Phys.* **2005**, *122*, 244709.
(351) Alexandrov, V.; Rosso, K. M. Insights into the Mechanism of Fe(II) Adsorption and Oxidation at Fe−Clay Mineral Surfaces from First-Principles Calculations. *J. Phys. Chem. C* **2013**, *117*, 22880−22886.
(352) Alexandrov, V.; Neumann, A.; Scherer, M. M.; Rosso, K. M. Electron Exchange and Conduction in Nontronite from First-Principles. *J. Phys. Chem. C* **2013**, *117*, 2032−2040.
(353) Liu, X.; Dong, H.; Yang, X.; Kovarik, L.; Chen, Y.; Zeng, Q. Effects of Citrate on Hexavalent Chromium Reduction by Structural Fe(II) in Nontronite. *J. Hazard. Mater.* **2018**, *343*, 245−254.
(354) Jaisi, D. P.; Dong, H.; Morton, J. P. Partitioning of Fe(II) in Reduced Nontronite (NAU-2) to Reactive Sites: Reactivity in Terms of Tc(VII) Reduction. *Clays Clay Miner.* **2008**, *56*, 175−189.
(355) Taylor, R. W.; Shen, S.; Bleam, W. F.; Tu, S.-I. Chromate Removal by Dithionite-Reduced Clays: Evidence from Direct X-Ray Adsorption near Edge Spectroscopy (XANES) of Chromate Reduction at Clay Surfaces. *Clays Clay Miner.* **2000**, *48*, 648−654.
(356) Haderlein, S. B.; Weissmahr, K. W.; Schwarzenbach, R. P. Specific Adsorption of Nitroaromatic Explosives and Pesticides to Clay Minerals. *Environ. Sci. Technol.* **1996**, *30*, 612−622.
(357) Amonette, J. E.; Workman, D. J.; Kennedy, D. W.; Fruchter, J. S.; Gorby, Y. A. Dechlorination of Carbon Tetrachloride by Fe(II) Associated with Goethite. *Environ. Sci. Technol.* **2000**, *34*, 4606−4613.
(358) Maithreepala, R.; Doong, R.-a. Synergistic Effect of Copper Ion on the Reductive Dechlorination of Carbon Tetrachloride by Surface-Bound Fe(II) Associated with Goethite. *Environ. Sci. Technol.* **2004**, *38*, 260−268.
(359) Zwank, L.; Elsner, M.; Aeberhard, A.; Schwarzenbach, R. P.; Haderlein, S. B. Carbon Isotope Fractionation in the Reductive Dehalogenation of Carbon Tetrachloride at Iron (Hydr)Oxide and Iron Sulfide Minerals. *Environ. Sci. Technol.* **2005**, *39*, 5634−5641.
(360) Shao, H.; Butler, E. C. The Influence of Iron and Sulfur Mineral Fractions on Carbon Tetrachloride Transformation in Model Anaerobic Soils and Sediments. *Chemosphere* **2007**, *68*, 1807−1813.
(361) Elsner, M.; Schwarzenbach, R. P.; Haderlein, S. B. Reactivity of Fe(II)-Bearing Minerals toward Reductive Transformation of Organic Contaminants. *Environ. Sci. Technol.* **2004**, *38*, 799−807.
(362) Chun, C. L.; Penn, R. L.; Arnold, W. A. Kinetic and Microscopic Studies of Reductive Transformations of Organic Contaminants on Goethite. *Environ. Sci. Technol.* **2006**, *40*, 3299−3304.
(363) Jones, A. M.; Kinsela, A. S.; Collins, R. N.; Waite, T. D. The Reduction of 4-Chloronitrobenzene by Fe(II)-Fe(III) Oxide Systems - Correlations with Reduction Potential and Inhibition by Silicate. *J. Hazard. Mater.* **2016**, *320*, 143−149.
(364) Vindedahl, A. M.; Stemig, M. S.; Arnold, W. A.; Penn, R. L. Character of Humic Substances as a Predictor for Goethite Nanoparticle Reactivity and Aggregation. *Environ. Sci. Technol.* **2016**, *50*, 1200−1208.
(365) Colón, D.; Weber, E. J.; Anderson, J. L. Effect of Natural Organic Matter on the Reduction of Nitroaromatics by Fe(II) Species. *Environ. Sci. Technol.* **2008**, *42*, 6538−6543.
(366) Tao, L.; Zhu, Z.; Li, F. Fe(II)/Cu(II) Interaction on $\alpha$-FeOOH, Kaolin and $TiO_2$ for Interfacial Reactions of 2-Nitrophenol Reductive Transformation. *Colloids Surf., A* **2013**, *425*, 92−98.
(367) Luan, F.; Xie, L.; Li, J.; Zhou, Q. Abiotic Reduction of Nitroaromatic Compounds by Fe (II) Associated with Iron Oxides and Humic Acid. *Chemosphere* **2013**, *91*, 1035−1041.
(368) Wang, S.; Arnold, W. A. Abiotic Reduction of Dinitroaniline Herbicides. *Water Res.* **2003**, *37*, 4191−4201.
(369) Strathmann, T. J.; Stone, A. T. Mineral Surface Catalysis of Reactions between $Fe^{II}$ and Oxime Carbamate Pesticides. *Geochim. Cosmochim. Acta* **2003**, *67*, 2775−2791.
(370) Klupinski, T. P.; Chin, Y.-P.; Traina, S. J. Abiotic Degradation of Pentachloronitrobenzene by Fe(II): Reactions on Goethite and Iron Oxide Nanoparticles. *Environ. Sci. Technol.* **2004**, *38*, 4353−4360.
(371) Chun, C. L.; Hozalski, R. M.; Arnold, W. A. Degradation of Drinking Water Disinfection Byproducts by Synthetic Goethite and Magnetite. *Environ. Sci. Technol.* **2005**, *39*, 8525−8532.
(372) Amstaetter, K.; Borch, T.; Larese-Casanova, P.; Kappler, A. Redox Transformation of Arsenic by Fe(II)-Activated Goethite ($\alpha$-FeOOH). *Environ. Sci. Technol.* **2010**, *44*, 102−108.
(373) Felmy, A. R.; Moore, D. A.; Rosso, K. M.; Qafoku, O.; Rai, D.; Buck, E. C.; Ilton, E. S. Heterogeneous Reduction of $PuO_2$ with Fe(II): Importance of the Fe(III) Reaction Product. *Environ. Sci. Technol.* **2011**, *45*, 3952−3958.
(374) Jeon, B.-H.; Dempsey, B. A.; Burgos, W. D.; Barnett, M. O.; Roden, E. E. Chemical Reduction of U(VI) by Fe(II) at the Solid-Water Interface Using Natural and Synthetic Fe(III) Oxides. *Environ. Sci. Technol.* **2005**, *39*, 5642−5649.
(375) Liger, E.; Charlet, L.; Van Cappellen, P. Surface Catalysis of Uranium(VI) Reduction by Iron(II). *Geochim. Cosmochim. Acta* **1999**, *63*, 2939−2955.
(376) Jang, J.-H.; Dempsey, B. A.; Burgos, W. D. Reduction of U(VI) by Fe(II) in the Presence of Hydrous Ferric Oxide and Hematite: Effects of Solid Transformation, Surface Coverage, and Humic Acid. *Water Res.* **2008**, *42*, 2269−2277.
(377) Tai, Y.-L.; Dempsey, B. A. Nitrite Reduction with Hydrous Ferric Oxide and Fe(II): Stoichiometry, Rate, and Mechanism. *Water Res.* **2009**, *43*, 546−552.
(378) Sørensen, J.; Thorling, L. Stimulation by Lepidocrocite ($\Upsilon$-FeOOH) of Fe(II)-Dependent Nitrite Reduction. *Geochim. Cosmochim. Acta* **1991**, *55*, 1289−1294.
(379) Cui, D.; Eriksen, T. E. Reduction of Pertechnetate in Solution by Heterogeneous Electron Transfer from Fe(II)-Containing Geological Material. *Environ. Sci. Technol.* **1996**, *30*, 2263−2269.
(380) Peretyazhko, T.; Zachara, J. M.; Heald, S. M.; Kukkadapu, R. K.; Liu, C.; Plymale, A. E.; Resch, C. T. Reduction of Tc(VII) by Fe(II) Sorbed on Al (Hydr)Oxides. *Environ. Sci. Technol.* **2008**, *42*, 5499−5506.
(381) Li, F.-b.; Tao, L.; Feng, C.-h.; Li, X.-z.; Sun, K.-w. Electrochemical Evidences for Promoted Interfacial Reactions: The Role of Fe(II) Adsorbed onto $\gamma$-$Al_2O_3$ and $TiO_2$ in Reductive Transformation of 2-Nitrophenol. *Environ. Sci. Technol.* **2009**, *43*, 3656−3661.
(382) Zhu, Z.; Tao, L.; Li, F. Effects of Dissolved Organic Matter on Adsorbed Fe(II) Reactivity for the Reduction of 2-Nitrophenol in $TiO_2$ Suspensions. *Chemosphere* **2013**, *93*, 29−34.
(383) Chakraborty, S.; Bardelli, F.; Charlet, L. Reactivities of Fe(II) on Calcite: Selenium Reduction. *Environ. Sci. Technol.* **2010**, *44*, 1288−1294.
(384) Charlet, L.; Scheinost, A. C.; Tournassat, C.; Greneche, J. M.; Géhin, A.; Fernández-Martínez, A.; Coudert, S.; Tisserand, D.; Brendle, J. Electron Transfer at the Mineral/Water Interface: Selenium Reduction by Ferrous Iron Sorbed on Clay. *Geochim. Cosmochim. Acta* **2007**, *71*, 5731−5749.
(385) Chakraborty, S.; Favre, F.; Banerjee, D.; Scheinost, A. C.; Mullet, M.; Ehrhardt, J.-J.; Brendle, J.; Vidal, L. c.; Charlet, L. U(VI) Sorption and Reduction by Fe(II) Sorbed on Montmorillonite. *Environ. Sci. Technol.* **2010**, *44*, 3779−3785.
(386) Jaisi, D. P.; Dong, H.; Plymale, A. E.; Fredrickson, J. K.; Zachara, J. M.; Heald, S.; Liu, C. Reduction and Long-Term Immobilization of Technetium by Fe(II) Associated with Clay Mineral Nontronite. *Chem. Geol.* **2009**, *264*, 127−138.


https://doi.org/10.1021/acs.chemrev.0c01286
*Chem. Rev.* 2021, 121, 8161−8233

(387) Poulton, S. W.; Krom, M. D.; Raiswell, R. A Revised Scheme for the Reactivity of Iron (Oxyhydr)Oxide Minerals Towards Dissolved Sulfide. *Geochim. Cosmochim. Acta* **2004**, *68*, 3703−3715.
(388) Poulton, S.; Raiswell, R. The Low-Temperature Geochemical Cycle of Iron: From Continental Fluxes to Marine Sediment Deposition. *Am. J. Sci.* **2002**, *302*, 774−805.
(389) Chen, C.; Meile, C.; Wilmoth, J.; Barcellos, D.; Thompson, A. Influence of $pO_2$ on Iron Redox Cycling and Anaerobic Organic Carbon Mineralization in a Humid Tropical Forest Soil. *Environ. Sci. Technol.* **2018**, *52*, 7709−7719.
(390) Bhattacharyya, A.; Campbell, A. N.; Tfaily, M. M.; Lin, Y.; Silver, W. L.; Nico, P. S.; Pett-Ridge, J. Redox Fluctuations Control the Coupled Cycling of Iron and Carbon in Tropical Forest Soils. *Environ. Sci. Technol.* **2018**, *52*, 14129−12139.
(391) Zinder, B.; Furrer, G.; Stumm, W. The Coordination Chemistry of Weathering: II. Dissolution of Fe(III) Oxides. *Geochim. Cosmochim. Acta* **1986**, *50*, 1861−1869.
(392) Williams, A. G.; Scherer, M. M. Spectroscopic Evidence for Fe(II)-Fe(III) Electron Transfer at the Iron Oxide-Water Interface. *Environ. Sci. Technol.* **2004**, *38*, 4782−4790.
(393) Yanina, S. V.; Rosso, K. M. Linked Reactivity at Mineral-Water Interfaces through Bulk Crystal Conduction. *Science* **2008**, *320*, 218−222.
(394) Handler, R. M.; Beard, B. L.; Johnson, C. M.; Scherer, M. M. Atom Exchange between Aqueous Fe(II) and Goethite: An Fe Isotope Tracer Study. *Environ. Sci. Technol.* **2009**, *43*, 1102−1107.
(395) Pedersen, H. D.; Postma, D.; Jakobsen, R.; Larsen, O. Fast Transformation of Iron Oxyhydroxides by the Catalytic Action of Aqueous Fe(II). *Geochim. Cosmochim. Acta* **2005**, *69*, 3967−3977.
(396) Jones, A. M.; Collins, R. N.; Rose, J.; Waite, T. D. The Effect of Silica and Natural Organic Matter on the Fe(II)-Catalysed Transformation and Reactivity of Fe(III) Minerals. *Geochim. Cosmochim. Acta* **2009**, *73*, 4409−4422.
(397) Hansel, C. M.; Benner, S. G.; Fendorf, S. Competing Fe(II)-Induced Mineralization Pathways of Ferrihydrite. *Environ. Sci. Technol.* **2005**, *39*, 7147−7153.
(398) Boland, D. D.; Collins, R. N.; Miller, C. J.; Glover, C. J.; Waite, T. D. Effect of Solution and Solid-Phase Conditions on the Fe(II)-Accelerated Transformation of Ferrihydrite to Lepidocrocite and Goethite. *Environ. Sci. Technol.* **2014**, *48*, 5477−5485.
(399) Sheng, A.; Liu, J.; Li, X.; Qafoku, O.; Collins, R. N.; Jones, A. M.; Pearce, C. I.; Wang, C.; Ni, J.; Lu, A.; et al. Labile Fe(III) from Sorbed Fe(II) Oxidation Is the Key Intermediate in Fe(II)-Catalyzed Ferrihydrite Transformation. *Geochim. Cosmochim. Acta* **2020**, *272*, 105−120.
(400) Sheng, A.; Li, X.; Arai, Y.; Ding, Y.; Rosso, K. M.; Liu, J. Citrate Controls Fe(II)-Catalyzed Transformation of Ferrihydrite by Complexation of the Labile Fe(III) Intermediate. *Environ. Sci. Technol.* **2020**, *54*, 7309−7319.
(401) Qafoku, O.; Kovarik, L.; Bowden, M. E.; Nakouzi, E.; Sheng, A.; Liu, J.; Pearce, C. I.; Rosso, K. M. Nanoscale Observations of Fe(II)-Induced Ferrihydrite Transformation. *Environ. Sci.: Nano* **2020**, *7*, 2953−2967.
(402) Schwertmann, U.; Murad, E. Effect of pH on the Formation of Goethite and Hematite from Ferrihydrite. *Clays Clay Miner.* **1983**, *31*, 277−284.
(403) Polyakov, V. B.; Mineev, S. D. The Use of Mössbauer Spectroscopy in Stable Isotope Geochemistry. *Geochim. Cosmochim. Acta* **2000**, *64*, 849−865.
(404) Frierdich, A. J.; Beard, B. L.; Scherer, M. M.; Johnson, C. M. Determination of the $Fe(II)_{aq}$−Magnetite Equilibrium Iron Isotope Fractionation Factor Using the Three-Isotope Method and a Multi-Direction Approach to Equilibrium. *Earth Planet. Sci. Lett.* **2014**, *391*, 77−86.
(405) Joshi, P.; Gorski, C. A. Anisotropic Morphological Changes in Goethite During $Fe^{2+}$-Catalyzed Recrystallization. *Environ. Sci. Technol.* **2016**, *50*, 7315−7324.
(406) Handler, R. M.; Frierdich, A. J.; Johnson, C. M.; Rosso, K. M.; Beard, B. L.; Wang, C.; Latta, D. E.; Neumann, A.; Pasakarnis, T.; Premaratne, W. Fe(II)-Catalyzed Recrystallization of Goethite Revisited. *Environ. Sci. Technol.* **2014**, *48*, 11302−11311.
(407) Boland, D. D.; Collins, R. N.; Payne, T. E.; Waite, T. D. Effect of Amorphous Fe(III) Oxide Transformation on the Fe(II)-Mediated Reduction of U(VI). *Environ. Sci. Technol.* **2011**, *45*, 1327−1333.
(408) Pedersen, H. D.; Postma, D.; Jakobsen, R. Release of Arsenic Associated with the Reduction and Transformation of Iron Oxides. *Geochim. Cosmochim. Acta* **2006**, *70*, 4116−4129.
(409) Frierdich, A. J.; Catalano, J. G. Controls on Fe(II)-Activated Trace Element Release from Goethite and Hematite. *Environ. Sci. Technol.* **2012**, *46*, 1519−1526.
(410) Frierdich, A. J.; Scherer, M. M.; Bachman, J. E.; Engelhard, M. H.; Rapponotti, B. W.; Catalano, J. G. Inhibition of Trace Element Release During Fe(II)-Activated Recrystallization of Al-, Cr-, and Sn-Substituted Goethite and Hematite. *Environ. Sci. Technol.* **2012**, *46*, 10031−10039.
(411) Frierdich, A. J.; Beard, B. L.; Rosso, K. M.; Scherer, M. M.; Spicuzza, M. J.; Valley, J. W.; Johnson, C. M. Low Temperature, Non-Stoichiometric Oxygen-Isotope Exchange Coupled to Fe(II)−Goethite Interactions. *Geochim. Cosmochim. Acta* **2015**, *160*, 38−54.
(412) Gorski, C. A.; Fantle, M. S. Stable Mineral Recrystallization in Low Temperature Aqueous Systems: A Critical Review. *Geochim. Cosmochim. Acta* **2017**, *198*, 439−465.
(413) Roden, E. E. Microbial Iron-Redox Cycling in Subsurface Environments. *Biochem. Soc. Trans.* **2012**, *40*, 1249−1256.
(414) Nevin, K. P.; Lovley, D. R. Potential for Nonenzymatic Reduction of Fe(III) via Electron Shuttling in Subsurface Sediments. *Environ. Sci. Technol.* **2000**, *34*, 2472−2478.
(415) Lovley, D. R.; Phillips, E. J. Availability of Ferric Iron for Microbial Reduction in Bottom Sediments of the Freshwater Tidal Potomac River. *Appl. Environ. Microbiol.* **1986**, *52*, 751−757.
(416) Weiss, J. V.; Emerson, D.; Backer, S. M.; Megonigal, J. P. Enumeration of Fe(II)-Oxidizing and Fe(III)-Reducing Bacteria in the Root Zone of Wetland Plants: Implications for a Rhizosphere Iron Cycle. *Biogeochemistry* **2003**, *64*, 77−96.
(417) Bonneville, S.; Behrends, T.; Van Cappellen, P. Solubility and Dissimilatory Reduction Kinetics of Iron(III) Oxyhydroxides: A Linear Free Energy Relationship. *Geochim. Cosmochim. Acta* **2009**, *73*, 5273−5282.
(418) Roden, E. E.; Zachara, J. M. Microbial Reduction of Crystalline Iron(III) Oxides: Influence of Oxide Surface Area and Potential for Cell Growth. *Environ. Sci. Technol.* **1996**, *30*, 1618−1628.
(419) Chan, C. S.; De Stasio, G.; Welch, S. A.; Girasole, M.; Frazer, B. H.; Nesterova, M. V.; Fakra, S.; Banfield, J. F. Microbial Polysaccharides Template Assembly of Nanocrystal Fibers. *Science* **2004**, *303*, 1656−1658.
(420) Glasauer, S.; Langley, S.; Beveridge, T. Sorption of Fe (Hydr)Oxides to the Surface of *Shewanella Putrefaciens*: Cell-Bound Fine-Grained Minerals Are Not Always Formed De Novo. *Appl. Environ. Microbiol.* **2001**, *67*, 5544−5550.
(421) Huang, J.; Dai, Y.; Singewald, K.; Liu, C.-C.; Saxena, S.; Zhang, H. Effects of $MnO_2$ of Different Structures on Activation of Peroxymonosulfate for Bisphenol a Degradation under Acidic Conditions. *Chem. Eng. J.* **2019**, *370*, 906−915.
(422) Xiao, W.; Jones, A. M.; Collins, R. N.; Waite, T. D. Investigating the Effect of Ascorbate on the Fe(II)-Catalyzed Transformation of the Poorly Crystalline Iron Mineral Ferrihydrite. *Biochim. Biophys. Acta, Gen. Subj.* **2018**, *1862*, 1760−1769.
(423) Gorski, C. A.; Edwards, R.; Sander, M.; Hofstetter, T. B.; Stewart, S. M. Thermodynamic Characterization of Iron Oxide−Aqueous $Fe^{2+}$ Redox Couples. *Environ. Sci. Technol.* **2016**, *50*, 8538−8547.
(424) Luther, G. The Frontier-Molecular-Orbital Theory Approach in Geochemical Processes. *Aquatic chemical kinetics: reaction rates of processes in natural waters* **1990**, 173−198.
(425) Stewart, S. M.; Hofstetter, T. B.; Joshi, P.; Gorski, C. A. Linking Thermodynamics to Pollutant Reduction Kinetics by $Fe^{2+}$ Bound to Iron Oxides. *Environ. Sci. Technol.* **2018**, *52*, 5600−5609.


https://doi.org/10.1021/acs.chemrev.0c01286
*Chem. Rev.* 2021, 121, 8161−8233

(426) Fan, D.; Bradley, M. J.; Hinkle, A. W.; Johnson, R. L.; Tratnyek, P. G. Chemical Reactivity Probes for Assessing Abiotic Natural Attenuation by Reducing Iron Minerals. *Environ. Sci. Technol.* **2016**, *50*, 1868−1876.
(427) Park, B.; Dempsey, B. A. Heterogeneous Oxidation of Fe(II) on Ferric Oxide at Neutral pH and a Low Partial Pressure of $O_2$. *Environ. Sci. Technol.* **2005**, *39*, 6494−6500.
(428) Jones, A. M.; Collins, R. N.; Waite, T. D. Redox Characterization of the Fe(II)-Catalyzed Transformation of Ferrihydrite to Goethite. *Geochim. Cosmochim. Acta* **2017**, *218*, 257−272.
(429) Assaf, N. W.; Altarawneh, M.; Oluwoye, I.; Radny, M.; Lomnicki, S. M.; Dlugogorski, B. Z. Formation of Environmentally Persistent Free Radicals on $\alpha$-$Al_2O_3$. *Environ. Sci. Technol.* **2016**, *50*, 11094−11102.
(430) Felmy, A. R.; Ilton, E. S.; Rosso, K. M.; Zachara, J. M. Interfacial Reactivity of radionuclide: Emerging Paradigms from Molecular-level Observations. *Mineral. Mag.* **2011**, *75*, 2379−2391.
(431) Silvester, E.; Charlet, L.; Tournassat, C.; Géhin, A.; Grenèche, J.-M.; Liger, E. Redox Potential Measurements and Mössbauer Spectrometry of $Fe^{II}$ Adsorbed onto $Fe^{III}$ (Oxyhydr)Oxides. *Geochim. Cosmochim. Acta* **2005**, *69*, 4801−4815.
(432) Buerge, I. J.; Hug, S. J. Influence of Mineral Surfaces on Chromium(VI) Reduction by Iron(II). *Environ. Sci. Technol.* **1999**, *33*, 4285−4291.
(433) Buerge, I. J.; Hug, S. J. Kinetics and pH Dependence of Chromium(VI) Reduction by Iron(II). *Environ. Sci. Technol.* **1997**, *31*, 1426−1432.
(434) Amirbahman, A.; Kent, D. B.; Curtis, G. P.; Marvin-DiPasquale, M. C. Kinetics of Homogeneous and Surface-Catalyzed Mercury(II) Reduction by Iron(II). *Environ. Sci. Technol.* **2013**, *47*, 7204−7213.
(435) Frierdich, A. J.; Helgeson, M.; Liu, C.; Wang, C.; Rosso, K. M.; Scherer, M. M. Iron Atom Exchange between Hematite and Aqueous Fe(II). *Environ. Sci. Technol.* **2015**, *49*, 8479−8486.
(436) Waychunas, G. A.; Kim, C. S.; Banfield, J. F. Nanoparticulate Iron Oxide Minerals in Soils and Sediments: Unique Properties and Contaminant Scavenging Mechanisms. *J. Nanopart. Res.* **2005**, *7*, 409−433.
(437) Cwiertny, D. M.; Handler, R. M.; Schaefer, M. V.; Grassian, V. H.; Scherer, M. M. Interpreting Nanoscale Size-Effects in Aggregated Fe-Oxide Suspensions: Reaction of Fe(II) with Goethite. *Geochim. Cosmochim. Acta* **2008**, *72*, 1365−1380.
(438) Stemig, A. M.; Do, T. A.; Yuwono, V. M.; Arnold, W. A.; Penn, R. L. Goethite Nanoparticle Aggregation: Effects of Buffers, Metal Ions, and 4-Chloronitrobenzene Reduction. *Environ. Sci.: Nano* **2014**, *1*, 478−487.
(439) Torrent, J.; Schwertmann, U.; Barron, V. The Reductive Dissolution of Synthetic Goethite and Hematite in Dithionite. *Clay Miner.* **1987**, *22*, 329−337.
(440) Dominik, P.; Pohl, H. N.; Bousserrhine, N.; Berthelin, J.; Kaupenjohann, M. Limitations to the Reductive Dissolution of Al-Substituted Goethites by Clostridium Butyricum. *Soil Biol. Biochem.* **2002**, *34*, 1147−1155.
(441) Ekstrom, E. B.; Learman, D. R.; Madden, A. S.; Hansel, C. M. Contrasting Effects of Al Substitution on Microbial Reduction of Fe(III) (Hydr)Oxides. *Geochim. Cosmochim. Acta* **2010**, *74*, 7086−7099.
(442) Hansel, C.; Learman, D.; Lentini, C.; Ekstrom, E. Effect of Adsorbed and Substituted Al on Fe(II)-Induced Mineralization Pathways of Ferrihydrite. *Geochim. Cosmochim. Acta* **2011**, *75*, 4653−4666.
(443) Masue-Slowey, Y.; Loeppert, R. H.; Fendorf, S. Alteration of Ferrihydrite Reductive Dissolution and Transformation by Adsorbed as and Structural Al: Implications for as Retention. *Geochim. Cosmochim. Acta* **2011**, *75*, 870−886.
(444) Latta, D. E.; Bachman, J. E.; Scherer, M. M. Fe Electron Transfer and Atom Exchange in Goethite: Influence of Al-Substitution and Anion Sorption. *Environ. Sci. Technol.* **2012**, *46*, 10614−10623.
(445) Huang, X.; Hou, X.; Zhang, X.; Rosso, K.; Zhang, L. Facet-Dependent Contaminant Removal Properties of Hematite Nanocrystals and Their Environmental Implications. *Environ. Sci.: Nano* **2018**, *5*, 1790−1806.
(446) Taylor, S. D.; Kovarik, L.; Cliff, J. B.; Rosso, K. M. Facet-Selective Adsorption of Fe(II) on Hematite Visualized by Nanoscale Secondary Ion Mass Spectrometry. *Environ. Sci.: Nano* **2019**, *6*, 2429−2440.
(447) Catalano, J. G.; Fenter, P.; Park, C.; Zhang, Z.; Rosso, K. M. Structure and Oxidation State of Hematite Surfaces Reacted with Aqueous Fe(II) at Acidic and Neutral pH. *Geochim. Cosmochim. Acta* **2010**, *74*, 1498−1512.
(448) Huang, X.; Hou, X.; Wang, F.; Guo, B.; Song, F.; Ling, L.; Zhao, J.; Zhang, L. Molecular-Scale Structures of Uranyl Surface Complexes on Hematite Facets. *Environ. Sci.: Nano* **2019**, *6*, 892−903.
(449) Huang, X.; Hou, X.; Zhao, J.; Zhang, L. Hematite Facet Confined Ferrous Ions as High Efficient Fenton Catalysts to Degrade Organic Contaminants by Lowering $H_2O_2$ Decomposition Energetic Span. *Appl. Catal., B* **2016**, *181*, 127−137.
(450) Huang, X.; Hou, X.; Song, F.; Zhao, J.; Zhang, L. Facet-Dependent Cr(VI) Adsorption of Hematite Nanocrystals. *Environ. Sci. Technol.* **2016**, *50*, 1964−1972.
(451) Huang, X.; Hou, X.; Song, F.; Zhao, J.; Zhang, L. Ascorbate Induced Facet Dependent Reductive Dissolution of Hematite Nanocrystals. *J. Phys. Chem. C* **2017**, *121*, 1113−1121.
(452) Huang, X.; Hou, X.; Jia, F.; Song, F.; Zhao, J.; Zhang, L. Ascorbate-Promoted Surface Iron Cycle for Efficient Heterogeneous Fenton Alachlor Degradation with Hematite Nanocrystals. *ACS Appl. Mater. Interfaces* **2017**, *9*, 8751−8758.
(453) Huang, X.; Chen, Y.; Walter, E.; Zong, M.; Wang, Y.; Zhang, X.; Qafoku, O.; Wang, Z.; Rosso, K. M. Facet-Specific Photocatalytic Degradation of Organics by Heterogeneous Fenton Chemistry on Hematite Nanoparticles. *Environ. Sci. Technol.* **2019**, *53*, 10197−10207.
(454) Notini, L.; Latta, D. E.; Neumann, A.; Pearce, C. I.; Sassi, M.; N'Diaye, A. T.; Rosso, K. M.; Scherer, M. M. The Role of Defects in Fe(II)−Goethite Electron Transfer. *Environ. Sci. Technol.* **2018**, *52*, 2751−2759.
(455) Eggleston, C. M.; Stack, A. G.; Rosso, K. M.; Bice, A. M. Adatom Fe(III) on the Hematite Surface: Observation of a Key Reactive Surface Species. *Geochem. Trans.* **2004**, *5*, 33−40.
(456) Eggleston, C. M.; Stack, A. G.; Rosso, K. M.; Higgins, S. R.; Bice, A. M.; Boese, S. W.; Pribyl, R. D.; Nichols, J. J. The Structure of Hematite ($\alpha$-$Fe_2O_3$) (001) Surfaces in Aqueous Media: Scanning Tunneling Microscopy and Resonant Tunneling Calculations of Coexisting O and Fe Terminations. *Geochim. Cosmochim. Acta* **2003**, *67*, 985−1000.
(457) Weidler, P. G.; Schwinn, T.; Gaub, H. E. Vicinal Faces on Synthetic Goethite Observed by Atomic Force Microscopy. *Clays Clay Miner.* **1996**, *44*, 437−442.
(458) Weidler, P. G.; Hug, S. J.; Wetche, T. P.; Hiemstra, T. Determination of Growth Rates of (100) and (110) Faces of Synthetic Goethite by Scanning Force Microscopy. *Geochim. Cosmochim. Acta* **1998**, *62*, 3407−3412.
(459) Taylor, S. D.; Liu, J.; Zhang, X.; Arey, B. W.; Kovarik, L.; Schreiber, D. K.; Perea, D. E.; Rosso, K. M. Visualizing the Iron Atom Exchange Front in the Fe(II)-Catalyzed Recrystallization of Goethite by Atom Probe Tomography. *Proc. Natl. Acad. Sci. U. S. A.* **2019**, *116*, 2866−2874.
(460) Russell, B.; Payne, M.; Ciacchi, L. C. Density Functional Theory Study of Fe(II) Adsorption and Oxidation on Goethite Surfaces. *Phys. Rev. B: Condens. Matter Mater. Phys.* **2009**, *79*, 165101.
(461) Alexandrov, V.; Rosso, K. M. Ab Initio Modeling of Fe(II) Adsorption and Interfacial Electron Transfer at Goethite ($\alpha$-FeOOH) Surfaces. *Phys. Chem. Chem. Phys.* **2015**, *17*, 14518−14531.
(462) Huang, J.; Zhang, H. Redox Reactions of Iron and Manganese Oxides in Complex Systems. *Front. Environ. Sci. Eng.* **2020**, *14*, 76−87.
(463) Zhang, Y.; Charlet, L.; Schindler, P. Adsorption of Protons, Fe(II) and Al(III) on Lepidocrocite ($\Upsilon$-FeOOH). *Colloids Surf.* **1992**, *63*, 259−268.


https://doi.org/10.1021/acs.chemrev.0c01286
*Chem. Rev.* 2021, 121, 8161−8233

(464) Larese-Casanova, P.; Scherer, M. M. Fe(II) Sorption on Hematite: New Insights Based on Spectroscopic Measurements. *Environ. Sci. Technol.* **2007**, *41*, 471−477.
(465) Larese-Casanova, P.; Cwiertny, D. M.; Scherer, M. M. Nanogoethite Formation from Oxidation of Fe(II) Sorbed on Aluminum Oxide: Implications for Contaminant Reduction. *Environ. Sci. Technol.* **2010**, *44*, 3765−3771.
(466) Charlet, L.; Bosbach, D.; Peretyashko, T. Natural Attenuation of TCE, As, Hg Linked to the Heterogeneous Oxidation of Fe(II): An AFM Study. *Chem. Geol.* **2002**, *190*, 303−319.
(467) Notini, L.; Latta, D. E.; Neumann, A.; Pearce, C. I.; Sassi, M. J.; N'Diaye, A. T.; Rosso, K. M.; Scherer, M. M. A Closer Look at Fe(II) Passivation of Goethite. *ACS Earth Space Chem.* **2019**, *3*, 2717−2725.
(468) Taujale, S.; Baratta, L. R.; Huang, J.; Zhang, H. Interactions in Ternary Mixtures of $MnO_2$, $Al_2O_3$, and Natural Organic Matter (NOM) and the Impact on $MnO_2$ Oxidative Reactivity. *Environ. Sci. Technol.* **2016**, *50*, 2345−2353.
(469) Zhang, H.; Taujale, S.; Huang, J.; Lee, G.-J. Effects of Nom on Oxidative Reactivity of Manganese Dioxide in Binary Oxide Mixtures with Goethite or Hematite. *Langmuir* **2015**, *31*, 2790−2799.
(470) ThomasArrigo, L. K.; Kaegi, R.; Kretzschmar, R. Ferrihydrite Growth and Transformation in the Presence of Ferrous Iron and Model Organic Ligands. *Environ. Sci. Technol.* **2019**, *53*, 13636−13647.
(471) Zhou, Z.; Latta, D. E.; Noor, N.; Thompson, A.; Borch, T.; Scherer, M. M. Fe(II)-Catalyzed Transformation of Organic Matter−Ferrihydrite Coprecipitates: A Closer Look Using Fe Isotopes. *Environ. Sci. Technol.* **2018**, *52*, 11142−11150.
(472) Vikesland, P. J.; Valentine, R. L. Iron Oxide Surface-Catalyzed Oxidation of Ferrous Iron by Monochloramine: Implications of Oxide Type and Carbonate on Reactivity. *Environ. Sci. Technol.* **2002**, *36*, 512−519.
(473) Taylor, S. D.; Becker, U.; Rosso, K. M. Electron Transfer Pathways Facilitating U(VI) Reduction by Fe(II) on Al- vs Fe-Oxides. *J. Phys. Chem. C* **2017**, *121*, 19887−19903.
(474) Neumann, A.; Olson, T. L.; Scherer, M. M. Spectroscopic Evidence for Fe(II)−Fe(III) Electron Transfer at Clay Mineral Edge and Basal Sites. *Environ. Sci. Technol.* **2013**, *47*, 6969−6977.
(475) Schultz, C. A.; Grundl, T. J. pH Dependence on Reduction Rate of 4-Cl-Nitrobenzene by Fe (II)/Montmorillonite Systems. *Environ. Sci. Technol.* **2000**, *34*, 3641−3648.
(476) Tsarev, S.; Waite, T. D.; Collins, R. N. Uranium Reduction by Fe(II) in the Presence of Montmorillonite and Nontronite. *Environ. Sci. Technol.* **2016**, *50*, 8223−8230.
(477) Latta, D. E.; Neumann, A.; Premaratne, W.; Scherer, M. M. Fe(II)−Fe(III) Electron Transfer in a Clay Mineral with Low Fe Content. *ACS Earth Space Chem.* **2017**, *1*, 197−208.
(478) Soltermann, D.; Marques Fernandes, M.; Baeyens, B.; Dähn, R.; Joshi, P. A.; Scheinost, A. C.; Gorski, C. A. Fe(II) Uptake on Natural Montmorillonites. I. Macroscopic and Spectroscopic Characterization. *Environ. Sci. Technol.* **2014**, *48*, 8688−8697.
(479) Schaefer, M. V.; Gorski, C. A.; Scherer, M. M. Spectroscopic Evidence for Interfacial Fe(II)−Fe(III) Electron Transfer in a Clay Mineral. *Environ. Sci. Technol.* **2011**, *45*, 540−545.
(480) Zhu, Y.; Elzinga, E. J. Formation of Layered Fe(II)-Hydroxides During Fe(II) Sorption onto Clay and Metal-Oxide Substrates. *Environ. Sci. Technol.* **2014**, *48*, 4937−4945.
(481) Starcher, A. N.; Li, W.; Kukkadapu, R. K.; Elzinga, E. J.; Sparks, D. L. Fe(II) Sorption on Pyrophyllite: Effect of Structural Fe(III) (Impurity) in Pyrophyllite on Nature of Layered Double Hydroxide (LDH) Secondary Mineral Formation. *Chem. Geol.* **2016**, *439*, 152−160.
(482) Géhin, A.; Grenèche, J. M.; Tournassat, C.; Brendlé, J.; Rancourt, D. G.; Charlet, L. Reversible Surface-Sorption-Induced Electron-Transfer Oxidation of Fe(II) at Reactive Sites on a Synthetic Clay Mineral. *Geochim. Cosmochim. Acta* **2007**, *71*, 863−876.
(483) Jaisi, D. P.; Kukkadapu, R. K.; Eberl, D. D.; Dong, H. Control of Fe(III) Site Occupancy on the Rate and Extent of Microbial Reduction of Fe(III) in Nontronite. *Geochim. Cosmochim. Acta* **2005**, *69*, 5429−5440.
(484) Russell, J.; Goodman, B.; Fraser, A. J. C.; Minerals, C. Infrared and Mössbauer Studies of Reduced Nontronites. *Clays Clay Miner.* **1979**, *27*, 63−71.
(485) Neumann, A.; Wu, L.; Li, W.; Beard, B. L.; Johnson, C. M.; Rosso, K. M.; Frierdich, A. J.; Scherer, M. M. Atom Exchange between Aqueous Fe(II) and Structural Fe in Clay Minerals. *Environ. Sci. Technol.* **2015**, *49*, 2786−2795.
(486) Orsetti, S.; Laskov, C.; Haderlein, S. B. Electron Transfer between Iron Minerals and Quinones: Estimating the Reduction Potential of the Fe(II)-Goethite Surface from Aqds Speciation. *Environ. Sci. Technol.* **2013**, *47*, 14161−14168.
(487) Li, X.; Liu, L.; Wu, Y.; Liu, T. Determination of the Redox Potentials of Solution and Solid Surface of Fe(II) Associated with Iron Oxyhydroxides. *ACS Earth Space Chem.* **2019**, *3*, 711−717.
(488) Wehrli, B.; Sulzberger, B.; Stumm, W. Redox Processes Catalyzed by Hydrous Oxide Surfaces. *Chem. Geol.* **1989**, *78*, 167−179.
(489) Huang, J.; Wang, Q.; Wang, Z.; Zhang, H. J. Interactions and Reductive Reactivity in Ternary Mixtures of Fe(II), Goethite, and Phthalic Acid Based on a Combined Experimental and Modeling Approach. *Langmuir* **2019**, *35*, 8220−8227.
(490) Merola, R. B.; Fournier, E. D.; McGuire, M. M. Spectroscopic Investigations of $Fe^{2+}$ Complexation on Nontronite Clay. *Langmuir* **2007**, *23*, 1223−1226.
(491) Gorski, C.; Scherer, M. $Fe^{2+}$ Sorption at the Fe Oxide-Water Interface: A Revised Conceptual Framework. In *Aquatic Redox Chemistry*; Tratnyek, P. G., Grundl, T. J., Haderlein, S. B., Eds.; ACS Symposium Series; American Chemical Society: Washington, DC, 2011; Vol. *1071*, Chapter 15, pp315−343.
(492) Taylor, S. D.; Liu, J.; Arey, B. W.; Schreiber, D. K.; Perea, D. E.; Rosso, K. M. Resolving Iron(II) Sorption and Oxidative Growth on Hematite (001) Using Atom Probe Tomography. *J. Phys. Chem. C* **2018**, *122*, 3903−3914.
(493) Rosso, K. M.; Smith, D. M. A.; Dupuis, M. An Ab Initio Model of Electron Transport in Hematite($\alpha$-$Fe_2O_3$) Basal Planes. *J. Chem. Phys.* **2003**, *118*, 6455−6466.
(494) Iordanova, N.; Dupuis, M.; Rosso, K. M. Charge Transport in Metal Oxides: A Theoretical Study of Hematite A-$Fe_2o_3$. *J. Chem. Phys.* **2005**, *122*, 144305.
(495) Kerisit, S.; Zarzycki, P.; Rosso, K. M. Computational Molecular Simulation of the Oxidative Adsorption of Ferrous Iron at the Hematite (001)−Water Interface. *J. Phys. Chem. C* **2015**, *119*, 9242−9252.
(496) Kerisit, S.; Rosso, K. M. Computer Simulation of Electron Transfer at Hematite Surfaces. *Geochim. Cosmochim. Acta* **2006**, *70*, 1888−1903.
(497) Kerisit, S.; Rosso, K. M. Charge Transfer in Feo: A Combined Molecular-Dynamics and Ab Initio Study. *J. Chem. Phys.* **2005**, *123*, 224712.
(498) Zarzycki, P.; Rosso, K. M. Surface Charge Effects on Fe(II) Sorption and Oxidation at (110) Goethite Surfaces. *J. Phys. Chem. C* **2018**, *122*, 10059−10066.
(499) Zarzycki, P.; Rosso, K. M. Stochastic Simulation of Isotopic Exchange Mechanisms for Fe(II)-Catalyzed Recrystallization of Goethite. *Environ. Sci. Technol.* **2017**, *51*, 7552−7559.
(500) Zarzycki, P.; Smith, D. M.; Rosso, K. M. Proton Dynamics on Goethite Nanoparticles and Coupling to Electron Transport. *J. Chem. Theory Comput.* **2015**, *11*, 1715−1724.
(501) Zarzycki, P.; Kerisit, S.; Rosso, K. M. Molecular Dynamics Study of Fe(II) Adsorption, Electron Exchange, and Mobility at Goethite ($\alpha$-FeOOH) Surfaces. *J. Phys. Chem. C* **2015**, *119*, 3111−3123.
(502) Kerisit, S.; Rosso, K. M. Kinetic Monte Carlo Model of Charge Transport in Hematite ($\alpha$-$Fe_2O_3$). *J. Chem. Phys.* **2007**, *127*, 124706.
(503) Zarzycki, P.; Rosso, K. M. Energetics and the Role of Defects in Fe(II)-Catalyzed Goethite Recrystallization from Molecular Simulations. *ACS Earth Space Chem.* **2019**, *3*, 262−272.
(504) Rosso, K. M.; Yanina, S. V.; Gorski, C. A.; Larese-Casanova, P.; Scherer, M. M. Connecting Observations of Hematite ($\alpha$-$Fe_2O_3$) Growth Catalyzed by Fe(II). *Environ. Sci. Technol.* **2010**, *44*, 61−67.


https://doi.org/10.1021/acs.chemrev.0c01286
*Chem. Rev.* 2021, 121, 8161−8233

(505) Tratnyek, P. G.; Salter-Blanc, A. J.; Nurmi, J. T.; Amonette, J. E.; Liu, J.; Wang, C.; Dohnalkova, A.; Baer, D. R. Reactivity of Zerovalent Metals in Aquatic Media: Effects of Organic Surface Coatings. In *Aquatic Redox Chemistry*; Tratnyek, P. G., Grundl, T. J., Haderlein, S. B., Eds.; ACS Symposium Series; American Chemical Society: Washington, DC, 2011; Vol. *1071*, Chapter 18, pp 381−406.
(506) Phenrat, T.; Lowry, G. V.; Babakhani, P. Nanoscale Zerovalent Iron (NZVI) for Environmental Decontamination: A Brief History of 20 Years of Research and Field-scale Application. In *Nanoscale Zerovalent Iron Particles for Environmental Restoration: From Fundamental Science to Field Scale Engineering Applications*; Phenrat, T., Lowry, G. V., Eds.; Springer International Publishing: Cham, 2019; pp 1−43.
(507) Bae, S.; Collins, R. N.; Waite, T. D.; Hanna, K. Advances in Surface Passivation of Nanoscale Zerovalent Iron: A Critical Review. *Environ. Sci. Technol.* **2018**, *52*, 12010−12025.
(508) Fan, D.; Lan, Y.; Tratnyek, P. G.; Johnson, R. L.; Filip, J.; O'Carroll, D. M.; Nunez Garcia, A.; Agrawal, A. Sulfidation of Iron-Based Materials: A Review of Processes and Implications for Water Treatment and Remediation. *Environ. Sci. Technol.* **2017**, *51*, 13070−13085.
(509) Shi, Z.; Fan, D.; Johnson, R. L.; Tratnyek, P. G.; Nurmi, J. T.; Wu, Y.; Williams, K. H. Methods for Characterizing the Fate and Effects of Nano Zerovalent Iron During Groundwater Remediation. *J. Contam. Hydrol.* **2015**, *181*, 17−35.
(510) Henderson, A. D.; Demond, A. H. Long-Term Performance of Zero-Valent Iron Permeable Reactive Barriers: A Critical Review. *Environ. Eng. Sci.* **2007**, *24*, 401−423.
(511) Tratnyek, P. G.; Scherer, M. M.; Johnson, T. L.; Matheson, L. J. Permeable Reactive Barriers of Iron and Other Zero-Valent Metals. In *Chemical Degradation Methods for Wastes and Pollutants: Environmental and Industrial Applications*; Tarr, M. A., Ed.; Marcel Dekker: New York, 2003; pp 371−421.
(512) Phillips, D. H.; Nooten, T. V.; Bastiaens, L.; Russell, M.; Dickson, K.; Plant, S.; Ahad, J.; Newton, T.; Elliot, T.; Kalin, R. M. Ten Year Performance Evaluation of a Field-Scale Zero-Valent Iron Permeable Reactive Barrier Installed to Remediate Trichloroethene Contaminated Groundwater. *Environ. Sci. Technol.* **2010**, *44*, 3861−3869.
(513) Phillips, D. H.; Gu, B.; Watson, D. B.; Roh, Y.; Liang, L.; Lee, S. Performance Evaluation of a Zerovalent Iron Reactive Barrier: Mineralogical Characteristics. *Environ. Sci. Technol.* **2000**, *34*, 4169−4176.
(514) Johnson, R.; Thoms, R.; O'Brien Johnson, R.; Nurmi, J.; Tratnyek, P. G. Mineral Precipitation Upgradient from a Zero-Valent Iron Permeable Reactive Barrier. *Groundwater Monit. Rem.* **2008**, *28*, 56−64.
(515) Kocur, C. M.; Lomheim, L.; Boparai, H. K.; Chowdhury, A. I.; Weber, K. P.; Austrins, L. M.; Edwards, E. A.; Sleep, B. E.; O'Carroll, D. M. Contributions of Abiotic and Biotic Dechlorination Following Carboxymethyl Cellulose Stabilized Nanoscale Zero Valent Iron Injection. *Environ. Sci. Technol.* **2015**, *49*, 8648−8656.
(516) Dong, H.; Li, L.; Lu, Y.; Cheng, Y.; Wang, Y.; Ning, Q.; Wang, B.; Zhang, L.; Zeng, G. Integration of Nanoscale Zero-Valent Iron and Functional Anaerobic Bacteria for Groundwater Remediation: A Review. *Environ. Int.* **2019**, *124*, 265−277.
(517) Scherer, M. M.; Balko, B. A.; Tratnyek, P. G. The Role of Oxides in Reduction Reactions at the Metal-Water Interface. In *Mineral-Water Interfacial Reactions*; ACS Symposium Series; American Chemical Society: Washington, DC, 1998; Vol. *715*, Chapter 15, pp 301−322.
(518) Gaspar, D. J.; Lea, A. S.; Engelhard, M. H.; Baer, D. R.; Miehr, R.; Tratnyek, P. G. Evidence for Localization of Reaction Upon Reduction of Carbon Tetrachloride by Granular Iron. *Langmuir* **2002**, *18*, 7688−7693.
(519) Liu, T.; Li, X.; Waite, T. D. Depassivation of Aged $Fe^0$ by Inorganic Salts: Implications to Contaminant Degradation in Seawater. *Environ. Sci. Technol.* **2013**, *47*, 7350−7356.
(520) Balko, B. A.; Tratnyek, P. G. Photoeffects on the Reduction of Carbon Tetrachloride by Zero-Valent Iron. *J. Phys. Chem. B* **1998**, *102*, 1459−1465.
(521) Johnson, T. L.; Fish, W.; Gorby, Y. A.; Tratnyek, P. G. Degradation of Carbon Tetrachloride by Iron Metal: Complexation Effects on the Oxide Surface. *J. Contam. Hydrol.* **1998**, *29*, 379−398.
(522) Liu, T.; Li, X.; Waite, T. D. Depassivation of Aged $Fe^0$ by Ferrous Ions: Implications to Contaminant Degradation. *Environ. Sci. Technol.* **2013**, *47*, 13712−13720.
(523) Jeong, H. Y.; Anantharaman, K.; Hyun, S. P.; Son, M.; Hayes, K. F. pH Impact on Reductive Dechlorination of cis-Dichloroethylene by Fe Precipitates: An X-Ray Absorption Spectroscopy Study. *Water Res.* **2013**, *47*, 6639−6649.
(524) He, Y.; Wilson, J.; Su, C.; Wilkin, R. Review of Abiotic Degradation of Chlorinated Solvents by Reactive Iron Minerals in Aquifers. *Groundwater Monit. Rem.* **2015**, *35*, 57−75.
(525) Johnson, T. L.; Scherer, M. M.; Tratnyek, P. G. Kinetics of Halogenated Organic Compound Degradation by Iron Metal. *Environ. Sci. Technol.* **1996**, *30*, 2634−2640.
(526) Miehr, R.; Tratnyek, P. G.; Bandstra, J. Z.; Scherer, M. M.; Alowitz, M. J.; Bylaska, E. J. Diversity of Contaminant Reduction Reactions by Zerovalent Iron: Role of the Reductate. *Environ. Sci. Technol.* **2004**, *38*, 139−147.
(527) Nurmi, J. T.; Tratnyek, P. G.; Sarathy, V.; Baer, D. R.; Amonette, J. E.; Pecher, K.; Wang, C.; Linehan, J. C.; Matson, D. W.; Penn, R. L.; et al. Characterization and Properties of Metallic Iron Nanoparticles: Spectroscopy, Electrochemistry, and Kinetics. *Environ. Sci. Technol.* **2005**, *39*, 1221−1230.
(528) Tratnyek, P. G.; Salter, A. J.; Nurmi, J. T.; Sarathy, V. Environmental Applications of Zerovalent Metals: Iron vs. Zinc. In *Nanoscale Materials in Chemistry: Environmental Applications*; Erickson, L. E., Koodali, R. T., Richards, R. M., Eds.; ACS Symposium Series; American Chemical Society: Washington, DC, 2010; Vol. *1045*, pp 165−178.
(529) Sarathy, V.; Salter, A. J.; Nurmi, J. T.; O'Brien Johnson, G.; Johnson, R. L.; Tratnyek, P. G. Degradation of 1, 2, 3-Trichloropropane (TCP): Hydrolysis, Elimination, and Reduction by Iron and Zinc. *Environ. Sci. Technol.* **2010**, *44*, 787−793.
(530) Liu, Y.; Wang, J. Reduction of Nitrate by Zero Valent Iron (ZVI)-Based Materials: A Review. *Sci. Total Environ.* **2019**, *671*, 388−403.
(531) Kharisov, B. I.; Rasika Dias, H. V.; Kharissova, O. V.; Manuel Jiménez-Pérez, V.; Olvera Pérez, B.; Muñoz Flores, B. Iron-Containing Nanomaterials: Synthesis, Properties, and Environmental Applications. *RSC Adv.* **2012**, *2*, 9325−9358.
(532) Su, C. Environmental Implications and Applications of Engineered Nanoscale Magnetite and Its Hybrid Nanocomposites: A Review of Recent Literature. *J. Hazard. Mater.* **2017**, *322*, 48−84.
(533) Chen, A.; Shang, C.; Shao, J.; Zhang, J.; Huang, H. The Application of Iron-Based Technologies in Uranium Remediation: A Review. *Sci. Total Environ.* **2017**, *575*, 1291−1306.
(534) Lee, W.; Batchelor, B. Reductive Capacity of Natural Reductants. *Environ. Sci. Technol.* **2003**, *37*, 535−541.
(535) Lee, W.; Batchelor, B. Abiotic Reductive Dechlorination of Chlorinated Ethylenes by Iron-Bearing Phyllosilicates. *Chemosphere* **2004**, *56*, 999−1009.
(536) He, F.; Gong, L.; Fan, D.; Tratnyek, P. G.; Lowry, G. V. Quantifying the Efficiency and Selectivity of Organohalide Dechlorination by Zerovalent Iron. *Environ. Sci. Process Impacts* **2020**, *22*, 528−542.
(537) Wolfe, N.; Kitchens, B.; Macalady, D.; Grundl, T. Physical and Chemical Factors That Influence the Anaerobic Degradation of Methyl Parathion in Sediment Systems. *Environ. Toxicol. Chem.* **1986**, *5*, 1019−1026.
(538) Christensen, T. H.; Bjerg, P. L.; Banwart, S. A.; Jakobsen, R.; Heron, G.; Albrechtsen, H.-J. Characterization of Redox Conditions in Groundwater Contaminant Plumes. *J. Contam. Hydrol.* **2000**, *45*, 165−241.
(539) Kocur, C. M. D.; Fan, D.; Tratnyek, P. G.; Johnson, R. L. Predicting Abiotic Reduction Rates Using Cryogenically Collected Soil Cores and Mediated Reduction Potential Measurements. *Environ. Sci. Technol. Lett.* **2020**, *7*, 20−26.


https://doi.org/10.1021/acs.chemrev.0c01286
*Chem. Rev.* 2021, 121, 8161−8233

(540) Baker, B. J.; Banfield, J. F. Microbial Communities in Acid Mine Drainage. *FEMS Microbiol. Ecol.* **2003**, *44*, 139−152.
(541) Chan, C.; Emerson, D.; Luther, G., III The Role of Microaerophilic Fe-Oxidizing Micro-Organisms in Producing Banded Iron Formations. *Geobiology* **2016**, *14*, 509−528.
(542) Chiu, B. K.; Kato, S.; McAllister, S. M.; Field, E. K.; Chan, C. S. Novel Pelagic Iron-Oxidizing Zetaproteobacteria from the Chesapeake Bay Oxic−Anoxic Transition Zone. *Front. Microbiol.* **2017**, *8*, 1280.
(543) Laufer, K.; Nordhoff, M.; Halama, M.; Martinez, R. E.; Obst, M.; Nowak, M.; Stryhanyuk, H.; Richnow, H. H.; Kappler, A. Microaerophilic Fe(II)-Oxidizing Zetaproteobacteria Isolated from Low-Fe Marine Coastal Sediments: Physiology and Composition of Their Twisted Stalks. *Appl. Environ. Microbiol.* **2017**, *83*, e03118−03116.
(544) Chan, C. S.; Fakra, S. C.; Emerson, D.; Fleming, E. J.; Edwards, K. J. Lithotrophic Iron-Oxidizing Bacteria Produce Organic Stalks to Control Mineral Growth: Implications for Biosignature Formation. *ISME J.* **2011**, *5*, 717−727.
(545) Straub, K. L.; Benz, M.; Schink, B.; Widdel, F. Anaerobic, Nitrate-Dependent Microbial Oxidation of Ferrous Iron. *Appl. Environ. Microbiol.* **1996**, *62*, 1458−1460.
(546) Klueglein, N.; Kappler, A. Abiotic Oxidation of Fe(II) by Reactive Nitrogen Species in Cultures of the Nitrate-Reducing Fe(II) Oxidizer *Acidovorax* Sp. Bofen1−Questioning the Existence of Enzymatic Fe(II) Oxidation. *Geobiology* **2013**, *11*, 180−190.
(547) Klueglein, N.; Zeitvogel, F.; Stierhof, Y.-D.; Floetenmeyer, M.; Konhauser, K. O.; Kappler, A.; Obst, M. Potential Role of Nitrite for Abiotic Fe(II) Oxidation and Cell Encrustation During Nitrate Reduction by Denitrifying Bacteria. *Appl. Environ. Microbiol.* **2014**, *80*, 1051−1061.
(548) Bryce, C.; Blackwell, N.; Schmidt, C.; Otte, J.; Huang, Y. M.; Kleindienst, S.; Tomaszewski, E.; Schad, M.; Warter, V.; Peng, C. Microbial Anaerobic Fe(II) Oxidation−Ecology, Mechanisms and Environmental Implications. *Environ. Microbiol.* **2018**, *20*, 3462−3483.
(549) Tominski, C.; Lösekann-Behrens, T.; Ruecker, A.; Hagemann, N.; Kleindienst, S.; Mueller, C. W.; Höschen, C.; Kögel-Knabner, I.; Kappler, A.; Behrens, S. FISH-SIMS Imaging of an Autotrophic, Nitrate-Reducing, Fe(II)-Oxidizing Enrichment Culture Provides Insights into Carbon Metabolism. *Appl. Environ. Microbiol.* **2018**, DOI: 10.1128/AEM.02166-17.
(550) He, S.; Tominski, C.; Kappler, A.; Behrens, S.; Roden, E. E. Metagenomic Analyses of the Autotrophic Fe(II)-Oxidizing, Nitrate-Reducing Enrichment Culture KS. *Appl. Environ. Microbiol.* **2016**, *82*, 2656−2668.
(551) Laufer, K.; Røy, H.; Jørgensen, B. B.; Kappler, A. Evidence for the Existence of Autotrophic Nitrate-Reducing Fe(II)-Oxidizing Bacteria in Marine Coastal Sediment. *Appl. Environ. Microbiol.* **2016**, *82*, 6120−6131.
(552) Posth, N.; Canfield, D. E.; Kappler, A. Biogenic Fe(III) Minerals: From Formation to Diagenesis and Preservation in the Rock Record. *Earth-Sci. Rev.* **2014**, *135*, 103−121.
(553) Posth, N. R.; Konhauser, K. O.; Kappler, A. Microbiological Processes in Banded Iron Formation Deposition. *Sedimentology* **2013**, *60*, 1733−1754.
(554) Singer, P. C.; Stumm, W. Acidic Mine Drainage: The Rate-Determining Step. *Science* **1970**, *167*, 1121−1123.
(555) Porsch, K.; Kappler, A. $Fe^{II}$ Oxidation by Molecular $O_2$ During HCl Extraction. *Environ. Chem.* **2011**, *8*, 190−197.
(556) Houben, G. J.; Sitnikova, M. A.; Post, V. E. Terrestrial Sedimentary Pyrites as a Potential Source of Trace Metal Release to Groundwater−a Case Study from the Emsland, Germany. *Appl. Geochem.* **2017**, *76*, 99−111.
(557) Druschel, G. K.; Emerson, D.; Sutka, R.; Suchecki, P.; Luther, G. W., III Low-Oxygen and Chemical Kinetic Constraints on the Geochemical Niche of Neutrophilic Iron(II) Oxidizing Microorganisms. *Geochim. Cosmochim. Acta* **2008**, *72*, 3358−3370.
(558) Lueder, U.; Druschel, G.; Emerson, D.; Kappler, A.; Schmidt, C. Quantitative Analysis of $O_2$ and $Fe^{2+}$ Profiles in Gradient Tubes for Cultivation of Microaerophilic Iron(II)-Oxidizing Bacteria. *FEMS Microbiol. Ecol.* **2018**, *94*, fix177.
(559) Maisch, M.; Lueder, U.; Laufer, K.; Scholze, C.; Kappler, A.; Schmidt, C. Contribution of Microaerophilic Iron(II)-Oxidizers to Iron(III) Mineral Formation. *Environ. Sci. Technol.* **2019**, *53*, 8197−8204.
(560) Sobolev, D.; Roden, E. E. Suboxic Deposition of Ferric Iron by Bacteria in Opposing Gradients of Fe(II) and Oxygen at Circumneutral pH. *Appl. Environ. Microbiol.* **2001**, *67*, 1328−1334.
(561) Larese-Casanova, P.; Haderlein, S. B.; Kappler, A. Biomineralization of Lepidocrocite and Goethite by Nitrate-Reducing Fe(II)-Oxidizing Bacteria: Effect of pH, Bicarbonate, Phosphate, and Humic Acids. *Geochim. Cosmochim. Acta* **2010**, *74*, 3721−3734.
(562) Pantke, C.; Obst, M.; Benzerara, K.; Morin, G.; Ona-Nguema, G.; Dippon, U.; Kappler, A. Green Rust Formation During Fe(II) Oxidation by the Nitrate-Reducing Acidovorax Sp. Strain BoFeN1. *Environ. Sci. Technol.* **2012**, *46*, 1439−1446.
(563) Peng, C.; Bryce, C.; Sundman, A.; Borch, T.; Kappler, A. Organic Matter Complexation Promotes Fe(II) Oxidation by the Photoautotrophic Fe(II)-Oxidizer Rhodopseudomonas Palustris TIE-1. *ACS Earth Space Chem.* **2019**, *3*, 531−536.
(564) Gledhill, M.; Buck, K. N. The Organic Complexation of Iron in the Marine Environment: A Review. *Front. Microbiol.* **2012**, *3*, 69.
(565) Kappler, A.; Newman, D. K. Formation of Fe(III)-Minerals by Fe(II)-Oxidizing Photoautotrophic Bacteria. *Geochim. Cosmochim. Acta* **2004**, *68*, 1217−1226.
(566) Han, X.; Tomaszewski, E.; Sorwat, J.; Pan, Y.; Kappler, A.; Byrne, J. Oxidation of Green Rust by Anoxygenic Phototrophic Fe(II)-Oxidising Bacteria. *Geochem. Perspect. Lett.* **2020**, *12*, 52−57.
(567) Etique, M.; Jorand, F. d. r. P.; Zegeye, A.; Grégoire, B.; Despas, C.; Ruby, C. Abiotic Process for Fe(II) Oxidation and Green Rust Mineralization Driven by a Heterotrophic Nitrate Reducing Bacteria (*Klebsiella mobilis*). *Environ. Sci. Technol.* **2014**, *48*, 3742−3751.
(568) Miot, J.; Li, J.; Benzerara, K.; Sougrati, M. T.; Ona-Nguema, G.; Bernard, S.; Jumas, J.-C.; Guyot, F. Formation of Single Domain Magnetite by Green Rust Oxidation Promoted by Microbial Anaerobic Nitrate-Dependent Iron Oxidation. *Geochim. Cosmochim. Acta* **2014**, *139*, 327−343.
(569) Weber, K. A.; Picardal, F. W.; Roden, E. E. Microbially Catalyzed Nitrate-Dependent Oxidation of Biogenic Solid-Phase Fe(II) Compounds. *Environ. Sci. Technol.* **2001**, *35*, 1644−1650.
(570) Jiao, Y.; Kappler, A.; Croal, L. R.; Newman, D. K. Isolation and Characterization of a Genetically Tractable Photoautotrophic Fe(II)-Oxidizing Bacterium, *Rhodopseudomonas Palustris* Strain Tie-1. *Appl. Environ. Microbiol.* **2005**, *71*, 4487−4496.
(571) Sand, W.; Gehrke, T.; Jozsa, P.-G.; Schippers, A. (Bio)-Chemistry of Bacterial Leaching—Direct vs. Indirect Bioleaching. *Hydrometallurgy* **2001**, *59*, 159−175.
(572) Percak-Dennett, E.; He, S.; Converse, B.; Konishi, H.; Xu, H.; Corcoran, A.; Noguera, D.; Chan, C.; Bhattacharyya, A.; Borch, T. Microbial Acceleration of Aerobic Pyrite Oxidation at Circumneutral pH. *Geobiology* **2017**, *15*, 690−703.
(573) Haaijer, S. C.; Lamers, L. P.; Smolders, A. J.; Jetten, M. S.; Op den Camp, H. J. Iron Sulfide and Pyrite as Potential Electron Donors for Microbial Nitrate Reduction in Freshwater Wetlands. *Geomicrobiol. J.* **2007**, *24*, 391−401.
(574) Juncher Jørgensen, C.; Jacobsen, O. S.; Elberling, B.; Aamand, J. Microbial Oxidation of Pyrite Coupled to Nitrate Reduction in Anoxic Groundwater Sediment. *Environ. Sci. Technol.* **2009**, *43*, 4851−4857.
(575) Edwards, K. J.; Rogers, D. R.; Wirsen, C. O.; McCollom, T. Isolation and Characterization of Novel Psychrophilic, Neutrophilic, Fe-Oxidizing, Chemolithoautotrophic $\alpha$-and $\gamma$-*Proteobacteria* from the Deep Sea. *Appl. Environ. Microbiol.* **2003**, *69*, 2906−2913.
(576) Bosch, J.; Lee, K.-Y.; Jordan, G.; Kim, K.-W.; Meckenstock, R. U. Anaerobic, Nitrate-Dependent Oxidation of Pyrite Nanoparticles by Thiobacillus Denitrificans. *Environ. Sci. Technol.* **2012**, *46*, 2095−2101.
(577) Yan, R.; Kappler, A.; Peiffer, S. Interference of Nitrite with Pyrite under Acidic Conditions: Implications for Studies of Chemo-

lithotrophic Denitrification. *Environ. Sci. Technol.* **2015**, *49*, 11403−11410.
(578) Yan, R.; Kappler, A.; Muehe, E. M.; Knorr, K.-H.; Horn, M. A.; Poser, A.; Lohmayer, R.; Peiffer, S. Effect of Reduced Sulfur Species on Chemolithoautotrophic Pyrite Oxidation with Nitrate. *Geomicrobiol. J.* **2019**, *36*, 19−29.
(579) Zhao, L.; Dong, H.; Edelmann, R. E.; Zeng, Q.; Agrawal, A. Coupling of Fe(II) Oxidation in Illite with Nitrate Reduction and Its Role in Clay Mineral Transformation. *Geochim. Cosmochim. Acta* **2017**, *200*, 353−366.
(580) Shelobolina, E. S.; VanPraagh, C. G.; Lovley, D. R. Use of Ferric and Ferrous Iron Containing Minerals for Respiration by Desulfitobacterium Frappieri. *Geomicrobiol. J.* **2003**, *20*, 143−156.
(581) Agnel, M. I.; Grangeon, S.; Fauth, F.; Elkaïm, E.; Claret, F.; Roulet, M.; Warmont, F.; Tournassat, C. Mechanistic and Thermodynamic Insights into Anion Exchange by Green Rust. *Environ. Sci. Technol.* **2020**, *54*, 851−861.
(582) Hegler, F.; Posth, N. R.; Jiang, J.; Kappler, A. Physiology of Phototrophic Iron(II)-Oxidizing Bacteria: Implications for Modern and Ancient Environments. *FEMS Microbiol. Ecol.* **2008**, *66*, 250−260.
(583) Rosso, L.; Lobry, J.; Bajard, S.; Flandrois, J.-P. Convenient Model to Describe the Combined Effects of Temperature and pH on Microbial Growth. *Appl. Environ. Microbiol.* **1995**, *61*, 610−616.
(584) Wu, W.; Swanner, E. D.; Hao, L.; Zeitvogel, F.; Obst, M.; Pan, Y.; Kappler, A. Characterization of the Physiology and Cell−Mineral Interactions of the Marine Anoxygenic Phototrophic Fe(II) Oxidizer Rhodovulum Iodosum−Implications for Precambrian Fe(II) Oxidation. *FEMS Microbiol. Ecol.* **2014**, *88*, 503−515.
(585) Laufer, K.; Niemeyer, A.; Nikeleit, V.; Halama, M.; Byrne, J. M.; Kappler, A. Physiological Characterization of a Halotolerant Anoxygenic Phototrophic Fe(II)-Oxidizing Green-Sulfur Bacterium Isolated from a Marine Sediment. *FEMS Microbiol. Ecol.* **2017**, *93*, 1−13.
(586) Gauger, T.; Byrne, J. M.; Konhauser, K. O.; Obst, M.; Crowe, S.; Kappler, A. Influence of Organics and Silica on Fe(II) Oxidation Rates and Cell−Mineral Aggregate Formation by the Green-Sulfur Fe(II)-Oxidizing Bacterium Chlorobium Ferrooxidans Kofox−Implications for Fe(II) Oxidation in Ancient Oceans. *Earth Planet. Sci. Lett.* **2016**, *443*, 81−89.
(587) Nordhoff, M.; Tominski, C.; Halama, M.; Byrne, J. M.; Obst, M.; Kleindienst, S.; Behrens, S.; Kappler, A. Insights into Nitrate-Reducing Fe(II) Oxidation Mechanisms through Analysis of Cell-Mineral Associations, Cell Encrustation, and Mineralogy in the Chemolithoautotrophic Enrichment Culture KS. *Appl. Environ. Microbiol.* **2017**, *83*, 1−19.
(588) Tominski, C.; Heyer, H.; Lösekann-Behrens, T.; Behrens, S.; Kappler, A. Growth and Population Dynamics of the Anaerobic Fe(II)-Oxidizing and Nitrate-Reducing Enrichment Culture KS. *Appl. Environ. Microbiol.* **2018**, *84*, e02173−02117.
(589) Otte, J. M.; Harter, J.; Laufer, K.; Blackwell, N.; Straub, D.; Kappler, A.; Kleindienst, S. The Distribution of Active Iron-Cycling Bacteria in Marine and Freshwater Sediments Is Decoupled from Geochemical Gradients. *Environ. Microbiol.* **2018**, *20*, 2483−2499.
(590) Byrne, J. M.; Klueglein, N.; Pearce, C.; Rosso, K. M.; Appel, E.; Kappler, A. Redox Cycling of Fe(II) and Fe(III) in Magnetite by Fe-Metabolizing Bacteria. *Science* **2015**, *347*, 1473−1476.
(591) Byrne, J. M.; Van Der Laan, G.; Figueroa, A. I.; Qafoku, O.; Wang, C.; Pearce, C. I.; Jackson, M.; Feinberg, J.; Rosso, K. M.; Kappler, A. Size Dependent Microbial Oxidation and Reduction of Magnetite Nano-and Micro-Particles. *Sci. Rep.* **2016**, *6*, 1−13.
(592) Aulenta, F.; Rossetti, S.; Amalfitano, S.; Majone, M.; Tandoi, V. Conductive Magnetite Nanoparticles Accelerate the Microbial Reductive Dechlorination of Trichloroethene by Promoting Interspecies Electron Transfer Processes. *ChemSusChem* **2013**, *6*, 433−436.
(593) Cruz Viggi, C.; Rossetti, S.; Fazi, S.; Paiano, P.; Majone, M.; Aulenta, F. Magnetite Particles Triggering a Faster and More Robust Syntrophic Pathway of Methanogenic Propionate Degradation. *Environ. Sci. Technol.* **2014**, *48*, 7536−7543.
(594) Kato, S.; Hashimoto, K.; Watanabe, K. Methanogenesis Facilitated by Electric Syntrophy via (Semi) Conductive Iron-Oxide Minerals. *Environ. Microbiol.* **2012**, *14*, 1646−1654.
(595) Kato, S.; Hashimoto, K.; Watanabe, K. Microbial Interspecies Electron Transfer via Electric Currents through Conductive Minerals. *Proc. Natl. Acad. Sci. U. S. A.* **2012**, *109*, 10042−10046.
(596) Rotaru, A.-E.; Calabrese, F.; Stryhanyuk, H.; Musat, F.; Shrestha, P. M.; Weber, H. S.; Snoeyenbos-West, O. L.; Hall, P. O.; Richnow, H. H.; Musat, N. Conductive Particles Enable Syntrophic Acetate Oxidation between Geobacter and Methanosarcina from Coastal Sediments. *mBio* **2018**, *9*, e00226−00218.
(597) Rotaru, A.-E.; Posth, N. R.; Löscher, C. R.; Miracle, M. R.; Vicente, E.; Cox, R. P.; Thompson, J.; Poulton, S. W.; Thamdrup, B. Interspecies Interactions Mediated by Conductive Minerals in the Sediments of the Iron Rich Meromictic Lake La Cruz. *Spain. Limnetica* **2019**, *38*, 21−40.
(598) Zhuang, L.; Ma, J.; Yu, Z.; Wang, Y.; Tang, J. Magnetite Accelerates Syntrophic Acetate Oxidation in Methanogenic Systems with High Ammonia Concentrations. *Microb. Biotechnol.* **2018**, *11*, 710−720.
(599) Zhuang, L.; Xu, J.; Tang, J.; Zhou, S. Effect of Ferrihydrite Biomineralization on Methanogenesis in an Anaerobic Incubation from Paddy Soil. *J. Geophys. Res.: Biogeosci.* **2015**, *120*, 876−886.
(600) Wang, C.; Ye, L.; Jin, J.; Chen, H.; Xu, X.; Zhu, L. Magnetite Nanoparticles Enhance the Performance of a Combined Bioelectrode-Uasb Reactor for Reductive Transformation of 2, 4-Dichloronitrobenzene. *Sci. Rep.* **2017**, *7*, 1−10.
(601) Ye, Q.; Zhang, Z.; Huang, Y.; Fang, T.; Cui, Q.; He, C.; Wang, H. Enhancing Electron Transfer by Magnetite During Phenanthrene Anaerobic Methanogenic Degradation. *Int. Biodeterior. Biodegrad.* **2018**, *129*, 109−116.
(602) Kappler, A.; Bryce, C. Cryptic Biogeochemical Cycles: Unravelling Hidden Redox Reactions. *Environ. Microbiol.* **2017**, *19*, 842−846.
(603) Peng, C.; Bryce, C.; Sundman, A.; Kappler, A. Cryptic Cycling of Complexes Containing Fe(III) and Organic Matter by Phototrophic Fe(II)-Oxidizing Bacteria. *Appl. Environ. Microbiol.* **2019**, *85*, No. e02826.
(604) Berg, J. S.; Michellod, D.; Pjevac, P.; Martinez-Perez, C.; Buckner, C. R.; Hach, P. F.; Schubert, C. J.; Milucka, J.; Kuypers, M. M. Intensive Cryptic Microbial Iron Cycling in the Low Iron Water Column of the Meromictic Lake Cadagno. *Environ. Microbiol.* **2016**, *18*, 5288−5302.
(605) Miot, J.; Benzerara, K.; Morin, G.; Kappler, A.; Bernard, S.; Obst, M.; Férard, C.; Skouri-Panet, F.; Guigner, J.-M.; Posth, N. Iron Biomineralization by Anaerobic Neutrophilic Iron-Oxidizing Bacteria. *Geochim. Cosmochim. Acta* **2009**, *73*, 696−711.
(606) Muehe, E. M.; Gerhardt, S.; Schink, B.; Kappler, A. Ecophysiology and the Energetic Benefit of Mixotrophic Fe(II) Oxidation by Various Strains of Nitratereducing Bacteria. *FEMS Microbiol. Ecol.* **2009**, *70*, 335−343.
(607) Frey, P. A.; Reed, G. H. The Ubiquity of Iron. *ACS Chem. Biol.* **2012**, *7*, 1477−1481.
(608) Emerson, D.; Scott, J. J.; Benes, J.; Bowden, W. B. Microbial Iron Oxidation in the Arctic Tundra and Its Implications for Biogeochemical Cycling. *Appl. Environ. Microbiol.* **2015**, *81*, 8066−8075.
(609) Fimmen, R. L.; Richter, D. d.; Vasudevan, D.; Williams, M. A.; West, L. T. Rhizogenic Fe-C Redox Cycling: A Hypothetical Biogeochemical Mechanism That Drives Crustal Weathering in Upland Soils. *Biogeochemistry* **2008**, *87*, 127−141.
(610) Chen, C.; Barcellos, D.; Richter, D. D.; Schroeder, P. A.; Thompson, A. Redoximorphic Bt Horizons of the Calhoun CZO Soils Exhibit Depth-Dependent Iron-Oxide Crystallinity. *J. Soils Sediments* **2019**, *19*, 785−797.
(611) Ahmed, I. A. M.; Maher, B. A. Identification and Paleoclimatic Significance of Magnetite Nanoparticles in Soils. *Proc. Natl. Acad. Sci. U.S.A.* **2018**, *115*, 1736−1741.


https://doi.org/10.1021/acs.chemrev.0c01286
*Chem. Rev.* 2021, 121, 8161−8233

(612) Herndon, E. M.; Kinsman-Costello, L.; Duroe, K. A.; Mills, J.; Kane, E. S.; Sebestyen, S. D.; Thompson, A. A.; Wullschleger, S. D. Iron (Oxyhydr)oxides Serve as Phosphate Traps in Tundra and Boreal Peat Soils. *JGR Biogeosci.* **2019**, *124*, 227−246.
(613) Hall, S. J.; Silver, W. L.; Timokhin, V. I.; Hammel, K. E. Lignin Decomposition Is Sustained under Fluctuating Redox Conditions in Humid Tropical Forest Soils. *Glob. Chang. Biol.* **2015**, *21*, 2818−2828.
(614) Chen, C.; Hall, S. J.; Coward, E.; Thompson, A. Iron-Mediated Organic Matter Decomposition in Humid Soils Can Counteract Protection. *Nat. Commun.* **2020**, *11*, 1−13.
(615) Krichels, A. H.; Sipic, E.; Yang, W. H. Iron Redox Reactions Can Drive Microtopographic Variation in Upland Soil Carbon Dioxide and Nitrous Oxide Emissions. *Soil Syst.* **2019**, *3*, 60.
(616) Thompson, A.; Chadwick, O. A.; Rancourt, D. G.; Chorover, J. Iron-Oxide Crystallinity Increases During Soil Redox Oscillations. *Geochim. Cosmochim. Acta* **2006**, *70*, 1710−1727.
(617) Tishchenko, V.; Meile, C.; Scherer, M. M.; Pasakarnis, T. S.; Thompson, A. $Fe^{2+}$ Catalyzed Iron Atom Exchange and Re-Crystallization in a Tropical Soil. *Geochim. Cosmochim. Acta* **2015**, *148*, 191−202.
(618) Kleber, M.; Eusterhues, K.; Keiluweit, M.; Mikutta, C.; Mikutta, R.; Nico, P. S. Mineral-Organic Associations: Formation, Properties, and Relevance in Soil Environments. In *Advances in Agronomy*; Sparks, D. L., Ed.; Academic Press, 2015; Vol. *130*, Chapter 1, pp 1−140.
(619) Kögel-Knabner, I.; Guggenberger, G.; Kleber, M.; Kandeler, E.; Kalbitz, K.; Scheu, S.; Eusterhues, K.; Leinweber, P. Organo-Mineral Associations in Temperate Soils: Integrating Biology, Mineralogy, and Organic Matter Chemistry. *J. Plant Nutr. Soil Sci.* **2008**, *171*, 61−82.
(620) Yang, W. H.; Weber, K. A.; Silver, W. L. Nitrogen Loss from Soil through Anaerobic Ammonium Oxidation Coupled to Iron Reduction. *Nat. Geosci.* **2012**, *5*, 538−541.
(621) Li, Y.; Yu, S.; Strong, J.; Wang, H. Are the Biogeochemical Cycles of Carbon, Nitrogen, Sulfur, and Phosphorus Driven by the "$Fe^{III}$−$Fe^{II}$ Redox Wheel" in Dynamic Redox Environments? *J. Soils Sediments* **2012**, *12*, 683−693.
(622) Kögel-Knabner, I.; Amelung, W.; Cao, Z.; Fiedler, S.; Frenzel, P.; Jahn, R.; Kalbitz, K.; Kölbl, A.; Schloter, M. Biogeochemistry of Paddy Soils. *Geoderma* **2010**, *157*, 1−14.
(623) Wang, M.; Hu, R.; Ruser, R.; Schmidt, C.; Kappler, A. Role of Chemodenitrification for $N_2O$ Emissions from Nitrate Reduction in Rice Paddy Soils. *ACS Earth Space Chem.* **2020**, *4*, 122−132.
(624) Kampschreur, M. J.; Kleerebezem, R.; de Vet, W. W. J. M.; van Loosdrecht, M. C. M. Reduced Iron Induced Nitric Oxide and Nitrous Oxide Emission. *Water Res.* **2011**, *45*, 5945−5952.
(625) Burdige, D. J.; Komada, T. Iron Redox Cycling, Sediment Resuspension and the Role of Sediments in Low Oxygen Environments as Sources of Iron to the Water Column. *Mar. Chem.* **2020**, *223*, 103793.
(626) Halevy, I.; Alesker, M.; Schuster, E. M.; Popovitz-Biro, R.; Feldman, Y. A Key Role for Green Rust in the Precambrian Oceans and the Genesis of Iron Formations. *Nat. Geosci.* **2017**, *10*, 135−139.
(627) Scholz, F.; Löscher, C. R.; Fiskal, A.; Sommer, S.; Hensen, C.; Lomnitz, U.; Wuttig, K.; Göttlicher, J.; Kossel, E.; Steininger, R.; et al. Nitrate-Dependent Iron Oxidation Limits Iron Transport in Anoxic Ocean Regions. *Earth Planet. Sci. Lett.* **2016**, *454*, 272−281.
(628) Schindler, D. W.; Carpenter, S. R.; Chapra, S. C.; Hecky, R. E.; Orihel, D. M. Reducing Phosphorus to Curb Lake Eutrophication Is a Success. *Environ. Sci. Technol.* **2016**, *50*, 8923−8929.
(629) Paytan, A.; Roberts, K.; Watson, S.; Peek, S.; Chuang, P.-C.; Defforey, D.; Kendall, C. Internal Loading of Phosphate in Lake Erie Central Basin. *Sci. Total Environ.* **2017**, *579*, 1356−1365.
(630) Gao, L.; Wei, Q.; Fu, F.; Shao, H. Influence of Outbreak of Macroalgal Blooms on Phosphorus Release from the Sediments in Swan Lake Wetland. *China. Plant Biosyst.* **2013**, *147*, 1175−1183.
(631) Pearce, A. R.; Rizzo, D. M.; Watzin, M. C.; Druschel, G. K. Unraveling Associations between Cyanobacteria Blooms and in-Lake Environmental Conditions in Missisquoi Bay, Lake Champlain, USA, Using a Modified Self-Organizing Map. *Environ. Sci. Technol.* **2013**, *47*, 14267−14274.
(632) Gaoa, L. Phosphorus Release from the Sediments in Rongcheng Swan Lake under Different pH Conditions. *Procedia Environ. Sci.* **2012**, *13*, 2077−2084.
(633) Robertson, E. K.; Roberts, K. L.; Burdorf, L. D. W.; Cook, P.; Thamdrup, B. Dissimilatory Nitrate Reduction to Ammonium Coupled to Fe(II) Oxidation in Sediments of a Periodically Hypoxic Estuary. *Liminol. Oceanogr.* **2016**, *61*, 365−381 DOI: 10.1002/lno.10220.
(634) Smith, R. L.; Kent, D. B.; Repert, D. A.; Böhlke, J. K. Anoxic Nitrate Reduction Coupled with Iron Oxidation and Attenuation of Dissolved Arsenic and Phosphate in a Sand and Gravel Aquifer. *Geochim. Cosmochim. Acta* **2017**, *196*, 102−120.
(635) Robertson, E. K.; Thamdrup, B. The Fate of Nitrogen Is Linked to Iron(II) Availability in a Freshwater Lake Sediment. *Geochim. Cosmochim. Acta* **2017**, *205*, 84−99.
(636) Trusiak, A.; Treibergs, L. A.; Kling, G. W.; Cory, R. M. The Role of Iron and Reactive Oxygen Species in the Production of $CO_2$ in Arctic Soil Waters. *Geochim. Cosmochim. Acta* **2018**, *224*, 80−95.
(637) Miller, C. J.; Rose, A. L.; Waite, T. D. Hydroxyl Radical Production by $H_2O_2$-Mediated Oxidation of Fe(II) Complexed by Suwannee River Fulvic Acid under Circumneutral Freshwater Conditions. *Environ. Sci. Technol.* **2013**, *47*, 829−835.
(638) Miller, C. J.; Rose, A. L.; Waite, T. D. Importance of Iron Complexation for Fenton-Mediated Hydroxyl Radical Production at Circumneutral pH. *Front. Mar. Sci.* **2016**, *3*, 134.
(639) Sevcikova, M.; Modra, H.; Slaninova, A.; Svobodova, Z. Metals as a Cause of Oxidative Stress in Fish: A Review. *Vet. Med.* **2011**, *56*, 537−546.
(640) Ilbert, M.; Bonnefoy, V. Insight into the Evolution of the Iron Oxidation Pathways. *Biochim. Biophys. Acta, Bioenerg.* **2013**, *1827*, 161−175.
(641) Canfield, D. E.; Raiswell, R.; Bottrell, S. H. The Reactivity of Sedimentary Iron Minerals toward Sulfide. *Am. J. Sci.* **1992**, *292*, 659−683.
(642) Vraspir, J. M.; Butler, A. Chemistry of Marine Ligands and Siderophores. *Annu. Rev. Mar. Sci.* **2009**, *1*, 43−63.
(643) Fujii, M.; Dang, T.; Rose, A. L.; Omura, T.; Waite, T. Effect of Light on Iron Uptake by the Freshwater Cyanobacterium Microcystis Aeruginosa. *Environ. Sci. Technol.* **2011**, *45*, 1391−1398.
(644) Rose, A. The Influence of Extracellular Superoxide on Iron Redox Chemistry and Bioavailability to Aquatic Microorganisms. *Front. Microbiol.* **2012**, *3*, 124.
(645) Laufer, K.; Nordhoff, M.; Røy, H.; Schmidt, C.; Behrens, S.; Jørgensen, B. B.; Kappler, A. Coexistence of Microaerophilic, Nitrate-Reducing, and Phototrophic Fe(II) Oxidizers and Fe(III) Reducers in Coastal Marine Sediment. *Appl. Environ. Microbiol.* **2016**, *82*, 1433−1447.
(646) Tollefson, J. Iron-Dumping Ocean Experiment Sparks Controversy. *Nature* **2017**, *545*, 393
(647) Martin, J. H.; Coale, K.; Johnson, K.; Fitzwater, S.; Gordon, R.; Tanner, S.; Hunter, C.; Elrod, V.; Nowicki, J.; Coley, T. Testing the Iron Hypothesis in Ecosystems of the Equatorial Pacific Ocean. *Nature* **1994**, *371*, 123−129.
(648) Emerson, D. Biogenic Iron Dust: A Novel Approach to Ocean Iron Fertilization as a Means of Large Scale Removal of Carbon Dioxide from the Atmosphere. *Front. Mar. Sci.* **2019**, *6*, 22.
(649) Chisholm, S. W.; Falkowski, P. G.; Cullen, J. J. Dis-Crediting Ocean Fertilization. *Science* **2001**, *294*, 309−310.
(650) Fenton, H. J. H. LXXIII.—Oxidation of Tartaric Acid in Presence of Iron. *J. Chem. Soc., Trans.* **1894**, *65*, 899−910.
(651) Bray, W. C.; Gorin, M. Ferryl Ion, a Compound of Tetravalent Iron. *J. Am. Chem. Soc.* **1932**, *54*, 2124−2125.
(652) Haber, F.; Weiss, J.; Pope, W. J. The Catalytic Decomposition of Hydrogen Peroxide by Iron Salts. *Proc. Math. Phys. Eng. Sci.* **1934**, *147*, 332−351.
(653) Zhu, Y.; Zhu, R.; Xi, Y.; Zhu, J.; Zhu, G.; He, H. Strategies for Enhancing the Heterogeneous Fenton Catalytic Reactivity: A Review. *Appl. Catal., B* **2019**, *255*, 117739.
(654) Munoz, M.; de Pedro, Z. M.; Casas, J. A.; Rodriguez, J. J. Preparation of Magnetite-Based Catalysts and Their Application in

Heterogeneous Fenton Oxidation − a Review. *Appl. Catal., B* **2015**, *176*−*177*, 249−265.
(655) Buda, F.; Ensing, B.; Gribnau, M. C. M.; Baerends, E. J. DFT Study of the Active Intermediate in the Fenton Reaction. *Chem. - Eur. J.* **2001**, *7*, 2775−2783.
(656) Deguillaume, L.; Leriche, M.; Chaumerliac, N. Impact of Radical Versus Non-Radical Pathway in the Fenton Chemistry on the Iron Redox Cycle in Clouds. *Chemosphere* **2005**, *60*, 718−724.
(657) Bataineh, H.; Pestovsky, O.; Bakac, A. pH-Induced Mechanistic Changeover from Hydroxyl Radicals to Iron(IV) in the Fenton Reaction. *Chem. Sci.* **2012**, *3*, 1594−1599.
(658) Enami, S.; Sakamoto, Y.; Colussi, A. J. Fenton Chemistry at Aqueous Interfaces. *Proc. Natl. Acad. Sci. U. S. A.* **2014**, *111*, 623−628.
(659) Remucal, C. K.; Sedlak, D. L. The Role of Iron Coordination in the Production of Reactive Oxidants from Ferrous Iron Oxidation by Oxygen and Hydrogen Peroxide. In *Aquatic Redox Chemistry*; Tratnyek, P. G., Grundl, T. J., Haderlein, S. B., Eds.; ACS Symposium Series; American Chemical Society: Washington, DC, 2011; Vol. *1071*, Chapter 9, pp177−197.
(660) Miller, C. J.; Wadley, S.; Waite, T. D. Fenton, Photo-Fenton and Fenton-like Processes. In *Advanced Oxidation Processes for Water Treatment: Fundamentals and Applications*; Stefan, M. I., Ed.; IWA Publishing, 2017; Chapter 7, pp297−332.
(661) Zhang, Y.; Zhou, M. A Critical Review of the Application of Chelating Agents to Enable Fenton and Fenton-Like Reactions at High pH Values. *J. Hazard. Mater.* **2019**, *362*, 436−450.
(662) He, J.; Yang, X.; Men, B.; Wang, D. Interfacial Mechanisms of Heterogeneous Fenton Reactions Catalyzed by Iron-Based Materials: A Review. *J. Environ. Sci.* **2016**, *39*, 97−109.
(663) Pignatello, J. J.; Oliveros, E.; MacKay, A. Advanced Oxidation Processes for Organic Contaminant Destruction Based on the Fenton Reaction and Related Chemistry. *Crit. Rev. Environ. Sci. Technol.* **2006**, *36*, 1−84.
(664) Lin, S.-S.; Gurol, M. D. Catalytic Decomposition of Hydrogen Peroxide on Iron Oxide: Kinetics, Mechanism, and Implications. *Environ. Sci. Technol.* **1998**, *32*, 1417−1423.
(665) Kwan, W. P.; Voelker, B. M. Rates of Hydroxyl Radical Generation and Organic Compound Oxidation in Mineral-Catalyzed Fenton-Like Systems. *Environ. Sci. Technol.* **2003**, *37*, 1150−1158.
(666) Pham, A. L.-T.; Lee, C.; Doyle, F. M.; Sedlak, D. L. A Silica-Supported Iron Oxide Catalyst Capable of Activating Hydrogen Peroxide at Neutral pH Values. *Environ. Sci. Technol.* **2009**, *43*, 8930−8935.
(667) González-Davila, M.; Santana-Casiano, J. M.; Millero, F. J. Oxidation of Iron(II) Nanomolar with $H_2O_2$ in Seawater. *Geochim. Cosmochim. Acta* **2005**, *69*, 83−93.
(668) Lee, C.; Keenan, C. R.; Sedlak, D. L. Polyoxometalate-Enhanced Oxidation of Organic Compounds by Nanoparticulate Zero-Valent Iron and Ferrous Ion in the Presence of Oxygen. *Environ. Sci. Technol.* **2008**, *42*, 4921−4926.
(669) Messele, S. A.; Bengoa, C.; Stüber, F. E.; Giralt, J.; Fortuny, A.; Fabregat, A.; Font, J. Enhanced Degradation of Phenol by a Fenton-Like System (Fe/EDTA/$H_2O_2$) at Circumneutral pH. *Catalysts* **2019**, *9*, 474.
(670) Rastogi, A.; Al-Abed, S. R.; Dionysiou, D. D. Effect of Inorganic, Synthetic and Naturally Occurring Chelating Agents on Fe(II) Mediated Advanced Oxidation of Chlorophenols. *Water Res.* **2009**, *43*, 684−694.
(671) Wang, Z.; Bush, R. T.; Liu, J. Arsenic(III) and Iron(II) Co-Oxidation by Oxygen and Hydrogen Peroxide: Divergent Reactions in the Presence of Organic Ligands. *Chemosphere* **2013**, *93*, 1936−1941.
(672) Hou, X.; Huang, X.; Ai, Z.; Zhao, J.; Zhang, L. Ascorbic Acid/Fe@$Fe_2O_3$: A Highly Efficient Combined Fenton Reagent to Remove Organic Contaminants. *J. Hazard. Mater.* **2016**, *310*, 170−178.
(673) Chen, L.; Ma, J.; Li, X.; Zhang, J.; Fang, J.; Guan, Y.; Xie, P. Strong Enhancement on Fenton Oxidation by Addition of Hydroxylamine to Accelerate the Ferric and Ferrous Iron Cycles. *Environ. Sci. Technol.* **2011**, *45*, 3925−3930.
(674) Hou, X.; Zhan, G.; Huang, X.; Wang, N.; Ai, Z.; Zhang, L. Persulfate Activation Induced by Ascorbic Acid for Efficient Organic Pollutants Oxidation. *Chem. Eng. J.* **2020**, *382*, 122355.
(675) Hou, X.; Huang, X.; Ai, Z.; Zhao, J.; Zhang, L. Ascorbic Acid Induced Atrazine Degradation. *J. Hazard. Mater.* **2017**, *327*, 71−78.
(676) Hou, X.; Shen, W.; Huang, X.; Ai, Z.; Zhang, L. Ascorbic Acid Enhanced Activation of Oxygen by Ferrous Iron: A Case of Aerobic Degradation of Rhodamine B. *J. Hazard. Mater.* **2016**, *308*, 67−74.
(677) Zou, J.; Ma, J.; Chen, L.; Li, X.; Guan, Y.; Xie, P.; Pan, C. Rapid Acceleration of Ferrous Iron/Peroxymonosulfate Oxidation of Organic Pollutants by Promoting Fe(III)/Fe(II) Cycle with Hydroxylamine. *Environ. Sci. Technol.* **2013**, *47*, 11685−11691.
(678) Tachiev, G.; Roth, J. A.; Bowers, A. R. Kinetics of Hydrogen Peroxide Decomposition with Complexed and "Free" Iron Catalysts. *Int. J. Chem. Kinet.* **2000**, *32*, 24−35.
(679) Matta, R.; Hanna, K.; Chiron, S. Fenton-Like Oxidation of 2,4,6-Trinitrotoluene Using Different Iron Minerals. *Sci. Total Environ.* **2007**, *385*, 242−251.
(680) Usman, M.; Faure, P.; Ruby, C.; Hanna, K. Remediation of PAH-Contaminated Soils by Magnetite Catalyzed Fenton-Like Oxidation. *Appl. Catal., B* **2012**, *117*−*118*, 10−17.
(681) Sun, H.; Xie, G.; He, D.; Zhang, L. Ascorbic Acid Promoted Magnetite Fenton Degradation of Alachlor: Mechanistic Insights and Kinetic Modeling. *Appl. Catal., B* **2020**, *267*, 118383.
(682) Costa, R. C. C.; Lelis, M. F. F.; Oliveira, L. C. A.; Fabris, J. D.; Ardisson, J. D.; Rios, R. R. V. A.; Silva, C. N.; Lago, R. M. Novel Active Heterogeneous Fenton System Based on $Fe_{3-x}M_xO_4$ (Fe, Co, Mn, Ni): The Role of $M^{2+}$ Species on the Reactivity Towards $H_2O_2$ Reactions. *J. Hazard. Mater.* **2006**, *129*, 171−178.
(683) Fang, G.-D.; Zhou, D.-M.; Dionysiou, D. D. Superoxide Mediated Production of Hydroxyl Radicals by Magnetite Nanoparticles: Demonstration in the Degradation of 2-Chlorobiphenyl. *J. Hazard. Mater.* **2013**, *250*−*251*, 68−75.
(684) Costa, R. C. C.; Moura, F. C. C.; Ardisson, J. D.; Fabris, J. D.; Lago, R. M. Highly Active Heterogeneous Fenton-Like Systems Based on $Fe^0/Fe_3O_4$ Composites Prepared by Controlled Reduction of Iron Oxides. *Appl. Catal., B* **2008**, *83*, 131−139.
(685) Xue, X.; Hanna, K.; Despas, C.; Wu, F.; Deng, N. Effect of Chelating Agent on the Oxidation Rate of PCP in the Magnetite/$H_2O_2$ System at Neutral pH. *J. Mol. Catal. A: Chem.* **2009**, *311*, 29−35.
(686) Zhang, P.; Yuan, S.; Liao, P. Mechanisms of Hydroxyl Radical Production from Abiotic Oxidation of Pyrite under Acidic Conditions. *Geochim. Cosmochim. Acta* **2016**, *172*, 444−457.
(687) Schoonen, M. A. A.; Harrington, A. D.; Laffers, R.; Strongin, D. R. Role of Hydrogen Peroxide and Hydroxyl Radical in Pyrite Oxidation by Molecular Oxygen. *Geochim. Cosmochim. Acta* **2010**, *74*, 4971−4987.
(688) Zhang, P.; Yuan, S. Production of Hydroxyl Radicals from Abiotic Oxidation of Pyrite by Oxygen under Circumneutral Conditions in the Presence of Low-Molecular-Weight Organic Acids. *Geochim. Cosmochim. Acta* **2017**, *218*, 153−166.
(689) Cheng, D.; Neumann, A.; Yuan, S.; Liao, W.; Qian, A. Oxidative Degradation of Organic Contaminants by FeS in the Presence of $O_2$. *Environ. Sci. Technol.* **2020**, *54*, 4091−4101.
(690) Joo, S. H.; Feitz, A. J.; Sedlak, D. L.; Waite, T. D. Quantification of the Oxidizing Capacity of Nanoparticulate Zero-Valent Iron. *Environ. Sci. Technol.* **2005**, *39*, 1263−1268.
(691) Joo, S. H.; Feitz, A. J.; Waite, T. D. Oxidative Degradation of the Carbothioate Herbicide, Molinate, Using Nanoscale Zero-Valent Iron. *Environ. Sci. Technol.* **2004**, *38*, 2242−2247.
(692) He, D.; Ma, J.; Collins, R. N.; Waite, T. D. Effect of Structural Transformation of Nanoparticulate Zero-Valent Iron on Generation of Reactive Oxygen Species. *Environ. Sci. Technol.* **2016**, *50*, 3820−3828.
(693) Liu, W.; Ai, Z.; Cao, M.; Zhang, L. Ferrous Ions Promoted Aerobic Simazine Degradation with Fe@$Fe_2O_3$ Core−Shell Nanowires. *Appl. Catal., B* **2014**, *150*−*151*, 1−11.
(694) Shi, J.; Ai, Z.; Zhang, L. Fe@$Fe_2O_3$ Core-Shell Nanowires Enhanced Fenton Oxidation by Accelerating the Fe(III)/Fe(II) Cycles. *Water Res.* **2014**, *59*, 145−153.


https://doi.org/10.1021/acs.chemrev.0c01286
*Chem. Rev.* 2021, 121, 8161−8233

(695) Xie, W.; Yuan, S.; Tong, M.; Ma, S.; Liao, W.; Zhang, N.; Chen, C. Contaminant Degradation by •OH During Sediment Oxygenation: Dependence on Fe(II) Species. *Environ. Sci. Technol.* **2020**, *54*, 2975−2984.
(696) Tong, M.; Yuan, S.; Ma, S.; Jin, M.; Liu, D.; Cheng, D.; Liu, X.; Gan, Y.; Wang, Y. Production of Abundant Hydroxyl Radicals from Oxygenation of Subsurface Sediments. *Environ. Sci. Technol.* **2016**, *50*, 214−221.
(697) Zhu, J.; Zhang, P.; Yuan, S.; Liao, P.; Qian, A.; Liu, X.; Tong, M.; Li, L. Production of Hydroxyl Radicals from Oxygenation of Simulated AMD Due to $CaCO_3$-Induced pH Increase. *Water Res.* **2017**, *111*, 118−126.
(698) Hou, X.; Huang, X.; Jia, F.; Ai, Z.; Zhao, J.; Zhang, L. Hydroxylamine Promoted Goethite Surface Fenton Degradation of Organic Pollutants. *Environ. Sci. Technol.* **2017**, *51*, 5118−5126.
(699) Pereira, M. C.; Oliveira, L. C. A.; Murad, E. Iron Oxide Catalysts: Fenton and Fentonlike Reactions − a Review. *Clay Miner.* **2012**, *47*, 285−302.
(700) Garrido-Ramírez, E. G.; Theng, B. K. G.; Mora, M. L. Clays and Oxide Minerals as Catalysts and Nanocatalysts in Fenton-Like Reactions — a Review. *Appl. Clay Sci.* **2010**, *47*, 182−192.
(701) Duesterberg, C. K.; Mylon, S. E.; Waite, T. D. pH Effects on Iron-Catalyzed Oxidation Using Fenton's Reagent. *Environ. Sci. Technol.* **2008**, *42*, 8522−8527.
(702) Zazo, J. A.; Pliego, G.; Blasco, S.; Casas, J. A.; Rodriguez, J. J. Intensification of the Fenton Process by Increasing the Temperature. *Ind. Eng. Chem. Res.* **2011**, *50*, 866−870.
(703) Liang, C.; Bruell, C. J.; Marley, M. C.; Sperry, K. L. Persulfate Oxidation for in Situ Remediation of TCE. I. Activated by Ferrous Ion with and without a Persulfate−Thiosulfate Redox Couple. *Chemosphere* **2004**, *55*, 1213−1223.
(704) Rastogi, A.; Al-Abed, S. R.; Dionysiou, D. D. Sulfate Radical-Based Ferrous−Peroxymonosulfate Oxidative System for PCBs Degradation in Aqueous and Sediment Systems. *Appl. Catal., B* **2009**, *85*, 171−179.
(705) Vicente, F.; Santos, A.; Romero, A.; Rodriguez, S. Kinetic Study of Diuron Oxidation and Mineralization by Persulphate: Effects of Temperature, Oxidant Concentration and Iron Dosage Method. *Chem. Eng. J.* **2011**, *170*, 127−135.
(706) Wang, Z.; Jiang, J.; Pang, S.; Zhou, Y.; Guan, C.; Gao, Y.; Li, J.; Yang, Y.; Qiu, W.; Jiang, C. Is Sulfate Radical Really Generated from Peroxydisulfate Activated by Iron(II) for Environmental Decontamination? *Environ. Sci. Technol.* **2018**, *52* (19), 11276−11284.
(707) Wang, S.; Wu, J.; Lu, X.; Xu, W.; Gong, Q.; Ding, J.; Dan, B.; Xie, P. Removal of Acetaminophen in the $Fe^{2+}$/Persulfate System: Kinetic Model and Degradation Pathways. *Chem. Eng. J.* **2019**, *358*, 1091−1100.
(708) Dong, H.; Li, Y.; Wang, S.; Liu, W.; Zhou, G.; Xie, Y.; Guan, X. Both Fe(IV) and Radicals Are Active Oxidants in the Fe(II)/Peroxydisulfate Process. *Environ. Sci. Technol. Lett.* **2020**, *7*, 219−224.
(709) Qiu, Q.; Li, G.; Dai, Y.; Xu, Y.; Bao, P. Removal of Antibiotic Resistant Microbes by Fe(II)-Activated Persulfate Oxidation. *J. Hazard. Mater.* **2020**, *396*, 122733.
(710) Liang, C.; Bruell, C. J.; Marley, M. C.; Sperry, K. L. Persulfate Oxidation for in Situ Remediation of TCE. II. Activated by Chelated Ferrous Ion. *Chemosphere* **2004**, *55*, 1225−1233.
(711) Wu, X.; Gu, X.; Lu, S.; Xu, M.; Zang, X.; Miao, Z.; Qiu, Z.; Sui, Q. Degradation of Trichloroethylene in Aqueous Solution by Persulfate Activated with Citric Acid Chelated Ferrous Ion. *Chem. Eng. J.* **2014**, *255*, 585−592.
(712) Ji, Y.; Ferronato, C.; Salvador, A.; Yang, X.; Chovelon, J.-M. Degradation of Ciprofloxacin and Sulfamethoxazole by Ferrous-Activated Persulfate: Implications for Remediation of Groundwater Contaminated by Antibiotics. *Sci. Total Environ.* **2014**, *472*, 800−808.
(713) Han, D.; Wan, J.; Ma, Y.; Wang, Y.; Li, Y.; Li, D.; Guan, Z. New Insights into the Role of Organic Chelating Agents in Fe(II) Activated Persulfate Processes. *Chem. Eng. J.* **2015**, *269*, 425−433.
(714) Wang, Z.; Qiu, W.; Pang, S.; Jiang, J. Effect of Chelators on the Production and Nature of the Reactive Intermediates Formed in Fe(II) Activated Peroxydisulfate and Hydrogen Peroxide Processes. *Water Res.* **2019**, *164*, 114957.
(715) Oh, S.-Y.; Kang, S.-G.; Kim, D.-W.; Chiu, P. C. Degradation of 2, 4-Dinitrotoluene by Persulfate Activated with Iron Sulfides. *Chem. Eng. J.* **2011**, *172*, 641−646.
(716) Fang, G.-D.; Dionysiou, D. D.; Al-Abed, S. R.; Zhou, D.-M. Superoxide Radical Driving the Activation of Persulfate by Magnetite Nanoparticles: Implications for the Degradation of Pcbs. *Appl. Catal., B* **2013**, *129*, 325−332.
(717) Fan, J.; Gu, L.; Wu, D.; Liu, Z. Mackinawite (FeS) Activation of Persulfate for the Degradation of p-Chloroaniline: Surface Reaction Mechanism and Sulfur-Mediated Cycling of Iron Species. *Chem. Eng. J.* **2018**, *333*, 657−664.
(718) Lai, L.; Zhou, H.; Zhang, H.; Ao, Z.; Pan, Z.; Chen, Q.; Xiong, Z.; Yao, G.; Lai, B. Activation of Peroxydisulfate by Natural Titanomagnetite for Atrazine Removal via Free Radicals and High-Valent Iron-Oxo Species. *Chem. Eng. J.* **2020**, *387*, 124165.
(719) Wang, X.; Wang, Y.; Chen, N.; Shi, Y.; Zhang, L. Pyrite Enables Persulfate Activation for Efficient Atrazine Degradation. *Chemosphere* **2020**, *244*, 125568.
(720) Do, S.-H.; Kwon, Y.-J.; Kong, S.-H. Effect of Metal Oxides on the Reactivity of Persulfate/Fe(II) in the Remediation of Diesel-Contaminated Soil and Sand. *J. Hazard. Mater.* **2010**, *182*, 933−936.
(721) Hu, P.; Long, M. Cobalt-Catalyzed Sulfate Radical-Based Advanced Oxidation: A Review on Heterogeneous Catalysts and Applications. *Appl. Catal., B* **2016**, *181*, 103−117.
(722) Huang, J.; Zhang, H. Mn-Based Catalysts for Sulfate Radical-Based Advanced Oxidation Processes: A Review. *Environ. Int.* **2019**, *133*, 105141.
(723) Ghanbari, F.; Moradi, M. Application of Peroxymonosulfate and Its Activation Methods for Degradation of Environmental Organic Pollutants: Review. *Chem. Eng. J.* **2017**, *310* (Part 1), 41−62.
(724) Wang, J.; Wang, S. Activation of Persulfate (PS) and Peroxymonosulfate (PMS) and Application for the Degradation of Emerging Contaminants. *Chem. Eng. J.* **2018**, *334*, 1502−1517.
(725) Liu, C. S.; Shih, K.; Sun, C. X.; Wang, F. Oxidative Degradation of Propachlor by Ferrous and Copper Ion Activated Persulfate. *Sci. Total Environ.* **2012**, *416*, 507−512.
(726) Wang, P.; He, X.; Zhang, W.; Ma, J.; Jiang, J.; Huang, Z.; Cheng, H.; Pang, S.; Zhou, Y.; Zhai, X. Highly Efficient Removal of p-Arsanilic Acid with Fe(II)/Peroxydisulfate under near-Neutral Conditions. *Water Res.* **2020**, *177*, 115752.
(727) Wang, Z.; Qiu, W.; Pang, S.-y.; Zhou, Y.; Gao, Y.; Guan, C.; Jiang, J. Further Understanding the Involvement of Fe(IV) in Peroxydisulfate and Peroxymonosulfate Activation by Fe(II) for Oxidative Water Treatment. *Chem. Eng. J.* **2019**, *371*, 842−847.
(728) Pestovsky, O.; Bakac, A. Aqueous Ferryl(IV) Ion: Kinetics of Oxygen Atom Transfer to Substrates and Oxo Exchange with Solvent Water. *Inorg. Chem.* **2006**, *45*, 814−820.
(729) Ahn, S.; Peterson, T. D.; Righter, J.; Miles, D. M.; Tratnyek, P. G. Disinfection of Ballast Water with Iron Activated Persulfate. *Environ. Sci. Technol.* **2013**, *47*, 11717−11725.
(730) Kim, C.; Ahn, J.-Y.; Kim, T. Y.; Shin, W. S.; Hwang, I. Activation of Persulfate by Nanosized Zero-Valent Iron (NZVI): Mechanisms and Transformation Products of Nzvi. *Environ. Sci. Technol.* **2018**, *52*, 3625−3633.
(731) Yuan, Y.; Tao, H.; Fan, J.; Ma, L. Degradation of P-Chloroaniline by Persulfate Activated with Ferrous Sulfide Ore Particles. *Chem. Eng. J.* **2015**, *268*, 38−46.
(732) Gorski, C. A.; Aeschbacher, M.; Soltermann, D.; Voegelin, A.; Baeyens, B.; Marques Fernandes, M.; Hofstetter, T. B.; Sander, M. Redox Properties of Structural Fe in Clay Minerals. 1. Electrochemical Quantification of Electron-Donating and -Accepting Capacities of Smectites. *Environ. Sci. Technol.* **2012**, *46*, 9360−9368.
(733) Tratnyek, P. G.; Weber, E. J.; Schwarzenbach, R. P. Quantitative Structure-Activity Relationships for Chemical Reductions of Organic Contaminants. *Environ. Toxicol. Chem.* **2003**, *22*, 1733−1742.
(734) Colón, D.; Weber, E. J.; Anderson, J. L.; Winget, P.; Suárez, L. A. Reduction of Nitrosobenzenes and N-Hydroxylanilines by Fe(II)


https://doi.org/10.1021/acs.chemrev.0c01286
*Chem. Rev.* 2021, 121, 8161−8233

Species: Elucidation of the Reaction Mechanism. *Environ. Sci. Technol.* **2006**, *40*, 4449−4454.
(735) Jeon, B.-H.; Dempsey, B. A.; Burgos, W. D. Kinetics and Mechanisms for Reactions of Fe(II) with Iron(III) Oxides. *Environ. Sci. Technol.* **2003**, *37*, 3309−3315.
(736) Coughlin, B. R.; Stone, A. T. Nonreversible Adsorption of Divalent Metal Ions ($Mn^{II}$, $Co^{II}$, $Ni^{II}$, $Cu^{II}$, and $Pb^{II}$) onto Goethite: Effects of Acidification, $Fe^{II}$ Addition, and Picolinic Acid Addition. *Environ. Sci. Technol.* **1995**, *29*, 2445−2455.
(737) Jeon, B.-H.; Dempsey, B. A.; Burgos, W. D.; Royer, R. A. Reactions of Ferrous Iron with Hematite. *Colloids Surf., A* **2001**, *191*, 41−55.
(738) Schaedler, F.; Kappler, A.; Schmidt, C. A Revised Iron Extraction Protocol for Environmental Samples Rich in Nitrite and Carbonate. *Geomicrobiol. J.* **2018**, *35*, 23−30.
(739) Peiffer, S.; Behrends, T.; Hellige, K.; Larese-Casanova, P.; Wan, M.; Pollok, K. Pyrite Formation and Mineral Transformation Pathways Upon Sulfidation of Ferric Hydroxides Depend on Mineral Type and Sulfide Concentration. *Chem. Geol.* **2015**, *400*, 44−55.
(740) Kim, W.; Suh, C.-Y.; Cho, S.-W.; Roh, K.-M.; Kwon, H.; Song, K.; Shon, I.-J. A New Method for the Identification and Quantification of Magnetite−Maghemite Mixture Using Conventional X-Ray Diffraction Technique. *Talanta* **2012**, *94*, 348−352.
(741) Mos, Y. M.; Vermeulen, A. C.; Buisman, C. J. N.; Weijma, J. X-Ray Diffraction of Iron Containing Samples: The Importance of a Suitable Configuration. *Geomicrobiol. J.* **2018**, *35*, 511−517.
(742) Lennie, A.; Redfern, S. A.; Schofield, P.; Vaughan, D. J. M. M. Synthesis and Rietveld Crystal Structure Refinement of Mackinawite. *Mineral. Mag.* **1995**, *59*, 677−683.
(743) Gorski, C. A.; Scherer, M. M. Determination of Nanoparticulate Magnetite Stoichiometry by Mössbauer Spectroscopy, Acidic Dissolution, and Powder X-Ray Diffraction: A Critical Review. *Am. Mineral.* **2010**, *95*, 1017−1026.
(744) Li, X.; Zhu, K.; Pang, J.; Tian, M.; Liu, J.; Rykov, A. I.; Zheng, M.; Wang, X.; Zhu, X.; Huang, Y. Unique Role of Mössbauer Spectroscopy in Assessing Structural Features of Heterogeneous Catalysts. *Appl. Catal., B* **2018**, *224*, 518−532.
(745) Mullet, M.; Boursiquot, S.; Abdelmoula, M.; Génin, J.-M.; Ehrhardt, J.-J. Surface Chemistry and Structural Properties of Mackinawite Prepared by Reaction of Sulfide Ions with Metallic Iron. *Geochim. Cosmochim. Acta* **2002**, *66*, 829−836.
(746) Zboril, R.; Mashlan, M.; Petridis, D. Iron(III) Oxides from Thermal Processessynthesis, Structural and Magnetic Properties, Mössbauer Spectroscopy Characterization, and Applications. *Chem. Mater.* **2002**, *14*, 969−982.
(747) Vandenberghe, R. E.; Barrero, C. A.; da Costa, G. M.; Van San, E.; De Grave, E. Mössbauer Characterization of Iron Oxides and (Oxy)Hydroxides: The Present State of the Art. *Hyperfine Interact.* **2000**, *126*, 247−259.
(748) da Costa, G. M.; de Grave, E.; De Barker, P. M. A.; Vandenberghe, R. E. Influence of Nonstoichiometry and the Presence of Maghemite on the Mössbauer Spectrum of Magnetite. *Clays Clay Miner.* **1995**, *43*, 656−668.
(749) Notini, L.; Byrne, J. M.; Tomaszewski, E. J.; Latta, D. E.; Zhou, Z.; Scherer, M. M.; Kappler, A. Mineral Defects Enhance Bioavailability of Goethite toward Microbial Fe(III) Reduction. *Environ. Sci. Technol.* **2019**, *53*, 8883−8891.
(750) Yamashita, T.; Hayes, P. Analysis of XPS Spectra of $Fe^{2+}$ and $Fe^{3+}$ Ions in Oxide Materials. *Appl. Surf. Sci.* **2008**, *254*, 2441−2449.
(751) Hochella, M., Jr; Ponader, H.; Turner, A.; Harris, D. The Complexity of Mineral Dissolution as Viewed by High Resolution Scanning Auger Microscopy: Labradorite under Hydrothermal Conditions. *Geochim. Cosmochim. Acta* **1988**, *52*, 385−394.
(752) Stern, L.-A.; Feng, L.; Song, F.; Hu, X. $Ni_2P$ as a Janus Catalyst for Water Splitting: The Oxygen Evolution Activity of $Ni_2P$ Nanoparticles. *Energy Environ. Sci.* **2015**, *8*, 2347−2351.
(753) Lettenmeier, P.; Wang, L.; Golla-Schindler, U.; Gazdzicki, P.; Cañas, N. A.; Handl, M.; Hiesgen, R.; Hosseiny, S. S.; Gago, A. S.; Friedrich, K. A. Nanosized Irox−Ir Catalyst with Relevant Activity for Anodes of Proton Exchange Membrane Electrolysis Produced by a Cost-Effective Procedure. *Angew. Chem.* **2016**, *128*, 752−756.
(754) Hochella, M. F., Jr; Brown, G. E., Jr Aspects of Silicate Surface and Bulk Structure Analysis Using X-Ray Photoelectron Spectroscopy (XPS). *Geochim. Cosmochim. Acta* **1988**, *52*, 1641−1648.
(755) Fujii, T. d.; De Groot, F.; Sawatzky, G.; Voogt, F.; Hibma, T.; Okada, K. In Situ XPS Analysis of Various Iron Oxide Films Grown by $NO_2$-Assisted Molecular-Beam Epitaxy. *Phys. Rev. B: Condens. Matter Mater. Phys.* **1999**, *59*, 3195.
(756) Panzmer, G.; Egert, B. The Bonding State of Sulfur Segregated to A-Iron Surfaces and on Iron Sulfide Surfaces Studied by XPS, AES and ELS. *Surf. Sci.* **1984**, *144*, 651−664.
(757) Yamashita, T.; Hayes, P. Effect of Curve Fitting Parameters on Quantitative Analysis of $Fe_{0.94}O$ and $Fe_2O_3$ Using XPS. *J. Electron Spectrosc. Relat. Phenom.* **2006**, *152*, 6−11.
(758) Adhikari, D.; Zhao, Q.; Das, K.; Mejia, J.; Huang, R.; Wang, X.; Poulson, S. R.; Tang, Y.; Roden, E. E.; Yang, Y. Dynamics of Ferrihydrite-Bound Organic Carbon During Microbial Fe Reduction. *Geochim. Cosmochim. Acta* **2017**, *212*, 221−233.
(759) Zeng, Q.; Huang, L.; Ma, J.; Zhu, Z.; He, C.; Shi, Q.; Liu, W.; Wang, X.; Xia, Q.; Dong, H. Bio-Reduction of Ferrihydrite-Montmorillonite-Organic Matter Complexes: Effect of Montmorillonite and Fate of Organic Matter. *Geochim. Cosmochim. Acta* **2020**, *276*, 327−344.
(760) Nesbitt, H.; Muir, I.; Prarr, A. Oxidation of Arsenopyrite by Air and Air-Saturated, Distilled Water, and Implications for Mechanism of Oxidation. *Geochim. Cosmochim. Acta* **1995**, *59*, 1773−1786.
(761) Lim, S.-F.; Zheng, Y.-M.; Chen, J. P. Organic Arsenic Adsorption onto a Magnetic Sorbent. *Langmuir* **2009**, *25*, 4973−4978.
(762) Chowdhury, S. R.; Yanful, E. K.; Pratt, A. R. Arsenic Removal from Aqueous Solutions by Mixed Magnetite−Maghemite Nanoparticles. *Environ. Earth Sci.* **2011**, *64*, 411−423.
(763) Greczynski, G.; Hultman, L. Compromising Science by Ignorant Instrument Calibration - Need to Revisit Half a Century of Published XPS Data. *Angew. Chem., Int. Ed.* **2020**, *59*, 5002−5006.
(764) Swift, P. Adventitious Carbon—the Panacea for Energy Referencing? *Surf. Interface Anal.* **1982**, *4*, 47−51.
(765) Singh, B.; Grafe, M. *Synchrotron-Based Techniques in Soils and Sediments*; Elsevier Science: London, 2010; Vol. *34*.
(766) Wilke, M.; Farges, F.; Petit, P.-E.; Brown, G. E., Jr; Martin, F. Oxidation State and Coordination of Fe in Minerals: An Fe K-XANES Spectroscopic Study. *Am. Mineral.* **2001**, *86*, 714−730.
(767) Parsons, J.; Aldrich, M.; Gardea-Torresdey, J. Environmental and Biological Applications of Extended X-Ray Absorption Fine Structure (EXAFS) and X-Ray Absorption Near Edge Structure (XANES) Spectroscopies. *Appl. Spectrosc. Rev.* **2002**, *37*, 187−222.
(768) Brown, G. E.; Calas, G.; Waychunas, G. A.; Petiau, J. X-ray Absorption Spectroscopy and Its Applications in Mineralogy and Geochemistry. In *Spectroscopic Methods in Mineralogy and Geology*; Hawthorne, F. C., Eds.; De Gruyter: Berlin, Boston, 1988; Chapter 11, pp 431−512.
(769) Henderson, G. S.; de Groot, F. M. F.; Moulton, B. J. A. X-Ray Absorption near-Edge Structure (XANES) Spectroscopy. *Rev. Mineral. Geochem.* **2014**, *78*, 75−138.
(770) Jeong, H. Y.; Lee, J. H.; Hayes, K. F. Characterization of Synthetic Nanocrystalline Mackinawite: Crystal Structure, Particle Size, and Specific Surface Area. *Geochim. Cosmochim. Acta* **2008**, *72*, 493−505.
(771) Elzinga, E. J. Formation of Layered Fe(II)−Al(III)-Hydroxides During Reaction of Fe(II) with Aluminum Oxide. *Environ. Sci. Technol.* **2012**, *46*, 4894−4901.
(772) Budi, H.; Husain, H.; Supanun, L.; Suminar, P. *Mater. Sci. Forum* **2019**, *964*, 40−44.
(773) Yalçıntaş, E.; Scheinost, A. C.; Gaona, X.; Altmaier, M. Systematic XAS Study on the Reduction and Uptake of Tc by Magnetite and Mackinawite. *Dalton Trans.* **2016**, *45*, 17874−17885.
(774) Coker, V. S.; Gault, A. G.; Pearce, C. I.; van der Laan, G.; Telling, N. D.; Charnock, J. M.; Polya, D. A.; Lloyd, J. R. XAS and XMCD Evidence for Species-Dependent Partitioning of Arsenic


https://doi.org/10.1021/acs.chemrev.0c01286
*Chem. Rev.* 2021, 121, 8161−8233

During Microbial Reduction of Ferrihydrite to Magnetite. *Environ. Sci. Technol.* **2006**, *40*, 7745−7750.
(775) Simoulin, V. The Synchrotron Generations: Communities and Facilities at the Crossroads between the National and the International. *Rev. Fr. Sociol.* **2016**, *57*, 503−528.
(776) Scheinost, A. C.; Rossberg, A.; Vantelon, D.; Xifra, I.; Kretzschmar, R.; Leuz, A.-K.; Funke, H.; Johnson, C. A. Quantitative Antimony Speciation in Shooting-Range Soils by EXAFS Spectroscopy. *Geochim. Cosmochim. Acta* **2006**, *70*, 3299−3312.
(777) Madejová, J.; Pálková, H.; Komadel, P. IR Spectroscopy of Clay Minerals and Clay Nanocomposites. *Spectroscopic Properties of Inorganic and Organometallic Compounds* **2010**, *41*, 22−71.
(778) Nasrazadani, S. The Application of Infrared Spectroscopy to a Study of Phosphoric and Tannic Acids Interactions with Magnetite ($Fe_3O_4$), Goethite ($\alpha$-FeOOH) and Lepidocrocite ($\gamma$-FeOOH). *Corros. Sci.* **1997**, *39*, 1845−1859.
(779) Namduri, H.; Nasrazadani, S. Quantitative Analysis of Iron Oxides Using Fourier Transform Infrared Spectrophotometry. *Corros. Sci.* **2008**, *50*, 2493−2497.
(780) Xiao, W.; Jones, A. M.; Collins, R. N.; Bligh, M. W.; Waite, T. D. Use of Fourier Transform Infrared Spectroscopy to Examine the Fe(II)-Catalyzed Transformation of Ferrihydrite. *Talanta* **2017**, *175*, 30−37.
(781) Xiao, W.; Jones, A. M.; Li, X.; Collins, R. N.; Waite, T. D. Effect of *Shewanella Oneidensis* on the Kinetics of Fe(II)-Catalyzed Transformation of Ferrihydrite to Crystalline Iron Oxides. *Environ. Sci. Technol.* **2018**, *52*, 114−123.
(782) Nasrazadani, S.; Raman, A. The Application of Infrared Spectroscopy to the Study of Rust Systems—II. Study of Cation Deficiency in Magnetite ($Fe_3O_4$) Produced During Its Transformation to Maghemite ($\gamma$-$Fe_2O_3$) and Hematite ($\alpha$-$Fe_2O_3$). *Corros. Sci.* **1993**, *34*, 1355−1365.
(783) Raman, A.; Kuban, B.; Razvan, A. The Application of Infrared Spectroscopy to the Study of Atmospheric Rust Systems—I. Standard Spectra and Illustrative Applications to Identify Rust Phases in Natural Atmospheric Corrosion Products. *Corros. Sci.* **1991**, *32*, 1295−1306.
(784) Sklute, E. C.; Kashyap, S.; Dyar, M. D.; Holden, J. F.; Tague, T.; Wang, P.; Jaret, S. J. Spectral and Morphological Characteristics of Synthetic Nanophase Iron (Oxyhydr) Oxides. *Phys. Chem. Miner.* **2018**, *45*, 1−26.
(785) Southall, S. C.; Micklethwaite, S.; Wilson, S. A.; Frierdich, A. J. Changes in Crystallinity and Tracer-Isotope Distribution of Goethite During Fe(II)-Accelerated Recrystallization. *ACS Earth Space Chem.* **2018**, *2*, 1271−1282.
(786) Moens, C.; Waegeneers, N.; Fritzsche, A.; Nobels, P.; Smolders, E. A Systematic Evaluation of Flow Field Flow Fractionation and Single-Particle ICP-MS to Obtain the Size Distribution of Organo-Mineral Iron Oxyhydroxide Colloids. *J. Chromatogr. A* **2019**, *1599*, 203−214.
(787) Mansor, M.; Cantando, E.; Wang, Y.; Hernandez-Viezcas, J. A.; Gardea-Torresdey, J. L.; Hochella, M. F., Jr; Xu, J. Insights into the Biogeochemical Cycling of Cobalt: Precipitation and Transformation of Cobalt Sulfide Nanoparticles under Low-Temperature Aqueous Conditions. *Environ. Sci. Technol.* **2020**, *54*, 5598−5607.
(788) Mansor, M.; Berti, D.; Hochella, M. F., Jr; Murayama, M.; Xu, J. Phase, Morphology, Elemental Composition, and Formation Mechanisms of Biogenic and Abiogenic Fe-Cu-Sulfide Nanoparticles: A Comparative Study on Their Occurrences under Anoxic Conditions. *Am. Mineral.* **2019**, *104*, 703−717.
(789) Manson, M.; Winkler, C.; Hochella, M. F., Jr; Xu, J. Nanoparticulate Nickel-Hosting Phases in Sulfidic Environments: Effects of Ferrous Iron and Bacterial Presence on Mineral Formation Mechanism and Solid-Phase Nickel Distribution. *Front. Earth Sci.* **2019**, *7*, 1−15.
(790) Vindedahl, A. M.; Strehlau, J. H.; Arnold, W. A.; Penn, R. L. Organic Matter and Iron Oxide Nanoparticles: Aggregation, Interactions, and Reactivity. *Environ. Sci.: Nano* **2016**, *3*, 494−505.
(791) Vindedahl, A. M.; Arnold, W. A.; Penn, R. L. Impact of Pahokee Peat Humic Acid and Buffer Identity on Goethite Aggregation and Reactivity. *Environ. Sci.: Nano* **2015**, *2*, 509−517.
(792) Legg, B. A.; Zhu, M.; Comolli, L. R.; Gilbert, B.; Banfield, J. F. Determination of the Three-Dimensional Structure of Ferrihydrite Nanoparticle Aggregates. *Langmuir* **2014**, *30*, 9931−9940.
(793) Legg, B. A.; Zhu, M.; Comolli, L. R.; Gilbert, B.; Banfield, J. F. Impacts of Ionic Strength on Three-Dimensional Nanoparticle Aggregate Structure and Consequences for Environmental Transport and Deposition. *Environ. Sci. Technol.* **2014**, *48*, 13703−13710.
(794) Li, X.; Qin, F.; Chen, X.; Sheng, A.; Wang, Z.; Liu, J. Dissolution Behavior of Isolated and Aggregated Hematite Particles Revealed by in Situ Liquid Cell Transmission Electron Microscopy. *Environ. Sci. Technol.* **2019**, *53*, 2416−2425.
(795) Lee, C. W.; Ecker, D. J.; Raymond, K. N. Coordination Chemistry of Microbial Iron Transport Compounds. 34. The pH-Dependent Reduction of Ferric Enterobactin Probed by Electrochemical Methods and Its Implications for Microbial Iron Transport. *J. Am. Chem. Soc.* **1985**, *107*, 6920−6923.
(796) Kadish, K. M.; D'Souza, F.; Villard, A.; Autret, M.; Van Caemelbecke, E.; Bianco, P.; Antonini, A.; Tagliatesta, P. Effect of Porphyrin Ring Distortion on Redox Potentials Of. Beta.-Brominated-Pyrrole Iron(III) Tetraphenylporphyrins. *Inorg. Chem.* **1994**, *33*, 5169−5170.
(797) Doyle, R. W. The Origin of the Ferrous Ion-Ferric Oxide Nernst Potential in Environments Containing Dissolved Ferrous Iron. *Am. J. Sci.* **1968**, *266*, 840−859.
(798) Grenthe, I.; Stumm, W.; Laaksuharju, M.; Nilsson, A. C.; Wikberg, P. Redox Potentials and Redox Reactions in Deep Groundwater Systems. *Chem. Geol.* **1992**, *98*, 131−150.
(799) Macalady, D. L.; Langmuir, D.; Grundl, T.; Elzerman, A. Use of Model-Generated $Fe^{3+}$ Ion Activities To Compare Eh and Ferric Oxyhydroxide Solubilities in Anaerobic Systems. In *Chemical Modeling of Aqueous Systems II*; Melchior, D. C., Bassett, R. L., Eds.; ACS Symposium Series; American Chemical Society: Washington, DC, 1990; Vol. *416*, Chapter 28, pp350−367.
(800) Sander, M.; Hofstetter, T. B.; Gorski, C. A. Electrochemical Analyses of Redox-Active Iron Minerals: A Review of Non-Mediated and Mediated Approaches. *Environ. Sci. Technol.* **2015**, *49*, 5862−5878.
(801) Niu, Y.; Sun, F.; Xu, Y.; Cong, Z.; Wang, E. Applications of Electrochemical Techniques in Mineral Analysis. *Talanta* **2014**, *127*, 211−218.
(802) Shi, Z.; Nurmi, J. T.; Tratnyek, P. G. Effects of Nano Zero-Valent Iron on Oxidation− Reduction Potential. *Environ. Sci. Technol.* **2011**, *45*, 1586−1592.
(803) Helz, G.; Ciglenečki, I.; Krznarić, D.; Bura-Nakić, E. Voltammetry of Sulfide Nanoparticles and the FeS(aq) Problem. In *Aquatic Redox Chemistry*; Tratnyek, P. G., Grundl, T. J., Haderlein, S. B., Eds.; ACS Symposium Series; American Chemical Society: Washington, DC, 2011; Vol. *1071*, Chapter 13, pp265−282.
(804) Bura-Nakić, E.; Krznarić, D.; Helz, G. R.; Ciglenečki, I. Characterization of Iron Sulfide Species in Model Solutions by Cyclic Voltammetry. Revisiting an Old Problem. *Electroanalysis* **2011**, *23*, 1376−1382.
(805) Gorski, C. A.; Klüpfel, L.; Voegelin, A.; Sander, M.; Hofstetter, T. B. Redox Properties of Structural Fe in Clay Minerals. 2. Electrochemical and Spectroscopic Characterization of Electron Transfer Irreversibility in Ferruginous Smectite, SWA-1. *Environ. Sci. Technol.* **2012**, *46*, 9369−9377.
(806) Gorski, C. A.; Klüpfel, L. E.; Voegelin, A.; Sander, M.; Hofstetter, T. B. Redox Properties of Structural Fe in Clay Minerals: 3. Relationships between Smectite Redox and Structural Properties. *Environ. Sci. Technol.* **2013**, *47*, 13477−13485.
(807) Hoving, A. L.; Sander, M.; Bruggeman, C.; Behrends, T. Redox Properties of Clay-Rich Sediments as Assessed by Mediated Electrochemical Analysis: Separating Pyrite, Siderite and Structural Fe in Clay Minerals. *Chem. Geol.* **2017**, *457*, 149−161.


https://doi.org/10.1021/acs.chemrev.0c01286
*Chem. Rev.* 2021, 121, 8161−8233

(808) Cachet-Vivier, C.; Keddam, M.; Vivier, V.; Yu, L. T. Development of Cavity Microelectrode Devices and Their Uses in Various Research Fields. *J. Electroanal. Chem.* **2013**, *688*, 12−19.
(809) Nurmi, J. T.; Bandstra, J. Z.; Tratnyek, P. G. Packed Powder Electrodes for Characterizing the Reactivity of Granular Iron in Borate Solutions. *J. Electrochem. Soc.* **2004**, *151*, B347.
(810) Nurmi, J. T.; Tratnyek, P. G. Electrochemical Studies of Packed Iron Powder Electrodes: Effects of Common Constituents of Natural Waters on Corrosion Potential. *Corros. Sci.* **2008**, *50*, 144−154.
(811) Nurmi, J. T.; Sarathy, V.; Tratnyek, P. G.; Baer, D. R.; Amonette, J. E.; Karkamkar, A. Recovery of Iron/Iron Oxide Nanoparticles from Solution: Comparison of Methods and Their Effects. *J. Nanopart. Res.* **2011**, *13*, 1937−1952.
(812) Sarathy, V.; Tratnyek, P. G.; Nurmi, J. T.; Baer, D. R.; Amonette, J. E.; Chun, C. L.; Penn, R. L.; Reardon, E. J. Aging of Iron Nanoparticles in Aqueous Solution: Effects on Structure and Reactivity. *J. Phys. Chem. C* **2008**, *112*, 2286−2293.
(813) Turcio-Ortega, D.; Fan, D.; Tratnyek, P. G.; Kim, E.-J.; Chang, Y.-S. Reactivity of Fe/FeS Nanoparticles: Electrolyte Composition Effects on Corrosion Electrochemistry. *Environ. Sci. Technol.* **2012**, *46*, 12484−12492.
(814) Kim, E.-J.; Kim, J.-H.; Chang, Y.-S.; Turcio-Ortega, D.; Tratnyek, P. G. Effects of Metal Ions on the Reactivity and Corrosion Electrochemistry of Fe/FeS Nanoparticles. *Environ. Sci. Technol.* **2014**, *48*, 4002−4011.
(815) Bradley, M. J.; Tratnyek, P. G. Electrochemical Characterization of Magnetite with Agarose-Stabilized Powder Disk Electrodes and Potentiometric Methods. *ACS Earth Space Chem.* **2019**, *3*, 688−699.
(816) Shimizu, K.; Lasia, A.; Boily, J.-F. o. Electrochemical Impedance Study of the Hematite/Water Interface. *Langmuir* **2012**, *28*, 7914−7920.
(817) Shimizu, K.; Boily, J.-F. Electrochemical Properties and Relaxation Times of the Hematite/Water Interface. *Langmuir* **2014**, *30*, 9591−9598.
(818) Lucas, M.; Boily, J.-F. o. Mapping Electrochemical Heterogeneity at Iron Oxide Surfaces: A Local Electrochemical Impedance Study. *Langmuir* **2015**, *31*, 13618−13624.
(819) Shimizu, K.; Boily, J.-F. Electrochemical Signatures of Crystallographic Orientation and Counterion Binding at the Hematite/Water Interface. *J. Phys. Chem. C* **2015**, *119*, 5988−5994.
(820) Zarzycki, P.; Chatman, S.; Preočanin, T.; Rosso, K. M. Electrostatic Potential of Specific Mineral Faces. *Langmuir* **2011**, *27*, 7986−7990.
(821) Goldberg, S. Application of Surface Complexation Models to Anion Adsorption by Natural Materials. *Environ. Toxicol. Chem.* **2014**, *33*, 2172−2180.
(822) Venema, P.; Hiemstra, T.; van Riemsduk, W. H. Comparison of Different Site Binding Models for Cation Sorption: Description of pH Dependency, Salt Dependency, and Cation−Proton Exchange. *J. Colloid Interface Sci.* **1996**, *181*, 45−59.
(823) Goldberg, S. Modeling Selenite Adsorption Envelopes on Oxides, Clay Minerals, and Soils Using the Triple Layer Model. *Soil Sci. Soc. Am. J.* **2013**, *77*, 64−71.
(824) Adsorption Models Incorporated into Chemical Equilibrium Models. In *Chemical Equilibrium and Reaction Models*; Loeppert, R. H., Schwab, A. P., Goldberg, S., Eds.; 1995; Chapter 5, pp 75−95.
(825) Groenenberg, J. E.; Lofts, S. The Use of Assemblage Models to Describe Trace Element Partitioning, Speciation, and Fate: A Review. *Environ. Toxicol. Chem.* **2014**, *33*, 2181−2196.
(826) Wang, Z.; Giammar, D. E. Mass Action Expressions for Bidentate Adsorption in Surface Complexation Modeling: Theory and Practice. *Environ. Sci. Technol.* **2013**, *47*, 3982−3996.
(827) Westall, J. C.; Herbelin, A. *FITEQL: A Computer Program for Determination of Chemical Equilibrium Constants from Experimental Data, Version 4.0, Report 99-01*; Oregon State University: Corvallis, OR, 1999.
(828) Gustafsson, J. P. *Visual MINTEQ 3.0 User Guide*; Royal Institute of Technology: Stockholm, Sweden, 2011.
(829) Parkhurst, D. L.; Appelo, C. User's Guide to PHREEQC (Version 2): A Computer Program for Speciation, Batch-Reaction, One-Dimensional Transport, and Inverse Geochemical Calculations. *Water-Resour. Invest. Rep.* **1999**, 99−4259.
(830) Schecher, W. D.; mCavoy, D. C. *MINEQL+: A Chemical Equilibrium Modeling System, Version 4.6*; Environmental Research Software: Hallowell, ME, 2007.
(831) Ludwig, C. GRFIT: A Program, for Solving Speciation Problem, Evaluation of Equilibrium Constants, Concentraions and Their Physical Parameters, PhD Thesis, The University of Beme, Switzerland, 1992.
(832) Keizer, M.; Van Riemsdijk, W. ECOSAT: Technical Report of the Departments of Soil Science and Plant Nutrition, Wageningen University, Wageningen, The Netherlands, 1994.
(833) Lövgren, L. Complexation Reactions of Phthalic Acid and Aluminium(III) with the Surface of Goethite. *Geochim. Cosmochim. Acta* **1991**, *55*, 3639−3645.
(834) Swedlund, P.; Webster, J. Cu and Zn Ternary Surface Complex Formation with $SO_4$ on Ferrihydrite and Schwertmannite. *Appl. Geochem.* **2001**, *16*, 503−511.
(835) Buerge-Weirich, D.; Behra, P.; Sigg, L. Adsorption of Copper, Nickel, and Cadmium on Goethite in the Presence of Organic Ligands. *Aquat. Geochem.* **2003**, *9*, 65−85.
(836) Hiemstra, T.; van Riemsdijk, W. H. Adsorption and Surface Oxidation of Fe(II) on Metal (Hydr)Oxides. *Geochim. Cosmochim. Acta* **2007**, *71*, 5913−5933.
(837) Stumm, W.; Huang, C.; Jenkins, S. Specific Chemical Interaction Affecting Stability of Dispersed Systems. *Croat. Chem. Acta* **1970**, *42*, 223−245.
(838) Stumm, W.; Hohl, H.; Dalang, F. Interaction of Metal-Ions with Hydrous Oxide Surfaces. *Croat. Chem. Acta* **1976**, *48*, 491−504.
(839) Vasudevan, D.; Stone, A. T. Adsorption of Catechols, 2-Aminophenols, and 1, 2-Phenylenediamines at the Metal (Hydr)-Oxide/Water Interface: Effect of Ring Substituents on the Adsorption onto $Tio_2$. *Environ. Sci. Technol.* **1996**, *30*, 1604−1613.
(840) Vasudevan, D.; Stone, A. T. Adsorption of 4-Nitrocatechol, 4-Nitro-2-Aminophenol, and 4-Nitro-1, 2-Phenylenediamine at the Metal (Hydr) Oxide/Water Interface: Effect of Metal (Hydr)Oxide Properties. *J. Colloid Interface Sci.* **1998**, *202*, 1−19.
(841) de Oliveira, L. P.; Hudebine, D.; Guillaume, D.; Verstraete, J. J. A Review of Kinetic Modeling Methodologies for Complex Processes. *Oil Gas Sci. Technol.* **2016**, *71*, 45.
(842) Zhang, H.; Lemley, A. T. Reaction Mechanism and Kinetic Modeling of Deet Degradation by Flow-through Anodic Fenton Treatment (FAFT). *Environ. Sci. Technol.* **2006**, *40*, 4488−4494.
(843) Zeng, G.; Maeda, S.; Taketsugu, T.; Sakaki, S. Catalytic Transfer Hydrogenation by a Trivalent Phosphorus Compound: Phosphorus-Ligand Cooperation Pathway or $P^{III}/P^{V}$ Redox Pathway? *Angew. Chem., Int. Ed.* **2014**, *53*, 4633−4637 DOI: 10.1002/anie.201311104.
(844) Liao, R.-Z.; Li, X.-C.; Siegbahn, P. E. M. Reaction Mechanism of Water Oxidation Catalyzed by Iron Tetraamido Macrocyclic Ligand Complexes − a DFT Study. *Eur. J. Inorg. Chem.* **2014**, *2014*, 728−741.
(845) Chen, H.-L.; Li, H.-J.; Ho, J.-J. Quantum-Chemical Calculations on a Novel Reaction Mechanism of CNN with NO. *Chem. Phys. Lett.* **2007**, *442*, 35−41.
(846) Hartenbach, A. E.; Hofstetter, T. B.; Aeschbacher, M.; Sander, M.; Kim, D.; Strathmann, T. J.; Arnold, W. A.; Cramer, C. J.; Schwarzenbach, R. P. Variability of Nitrogen Isotope Fractionation During the Reduction of Nitroaromatic Compounds with Dissolved Reductants. *Environ. Sci. Technol.* **2008**, *42*, 8352−8359.
(847) Hofstetter, T. B.; Neumann, A.; Arnold, W. A.; Hartenbach, A. E.; Bolotin, J.; Cramer, C. J.; Schwarzenbach, R. P. Substituent Effects on Nitrogen Isotope Fractionation During Abiotic Reduction of Nitroaromatic Compounds. *Environ. Sci. Technol.* **2008**, *42*, 1997−2003.
(848) Burke, K.; Wagner, L. O. Dft in a Nutshell. *Int. J. Quantum Chem.* **2013**, *113*, 96−101.
(849) Stephens, P. J.; Devlin, F. J.; Chabalowski, C. F.; Frisch, M. J. Ab Initio Calculation of Vibrational Absorption and Circular Dichroism

Spectra Using Density Functional Force Fields. *J. Phys. Chem.* **1994**, *98*, 11623−11627.
(850) Kim, K.; Jordan, K. D. Comparison of Density Functional and MP2 Calculations on the Water Monomer and Dimer. *J. Phys. Chem.* **1994**, *98*, 10089−10094.
(851) Stephens, P.; Devlin, F.; Chabalowski, C.; Frisch, M. J. Ab Initio Calculation of Vibrational Absorption and Circular Dichroism Spectra Using Density Functional Force Fields. *J. Phys. Chem.* **1994**, *98*, 11623−11627.
(852) Scott, A. P.; Radom, L. Harmonic Vibrational Frequencies: An Evaluation of Hartree− Fock, Møller− Plesset, Quadratic Configuration Interaction, Density Functional Theory, and Semiempirical Scale Factors. *J. Phys. Chem.* **1996**, *100*, 16502−16513.
(853) Andersson, M. P.; Uvdal, P. New Scale Factors for Harmonic Vibrational Frequencies Using the B3lyp Density Functional Method with the Triple-Z Basis Set 6−311+G(D,P). *J. Phys. Chem. A* **2005**, *109*, 2937−2941.
(854) Anisimov, V. I.; Zaanen, J.; Andersen, O. K. Band Theory and Mott Insulators: Hubbard U Instead of Stoner I. *Phys. Rev. B: Condens. Matter Mater. Phys.* **1991**, *44*, 943−954.
(855) Anisimov, V. I.; Solovyev, I. V.; Korotin, M. A.; Czyżyk, M. T.; Sawatzky, G. A. Density-Functional Theory and Nio Photoemission Spectra. *Phys. Rev. B: Condens. Matter Mater. Phys.* **1993**, *48*, 16929−16934.
(856) Solovyev, I. V.; Dederichs, P. H.; Anisimov, V. I. Corrected Atomic Limit in the Local-Density Approximation and the Electronic Structure of D Impurities in Rb. *Phys. Rev. B: Condens. Matter Mater. Phys.* **1994**, *50*, 16861−16871.
(857) Rohrbach, A.; Hafner, J.; Kresse, G. Ab Initio Study of the (0001) Surfaces of Hematite and Chromia: Influence of Strong Electronic Correlations. *Phys. Rev. B: Condens. Matter Mater. Phys.* **2004**, *70*, 125426.
(858) Dzade, N. Y.; Roldan, A.; De Leeuw, N. H. A Density Functional Theory Study of the Adsorption of Benzene on Hematite ($\alpha$-$Fe_2O_3$) Surfaces. *Minerals* **2014**, *4*, 89−115.
(859) Jakobsen, S.; Mikkelsen, K. V.; Pedersen, S. U. Calculations of Intramolecular Reorganization Energies for Electron-Transfer Reactions Involving Organic Systems. *J. Phys. Chem.* **1996**, *100*, 7411−7417.
(860) Sharp, K. A. Calculation of Electron Transfer Reorganization Energies Using the Finite Difference Poisson-Boltzmann Model. *Biophys. J.* **1998**, *74*, 1241−1250.
(861) Peng, C.; Sundman, A.; Bryce, C.; Catrouillet, C.; Borch, T.; Kappler, A. Oxidation of Fe(II)-organic matter complexes in the presence of the mixotrophic nitrate-reducing Fe(II)-oxidizing bacterium Acidovorax sp. BoFeN1. *Environ. Sci. Technol.* **2018**, *52*, 5753−5763.
(862) Ehrlich, H. Microorganisms in Acid Drainage from a Copper Mine. *J. Bacteriol.* **1963**, *86*, 350.
(863) Tuovinen, O. H.; Niemelä, S.; Gyllenberg, H. Tolerance Ofthiobacillus Ferrooxidans to Some Metals. *Antonie van Leeuwenhoek* **1971**, *37*, 489−496.
(864) Zhang, L.; Dong, H.; Kukkadapu, R. K.; Jin, Q.; Kovarik, L. Electron Transfer between Sorbed Fe(II) and Structural Fe(III) in Smectites and Its Effect on Nitrate-Dependent Iron Oxidation by Pseudogulbenkiania sp. Strain 2002. *Geochim. Cosmochim. Acta* **2019**, *265*, 132−147.


https://doi.org/10.1021/acs.chemrev.0c01286
*Chem. Rev.* 2021, 121, 8161−8233